



DI Robert Macher-Ambrosch

TURBIDITY CONTROL

Dissertation

zur Erlangung des akademischen Grades
Doktor der technischen Wissenschaften

eingereicht an der
Technischen Universität Graz

Betreuer

Univ.-Prof. Dipl.-Ing. Dr.techn. Matthäus Siebenhofer

Institut für Chemische Verfahrenstechnik und Umwelttechnik

Graz, Februar 2018

*"Nichts auf dieser Welt, das sich zu haben lohnt, fällt
einem in den Schoß."*

Dr. Robert "Bob" Kelso, "Scrubs", season 4, episode 20

DANKSAGUNG

An dieser Stelle möchte ich allen danken, die zum Entstehen dieser Arbeit beigetragen haben.

Zuallererst möchte ich mich bei meinem Betreuer, Prof. Matthäus Siebenhofer bedanken, der sich nach einem unglücklichen ersten Versuch bereit erklärt hat, die Betreuung zu übernehmen und mit mir ein neues Thema auszuarbeiten. Vielen Dank für die große Unterstützung und die besondere Art, für jedes Problem die passende Lösung parat zu haben!

Ich möchte mich auch bei meinen Studenten bedanken, die mich in beiden Anläufen zu dieser Arbeit mit ihrer experimentellen Arbeit unterstützt haben: Daniel Habenbacher, Bianca Höller, Dorothea Leis, Tobias Maier, Dominik Otrin, Christin Pirmann, Aroonrat Poonyaratanasrihajon, Christoph Rohringer, Christina Staudinger, Chanita Tantichumnan, Tobias Thaler, Stephan Weixler

Ich hoffe, dass auch ihr ein wenig aus diesen Arbeiten mitnehmen könntet.

Außerdem möchte ich mich beim gesamten Team des ICVT für die schöne Zeit als Universitätsassistent bedanken. Ich werde auf die 4 Jahre am Institut immer positiv zurückblicken und hoffe, dass wir uns auch in Zukunft hin und wieder über den Weg laufen werden.

Abschließend möchte ich mich bei meiner gesamten Familie bedanken, insbesondere bei meiner Frau Patrizia und unserem Sohn Felix. Ohne eure Rücksicht und das große Verständnis für viele Stunden im Büro wäre eine Fertigstellung dieser Arbeit nicht möglich gewesen. Vielen Dank für die Unterstützung in dieser für uns alle entbehrungsreichen Zeit.

VIELEN DANK!

STATUTORY DECLARATION

I declare that I have authored this thesis independently, that I have not used other than the declared sources/resources, and that I have explicitly marked all material which has been quoted either literally or by content from the used sources.

Graz, _____
Date Signature

EIDESSTATTLICHE ERKLÄRUNG¹

Ich erkläre an Eides statt, dass ich die vorliegende Arbeit selbstständig verfasst, andere als die angegebenen Quellen/Hilfsmittel nicht benutzt, und die den benutzten Quellen wörtlich und inhaltlich entnommenen Stellen als solche kenntlich gemacht habe.

Graz, am _____
Datum Unterschrift

¹Beschluss der Curricula-Kommission für Bachelor-, Master- und Diplomstudien vom 10.11.2008; Genehmigung des Senates am 1.12.2008

ABSTRACT

In this research project, the electrical splitting of stable oil in water emulsions has been investigated. Particular attention has been paid to emulsions with a very low amount of solvent phase dispersed in the aqueous carrier phase, according to industrial applications in liquid-liquid extraction. These turbidities must be split in the electric field without electrolysis, therefore limited to the action of electrical field intensity.

To produce a reproducible stable turbidity, the stability of emulsions has been studied. For the system ShellSol-K/water the optimal number of revolutions was determined to be 1500 rpm. Below and above this number of revolutions the stability of the emulsion will drop. The stability was increased by adding the anionic surfactant 4-dodecylbenzenesulfonic acid. Stable turbidity was needed for comparison of different splitting techniques. Besides the splitting in the electric field, also the chemical splitting, splitting by centrifugation and flotation have been investigated. However, none of these techniques could satisfy the needs.

Splitting in the electric field has been investigated in different setups. It was observed, that inclination of the electrodes leads to faster separation compared to vertically arranged electrodes. A link between the electric field strength and the separation willingness was found. Expectedly, increasing electric field strength led to faster phase separation. On the contrary, the electrode distance at constant electric field strength did not show an influence on quality or duration of the separation. The number of electrodes also influenced the rate of separation.

With these findings, the optimal configuration was determined. In the three electrodes setup with a central anode and the outer cathodes best phase separation was achieved. The electrodes shall be inclined by an angle of 45 degrees.

A model has been developed to facilitate the prediction of splitting of emulsions in the electric field. The model correlates theoretically consolidated the electric field strength with the droplet diameter, which can just be separated.

KURZFASSUNG

In der vorliegenden Arbeit wurde die elektrische Spaltung von stabilen Öl in Wasser Emulsionen untersucht. Hauptaugenmerk wurde auf Emulsionen mit sehr geringem Anteil an Solventphase in wässriger Trägerlösung gelegt, wie sie in der industriellen Anwendung der Flüssig-Flüssig Extraktion vorkommen. Diese Feinsttrübungen wurden im elektrischen Feld ohne Elektrolyse behandelt, wodurch die Stärke des elektrischen Feldes limitiert war. Um eine reproduzierbare Feinsttrübung zu erzeugen, wurde im Vorfeld eine Studie hinsichtlich der Stabilität von Emulsionen durchgeführt. Für das Stoffsystem ShellSol-K/Wasser konnte eine optimale Drehzahl des Rührers von 1500 rpm gefunden werden. Unter und auch über dieser Drehzahl war die Stabilität der Emulsion geringer. Durch Zugabe des anionischen Tensides 4-Dodecylbenzolsulfonsäure konnte die Stabilität weiter gesteigert werden. Eine stabile Feinsttrübung war erforderlich, um in den Spaltversuchen verschiedene Verfahren vergleichen zu können. Neben der Spaltung im elektrischen Feld wurden auch die chemische Spaltung, die Spaltung mittels Zentrifugation und Flotation untersucht. Keines dieser Alternativverfahren konnte alle Anforderungen erfüllen.

Die elektrische Spaltung wurde in unterschiedlichen Varianten des Spaltapparates untersucht. So konnte festgestellt werden, dass eine Neigung der Elektroden im Vergleich zur vertikalen Ausrichtung eine schnellere Spaltung bewirkt. Weiters wurde ein Zusammenhang zwischen elektrischer Feldstärke und Trennverhalten gefunden, wobei erwartungsgemäß erhöhte Feldstärke schnellere Phasentrennung mit sich brachte. Dagegen hatte die Veränderung des Abstandes der Elektroden bei gleichbleibender elektrischer Feldstärke keinen Einfluss auf die Güte und die Dauer der Trennung. Auch die Anzahl der Elektroden beeinflusste die Geschwindigkeit der Spaltung. Die optimale Konfiguration war demnach eine Drei-Elektrodenanordnung, wobei die mittlere als Anode und die beiden äußeren als Kathode geschaltet waren. Zusätzlich sollten die Elektroden um 45° geneigt in den Spaltungsapparat eingebaut werden.

Um die Vorhersage des Spaltverhaltens einer Emulsion im elektrischen Feld zu erleichtern wurde ein Modell entwickelt. Dieses stellt theoretisch fundiert den Zusammenhang zwischen der elektrischen Feldstärke und dem Tropfendurchmesser, der gerade noch abgetrennt werden kann, her.

CONTENTS

Abstract	IV
Kurzfassung	V
1. Introduction	1
1.1. Definition and classification of emulsions	1
1.1.1. Definition	1
1.1.2. Classification	1
1.2. Processes and emulsions	2
1.2.1. Extraction	3
1.2.2. Secondary crude oil production	3
1.2.3. Cutting oil emulsions	3
1.3. Scope	4
I. Basics	5
2. Stabilisation mechanisms	6
2.1. DLVO-theory	6
2.1.1. Double layer repulsion	7
2.1.2. Van der Waals forces	9
2.2. Surfactants	9
2.2.1. Steric stabilisation	12
2.2.2. Membrane formation	12
2.3. Brownian motion	13
3. Emulsion formation techniques	15
3.1. Low energy consuming techniques	15
3.1.1. The Ouzo effect	16
3.1.2. Phase inversion	16
3.2. Intermediate energy consuming techniques	18
3.3. High energy consuming techniques	19
3.3.1. Rotor-stator systems	20
3.3.2. High pressure systems	20
3.3.3. Ultrasonic systems	20

4. Breakdown processes in emulsions	23
4.1. Coalescence	23
4.2. Creaming and sedimentation	23
4.3. Flocculation	26
4.4. Ostwald ripening	27
4.5. Phase Inversion	27
5. Splitting of stable emulsions	29
5.1. Chemical splitting	29
5.2. Electrical splitting	29
5.2.1. Theory of electrical splitting	30
5.2.2. Water-in-oil emulsions	32
5.2.3. Oil-in-water emulsions	32
5.3. Mechanical splitting	33
5.3.1. Filtration	34
5.3.2. Sedimentation	34
5.4. Thermal splitting	38
II. Experimental setup	39
6. Chemical system	40
7. Setup - Preparation of stable emulsions	42
7.1. Ultrasonic scanner	42
7.2. Experimental procedure	42
7.2.1. Preparation of saturated phases	43
7.2.2. Optical cell evaluation	44
7.2.3. Ultrasonic scanning experiments	44
8. Setup - Splitting of stable emulsions	46
8.1. Experimental procedure	46
8.2. Thermal splitting	47
8.3. Chemical splitting	47
8.4. Mechanical splitting	47
8.4.1. Centrifugation	47
8.4.2. Flotation	48
8.5. Electrical splitting	50
8.5.1. Direct current	50

8.6. Interpretation of monitoring results	52
III. Modelling	58
9. Sigmoidal modelling approach	59
10. Exponential modelling approach	62
IV. Results and discussion	68
11. Results - Preparation of stable emulsions	69
11.1. Influence of the agitation rate	69
11.1.1. Optical evaluation	69
11.1.2. Ultrasonic scanner	71
11.2. Influence of the hold-up	72
11.3. Influence of the surfactant	74
12. Results - Splitting of stable emulsions	76
12.1. Thermal splitting	76
12.2. Chemical splitting	77
12.3. Mechanical splitting	78
12.3.1. Centrifugation	78
12.3.2. Flotation	79
12.4. Electrical splitting - Direct current	81
12.4.1. Reproducibility	82
12.4.2. Comparison of different setups	84
12.4.3. Results of experiments with two plate electrodes	85
12.4.4. Results of experiments with three plate electrodes	90
12.4.5. Results of experiments with four plate electrodes	95
12.4.6. Results of experiments with four plate electrodes and 3 times 4 rod electrodes	97
12.4.7. Comparison of the different electrode arrangements	98
12.4.8. Electrical splitting of a multi component system using four plate electrodes	99
13. Results - Modelling of the electric field splitting progress	103
14. Summary	108

CONTENTS

Abbreviations	111
Bibliography	115
List of Figures	120
List of Tables	127
Appendix	130
Appendix A. Matlab Code	131
Appendix B. Thermal Splitting	157
Appendix C. Flotation	159
Appendix D. Calibration of the ultrasonic scanner	162
Appendix E. Reproducibility of the electric field experiments	164
Appendix F. Modelling results for the electrical field splitting	191
Appendix G. Publications	206

1. INTRODUCTION

1.1. DEFINITION AND CLASSIFICATION OF EMULSIONS

1.1.1. DEFINITION

An emulsion (macroemulsion) is a system containing two intensely mixed immiscible or partially miscible liquids. One of the liquids forms droplets, which are dispersed in the other one. The liquid forming droplets is called dispersed phase and the one representing the surrounding media is called the continuous phase. In most cases, one phase is an oil and the other one is aqueous. Oil in this case means an insoluble organic species. There are two types of emulsion, which can be distinguished looking at the continuous and the dispersed phase. There is the oil-in-water (o/w) emulsion, where the oil is dispersed in the water phase, and the water-in-oil (w/o) emulsion, where it is the other way around. There are several ways to identify the direction of the emulsification like solubilisation of a dye in the continuous phase or trying to dilute with water or oil. Depending on the continuous phase, it is possible to dilute with water (if water is the continuous phase) or with oil. Another option to find out the dispersion direction is to determine the electrical conductivity since oil usually has a lower conductivity than water. [1]

Emulsions may be significantly stable relative to the intended use, which covers a range from a few minutes to a few years. [2]

1.1.2. CLASSIFICATION

In general the droplet size of macroemulsions lies in the micrometre range (0.1 – 10 μm [3]), which means that gravity force influences the behaviour of the droplets [4]. Additionally, this size range covers the wavelength of visible light. Therefore, macroemulsions often scatter visible light and appear cloudy [3]. As mentioned in the previous section, intense mixing (or high energy input in general, see chapter 3 for more information) is necessary to form droplets small enough to produce a macroemulsion. Anyway, no matter how high the energy input into the emulsifying system might be, it is only kinetically stable. Therefore, several stabilising mechanisms (see chapter 2) have to be taken into account to produce macroemulsions as stable as possible.

Table 1.1.: Properties of different emulsion types [1, 3, 6]

<i>Property</i>	<i>Macroemulsion</i>	<i>Nanoemulsion</i>	<i>Microemulsion</i>
Appearance	Formulation-dependent	Transparent to milky	Transparent
Preparation method	Classic homogenization	High energy (pressure)	Low-energy emulsification
Surfactant load	Fairly low	Medium (<10 %)	Fairly high (10–20 %)
Droplet size	0.1 – 10 μm	50 – 200 nm	1 – 100 nm
Thermodynamic stability	Unstable; kinetically stable	Unstable; kinetically stable	Stable

A transparent or translucent type of emulsion is a so-called nanoemulsion. The size range of the dispersed droplets is 50 – 200 nm. They are kinetically stable but their long-term stability is sometimes referred to as “approaching thermodynamic stability.” [5]

A special case are so-called microemulsions, which form spontaneously and are thermodynamically stable. The range for the characteristic drop size is from 1 – 100 nm, which means that they do not scatter light. Microemulsions can be divided into two main types: the dispersed and the bicontinuous microemulsion. In the former, the droplets are stabilised by surfactants. In the latter, a network of water and oil – both continuous – is stabilised by amphiphilic membranes. [3]

In table 1.1, some properties of macro- nano- and microemulsions are listed. Additionally, the preparation mode is described, since this leads to big differences in emulsion behaviour. The same holds for the surfactant load.

1.2. PROCESSES AND EMULSIONS

Emulsions are used in many different industrial applications. There are several processes, where emulsions are desired. These processes include but are not limited to agricultural products, cosmetics, pharmaceuticals and foodstuff as well as metal working [3, 7]. However, emulsion formation is not always a desired process step. In the following sections, some examples for such processes are given. Additionally, the problems due to unwanted emulsification are addressed.

1.2.1. EXTRACTION

In liquid-liquid extraction, the feed phase with the constituent to be separated is contacted with a second liquid. The latter liquid shall be more or less immiscible with the feed phase. The goal is to separate two or more components from the feed phase. The solute shall preferentially dissolve in the solvent. [8] Since liquid-liquid extraction has always to be followed by a solvent recovery process, the extraction process needs complete phase separation [8, 9]. Therefore, stable emulsions are unwanted in solvent extraction. While primary separation is often easily achieved, complete separation into two clean (turbidity free) phases might take long separation time. The reason for this disadvantageous phenomenon is mainly the presence of surface-active components in the system. These components can be added intentionally, acting as catalyst (see [10] for more information) or occur unintended as part of fermentation broths or as degradation products. All cases show the same problem. The separation of the aqueous from the solvent phase is not complete. If the solvent or the target component are expensive chemicals, even traces lost in the aqueous raffinate phase may have a strong influence on the economic feasibility of a process. Another reason for the need of complete separation might be the toxicity of constituents.

1.2.2. SECONDARY CRUDE OIL PRODUCTION

Crude oil recovery from oil fields is usually performed using the natural energy of the reservoir. If this energy becomes too low with ongoing recovery, seawater is injected to elevate the pressure in the reservoir. Due to this process a stable emulsion (stability up to five months) with very fine water droplets in the crude oil is formed. The small droplet size together with naturally occurring surfactants lead to stabilization. These surfactants do not drop the interfacial tension but avoid coalescence by opposing film thinning (see chapter 2.2.2). [11] Obviously, the further processing of the crude oil is hindered by water dispersed into the oil, which therefore has to be removed.

1.2.3. CUTTING OIL EMULSIONS

Cutting oil emulsions are used during mechanical cutting and machining of metals, because they combine the properties of lubrication as well as cooling. A cutting fluid consists of water, a mineral oil and additives to meet the desired specifications. These specifications can be the resistance to bacterial growth or low corrosion capacity [12]. These properties

1. INTRODUCTION

may get lost due to aging by mainly thermal degradation and increasing concentration of metal particles during usage. Therefore, cutting oils have to be replaced on occasion. Due to the high content of surfactants and other organic compounds spent cutting oil emulsions are classified as environmentally toxic. These emulsions are designed to be very stable. This includes the admixture of surfactants. Additionally, the droplet size is very small, which can lead to turbidity formation. Therefore, splitting of cutting oil emulsions is very challenging and it might be necessary to combine two or more separation techniques. [13]

1.3. SCOPE

For the above-mentioned reasons the target of this work is the splitting of emulsions with very low amount of solvent (turbidity) dispersed in an aqueous carrier. For better understanding of emulsion splitting, a general review of the knowledge already discussed in literature is summarized. The stabilising effects as well as the breakdown processes will be discussed. The understanding of formation of stable emulsions is a basic need for the development of splitting technologies. Therefore, experiments on emulsion formation are necessary. Then, the breaking of a stable turbidity can be investigated. Different techniques are in principle available. However, the focus is laid on splitting of turbidity in the electric field without faradaic current. This topic is not intensively discussed in literature and claimed to be a slow technique [9]. Nevertheless, due to its advantages regarding setup complexity and the lack of safety hazards this technique deserves detailed attention. A standard apparatus consisting of two vertical electrodes, which are arranged in parallel, had to be optimized regarding number, shape and inclination of the electrodes. Additionally, a model for the prediction of splitting progress had to be developed relating the electric field strength with the size of the smallest removable droplets.

Part I.

Basics

2. STABILISATION MECHANISMS

In this section, the most important stabilisation mechanisms and parameters influencing the stability are described. Special attention is paid to this section since it is necessary to deal with emulsion stability preceding the investigation of the splitting mechanisms. Since this work mainly deals with o/w-emulsions, the focus is laid on the stabilisation mechanisms of this dispersion direction.

2.1. DLVO-THEORY

The DLVO-theory helps understanding the stability of colloids. It was named after the four developers of this theory Boris Derjaguin, Lew Landau, Evert Verwey and Theodoor Overbeek [14, 15]. In this theory the repulsive double layer forces as well as the attractive van der Waals forces, which act on short-range and long-range, respectively, are taken into account. This is used to describe the potential energy in the system as the sum of the repulsive potential energy due to the overlapping of the electrical double layer surrounding the colloid particles (in the case of emulsions: droplets) and the attractive van der Waals energy. [3]

In figure 2.1 net DLVO interaction is depicted for different interfacial tensions σ . The lower the interfacial tension the lower the energy barrier. Below a critical interfacial tension, there is no repulsive barrier anymore and the emulsion breaks due to coalescence because the attractive forces are predominant.

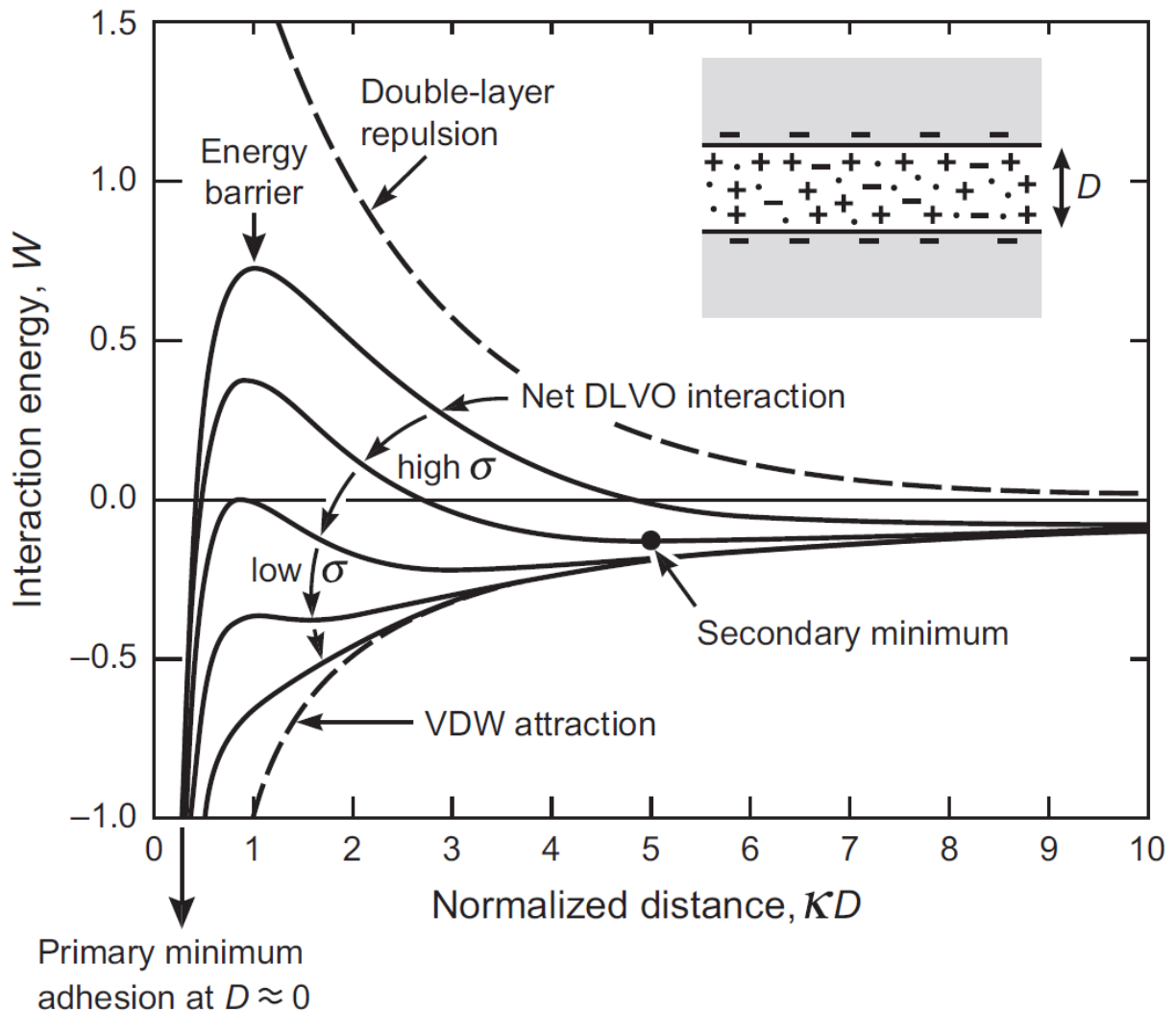


Figure 2.1.: Schematic energy versus distance profiles of the DLVO interaction [16]

2.1.1. DOUBLE LAYER REPULSION

Particles or droplets suspended in water, which has a high dielectric constant, are usually charged. Therefore, coalescence is often prevented by repulsive electrostatic forces [16]. This surface charge leads to the formation of an electrical double layer around the dispersed droplets [17]. The structure surrounding the droplet consists of the following parts (from inside to outside) and is depicted in figure 2.2:

2. STABILISATION MECHANISMS

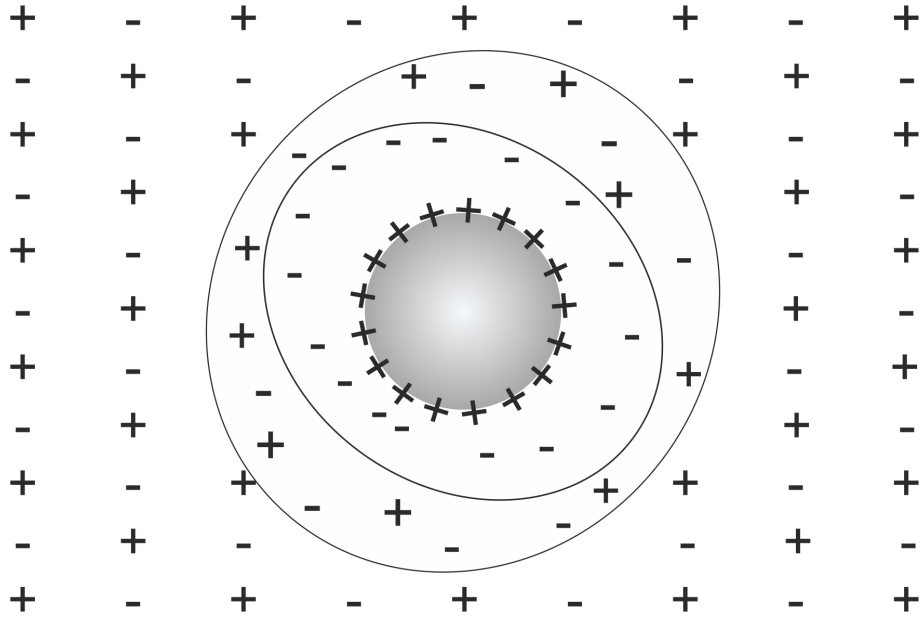


Figure 2.2.: Scheme of electrical stabilisation layers, adopted from [17]

- **Oil droplet**
- **Charged surface**
- **Stern layer:** A layer of oppositely charged ions (compared to the charged surface) close to the surface [17]. A part of the counterion charge is located here [18].
- **Diffuse layer:** A layer of oppositely charged ions (compared to the charged surface) next to the Stern layer. The remainder of the counterion charge is located here. [18]
- **Electric double layer:** The combination of the Stern layer and the diffuse layer. [17]
- **Surrounding aqueous phase**

The interaction due to the electrostatic forces is mostly influenced by the overlap of the electric double layers [18]. Therefore, it is important to define its spreading and quantify the strength. An important number describing the thickness of the double layer is the *Debye length*, $1/\kappa$. It is a measure for the decay of an electric field. Its magnitude is only dependent to the properties of the solution. The charged interface does not have any influence on it. For a monovalent electrolyte ($z = 1$) the Debye-length can be calculated as described in [16] as

$$\kappa^{-1} = \sqrt{\frac{\epsilon_0 \cdot \epsilon \cdot k_B \cdot T}{2 \cdot \rho_\infty \cdot e^2}} \quad . \quad (2.1)$$

The potential at the border between the Stern layer and the diffuse layer is quantified by the *zeta-potential*. It can be measured by electrophoresis. The higher the zeta potential the stronger is the repulsion between the droplets. [17]

2.1.2. VAN DER WAALS FORCES

The van der Waals forces arise from the interactions between dipoles, i.e. from the interactions between molecules on the surface of each droplet. For two flat infinite surfaces with a distance of h in vacuum the potential is

$$V = \frac{A_H}{12 \cdot \pi \cdot h^2} \quad [3]. \quad (2.2)$$

According to International Union of Pure and Applied Chemistry (IUPAC) van der Waals forces can be defined as follows:

“The attractive or repulsive forces between molecular entities (or between groups within the same molecular entity) other than those due to bond formation or to the electrostatic interaction of ions or of ionic groups with one another or with neutral molecules. The term includes: dipole-dipole, dipole-induced dipole and London (instantaneous induced dipole-induced dipole) forces.

The term is sometimes used loosely for the totality of nonspecific attractive or repulsive intermolecular forces.” [19]

2.2. SURFACTANTS

To stabilise mixtures of two immiscible liquids in such way to call the mixture an emulsion as it is defined in [2] (see chapter 1.1.1) it is necessary to add additional components to reach the required stability. These components are of amphiphilic character, which means they have a hydrophilic head and a hydrophobic tail (consisting of 10 - 20 carbon atoms [20]). Therefore, they adsorb onto the interface of the system to be emulsified and reduce the interfacial tension. [2]

These components are called surfactants, which is a contraction of the term **surface-active agent**. Surfactants are very versatile. They are used in motor oils, in pharmaceuticals, for detergents and many other things. Another important fact about surfactants is that they form micelles in the continuous phase. This characteristic does not occur at any concentration, but it starts above the *critical micelle concentration* (cmc). Until this concentration is reached, the surfactant molecules adsorb only onto the interface of the two-phase system. [2] The definition for the critical micelle concentration (cmc) according to the IUPAC is as follows:

2. STABILISATION MECHANISMS

Table 2.1.: Fields of application of surfactants with distinct HLB [23]

<i>HLB Range</i>	<i>Application</i>
4 – 6	w/o emulsifiers
7 – 9	Wetting agents
8 – 18	o/w emulsifiers
13 – 15	Detergents
15 – 18	Solubilizers

“Critical micelle concentration (cmc): *There is a relatively small range of concentrations separating the limit below which virtually no micelles are detected and the limit above which virtually all additional surfactant molecules form micelles. Many properties of surfactant solutions, if plotted against the concentration, appear to change at a different rate above and below this range. By extrapolating the loci of such a property above and below this range until they intersect, a value may be obtained known as the critical micellization concentration (critical micelle concentration), symbol Q , abbreviation cmc (or c.m.c.). As values obtained using different properties are not quite identical, the method by which the cmc is determined should be clearly stated.*” [19]

A general classification of surfactants regarding their activity can be done using the hydrophilic-lipophilic balance (HLB) [21]. This is an empirical number in the range between 1 and 20. The value indicates whether the surfactant is preferably in the aqueous or in the solvent phase. The more hydrophilic the surfactant the higher the HLB [3]. Adding surfactants with a high HLB value leads to formation of oil-in-water (o/w) emulsions while surfactants with low HLB values support the stability of water-in-oil (w/o) emulsions at a given temperature. Table 2.1 gives an overview about the application of a surfactant with a specific HLB-value. The formulas for calculating the HLB values of nonionic (equation 2.3) and ionic surfactants (equation 2.4) are given according to Griffin [21] and Davies [22], respectively.

$$HLB = 20 \cdot \left(\frac{M_H}{M_H + M_L} \right) \quad (2.3)$$

and

$$HLB = \left(\sum \text{hydrophilic group numbers} \right) - n \cdot \left(\sum \text{group numbers per } CH_2 \text{ group} \right) + 7, \quad (2.4)$$

2. STABILISATION MECHANISMS

Table 2.2.: HLB group numbers [22]

<i>Hydrophilic groups</i>	<i>group number</i>
-SO ₄ ⁻ Na ⁺	38.7
-COO ⁻ K ⁺	21.1
-COO ⁻ Na ⁺	19.1
N (tertiary amine)	9.4
Ester (sorbitan ring)	6.8
Ester (free)	2.4
-COOH	2.1
Hydroxyl (free)	1.9
-O-	1.3
Hydroxyl (sorbitan ring)	0.5
<i>Lipophilic groups</i>	
-CH-	
-CH ₂ -	-0.475
-CH ₃	
=CH-	
<i>Derived groups</i>	
-(CH ₂ -CH ₂ -O)-	0.33
-(CH ₂ -CH ₂ -CH ₂ -O)-	-0.15

where M_H is the molar mass of the hydrophilic part and M_L is the molar mass of the lipophilic part of the molecule. The hydrophilic group numbers as well as the group numbers per CH₂-group are shown in table 2.2. n stands for the number of lipophilic groups in the molecule.

The reason for this difference in calculation is that the ionic character of the hydrophilic part of the surfactant increases its hydrophilic character, which cannot be taken into account by the simple ratio between the molar masses of the hydrophilic part and the lipophilic part. Due to their simple character, both equations are only applicable for their own specific range. Equation 2.3 can be used for the HLB calculation of nonionic surfactants while equation 2.4 is in use for ionic surfactants and delivers good results. [24]

As already mentioned, regarding the ionisation of the hydrophilic group, there are four different types of surfactants.

2. STABILISATION MECHANISMS

Anionic surfactants: the hydrophilic group is negatively charged [20]

Cationic surfactants: the hydrophilic group is positively charged [20]

Nonionic surfactants: no functional group, which can be dissociated in water [20]

Amphoteric surfactants: the hydrophilic group has an anionic part and a cationic part [20]

The most important group of the aforementioned surfactants are the anionic surfactants. They are mainly used in cleansing agents. The same holds for nonionic surfactants but they are in use in a much smaller amount. Cationic surfactants are used in antiseptics, fabric softeners and different cosmetic products because they act antistatic. Amphoteric surfactants are used in low concentration washing-up liquids, shampoos and other cosmetics since the skin compatibility is very good. [20]

2.2.1. STERIC STABILISATION

Steric stabilisation occurs when polymeric surfactants adsorb at the interface. There they form tails and loops inside the two phases (see figure 2.3). Therefore, a layer is formed, which stabilises the emulsion due to the limited interpenetration of the polymer chains of the surfactant and leads to repulsion of the droplets approaching each other [3]. Steric stabilisation is an effective way of stabilising non-aqueous emulsions. [17]

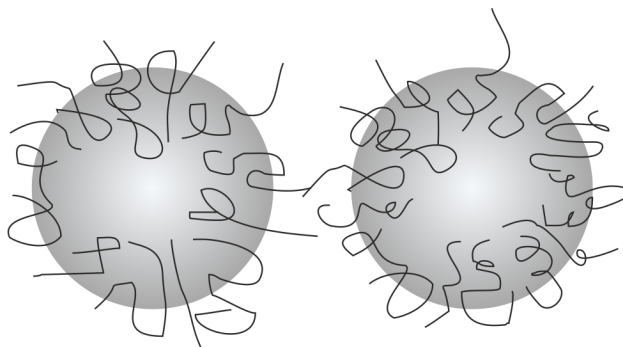


Figure 2.3.: Scheme of steric stabilisation of emulsions

2.2.2. MEMBRANE FORMATION

Since surfactants lower the interfacial tension, they favour the formation of small droplets and therefore new interfaces. When a new droplet is formed, the surface is mechanically stabilised by the surfactant forming a membrane at the interface. This leads to two static effects and one dynamic effect, which prevent coalescence. [17]

Static effects

- The reduction in interfacial tension leads to a decrease in the thermodynamic drive into coalescence. [25]
- A physical barrier is set up by the surfactant molecules, which prevents coalescence by its strength and elasticity. [25]

Dynamic effect

- The *Gibbs-Marangoni* effect stabilises the membrane itself. When two drops approach each other and their surfaces are insufficiently covered with surfactant they take up surfactant molecules while getting closer to each other. Due to an interfacial tension gradient at the interface of the droplets, which occurs due to the hindered adsorption in the film between the droplets, the surfaces move into the direction of the film. This causes streaming of the liquid along the surface, which drives the droplets apart. This self-stabilising effect is only possible if the surfactant is dissolved in the continuous phase. [25] (see figure 2.4)

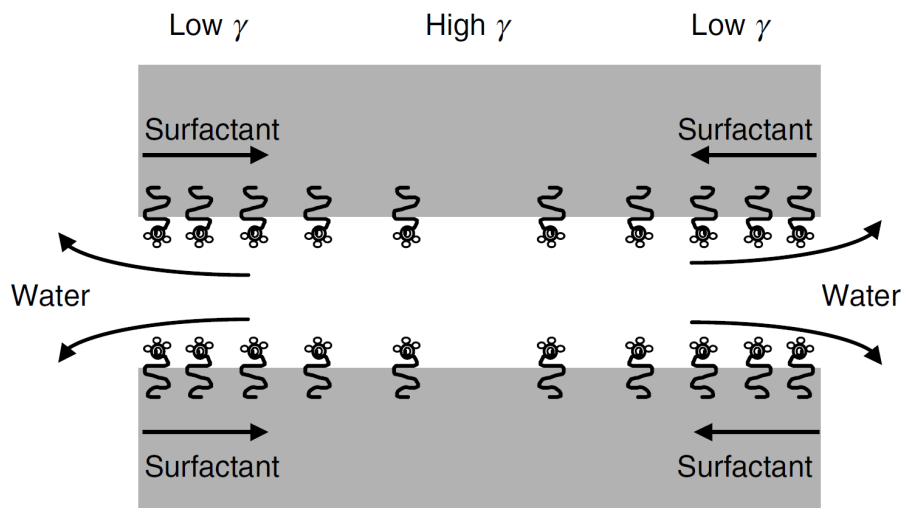


Figure 2.4.: Scheme of the Gibbs-Marangoni effect [26]

2.3. BROWNIAN MOTION

Brownian motion of small dispersed droplets is caused by the movement of the molecules of the continuous phase due to heat energy [27]. In contrast to gravity, which favours creaming (accumulation of the dispersed phase at the top, see chapter 4.2) or sedimentation (accumulation of the dispersed phase at the bottom, see chapter 4.2), Brownian motion favours a random distribution of the dispersed droplets in the whole emulsion. The reason

2. STABILISATION MECHANISMS

for this is that it maximises the configurational entropy of the system. Equation 2.5 shows the equilibrium distribution of droplets in an emulsion underlying both Brownian motion and creaming. [26]

$$\phi(h) = \phi_0 \cdot \exp\left(\frac{-4 \cdot \pi \cdot r^3 \cdot \Delta \cdot \rho \cdot g \cdot h}{3 \cdot k_B \cdot T}\right) \quad (2.5)$$

In this equation $\phi(h)$ is the hold-up of the dispersed phase at a distance h from the top of the emulsion. ϕ_0 represents the hold-up at the top of the emulsion. r represents the radius of the droplet, $\Delta\rho$ is the density difference of the continuous and the dispersed phase, g means the gravitational constant, k_B the Boltzmann constant and T the temperature. If $\phi(h) = \phi_0$ the dispersed phase is evenly distributed in the continuous phase. Therefore, Brownian motion dominates the system. If $\phi(h) \ll \phi_0$ the droplets tend to accumulate and the dispersed phase vanishes. [26]

3. EMULSION FORMATION TECHNIQUES

Emulsions on a submicronic scale with a narrow drop size distribution are needed in cosmetics, food and pharmaceutical industry. To produce these emulsions two ways are possible. Emulsification is either possible via a large amount of energy input or via a high surfactant content or combinations of both. [6] In the following sections the emulsion formation techniques are distinguished by energy input starting with low energy consuming techniques.

3.1. LOW ENERGY CONSUMING TECHNIQUES

The low energy consuming techniques take advantage of the physicochemical properties of the system [17]. Therefore, only a small amount of energy but a high amount of surfactant is necessary to produce finely dispersed emulsions. Additionally, the interfacial tension is reduced by surfactants, which also increases the emulsion stability. This effect is schematically depicted in figure 3.1. It is visible that there is an optimum surfactant concentration where the droplet size as well as the interfacial tension show a minimum, which leads to a maximum in emulsion stability.

In low energy emulsification, two main effects can be distinguished. The first one shows unique behaviour since emulsification occurs without addition of any surfactant.

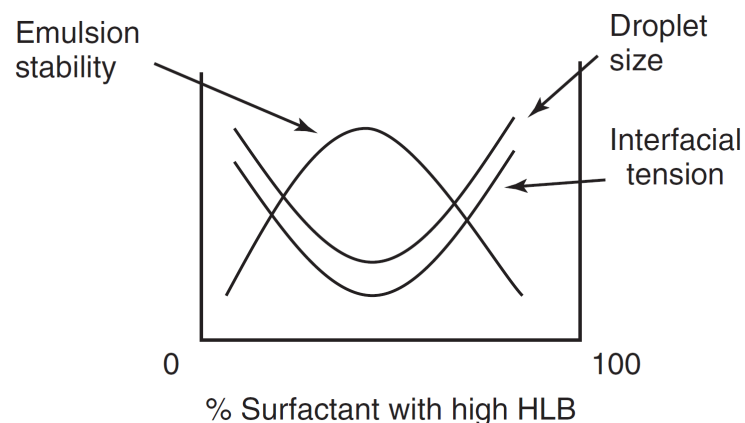


Figure 3.1.: Influence of surfactant concentration on emulsion stability, droplet size and interfacial tension [28]

3.1.1. THE OUZO EFFECT

This effect describes the addition of a solvent to a dilute binary system. The solute shows only limited solubility in this solvent. Therefore, supersaturation occurs and the solute rapidly separates from the solution. The dispersion produced is stable with very small droplets of solute without any mechanical energy input, stabilizers or surfactants. The dispersion shows a narrow droplet size distribution and droplet growth only takes place by Ostwald ripening (see chapter 4.4 for more information) [29]

The Ouzo effect only occurs in systems with three or more components. The name originated in the addition of water to ouzo, a beverage common in Greece, since the dissolved anise oil spontaneously nucleates and forms an opaque, milky liquid following the mechanisms described before. [29]

3.1.2. PHASE INVERSION

Phase inversion can be divided into two main classes. First, the phase inversion temperature (PIT) method shall be explained. Then, an explanation of the emulsification using the emulsion inversion point (EIP) method is given (see figure 3.2).

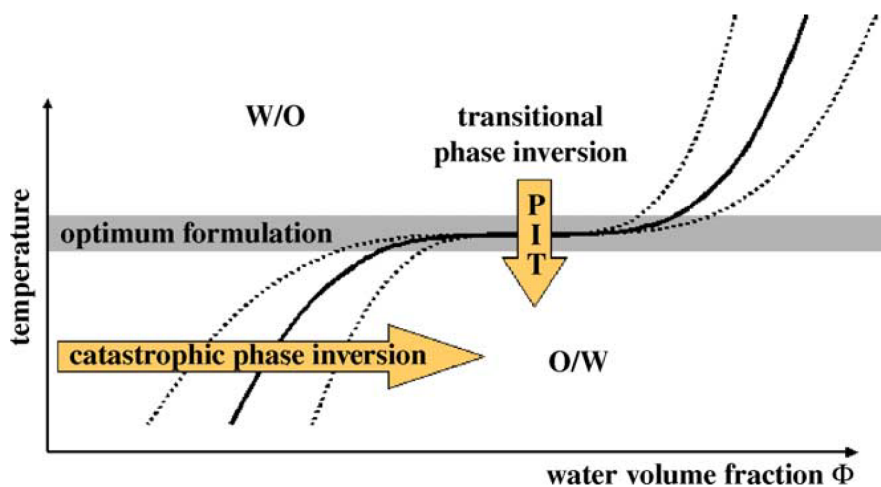


Figure 3.2.: Schematic illustration of transitional and catastrophic phase inversion [30]

PHASE INVERSION TEMPERATURE METHOD

The PIT method was first described by Shinoda et. al. in 1969 [31]. They found that many o/w emulsions, which are stabilised with a nonionic surfactant, show phase inversion at a

3. EMULSION FORMATION TECHNIQUES

critical temperature (phase inversion temperature) without changes in composition. The surfactants were subject of dehydration of the polyethylene oxide chain with increasing temperature and therefore became more lipophilic. At low temperature, stable o/w emulsions were formed as the surfactant had a higher affinity to the aqueous phase. At high temperatures, the stability of o/w emulsions decreased and both o/w and w/o emulsions became unstable. In this temperature zone, the interfacial tension reached a minimum and the system crossed a point of zero spontaneous curvature. At higher temperature w/o emulsions became stable. [32] Picture 3.3 shows this change in spontaneous curvature. The surfactant stabilising the reverse micelles of a w/o emulsion changes its preferred curvature from negative to positive curvature with decreasing temperature. Initially this leads to a lamellar structure of the emulsion before the dispersion direction changes and an o/w emulsion is formed.

A big advantage of emulsions prepared at temperatures close to the PIT is that the droplets are very small. However, they are unstable towards coalescence in this temperature range. Therefore, exiting this unstable zone by rapid cooling stabilises the emulsion and retains the small droplet size. [28]

Another option to stabilise emulsions is to increase the molar mass at given HLB. The enhanced stability is caused by steric hindrance due to the longer chains inside the surfactant molecules. (see chapter 2.2.1 for more information) [28]

The presence of electrolytes reduces the PIT. Therefore, surfactants with a higher PIT have to be chosen for stabilising electrolyte-containing emulsions at a given temperature. [28]

EMULSION INVERSION POINT METHOD

The EIP method takes advantage of the fact that the radius of curvature changes spontaneously when changing the phase ratio. For example, if water is added to oil the water phase becomes the dispersed phase and therefore forms droplets. With increasing amount of water the spontaneous curvature of the surfactant changes from w/o emulsion stabilisation to stabilizing o/w emulsions. [30]

Additionally, the point of phase inversion shows a hysteresis when emulsifying according to the EIP method, which means that addition of oil leads to a different result compared to the addition of water. Furthermore, the extent and technique of energy input during emulsification has an influence. [33]

3. EMULSION FORMATION TECHNIQUES

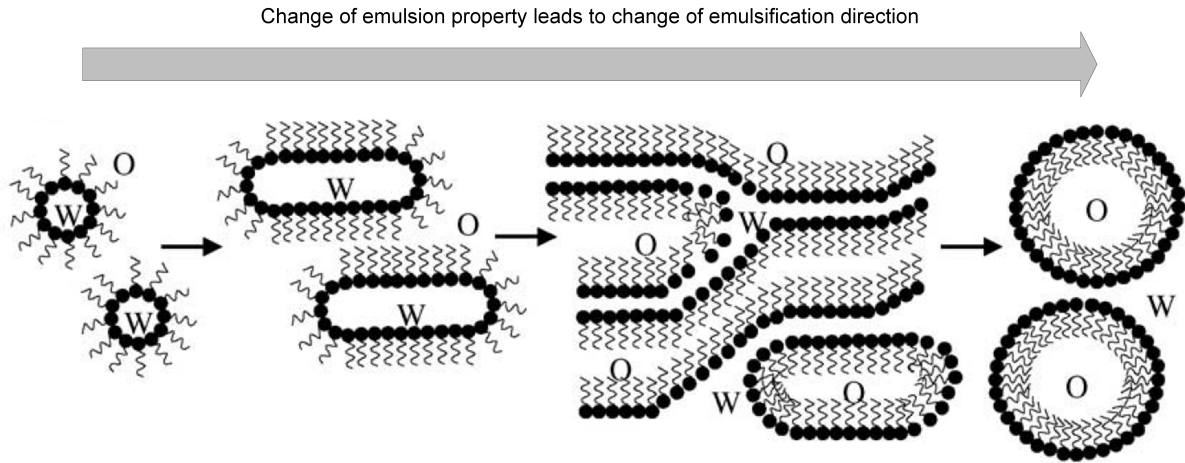


Figure 3.3.: Scheme of curvature change inside an emulsion due to transitional or catastrophic phase inversion (adopted from [30])

3.2. INTERMEDIATE ENERGY CONSUMING TECHNIQUES

The intermediate energy consuming techniques consist mainly of membrane applications for emulsification. Specifically, the direct emulsification using membranes shall be mentioned, as described in this section.

In 1992, Nakashima et al. proposed a new emulsification technique which proved to be beneficial compared to conventional emulsification techniques [34]. Especially the industry makes use of this method to create stable emulsions with a narrow drop size distribution [35]. Another important advantage of emulsification with membranes is that the drop size itself corresponds solely with the pore diameter of the membrane used. This means that a change in particle size can easily be achieved by changing the membrane [34]. Moreover, even emulsions containing a big amount of the dispersed phase can be stabilised using membrane emulsification [35]. A critical pressure P_c can be determined which has to be overcome to make the oil disperse and permeate the membrane (see 3.1). γ_{ow} means the interfacial tension between the organic and the water phase and Θ represents the oil/water contact angle while D_m corresponds with the average pore diameter of the membrane. [34]

$$P_c = \frac{4 \cdot \gamma_{ow} \cdot \cos(\Theta)}{D_m} \quad [34]. \quad (3.1)$$

Nakashima et al. found some additional aspects concerning emulsion formation in general and about the drop formation in specific.

3. EMULSION FORMATION TECHNIQUES

- Particle size D_p corresponds with the pore size D_m in a linear way. (see equation 3.2 [34, 35])

$$D_p = k \cdot D_m \quad (3.2)$$

In this equation, k means a linear correlation between D_p and D_m , which depends on the system to be dispersed and the membrane used [17].

- One of the most important requirements is that the membrane has to be wetted by the continuous phase. Additionally, adsorption of the surfactants on the membrane by stabilising the emulsion has to be avoided. Ionising the membrane surface or applying the same charge as the functional group of the surfactant can fulfil this recommendation. [34]
- An appropriate amount of surfactant has to be present in the system to form stable emulsions with a narrow drop size distribution. High concentrations do not lead to a change in droplet size or drop size distribution. [34]

On the contrary, a minimal velocity is needed to apply physical force on the fluid to be dispersed and to separate the droplets from the membrane surface [35].

3.3. HIGH ENERGY CONSUMING TECHNIQUES

To produce emulsions in large scale, conventional devices like ultrasonic transducers, high-pressure homogenizers or colloid mills are used [17]. The droplets are deformed because of the forces inside the equipment and finally break into smaller ones, if the Laplace pressure is overcome (see equation 3.3) [30]. This pressure corresponds to a pressure difference between the two sides of a curved interface and can be written as Δp_L (see equation 3.3). R_1 and R_2 are two radii of the curvature. For spherical droplets $R_1 = R_2$ holds.

$$\Delta p_L = \gamma \cdot \left(\frac{1}{R_1} + \frac{1}{R_2} \right) \quad (3.3)$$

In the following sections, the main high-energy consuming emulsification systems are briefly described.

3.3.1. ROTOR-STATOR SYSTEMS

Rotor-stator systems are widely used in industry because they offer a large variety of configurations. It is possible to operate these systems either in discontinuous or in continuous mode depending on the device applied. For producing coarse primary emulsions high speed mixers can be used. To produce smaller droplets the preformed emulsion is fed into a second homogenization equipment like colloid mills, which are much more efficient in reducing the size of droplets than in producing a primary emulsion. The force applied on the emulsion is caused by a combination of velocity gradients inside the vessel containing the mixing device or by shear stress in the gap between rotor and stator. [26]

3.3.2. HIGH PRESSURE SYSTEMS

High pressure homogenizers are the most important emulsification devices in industry for continuous production of finely dispersed emulsions. These systems use intense shear stress and cavitation to disrupt droplets. [36] This is the reason why mainly secondary emulsification is performed in such devices. [26] It is possible to produce mean droplet diameters of 0.1 μm even at high throughputs [6, 37]. However, a drawback has to be taken into account since the emulsion has to withstand high pressure gradients inside the equipment, which may not be usable for every system. [37]

3.3.3. ULTRASONIC SYSTEMS

The ultrasonic emulsification is based on the production of pressure variations due to the induced movement of piezoelectric or magnetostrictive materials. The induction is performed by exposure of piezoelectric materials to an electric field or by exposure of magnetostrictive materials to a magnetic field. The materials respond to this field with changing in dimensions, which are transferred to passive components to enhance the energy transfer. [38] Since the throughput is small, ultrasonic emulsification is only applied in lab scale, where a droplet size of 0.2 μm can be obtained [39].

In table 3.1 the high energy input emulsification techniques are summarized. It is obvious that depending on the emulsification system used the properties of the system to be emulsified as well as the produced emulsion differ. Especially the droplet size and the viscosity of the emulsions are very different. Rotor-stator systems for example offer a wide

3. EMULSION FORMATION TECHNIQUES

range of optimal viscosity from 20 to 5000 mPas for emulsification, while for high pressure systems and ultrasonication low to medium viscosities (1 to 200 mPas) are required.

Table 3.1.: Comparison of different types of emulsification systems [6]

<i>Emulsification system</i>	<i>Rotor–stator systems</i>	<i>High-pressure systems</i>	<i>Ultrasonic systems</i>
Examples	Mixers, agitators, colloid mills (Silverson, Ultra-Turrax)	Radial diffusers, valve homogenizers, jet dispersers, microfluidizer	Sonotrodes (sonication probes)
Droplet disruption mechanisms	Shear stress in laminar flow and/or shear and inertial stress in turbulent flow	Shear and inertial stress in turbulent flow; cavitation in laminar extension flow	Cavitation in microturbulent flows
Throughput	Medium to high	High	Low
Batch/continuous	Batch (mixers) or continuous (colloid mills)	Continuous	Batch or quasi-continuous
Minimum droplet size (μm)	1.0	0.1	0.1 – 0.2
Optimal range of viscosity	Low to high (20 – 5000 mPas)	Low to medium (1 – 200 mPas)	Low to medium
Application	Lab/industrial	Lab/industrial	Lab
Energy density	Low–high	Medium–high	Medium–high
Change of energy input through	Rotation speed, exposure time, gap distance, and disk design	Pressure, recirculation (exposure time), and nozzle design	Intensity and frequency of ultrasonic wave sonication time
Residence time in dispersing zone, t	$0.1 < t < 1$ s	$0.1 < t < 3$ ms	–
Required adsorption rate of emulsifier	Low to high	High to very high	Middle to high

4. BREAKDOWN PROCESSES IN EMULSIONS

There are several different processes involved in emulsion splitting. Some of them are applied simultaneously, others consecutively. [28] In figure 4.1 various breakdown processes are depicted. In the following sections, these processes are explained in detail.

4.1. COALESCENCE

Coalescence describes the fusion of two droplets or fusion of one droplet with its coherent phase [40]. It starts with the thinning of a liquid film between the phase boundaries, which finally leads to disruption of the film [28]. Three major steps can be distinguished until two drops (or one drop and an interface) coalesce [26, 40]. These steps are depicted in figure 4.2 and described below.

1. **Approaching:** When a droplet reaches an interface (it does not matter if it is a curved interface of a drop or a flat one of the coherent phase) the droplet as well as the interface are deformed. However, the film in between remains intact. Through the deformation possibly an oscillation is induced, which normally is restrained by the viscosity of the liquids. [40]
2. **Film thinning:** The film vanishes by flowing out of the gap between the two interfaces. Gravity force (or any other force strong enough to move the droplet, e.g. buoyancy, centrifugal or electric field force) pushes the interfaces closer together. This step takes the longest time and therefore is the decisive step for coalescence to take place. [40]
3. **Film rupture:** If the film thickness reaches a critical value, it gets ruptured and the droplet coalesces with the interface. At the critical film thickness the interfacial forces, which increase with decreasing film thickness, reach the order of magnitude of the hydrostatic forces in the system and therefore lead to coalescence. [40]

4.2. CREAMING AND SEDIMENTATION

Creaming and sedimentation describe the settling of the dispersed phase due to external forces, e.g. gravitational, centrifugal or electric field forces. They differ only in the settling

4. BREAKDOWN PROCESSES IN EMULSIONS

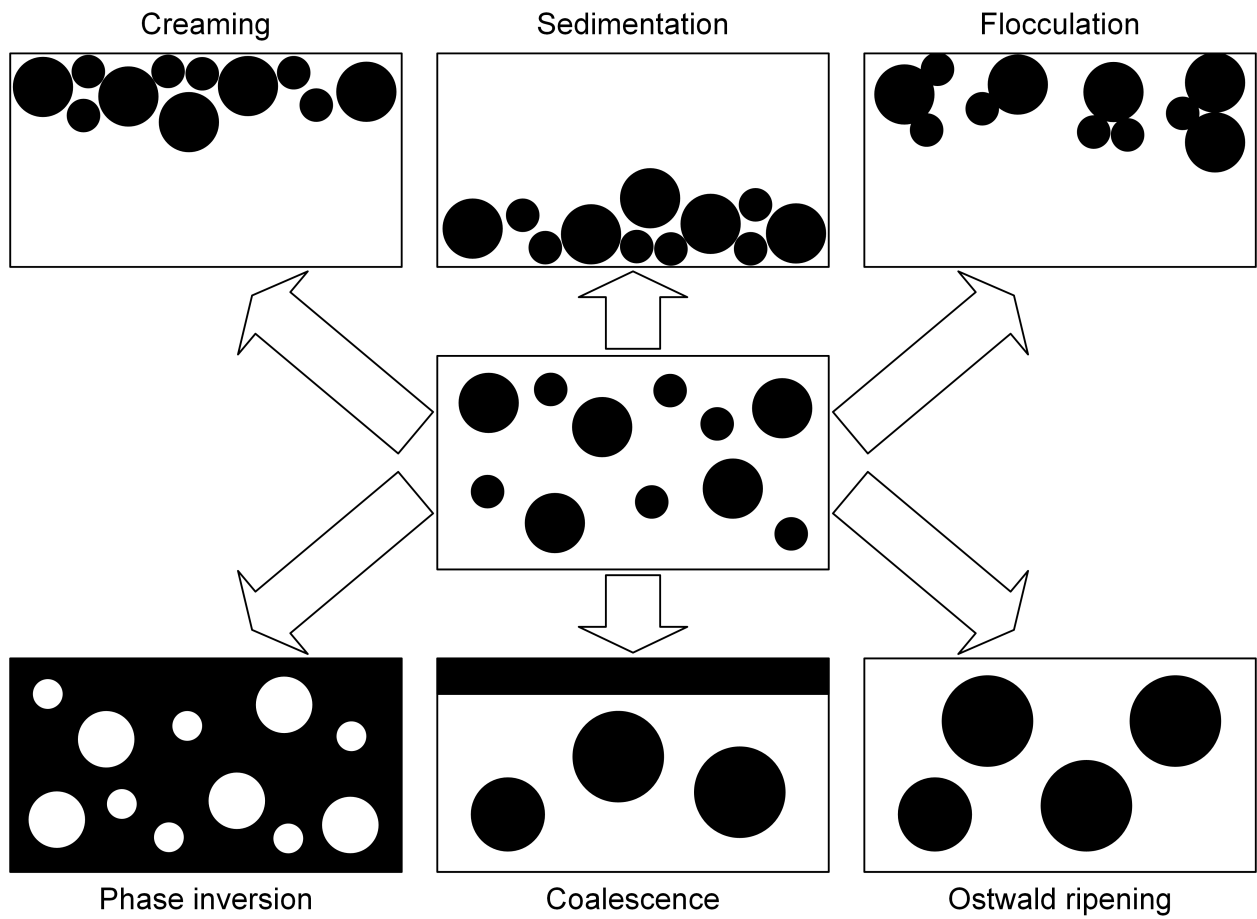


Figure 4.1.: Scheme of various breakdown processes in emulsions (adopted from [28])

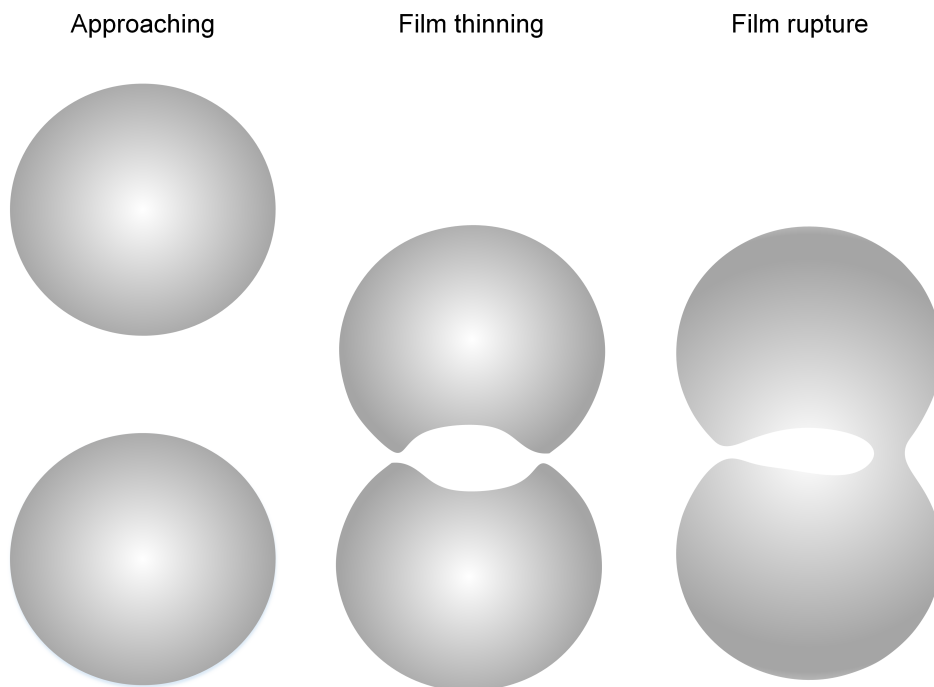


Figure 4.2.: Main coalescence steps (adopted from [40])

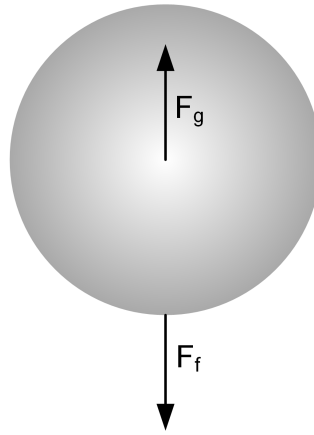


Figure 4.3.: Force balance of an ascending droplet

direction of the droplets. Creaming and Sedimentation mean the movement of droplets to the top and the bottom of the emulsion, respectively. If the dispersed phase has a lower density, creaming occurs. If the dispersed phase has a higher density, sedimentation takes place. [26, 28]

For dilute systems and rigid spheres, which is given for low hold-up and very small droplets, the Stokes' law can be applied to calculate the creaming or sedimentation velocity v . It can be obtained from equations 4.1 and 4.2 and a force balance for a droplet (see figure 4.3). [26]

$$F_g = -\frac{4}{3} \cdot \pi \cdot r^3 \cdot (\rho_2 - \rho_1) \cdot g \quad (4.1)$$

$$F_f = 6 \cdot \pi \cdot \eta_1 \cdot r \cdot v_{Stokes} \quad (4.2)$$

F_g describes the gravitational force while F_f stands for the frictional force. These two forces counteract, independently whether creaming or sedimentation occurs. The symbols ρ_1 and ρ_2 represent the density of the continuous and the dispersed phase, respectively. The shear viscosity of the continuous phase is described by η_1 .

$$v_{Stokes} = -\frac{2 \cdot g \cdot r^2 \cdot (\rho_2 - \rho_1)}{9 \cdot \eta_1} \quad (4.3)$$

The direction of droplet movement is determined by the signum of v_{Stokes} . A positive signum means the droplet moves upward (creaming) and a negative signum signals that the droplet moves downward (sedimentation). A rule of thumb tells that an emulsion with $v_{Stokes} < 1$ mm per day can be seen as stable toward creaming. [26]

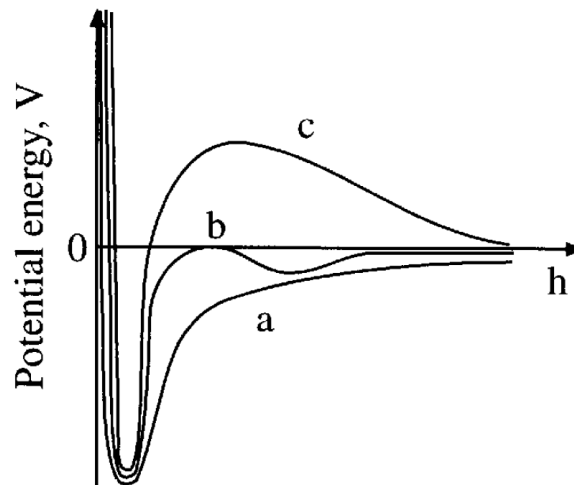


Figure 4.4.: different potential energy curves versus distance of droplets with charged surface [3]

4.3. FLOCCULATION

Flocculation describes the process of reversible aggregation. If aggregation is irreversible, it is termed coagulation [3]. This means that two or more droplets merge without losing their individual integrity. Due to flocculation, the gravitational separation rate is increased [26]. Additionally, the emulsion viscosity is increased, which may even lead to gel formation [41, 42]. This can have a stabilising effect in concentrated emulsions [43].

The DLVO theory describes in general terms whether flocculation or coagulation occurs. More generally, the stability of the emulsion can be described by the DLVO theory (see chapter 2.1). This can be illustrated by figure 4.4 where three different emulsions are depicted. For the first type of emulsion the potential energy curve is dominated by the attractive van der Waals forces, which will lead to coagulation (see figure 4.4 curve *a*). Coagulation is favoured in this case because the potential energy is minimized. For the second type of emulsion the attractive forces and the repulsive double-layer forces contribute in such way that a secondary minimum occurs in the potential energy curve. If the minimum is comparable to $k_B T$, reversible flocculation can take place, (see figure 4.4 curve *b*). For the third type of emulsions the repulsive forces contribute with significant values, which leads to a positive potential energy barrier. If this barrier is large enough (i.e. large compared to $k_B T$) the emulsion is kinetically stable (see figure 4.4 curve *c*). [3]

4.4. OSTWALD RIPENING

Ostwald ripening results from finite mutual solubility of the liquid phases, which increases with decreasing droplet diameter. Therefore, large droplets grow while smaller droplets dissolve (see figure 4.5) [26, 28, 44, 45]. The Ostwald ripening rate increases with increasing surfactant concentration [46]. This can be supported by the fact that solubility of the dispersed phase increases with decreasing droplet diameter, which is a consequence of higher surfactant concentration. The correlation of solubility and droplet size can be seen in equation 4.4. [47]

$$S(r) = S(\infty) \cdot \exp\left(\frac{2 \cdot \gamma \cdot M}{R \cdot T \cdot \rho \cdot r}\right) \quad (4.4)$$

In this equation $S(r)$ is the solubility of a droplet of radius r . Consequently, $S(\infty)$ is the solubility of a droplet with an infinitely large radius, i.e. a planar surface. Additionally, M represents the molar mass of the dispersed phase.

From equation 4.4 can be seen that the concentration of the dispersed phase is higher in the surrounding of small droplets because of the higher solubility of smaller droplets. Since this induces a concentration gradient, the molecules move towards the bigger droplets leading to a shrinkage of the small ones and a growth of the bigger ones. [26]

4.5. PHASE INVERSION

Phase inversion refers to the change of the dispersed phase to become the continuous phase and vice versa. [28] As described in chapter 3.1.2 this results from the change in curvature of the emulsion due to temperature change (PIT) or change in concentration of the dispersed phase (EIP).

4. BREAKDOWN PROCESSES IN EMULSIONS

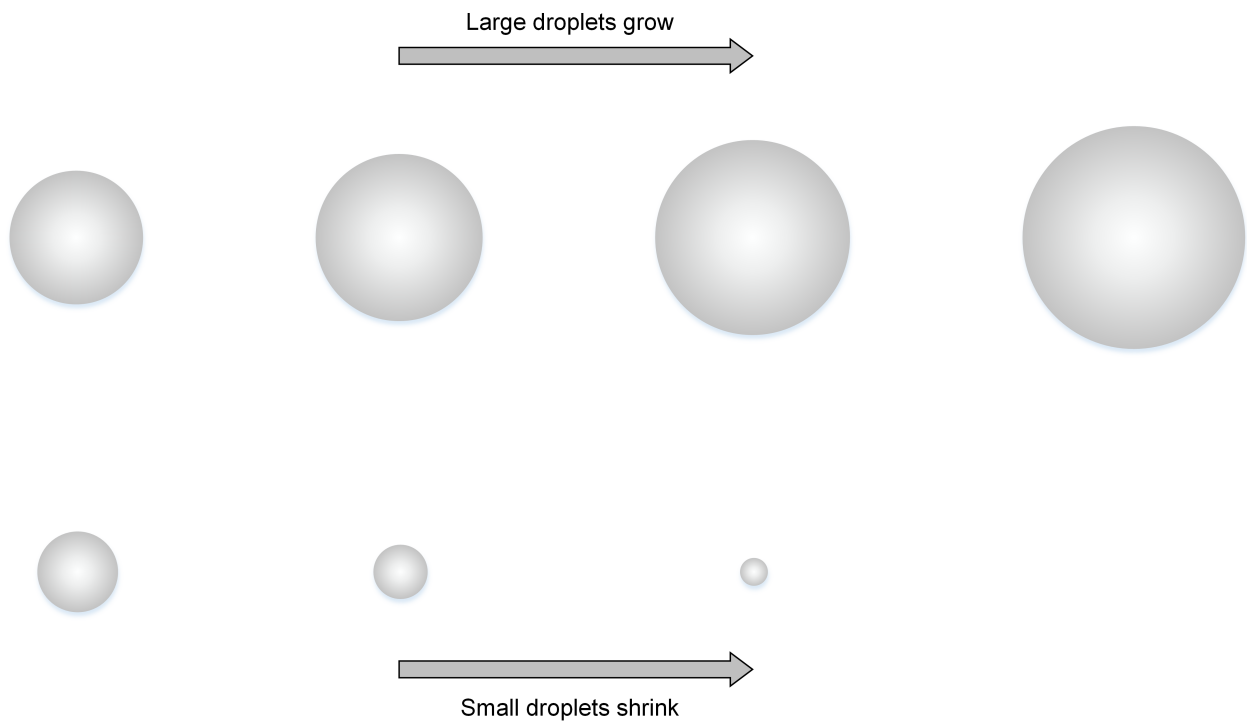


Figure 4.5.: Ostwald ripening (adopted from [26])

5. SPLITTING OF STABLE EMULSIONS

After producing a stable emulsion it is often intended to split it again. This chapter describes mechanisms of emulsion splitting and technologies that make use of the different mechanisms discussed in chapter 4.

5.1. CHEMICAL SPLITTING

Demulsification using chemical additives is known to be effective [48]. It is widely used for w/o and o/w emulsion separation in general and in crude-oil treatment in specific [48, 49]. However, there are some major drawbacks using this technology. Firstly, an additional separation step is necessary for recovery and recycle of the emulsion components, which makes it difficult to choose a chemical easy to remove after demulsification with the capability of neutralisation of emulsifiers [48, 50]. Secondly, the demulsifying agent must have very low water solubility and additionally show a high volatility to make separation easier. In many cases, butanol is therefore preferred over propanol due to the lower solubility and over tetradecane or oleic acid due to its higher volatility, which makes distillation possible as recovery step. [48] According to [51] the following steps have to be considered to attain chemical demulsification in o/w emulsions:

- sufficient amount of the chemical has to be provided
- intense mixing of the chemical with the emulsion has to be performed
- elevated temperatures help to enhance the splitting process
- enough residence time in the separation equipment has to be provided to enable settling

5.2. ELECTRICAL SPLITTING

Since the knowledge in the literature is very different regarding the dispersion direction, w/o and o/w emulsions are discussed separately in the chapters 5.2.2 and 5.2.3, respectively. In chapter 5.2.1 a general theoretical background is presented without taking the dispersion direction into account.

5.2.1. THEORY OF ELECTRICAL SPLITTING

It has already been discovered in 1911 that emulsions coalesce faster if they are exposed to an electric field compared to gravity [52]. The method found by Cottrell [52] has been used in the petroleum industry to demulsify brine dispersed in crude oil [48]. According to Draxler et al. [53] electrical splitting is used for splitting of emulsion liquid membranes in industrial scale. The biggest advantage of electrical splitting is that it is a strictly physical process, which allows recycling the phases without any additional separation step [48]. Additionally, it is advantageous regarding energy consumption compared to heating or centrifugation [54–56].

Three effects can be distinguished in electric field splitting:

- Dipole-dipole interaction
- Electrophoresis
- Dielectrophoresis

Dipole-dipole interaction occurs between two polarized droplets. The electric field induces a charge at the surface of the droplets which results in attraction forces between the droplets (see figure 5.1). The overall charge of the droplet remains unchanged. [57]

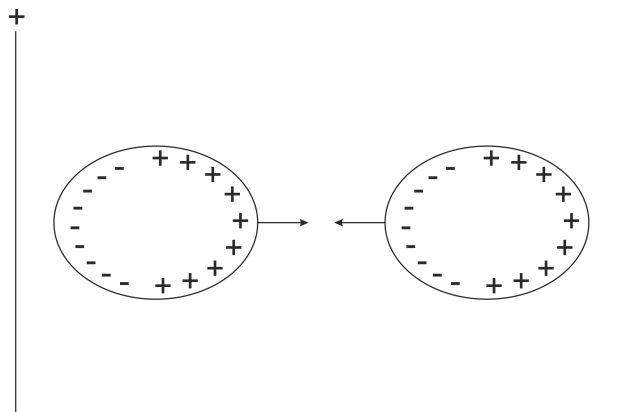


Figure 5.1.: Schematic of the dipole-dipole interaction [57]

Electrophoresis arises from movement of droplets in the electric field. If a charged droplet is formed through contact with an electrode, it is repulsed and attracted by the opposite electrode. The polarity of this droplet can now be reversed like in figure 5.2. It is also possible that one droplet hands over its charge to another one. However, the electrophoretic force decreases exponentially with time due to low conductivity in the continuous phase. Electrophoresis causes accidental movement of droplets in the emulsion which leads to accidental collisions and therefore to coalescence. [57]

5. SPLITTING OF STABLE EMULSIONS

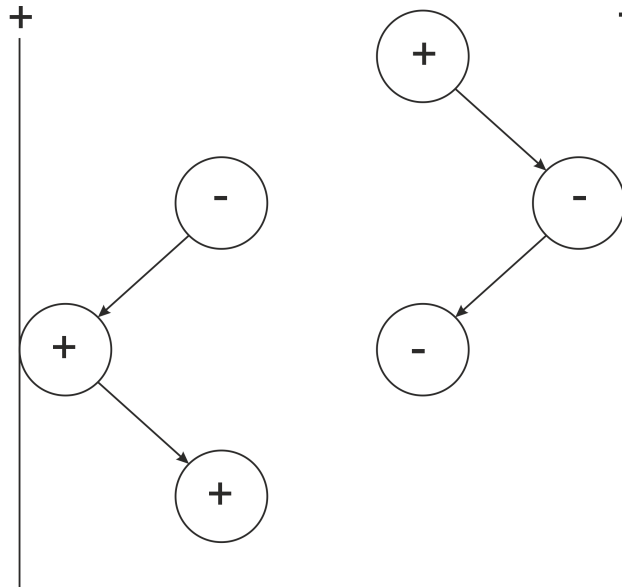


Figure 5.2.: Schematic of the electrophoresis [57]

Dielectrophoresis only occurs in inhomogeneous electric fields. This phenomenon describes the orientation of droplets towards the stronger field strength independent of the charge of the droplets or the electrodes. A higher electric field increases the force acting on the droplets and their velocity, which enhances collisions and coalescence. [57] Figure 5.3 shows the principle.

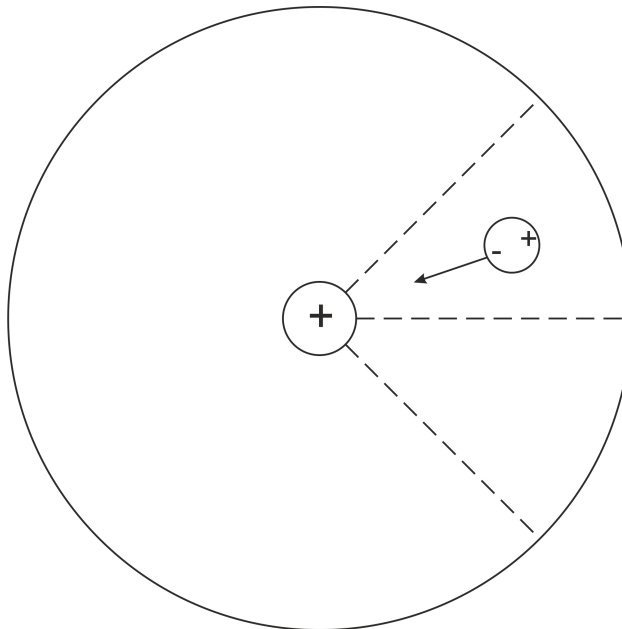


Figure 5.3.: Schematic of the dielectrophoresis [57]

It has to be mentioned that the predominant mechanism in emulsion systems depends on several parameters like electrode design and setup, emulsion properties as well as on the type of electric field applied. [56]

5.2.2. WATER-IN-OIL EMULSIONS

The splitting of w/o emulsions in the electric field has been studied for more than 100 years [52, 58]. Since a high electric AC field applied on a flowing emulsion leads to flocculation and coalescence of the water droplets, the technology has become very important in crude oil processing [52, 56, 58–60]. However, complete understanding and prediction of coalescence of droplets in the electric field is still missing. The reason for this lack of knowledge is the complexity of the electrostatic and hydrodynamic interactions and the difficulty in defining the electric field strength acting on the droplets [56].

AC is preferably applied for splitting w/o emulsions; DC has been used to split this emulsion type, too. Bare electrodes with 5 to 25 kV lead to demulsification of 60 to 70 % [61]. In addition, pulsed DC field has been investigated [62, 63]. Mhatre et al. conclude in their review that the application of AC or pulsed DC fields is favoured over constant DC fields to achieve efficient separation [64].

According to Chen et al. [65] a typical field strength in o/w splitting is 100,000 V/m. However, if the electric field strength is too high, drop breakage occurs and the emulsion is stabilised. [66]

5.2.3. OIL-IN-WATER EMULSIONS

Especially in the metalworking industries oily wastewaters are generated. These effluents often contain stable o/w emulsions, which originate in lubrication, surface cleaning or corrosion prevention. [67] In general, there are three different types of forces known which prevent demulsification of o/w emulsions. These are the electrical double layer force, which acts between electrically charged oil droplets [14, 15], the steric force, resulting from macromolecules adsorbed on the droplet surface [68, 69], and the hydration force acting between hydrated oil surfaces, which is a short range force [70, 71].

According to [9, 60] and [67] splitting of o/w emulsions should be performed using electrical splitting devices. The reasons are the simplicity of the apparatus and the process itself. However, demulsification of o/w emulsions by electrical splitting has not been intensively investigated for two main reasons. On the one hand, high electric field may

cause electrolysis of the aqueous phase, which leads to a contamination of the chemical products. On the other hand, the application of a low electric field for demulsification has been regarded as a slow process driven by electrophoresis of the droplets. The reduction of the surface charge due to electrolysis does cause corrosion of the electrodes, which increases the concentration of metal ions. Metal ions act as demulsifier. [9, 56, 60]

In figure 5.4 the mechanism of electrical splitting is depicted. The surface ions migrate in an electric field minimizing the difference in the electrostatic potential difference induced by the external field. Since the potential energy barrier is decreased with decreasing surface charge density, small droplets adjacent to this side of large droplets coalesce first. (right hand side of the big droplet in figure 5.4 [72])

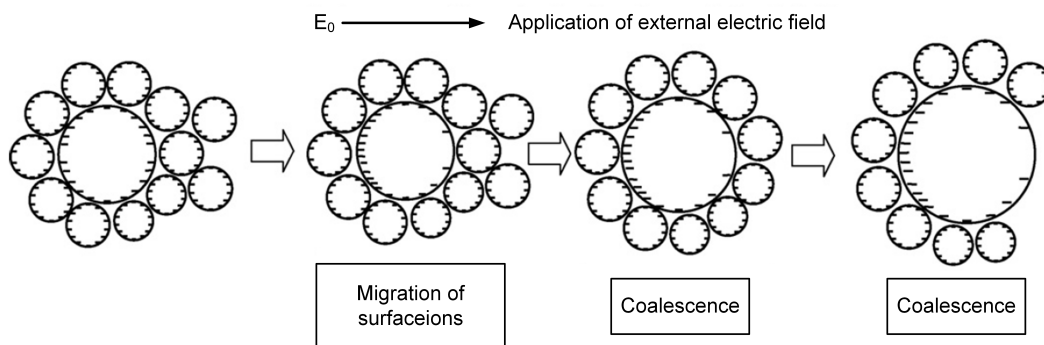


Figure 5.4.: Mechanism of electrical demulsification acc. to [72]

Two options can be found in literature to demulsify o/w emulsions in the electric field. On the one hand, the application of a uniform field is possible. On the other hand, a non-uniform electrical field can be applied. Both lead to good separation at optimal conditions. [9, 60, 72–75]

5.3. MECHANICAL SPLITTING

Regarding separation mechanical separation can be subdivided into filtration and sedimentation. The former separation mechanism is based on the relative particle size, while the latter uses mainly the relative particle density for separation. It has to be mentioned that particle size plays also a role in sedimentation. [50] The major technologies of mechanical splitting are discussed in the following chapters.

5.3.1. FILTRATION

The filtration mechanism works entirely on droplet size and to some extent on the shape of the droplets. The cutoff size is the characteristic measure of the filter medium. Since a pressure difference is necessary across this barrier, there are two modes of operation possible. In vacuum filters the suction is downstream of the filter while in pressure filters pressure is applied on the emulsion upstream the filter. [50] Filtration can be divided into the following categories [50, 76].

- macro filtration (particle/droplet size: 5 μm – 1 mm)
- micro filtration (particle/droplet size: 0.1 μm – 5 μm)
- ultra filtration (particle/droplet size: 0.01 – 0.1 μm)
- nano filtration (particle/droplet size: 0.001 – 0.01 μm)
- reverse osmosis (particle/droplet size: < 0.003 μm)

The lower limit of ultrafiltration is measured in molecular weight terms (dalton). In nanofiltration, the liquid stream is treated as solution without suspended matter. It is assumed that the membranes are tight without holes inside. However, small molecules are able to dissolve in it and diffuse through the membrane, which makes a high pressure difference necessary. [50]

Another classification of filtration devices is based on the filtration mechanism itself. In surface filtration, the barrier is thin compared to the diameter of the dispersed phase. Therefore, the filtration takes place upstream of the filter medium. Particles, which are smaller than the pore diameter, are able to pass the filter medium while larger particles are hold back on the upstream surface. Secondly, filtration may be based on depth filtration or depth straining. These mechanisms differ only in the effect how the droplet is trapped. In depth filtration, the droplet is trapped in a bed of fibres by adsorption onto the pore surface while in depth straining the droplet moves through the pore until it reaches a point where the pore gets too small and the droplet is hold back. [50]

5.3.2. SEDIMENTATION

The density difference of the two liquids to be separated can be used either for gravitational or centrifugal separation. The gravitational separation can be performed in basins with a circular or rectangular shape or in vessels with internals. Since the principle is the same for both types, they are discussed together. The application of centrifugal force on an emulsion

is possible either mechanically driven (centrifugation) or inertially driven (hydrocyclones). [50]

GRAVITATIONAL SEPARATION

Gravitational separation is a direct and low cost treatment of emulsions. However, bulky equipment with correct proportions is necessary to provide proper separation. [50]

In simple gravity separators, the dispersed phase is separated from the continuous phase and moves upward or downward according to the density difference. The principle is the same in so-called lamella separators but due to shorter sedimentation distances because of internals mounted in parallel a larger separation area is provided for sedimentation. The internals can be designed as plates or tubes. [50]

Another way to enhance separation in gravitational separation devices is the installation of coalescers. These use dense fibre beds or fibre mats for oil/water separation. The fibre material has to be chosen depending on the dispersed phase. Inorganic fibre material is used for dispersed water droplets, and lipophilic materials are chosen for solvents as dispersed phase. If the material is chosen in the way described, the droplets are intersected by the fibres and impinged on them. With time the film consisting of continuous phase between the droplet and the fibre is thinned and finally ruptured, which leads to attachment onto the fibre and to coalescence with other droplets. The growing droplets are broken from the fibre when they reach a certain size due to gravity and drag force and therefore separate from the emulsion. [50]

CENTRIFUGATION

All demulsification processes are enhanced and facilitated when using centrifuges, because the droplets of the dispersed phase are forced towards one end of the equipment. There, the interfacial membrane is ruptured, which leads to coalescence and therefore to phase separation. [26] The rupturing is facilitated due to the higher acceleration force (5,000 – 8,000 times higher) compared to gravitational force. Centrifuges can easily be applied to different separation requirements especially regarding the amount of emulsion to be split. [50]

HYDROCYCLONES

Hydrocyclones are dynamic separators used since the early 1980s [50, 77]. The operation principle is the inertial force, which is caused by the inflow velocity of the emulsion. The emulsion is forced to develop a vortex flow, which forces the high density liquid to the barrel side. [50] The operating principle can be seen in figure 5.5.

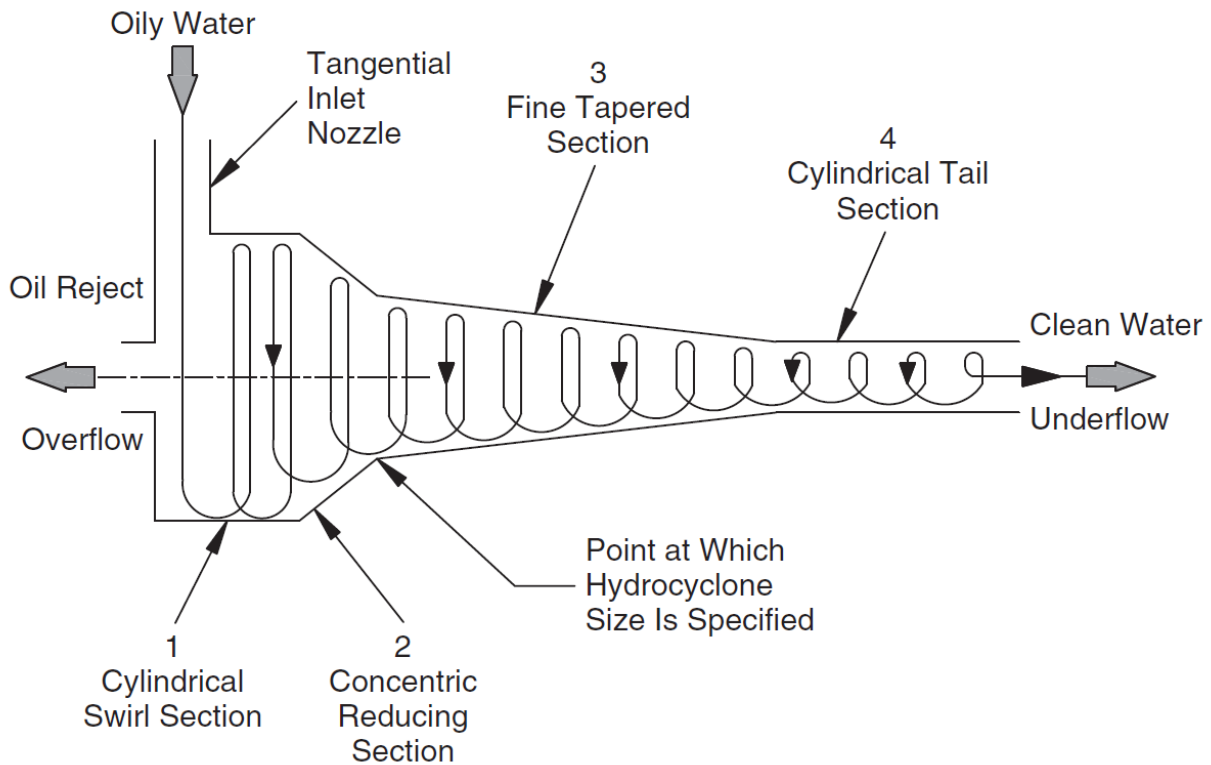


Figure 5.5.: Operation principle of a hydrocyclone [77]

FLOTATION

Flotation is a mechanical splitting technology, which artificially enlarges the density difference between the two phases with gas bubbles. As a prerequisite, the dispersed phase has to be the non polar solvent phase since adhesion between the droplets and the gas bubbles has to be big enough. In figure 5.6 the principle of flotation is depicted. The whole process can be divided into three intermediate steps. The first one is the formation of the gas bubbles, followed by the attachment of the droplets to the bubbles and finally the movement towards the upper interface of the emulsion leaving behind a clear hydrophilic liquid. [78] Flotation is used in the cleaning of effluents from the pulp and paper industry containing fibres, of effluents containing varnishes and of oily effluents produced in the food industry [79].

5. SPLITTING OF STABLE EMULSIONS

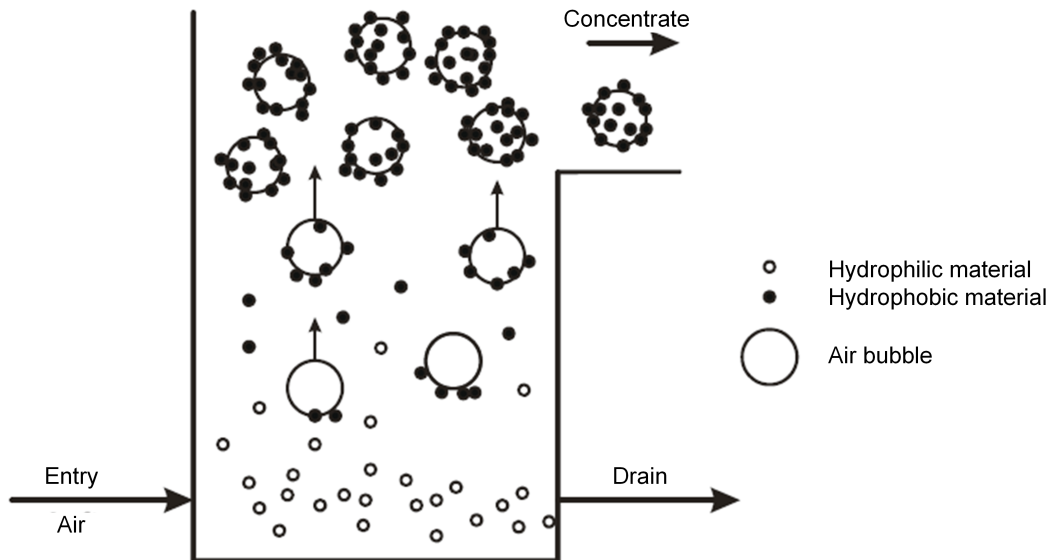


Figure 5.6.: Flotation principle, adopted from [79]

The different flotation techniques are divided into three main groups regarding the mechanism of bubble generation:

- Dissolved air flotation (DAF)
- Electroflotation
- Froth flotation

Dissolved air flotation (DAF) is the most commonly used flotation technique. In a separate tank, saturation of water with gas is performed at elevated pressure. By varying the pressure difference between this saturation tank and the separation tank, the number as well as the size of the gas bubbles can be modified. With increasing pressure difference, the bubble diameter is decreased. Depending on the pressure difference, a bubble size of 30 – 100 μm is obtained. [80, 81]

Electroflotation is also a widespread flotation separation technique. It is mostly used in the separation of light colloidal systems. The gas bubbles are produced by electrolysis with electrodes immersed in the liquid. At the cathode hydrogen is generated while oxygen is produced at the anode. The number of bubbles is proportional to the voltage. The advantage of this technique compared to other flotation techniques is that monodispersed gas bubbles with a diameter of 50 μm can be produced. [79]

In *froth flotation*, the bubbles are generated by inserting the gas to the flotation equipment at the bottom. With this technique, relatively large bubble diameters (app. 1 mm) are

obtained. The advantage of froth flotation is that operating cost is low, and there are no moving parts inside the system. [79]

5.4. THERMAL SPLITTING

Heating of emulsions is a widespread technique in w/o emulsions splitting [7]. There are various reasons for this application. [7]

- lower heat capacity of solvents compared to water reduces the huge amount of energy necessary
- heating reduces the viscosity as well as the density of solvents faster than those of water
- the solubility of surfactant is increased in the solvent as well as in the water phase, weakening the interfacial film

Thermal treatment is also the primary technique when demulsification of microemulsions is intended, because the amount of water dissolved in the solvent phase is decreased with increasing temperature [48].

Two major techniques are applied in industry when thermal splitting is used for demulsification, microwave irradiation and conventional heating. It has to be mentioned that the former works much more efficient regarding separation time and energy consumption compared to the latter [82–89]. Even without addition of chemical demulsifiers, microwave irradiation shows a higher efficiency in breaking o/w emulsions [84].

However, there are some major drawbacks regarding thermal splitting without application of other separation technologies. Most importantly thermal splitting is a very expensive operation [7]. Additionally, the demulsification kinetics are slow in thermal splitting [48].

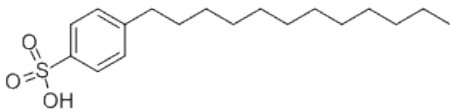
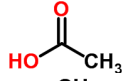
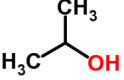
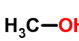
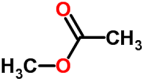

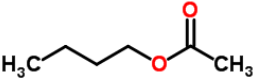

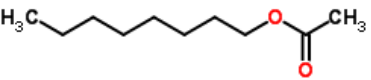

Part II.

Experimental setup

6. CHEMICAL SYSTEM

The chemicals used are shown in table 6.1. For the experiments Shellsol-K (SSK) as solvent phase and 4-dodecylbenzenesulfonic acid (4-DBSA) as surfactant have been used. To evaluate the electrical field splitting a highly stable emulsion resulting from a process intensification step has been investigated. To produce this emulsion acetic acid, methanol, *n*-butanol, *n*-octanol, *n*-undecane and 4-DBSA have been used. Methyl acetate, *n*-butyl acetate and *n*-octyl acetate are formed in the reaction and not added by hand. Isopropyl alcohol was used as solubilizer in the chemical splitting. Acetone was used for cleaning purposes only to remove impurities from the experimental equipment. Additionally, deionized water was used for both experimental reasons as continuous phase and for cleaning purposes.

Table 6.1.: Chemicals used

Chemical	CAS-number	Molecular weight in g/mol	Density in g/cm ³	Chemical characterization	Source
4-dodecyl- benzenesulfonic acid (4-DBSA)	121-65-3	326.49	1.2		[90, 91]
Acetic acid	64-19-7	60.05	1.05		[92, 93]
Isopropyl alcohol	67-63-0	60.10	0.78		[92, 93]
Methanol	67-56-1	32.04	0.79		[92, 93]
Methyl acetate	79-20-9	74.08	0.93		[92, 93]
<i>n</i> -butanol	71-36-3	74.12	0.81		[92, 93]
<i>n</i> -butyl acetate	123-86-4	116.16	0.88		[92, 93]
<i>n</i> -octanol	111-87-5	130.23	0.83		[92, 93]
<i>n</i> -octyl acetate	112-14-1	172.27	0.87		[92, 93]
<i>n</i> -undecane	1120-21-4	156.31	0.74		[92, 93]
ShellSol-K (SSK)	64742-47-8	174.00	0.792	Mixture of hydrocarbons, C11-C14, <i>n</i> -alkanes, isoalkanes, cyclenes, <2 % aromatics	[94]

7. SETUP - PREPARATION OF STABLE EMULSIONS

Before electric field splitting can be applied on a stable emulsion, the formation of such emulsions has to be investigated. To observe the splitting progress the experiments were analysed in an optical cell. Since the emulsion showed turbidity formation, also ultrasonic scanning has been applied using an ultrasonic suspension analyzer, type SUSS-2008 from Rhosonics Analytical B. V., Netherlands. The principles of the latter observation techniques are explained in the following chapter.

7.1. ULTRASONIC SCANNER

The principle of the ultrasonic scanner can be seen in figure 7.1. The sound waves generated by the ultrasonic scanner pass the emulsion. The direction of the sound waves is perpendicular to that of the phase separation going from the transducer T to the receiver R. On its way through the emulsion the wave is attenuated depending on the medium. A_0 is the amplitude directly after the transducer and A_t is the amplitude received by the receiver. Additionally, the speed of sound changes with changing solvent concentration. This is used to determine the concentration of the solvent phase. Important for getting accurate measurements is that the range of sound speed analysed is as narrow as possible. It is possible to generate sound waves with a sound speed between 1000 and 2500 m/s. The minimum and maximum speed of sound used for the system water/SSK are 1200 m/s and 1600 m/s, respectively. [95]

7.2. EXPERIMENTAL PROCEDURE

For performing separation experiments one preparation step has to be done. Each phase has to be saturated with the other one to avoid unwanted effects due to incomplete saturation in the experiment itself. When the separation after the saturation process is finished the two phases can be mixed again to perform the experiment. These two steps are explained in the following chapters.

7. SETUP - PREPARATION OF STABLE EMULSIONS

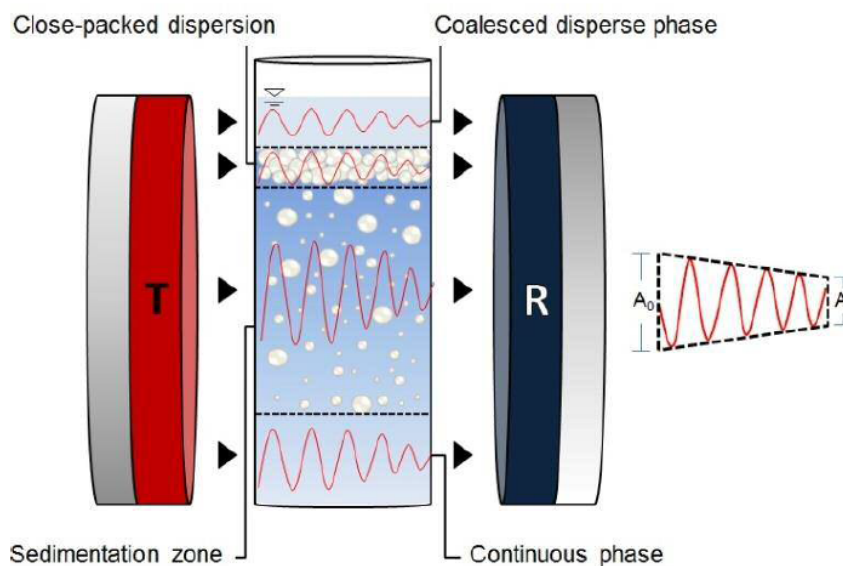


Figure 7.1.: Principle of the ultrasonic scanner [95]

7.2.1. PREPARATION OF SATURATED PHASES

Before saturation of the aqueous with the solvent phase and vice versa occurs, the two phases have to be mixed intensely. The mixing is performed in a standardized mixing cell shown in figure 7.2. It is also possible to observe the separation optically in this cell (see chapter 7.2.2). Therefore, two rods with propellers mounted are used. These rods are rotating into opposite directions to avoid unwanted circulation of the liquid after stopping the mixing process. The agitation rate for the saturation process was 800 rpm for 1 minute. After settling of the now saturated phases they are separated using a separation funnel (see figure 7.3).

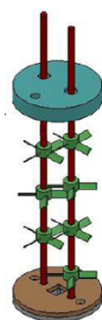


Figure 7.2.: Mixing unit with scheme

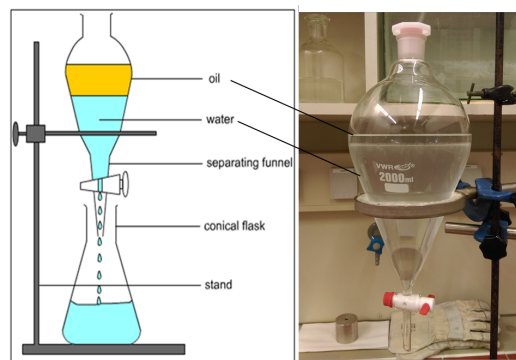


Figure 7.3.: Separation funnel [96]

7. SETUP - PREPARATION OF STABLE EMULSIONS

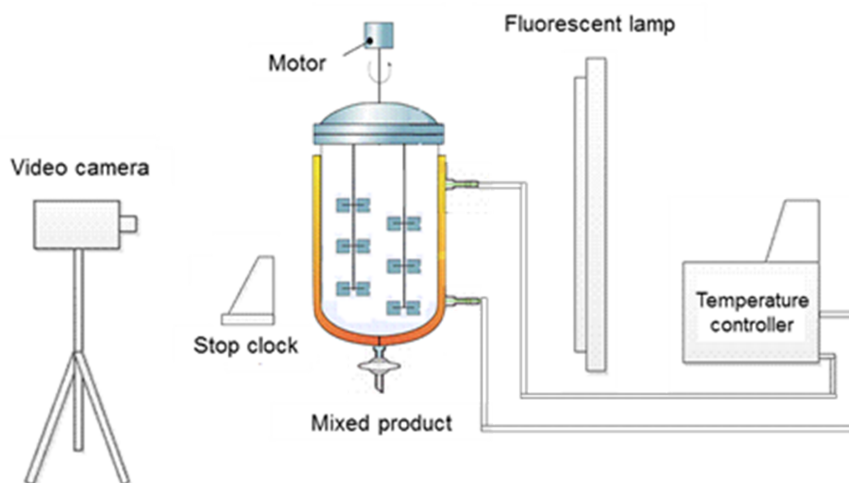


Figure 7.4.: Scheme of the optical cell equipment

7.2.2. OPTICAL CELL EVALUATION

For this observation, the mixing unit (see figure 7.2) was used as optical cell as well. A scale has been attached to the mixer, which contained an overall volume of 600 ml. The two phases were mixed for 1 minute at given rotational speed. After stopping the mixer, the sedimentation and coalescence behaviour was recorded using a video camera (Panasonic HDC-TM900). Additionally, the settling time was counted by a stop clock. A scheme of the optical cell equipment is shown in figure 7.4.

7.2.3. ULTRASONIC SCANNING EXPERIMENTS

To operate the ultrasonic scanner (see figure 7.5) the software *Rhosonics SUSS v1.11* has been installed on a computer mounted to the scanner. The end position of the scanner has to be added to adopt the scanned height to the height of the emulsion. Additionally, the duration of the scanning interval and the number of calibration points had to be entered. To operate the scanner properly the first scan was performed with deionized water only to calibrate the scanner on the decanter used. After the calibration was finished, the emulsion was prepared. For this reason, different amounts of SSK and water are added up to a total volume of 600 ml. The phase ratio has been varied to see whether it affects the emulsion stability. The mixture was then mixed for 1 minute at a distinct number of revolutions. The number of revolutions has been varied to find an optimum value for maximum stability. Additionally, experiments with and without surfactant have been performed. After that, the generated emulsion was poured into the decanter and the scanning started. For this

7. SETUP - PREPARATION OF STABLE EMULSIONS

system, the range of evaluated speed of sound has been 1200 – 1600 m/s. The temperature control system kept the temperature constant at 20 °C.



Figure 7.5.: Ultrasonic Scanner [97]

8. SETUP - SPLITTING OF STABLE EMULSIONS

Having performed several experiments on emulsion stability and finding the best setting this stable emulsion can be split again. For this reason, several different technologies are investigated. The experimental procedure is described in the following chapters.

8.1. EXPERIMENTAL PROCEDURE

The initial procedure of all experiments is the same for the different splitting technologies applied. Before the separation step the turbidity has to be formed. For this reason, an amount of water (depending on the splitting technology) is mixed with 0.5 wt.% of solvent phase, if not specified differently. The solvent phase consisted of the solvent SSK and 0.1 wt.% of the anionic surfactant 4-DBSA. The mixing is performed using an ULTRA-TURRAX T25 from the company JANKE & KUNKEL IKA-Labortechnik.

To prove the concept of electrical splitting the splitting of a model emulsion created in an intensification step of waste water treatment has also been investigated. This emulsion is prepared in a different way.

The model effluent containing 60 g/l acetic acid is cleaned by esterification of the carboxylic acid with one of the alcohols, methanol, *n*-butanol and octanol. The used alcohol is added in equimolar amount to the emulsion. The phase it is added to depends on the solubility of the alcohol. Methanol and *n*-butanol are added to the water phase, while octanol is added to the solvent phase. To enhance reaction kinetics 4-DBSA is used as catalyst. It is dissolved in the solvent phase consisting of *n*-undecane. The concentration of 4-DBSA was 20 wt.%. To achieve complete conversion the model effluent was heated to 60 °C and stirred overnight to provide a large interface between the solvent and the water phase. This was necessary for two reasons. First, the reaction takes place on the interface. If the latter is increased, more catalyst is available and the reaction rate is enhanced. Second, the products methyl-acetate, *n*-butyl acetate and octyl-acetate are hardly soluble in water and therefore need to migrate to the solvent phase. To enhance this process the interface has to be as large as possible, too. After the reaction is finished, the two phases are separated. However, a very stable o/w emulsion has been produced due to the catalyst acting as surfactant as well. The splitting behaviour of this emulsion in the electric field has then been investigated qualitatively.

Further detail to the process intensification step for isolating carboxylic acid from aqueous

effluents including theoretical background can be found in [10]. The equipment used is also described there in deep detail.

8.2. THERMAL SPLITTING

For thermal splitting the emulsion is put into a beaker and heated with a heat plate under continuous stirring until 60 °C are reached. This temperature is hold constant for a distinct time (14,500 seconds) to see whether there is a splitting effect or not.

8.3. CHEMICAL SPLITTING

The chemical breaking of the emulsion has been performed using isopropyl alcohol. To find the minimum amount of solubilizer the emulsion is added drop wise to a distinct amount of isopropyl alcohol. This operation is finished when the emulsion is not solubilized any more but grey stria occur inside the vessel. By using a stir bar an even distribution is realised.

8.4. MECHANICAL SPLITTING

8.4.1. CENTRIFUGATION

To investigate the stability of the emulsion a conventional splitting technology has to be applied. Therefore, the emulsion was put into a lab scale centrifuge and buoyancy force was applied for 18 min until the phases were separated. The radius r of the centrifuge has been 0.075 m and the centrifugation number has been set to 3000. The resulting number of revolutions can be calculated from the definition of the centrifugation number, which is the fraction of the buoyancy force F_b and the gravity force F_g (see equation 8.1).

$$z = \frac{F_b}{F_g} \quad (8.1)$$

The buoyancy force can be written as

$$F_b = r \cdot \omega^2 = r \cdot (2\pi \cdot n)^2 \quad , \quad (8.2)$$

where r is the radius of the centrifuge, ω is the circular velocity and n is the number of revolutions in Hz. Inserting equation 8.2 into 8.1 leads to equation 8.3 for n , which has to be set on the centrifuge.

$$n = \sqrt{\frac{z \cdot g}{r}} \cdot \frac{1}{2\pi} = 100 \text{ Hz} \quad (8.3)$$

8.4.2. FLOTATION

The flotation experiments are divided into two parts. As a first approach, pressurized air flotation was investigated. The equipment used can be seen in figure 8.1. A stopwatch for measuring the separation time, a vessel with a frit and a pressurized air inlet at the bottom was utilized for performing the experiment itself. To observe the separation progress a source of light was placed behind the vessel to see the turbidity changes. To document the separation progress a digital single-lens reflex camera (Nikon D90) was used. The program DCamCapture was used for time lapse image capturing. The timer was set to 1 or 20 minutes for separation in the electric field or in the gravitational field, respectively.

Through the frit the pressurized air is led into the emulsion as monodispersed bubbles. The bubbles generate foam containing separated solvent phase. With increasing separation progress, the emulsion becomes more and more translucent.

The second approach dealt with the emulsion splitting in an electroflotation equipment. An expanded metal plate and rod electrodes are used as electrodes. Additional parts of the equipment depicted in figure 8.2 are a multimeter to observe the current between the electrodes, a voltage source for power supply and again a light source behind the vessel to observe the separation progress. A test setup has been constructed to arrange the electrode parallel to the ground and in a distinct distance to the fixed rod electrodes. (see figure 8.3).

The experiment itself is performed as follows. At first, a picture of pure water and the electrodes placed inside is taken as a reference for complete separation. After that, the emulsion is prepared according to chapter 8.1 and filled inside the flotation cell. This is followed by taking a second picture with the electrodes inside as a reference for no separation. After this picture the separation experiment itself starts with applying the predefined voltage and taking pictures automatically every minute (or every 20 minutes for

8. SETUP - SPLITTING OF STABLE EMULSIONS

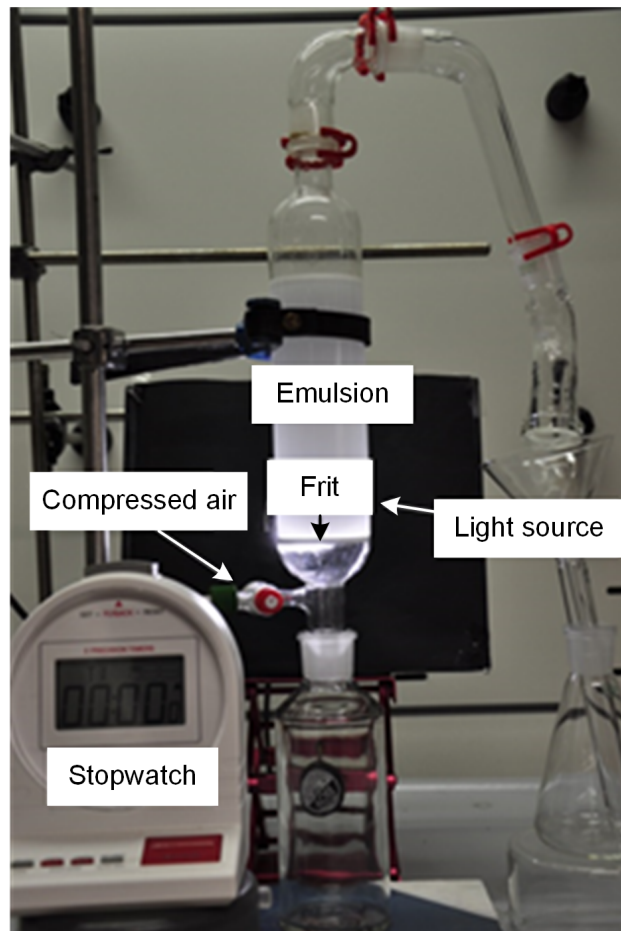


Figure 8.1.: Laboratory equipment pressurized air flotation

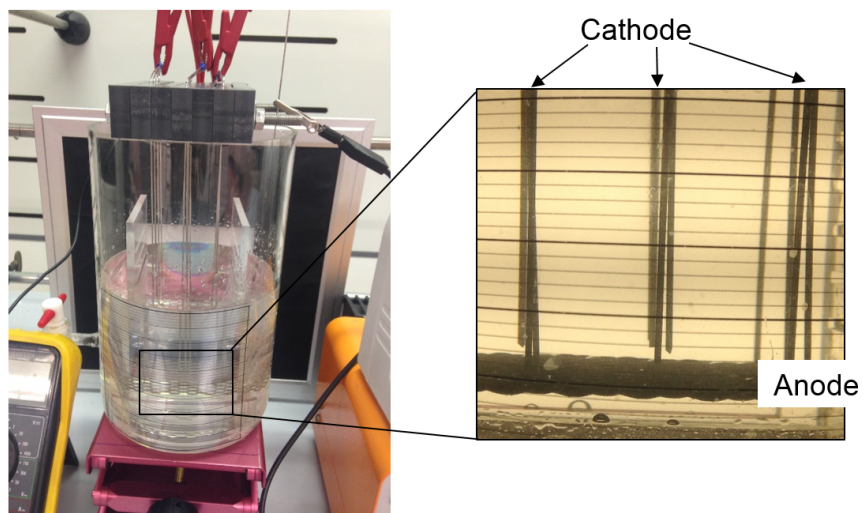


Figure 8.2.: Laboratory equipment electroflotation

8. SETUP - SPLITTING OF STABLE EMULSIONS

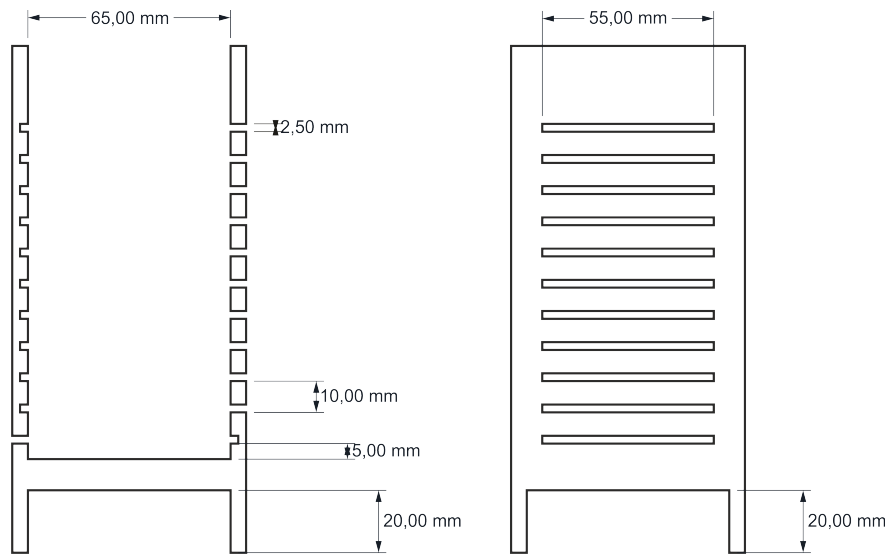


Figure 8.3.: Scheme of the electrode setup

gravitational experiments, but in this case the electrodes are not placed inside the flotation equipment). The electroflotation experiments end after 240 minutes. The gravitational experiments take several days.

8.5. ELECTRICAL SPLITTING

8.5.1. DIRECT CURRENT

The emulsion splitting experiments in a direct current electric field were performed with three different setups. First, a homogeneous electric field has been applied. For this reason, two to four plates are arranged in parallel. The distance between the electrodes (1 – 10 cm) as well as the applied voltage (1 – 14 V) have been varied to investigate the influence of the electric field. In figure 8.4 three plates are mounted in a distance of 1 cm. This leads to a homogeneous field, which is assumed to be stronger than it would be if only two plates in a distance of 2 cm were used. Second, an inhomogeneous electric field has been investigated. In this case, only the applied voltage has been varied from 1 to 3 V and the electrode configuration remained the same. The reason for this small range is the large electric field strength due to the inhomogeneous field and the small distance between the electrodes. This configuration can be seen in figure 8.5. Third, the influence of inclined electrodes has been investigated. For this reason, a new apparatus has been designed long enough to carry three plates inclined by 45 degrees in a distance of 60 mm or four plates in a distance of 20 mm (see figure 8.6). The angle can be chosen freely. The applied

8. SETUP - SPLITTING OF STABLE EMULSIONS

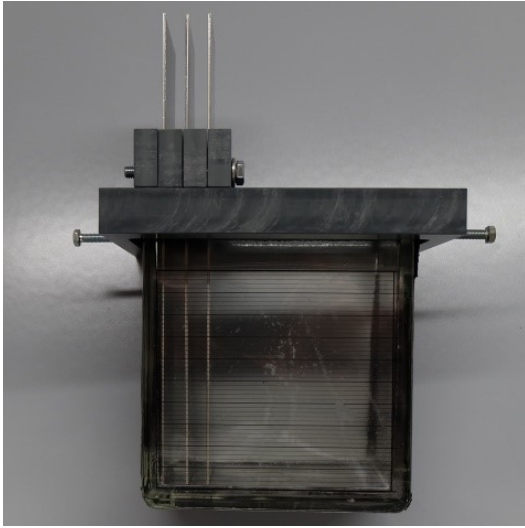


Figure 8.4.: Picture of the three plate arrangement; distance between electrodes: 1 cm

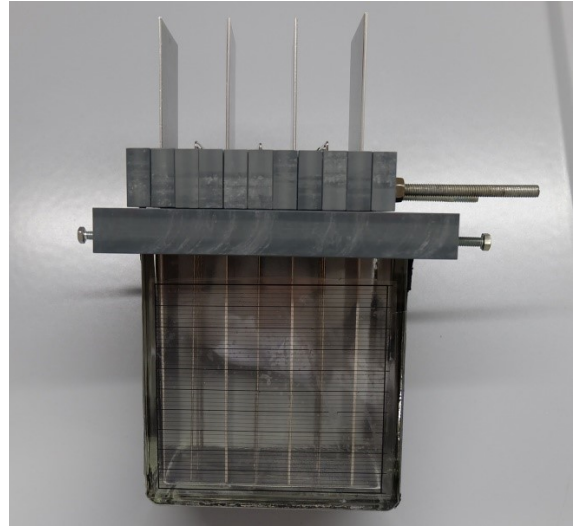


Figure 8.5.: Plate rod configuration with four plates and 3x4 rods; distance between electrodes: 1 cm

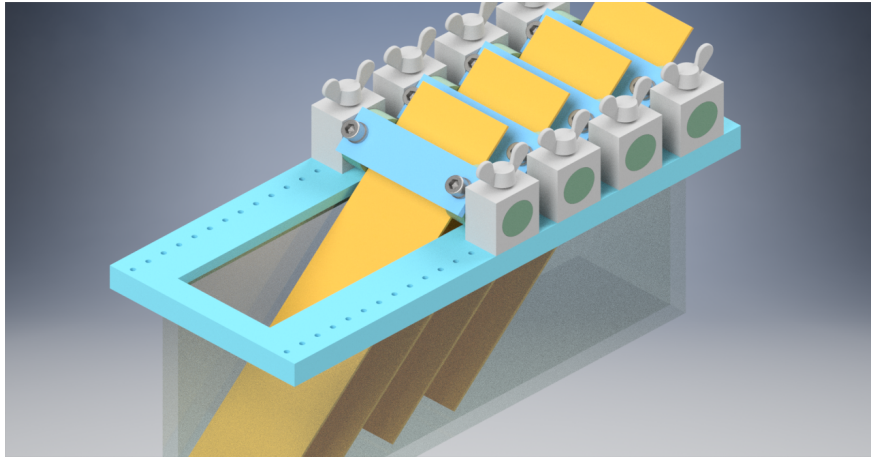


Figure 8.6.: Scheme of the apparatus for investigating the electric field with inclined plates

electric field strength is calculated according to equation 8.4. The graphical background of this equation is given in figure 8.7. The parameter d^* indicates the distance between the electrodes depending on the angle α , while d means the horizontal distance between the electrodes. The first distance is used for correct electric field strength calculation. The latter distance is used to describe the experiments, because this value is easier to measure and to set on the equipment.

$$d^* = d \cdot \cos(\alpha) \quad (8.4)$$

The experiments themselves are performed as follows without any difference concerning

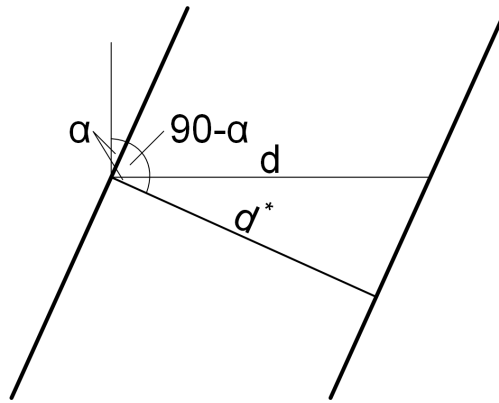


Figure 8.7.: Scheme of inclined plates and the electric field force applied between them

the electrode configuration. At first, a picture with pure water (and the electrodes placed inside) is taken as a reference for complete separation. After that, the emulsion is prepared according to chapter 8.1 and filled inside the electric field splitting cell. This is followed by taking a second picture with the electrodes inside as a reference for no separation. After this picture the separation experiment itself starts with applying the predefined voltage and taking pictures automatically every minute (or every 20 minutes for gravitational experiments, but in this case the electrodes are not placed inside the splitting equipment).

8.6. INTERPRETATION OF MONITORING RESULTS

To get the best results possible concerning the picture quality a light source is placed behind the separation cell (flotation or electric field) and illuminates the emulsion from the back side. The camera is placed directly in front of the separation cell. The optical zoom of the camera is adjusted in such way that the emulsion area is as big as possible but all important additional equipment can be seen on the picture. A schematic sketch of the documentation setup is depicted in figure 8.8. The whole separation area with the additional equipment can be seen in figure 8.9.

After performing the experiments, the pictures taken have to be analysed. For this reason, a MATLAB[®] function was developed. The complete code can be seen in appendix A. In this section only the features of the code are discussed.

The first setting is the analysis interval, which defines at what time intervals pictures are analysed. This is used to get results with limited data points generated. Then, the weight factor for the first point (zero separation at time zero) is defined by the user. By default they are set to unity for all experimental data. This step is followed by the definition of the

8. SETUP - SPLITTING OF STABLE EMULSIONS

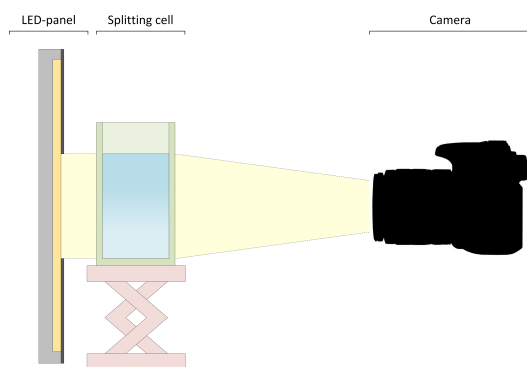


Figure 8.8.: Scheme of the monitoring setup



Figure 8.9.: Whole separation area with additional equipment devices

basic name of the output files. By default it consists of the analysis interval and the weight factor. Some other segments are added in the modelling and in the fitting part.

After defining the filename, the input is read. The input has to be written into a Microsoft Excel[®] spreadsheet. The spreadsheet contains all information about the experiment like date of performance, number of electrodes, system investigated, amount of solvent/aqueous phase etc. The spreadsheet is depicted in figure 8.10. The spreadsheet has to contain also information about which area of the picture has to be analysed. For this reason, the corners of the separation cell have to be determined inside the reference picture as well as inside one picture of the experiment. This input leads to cropped pictures, which are analysed for their overall brightness. This means that the separation is observed for the whole experimental equipment and not for individual segments. Therefore, the separation progress shows a number dependency instead of a volume dependency. In other words: One separated large drop changes the brightness of the emulsion less than many small ones with the same volume. Therefore, the separation change is less for one large droplet than for many small droplets.

The program stores an image containing the original pictures of the reference, the first and the last picture of the experiment as well as the cut ones. This is done to easily see whether the cutting was successful or the camera has been moved during the experiment (see figure 8.11). If the experiment has been carried out with inclined plates, the picture is rotated to have the region of interest in an upright position.

After analysis of the brightness, the sigmoidal fit is applied to the data generated (for details about the fit see chapter 9). This is done using the *fit* function of MATLAB[®]. How this function works is described in appendix A in deeper detail.

After the fitting is finished, the resulting function is plotted together with the separation data. This is depicted in figure 8.12 for an experiment with two plates in a distance of 10 cm

8. SETUP - SPLITTING OF STABLE EMULSIONS

Date	30.11.2016
Electrode configuration	2 plates
Anode	left
electrode distance	10 cm
aqueous phase	water
solvent phase	SSK 0.1 gew% SSK
phase ratio	0,005
voltage	10 V
experiment duration (approx.)	180 min
amount aq. phase	497,5
amount sol. phase	2,5
Notes	
photos to be deleted before exp. data (incl. reference)	1
photos to be deleted after exp. data (incl. reference)	0
interval between photos	1 min
time of first photograph	0
Information concerning the <u>reference</u> picture	
Number of reference picture	1
Cutting information	
Top left	
x-coordinate	1085
y-coordinate	1025
Bottom right	
x-coordinate	1980
y-coordinate	1650
Information concerning the <u>other</u> pictures in the experiment	
Cutting information	
Top left	
x-coordinate	1105
y-coordinate	965
Bottom right	
x-coordinate	2000
y-coordinate	1590

Figure 8.10.: Microsoft Excel[®] spreadsheet of the input



Figure 8.11.: Image containing the original reference, start and last picture of the experiment as well as the cut pictures

and an applied voltage of 10 V, therefore 100 V/m. It is clearly visible that the fit describes the experimental data very well.

Using the deadtime calculated with the sigmoidal fit the exponential model can be applied (for details about the model see chapter 10). This is also done applying the *fit* function of MATLAB[®] to the brightness data.

After the modelling is finished, the resulting function is plotted over the separation data (see figure 9.3).

Now all pictures are stored with the corresponding file name and the fit and modelling data are stored in a new spreadsheet (see figure 8.13).

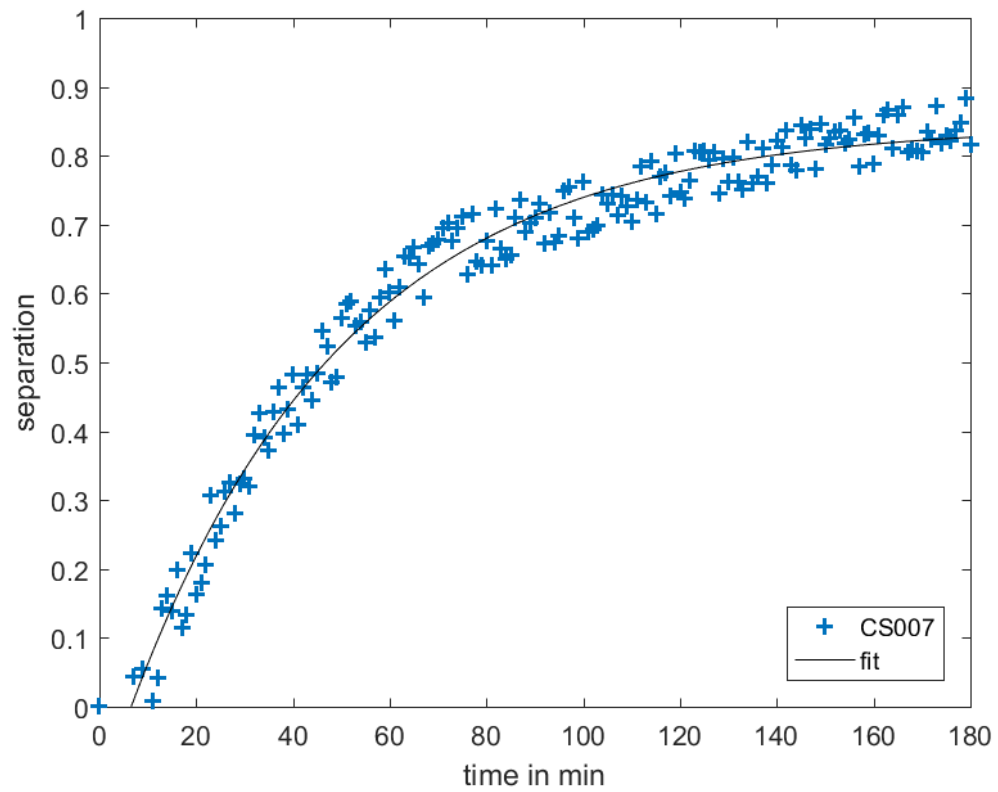


Figure 8.12.: Sigmoidal Fit and experimental data

time [min]	separation [-]	model data [-]	model data low	model data up	avg. brightness [-]	brightness ref. [-]	deadtime [min]	values parameter	confidence interval lower boundary	confidence interval upper boundary	goodness of fit message
0	0,043	0,000	0,000	0,000	0,604	0,999536134	7 am	0,843731161	0,832372607	0,855209716	sse 0,18448302
1	-0,020	0,019	0,018	0,020	0,578		bm	0,022574461	0,021609321	0,023539601	rsquare 0,37841556
2	0,055	0,037	0,035	0,039	0,609						dfe 172
3	-0,002	0,055	0,052	0,058	0,585		drop diameter	0,428842096	0,410507546	0,447176645	adrsquare 0,37823007
4	0,009	0,073	0,069	0,077	0,590						rmse 0,0327502
5	0,042	0,090	0,085	0,095	0,603						
6	0,142	0,107	0,101	0,113	0,645						
7	0,161	0,123	0,117	0,130	0,653						
8	0,138	0,139	0,132	0,147	0,643						
9	0,198	0,155	0,147	0,163	0,668						
10	0,115	0,171	0,162	0,179	0,634						
11	0,134	0,186	0,176	0,195	0,641						
12	0,222	0,200	0,190	0,210	0,678						
13	0,163	0,215	0,204	0,225	0,654						
14	0,179	0,229	0,217	0,240	0,660						
15	0,206	0,242	0,230	0,254	0,671						
16	0,307	0,256	0,243	0,268	0,713						
17	0,242	0,269	0,256	0,282	0,686						
18	0,261	0,282	0,268	0,295	0,694						
19	0,312	0,294	0,280	0,306	0,715						
20	0,325	0,307	0,292	0,321	0,720						
21	0,280	0,319	0,304	0,334	0,702						
22	0,324	0,330	0,315	0,346	0,720						
23	0,332	0,342	0,326	0,358	0,723						
24	0,320	0,353	0,337	0,369	0,718						
25	0,394	0,364	0,347	0,380	0,749						
26	0,426	0,375	0,358	0,391	0,762						
27	0,390	0,385	0,368	0,402	0,747						
28	0,373	0,395	0,378	0,413	0,740						
29	0,428	0,405	0,388	0,423	0,763						
30	0,464	0,415	0,397	0,433	0,778						

Figure 8.13.: Microsoft Excel[®] spreadsheet of the results of the modelling; the result file of the fit has a similar structure

Part III.

Modelling

9. SIGMOIDAL MODELLING APPROACH

In a first step, the beginning of the separation process has to be described. The necessity to do so comes from the obvious delay time, which occurs without any regularity. This can be seen in figures 9.1 and 9.2, where the results of two different experiments with two electrodes mounted in a distance of 10 cm and an applied voltage of 10 V are shown. In the first experiment, approximately 7 minutes of delay occur until the separation starts (red line) whereas in the second one hardly any delay is visible.

For this reason, a fit equation (see equation 9.1) containing the start parameter A_s was set up and the parameters B_s , C_s and D_s have been fitted to the experimental data. The physical meaning of these parameters can be calculated from the modelling of Bhumpong [98], who analysed the sedimentation of droplets in the gravitational field. This is not performed in this work since only the description of the inflow region is of interest using the sigmoidal fitting approach.

$$Sr = A_s + \frac{B_s - A_s}{1 + e^{-\frac{t-C_s}{D_s}}} \quad (9.1)$$

In order to not consider the delay in the modelling the separation values before the sigmoidal fit intersects with the abscissa are excluded. Figure 9.3 shows the experiment shown in figure 9.1 without the start delay.

9. SIGMOIDAL MODELLING APPROACH

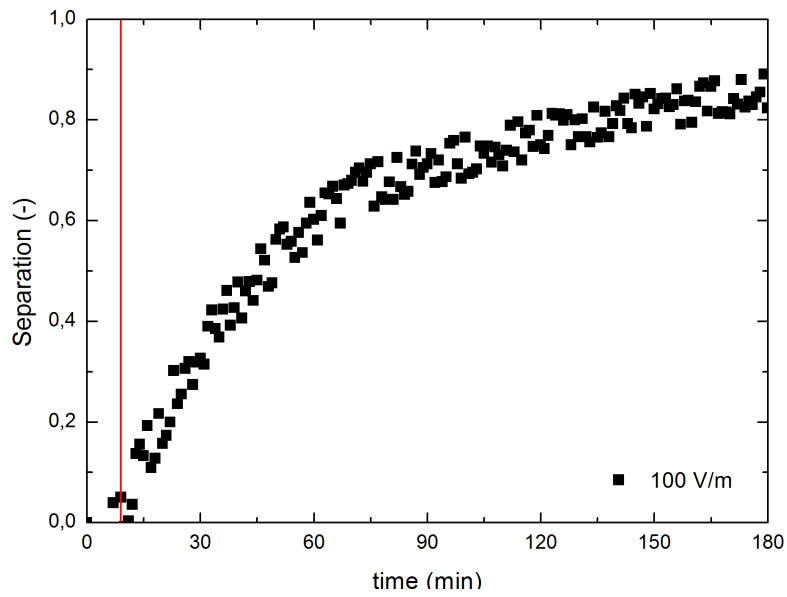


Figure 9.1.: delay of separation (red line); experiment performed with 2 electrodes with a distance of 10 cm and an applied voltage of 10 V (CS007)

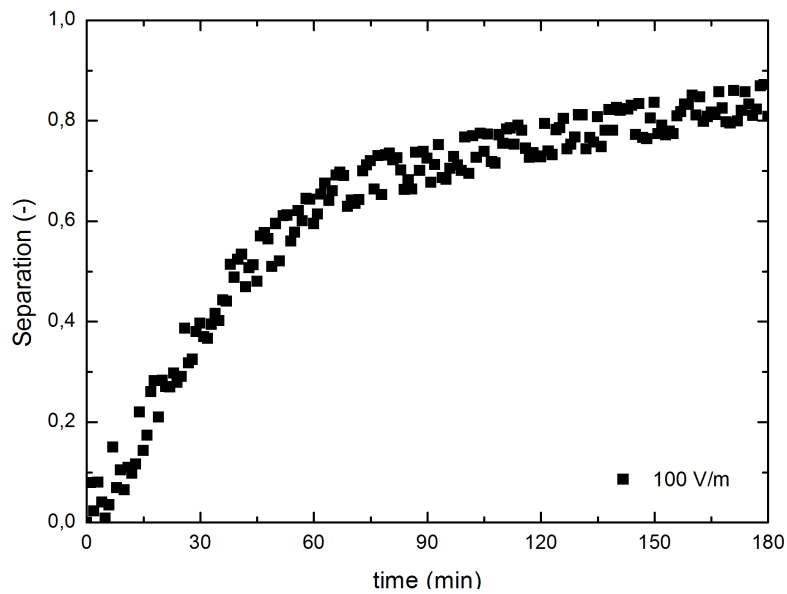


Figure 9.2.: No delay; experiment performed with two electrodes with a distance of 10 cm and an applied voltage of 10 V (CS012)

9. SIGMOIDAL MODELLING APPROACH

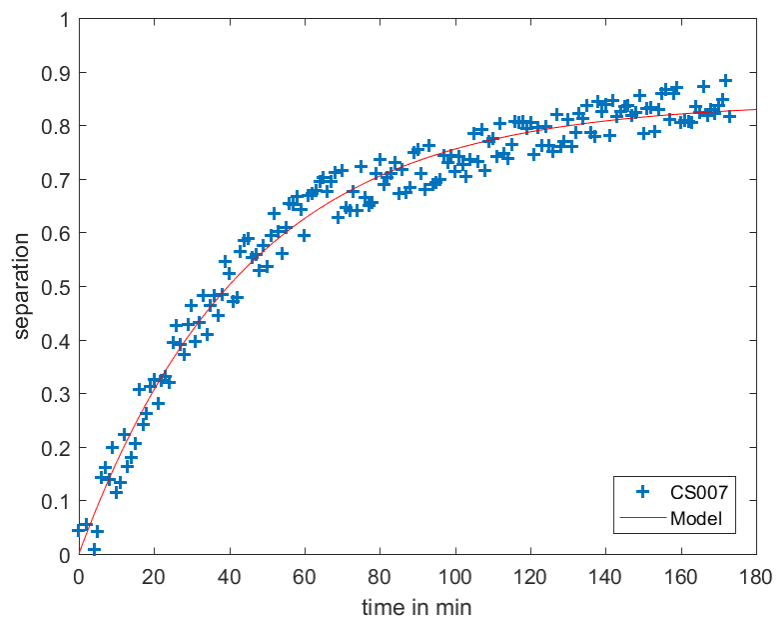


Figure 9.3.: Delay is not taken into account; experiment performed with two electrodes with a distance of 10 cm and an applied voltage of 10 V (CS007 without delay time of 7 min)

10. EXPONENTIAL MODELLING APPROACH

After the delay of the separation start is quantified and excluded the modelling itself can be performed.

The exponential modelling approach can be derived from a balance for the splitting equipment (see figure 10.1), which is set up in a general way as

$$F_V \cdot c_{E0} = F_V \cdot c_E - r'' \cdot A + \frac{dN_E}{dt} \quad . \quad (10.1)$$

In this equation F_V is the volume flow rate of the emulsion, c_{E0} represents the starting concentration of the dispersed phase, the actual concentration of the emulsion is c_E , r'' represents the area related rate of turbidity drop, A is the electrode (capacitor) area, N_E is the amount of dispersed phase and t is the experimental time. Since the volume flow rate F_V is 0 because the experiments were performed in batch mode all terms containing F_V can be rejected. For the turbidity depletion rate r'' and the amount of emulsion N_E we get

$$- r'' = w \cdot c \quad \text{and} \quad (10.2)$$

$$N_E = V \cdot c_E \quad , \quad (10.3)$$

with the particle migration rate w induced by the electric field and the concentration c , respectively, and the volume V , equation 10.1 can be rearranged as according to

$$- w \cdot c \cdot A = V \cdot \frac{dc}{dt} \quad . \quad (10.4)$$

Separation of variables and inserting the limits c_{E0} , c_E , 0 and t for concentration at the beginning and at time t leads to

$$\int_{c_{E0}}^{c_E} \frac{dc}{c} = - \frac{w \cdot A}{V} \int_0^t dt \quad . \quad (10.5)$$

Integration between limits leads to

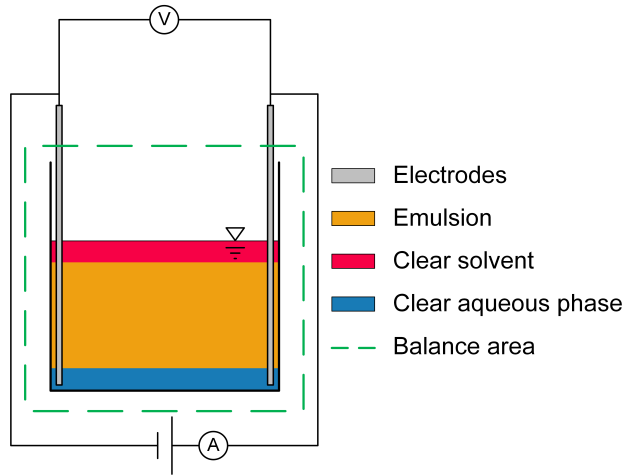


Figure 10.1.: Balance for the splitting equipment

$$\ln \frac{c_E}{c_{E0}} = -\frac{w \cdot A}{V} \cdot t \quad (10.6)$$

and rearranging equation 10.6 leads to

$$c_E = c_{E0} \cdot e^{-\frac{w \cdot A}{V} \cdot t} \quad , \quad (10.7)$$

which correlates the actual emulsion concentration c_E with respect to the initial concentration c_{E0} and the experimental time t . This equation has the same shape as the so-called "Deutsch-equation," which describes the separation of particles from gaseous carrier in the electric field. [99] Inserting

$$A = b \cdot h \quad \text{and} \quad (10.8)$$

$$V = b \cdot h \cdot d \quad , \quad (10.9)$$

where b , h and d are width, height and distance of the electrodes, respectively, equation 10.7 can be rewritten as

$$c_E = c_{E0} \cdot e^{-\frac{w}{d} \cdot t} \quad , \quad (10.10)$$

which means that the actual emulsion concentration only depends on the initial concentration c_{E0} , the average rate of migration of the emulsion droplets w , the electrode distance d and the time t .

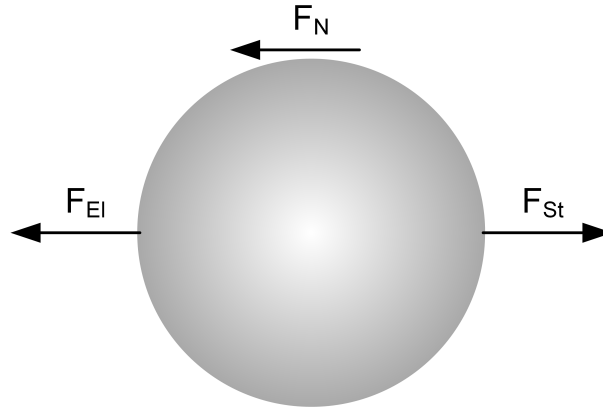


Figure 10.2.: Force balance for a droplet in the electric field

The separation efficiency Sr can now be developed.

$$Sr = 1 - \frac{c_E}{c_{E0}} = 1 - e^{-\frac{w}{d} \cdot t} \quad (10.11)$$

The rate of migration w in the electric field can be derived from the force balance for the single droplet in the electric field, also called Coulomb-force, F_{El} . Due to the motion into the direction of the field gradient the Stokes resistance force F_{St} acts into the opposite direction and reduces the resulting Newton force F_N . [100]

$$F_N = F_{El} - F_{St} \quad (10.12)$$

with

$$F_N = m \cdot \frac{dw}{dt} \quad , \quad (10.13)$$

$$F_{El} = q \cdot E_P \quad \text{and} \quad (10.14)$$

$$F_{St} = 3 \cdot \pi \cdot \eta_c \cdot x \cdot w(x) \quad (10.15)$$

leads after rearranging to

$$dw = (q \cdot E_P - 3 \cdot \pi \cdot \eta_c \cdot x \cdot w(x)) \cdot \frac{dt}{m} \quad . \quad (10.16)$$

In this set of equations m is the mass of the droplet, q represents the charge of the droplet and is defined in equation 10.17, E_P is the precipitating electric field as defined in 10.18, η_c is the dynamic viscosity of the continuous phase and x the droplet diameter. E_0 in equation

10.17 is the charging field strength defined in 10.19, where U is the applied voltage in V and d the distance between electrodes in m. [99, 100]

$$q = 3 \cdot E_0 \cdot \left(\frac{x}{2}\right)^2 \quad (10.17)$$

$$E_P = \sqrt{\frac{2 \cdot I}{K}} \quad \text{with} \quad (10.18)$$

I being the current applied per m of electrode and K being a constant describing the mobility of the ions, which lies in the range of $20 \text{ m}^3/2 \text{ kg}^{-1/2}$.

$$E_0 = \frac{U}{d} \quad (10.19)$$

The separation of variables and the integration are performed in the following way:

1. Separation of variables

$$\frac{dw}{q \cdot E_P - 3 \cdot \pi \cdot \eta_c \cdot x \cdot w(x)} = \frac{dt}{m} \quad (10.20)$$

2. Multiplying with the constants $3 \cdot \pi \cdot \eta_c \cdot x$

$$\frac{dw}{\frac{q \cdot E_P}{3 \cdot \pi \cdot \eta_c \cdot x} - w(x)} = \frac{3 \cdot \pi \cdot \eta_c \cdot x}{m} dt \quad (10.21)$$

3. Integration from 0 to $w(x)$ (left side) and from 0 to t (right side)

$$\frac{\ln\left(\frac{q \cdot E_P}{3 \cdot \pi \cdot \eta_c \cdot x} - w(x)\right)}{-1} = \frac{3 \cdot \pi \cdot \eta_c \cdot x}{m} \cdot t \quad (10.22)$$

4. Rearranging to get an expression for $w(x)$

$$\frac{q \cdot E_P}{3 \cdot \pi \cdot \eta_c \cdot x} - w(x) = e^{-\frac{3 \cdot \pi \cdot \eta_c \cdot x}{m} \cdot t} \quad (10.23)$$

$$w(x) = \frac{q \cdot E_P}{3 \cdot \pi \cdot \eta_c \cdot x} - e^{-\frac{3 \cdot \pi \cdot \eta_c \cdot x}{m} \cdot t} \quad (10.24)$$

Since the droplet diameter x is very small the mass of the droplet m becomes very small and may be neglected.

$$e^{-\frac{3 \cdot \pi \cdot \eta_c \cdot x}{m} \cdot t} \cong 0 \quad (10.25)$$

Therefore, the second part of equation 10.24 vanishes, simplifying equation 10.24 to

$$w(x) = \frac{q \cdot E_P}{3 \cdot \pi \cdot \eta_c \cdot x} \quad (10.26)$$

Inserting equation 10.17 for the charge of the droplet q , equation 10.26 can be rewritten as

$$w(x) = \frac{E_0 \cdot E_P \cdot x}{4 \cdot \pi \cdot \eta_c} \quad (10.27)$$

Since I in equation 10.18 must be 0 in electric field splitting of o/w emulsions to avoid Faradaic currents the precipitating field strength E_P is approaching the charging field strength E_0 , which leads to

$$w(x) = \frac{E_0^2 \cdot x}{4 \cdot \pi \cdot \eta_c} \quad (10.28)$$

This equation relates the rate of migration w with the (charging) electric field strength in the splitting equipment E_0 and the droplet diameter x . The rate can be compared regarding the electric field strength. It is obvious, that the distance between the electrodes does not have an influence on it. Combining equation 10.11 with 10.28 makes the determination of the droplet diameter for each experiment possible.

$$Sr = 1 - \frac{C_E}{C_{E0}} = 1 - e^{-\frac{E_0^2 \cdot x}{4 \cdot \pi \cdot \eta_c} \cdot t} \quad (10.29)$$

Since inaccuracies in experimental work will affect separation, an additional parameter a considers deviations. The inaccuracies can be caused by backmixing due to Brownian motion, mist on the glass, droplets sticking to the electrodes and many more.

$$Sr = a \cdot \left(1 - e^{-\frac{E_0^2 \cdot x}{4 \cdot \pi \cdot \eta_c \cdot d} \cdot t} \right) \quad (10.30)$$

Rearranging of equation 10.29 with respect to the droplet diameter x leads to equation 10.31, which enables the calculation of the droplet diameter with respect to the separation rate Sr at time t of an experiment with the electric field strength E_0 applied with electrodes in a distance d and the viscosity η_c of the continuous phase.

$$x = -\ln(1 - Sr) \cdot \frac{4 \cdot \pi \cdot \eta_c \cdot d}{E_0^2 \cdot t} \quad (10.31)$$

Equation 10.31 finally gives access to the droplet diameter at distinct time. To determine a representative mean droplet diameter for the whole experiment, equation 10.29 is rearranged. All parameters in the exponent except t are constant for one specific setting (parameter b in equation 10.32), therefore an average drop diameter for the experiment can be determined. The final rearrangement can be seen in equation 10.33.

$$b = \frac{E_0^2 \cdot x}{4 \cdot \pi \cdot \eta_c \cdot d} \quad (10.32)$$

$$x = \frac{4 \cdot \pi \cdot \eta_c \cdot d \cdot b}{E_0^2} \quad (10.33)$$

With the result of equation 10.33 the migration rate w can be determined using equation 10.28. However, this can only be done, if the unit conversion of the electric field strength from V/m to kg, m and s is performed according to [101]. The correlation between these units and between A and kg, m and s is shown in equation 10.34 and 10.35, respectively.

$$\frac{V}{m} = 1.05 \cdot 10^{-2} [kg^{0.5} \cdot m^{-0.5} \cdot s^{-1}] \quad (10.34)$$

$$A = \frac{3 \cdot 10^6}{\sqrt{10^3}} \cdot \frac{\sqrt{kg} \cdot m^{\frac{3}{2}}}{s^2} = 9.49 \cdot 10^4 \cdot \frac{\sqrt{kg} \cdot m^{\frac{3}{2}}}{s^2} \quad (10.35)$$

Part IV.

Results and discussion

11. RESULTS - PREPARATION OF STABLE EMULSIONS

This chapter deals with the emulsion formation experiments. The influence of the agitation rate (chapter 11.1), the hold-up (chapter 11.2) and the action of a surfactant (chapter 11.3) are presented and discussed in the following chapters.

11.1. INFLUENCE OF THE AGITATION RATE

In general, the determination of the separation progress by speed of sound is much easier than by optical measures. Therefore, only the agitation rate has been investigated using the optical cell. The other observations have been carried out in the ultrasonic scanner. The calibration of the ultrasonic scanner to connect the speed of sound with the actual hold-up can be seen in the appendix D.

11.1.1. OPTICAL EVALUATION

The settling behaviour in the system SSK-water has been investigated applying agitation rates from 300 to 1900 rpm. The amount of SSK was kept constant at 10 wt.%. Figure 11.1 shows the relation between the coalescence curve and the time. It was not possible to observe the sedimentation curve optically since it was hidden by a turbidity formed during mixing. For this reason not the final separation point was defined as end of the experiment, but a distinct height has been chosen. It is obvious that due to higher shear stress the droplet size decreases and therefore the coalescence time is increased until a maximum is reached (1500 rpm). Due to the small droplet diameter, the sedimentation rate is decreased. Therefore, it takes longer for them to reach the o/w interface.

Figure 11.2 shows the influence of the agitation rate on the time necessary for the coalescence interface to reach the predefined height. It is obvious that there is a maximum at 1500 rpm. After the maximum of coalescence time at 1500 rpm, the coalescence time decreases again. This phenomenon has not been investigated in detail. It may be caused by dissolution of fines combined with growth of coarse particles, similar to nucleation and particle growth in homogeneous crystallisation. Colloidal particles size would not be detected by the monitoring setup. As can be seen in figure 11.3 the decrease in coalescence time follows linear behaviour with increasing agitation rate.

11. RESULTS - PREPARATION OF STABLE EMULSIONS

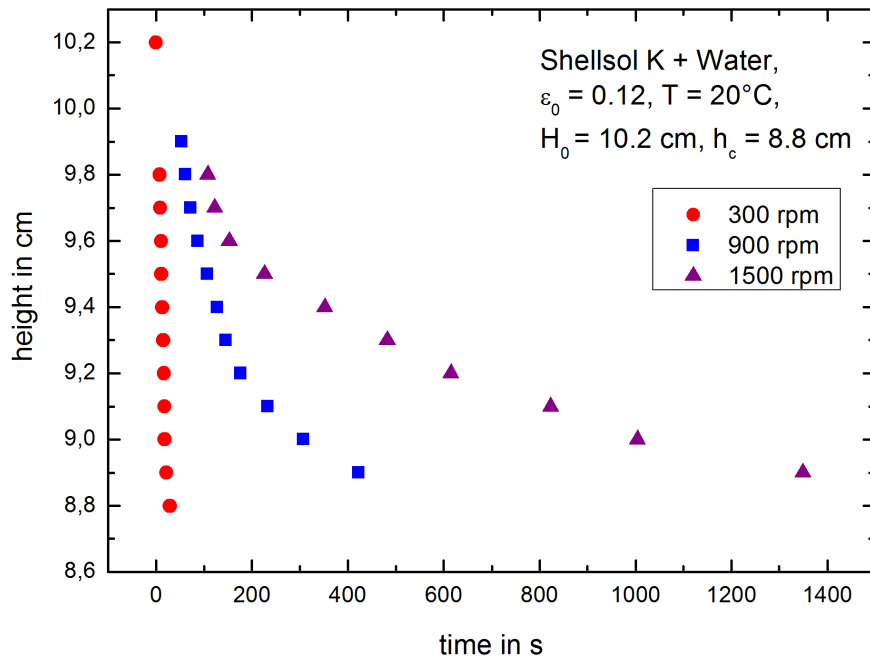


Figure 11.1.: Influence of the agitation rate on the coalescence curve

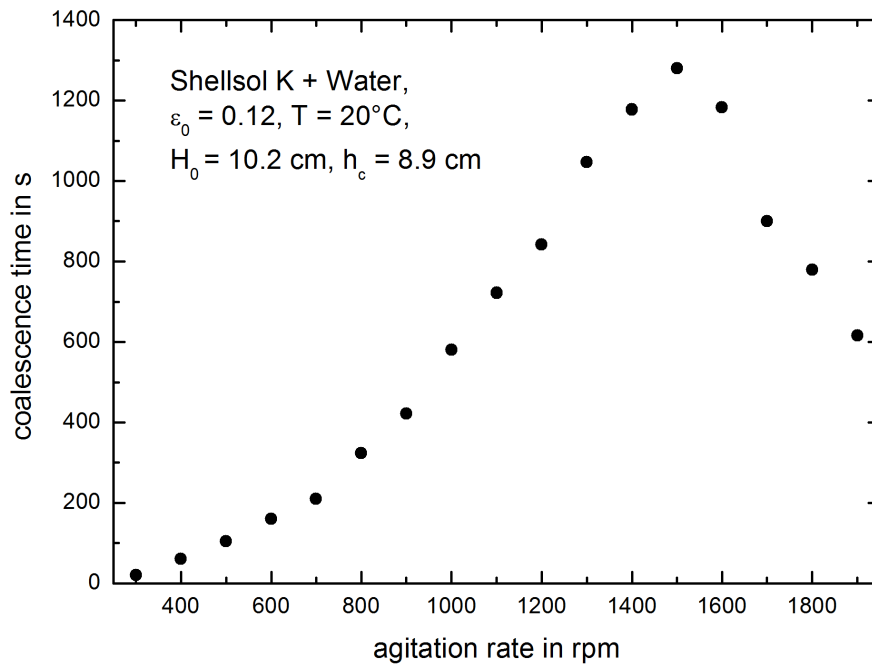


Figure 11.2.: Influence of the agitation rate on the coalescence time, optical evaluation

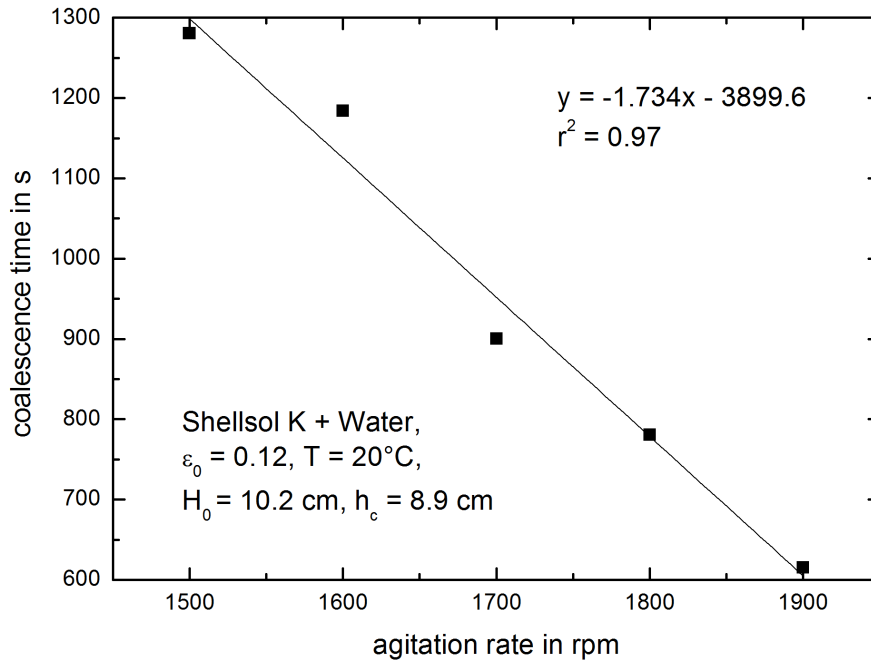


Figure 11.3.: Linear decrease of the coalescence time for agitation rate between 1500 and 1900 rpm, optical evaluation

11.1.2. ULTRASONIC SCANNER

The behaviour observed in the optical cell could be validated in the ultrasonic equipment. 30 wt.% SSK was dispersed in water and the separation behaviour was investigated for 6 agitation rates (900, 1100, 1300, 1500, 1700 and 1900 rpm). This means that a change in hold-up (from 12 to 30 wt.%) did not change the behaviour of the emulsion. The different shape of the results in figure 11.4 compared to figure 11.1 is due to the differences in hold-up and in cross sectional area of the equipment. The amount of liquid has been 600 ml in all experiments. However, the diameters of the optical cell and the decanter of the ultrasonic scanner differed in size (8.5 and 6 cm, respectively), which led to a different overall height of the emulsion in the two vessels.

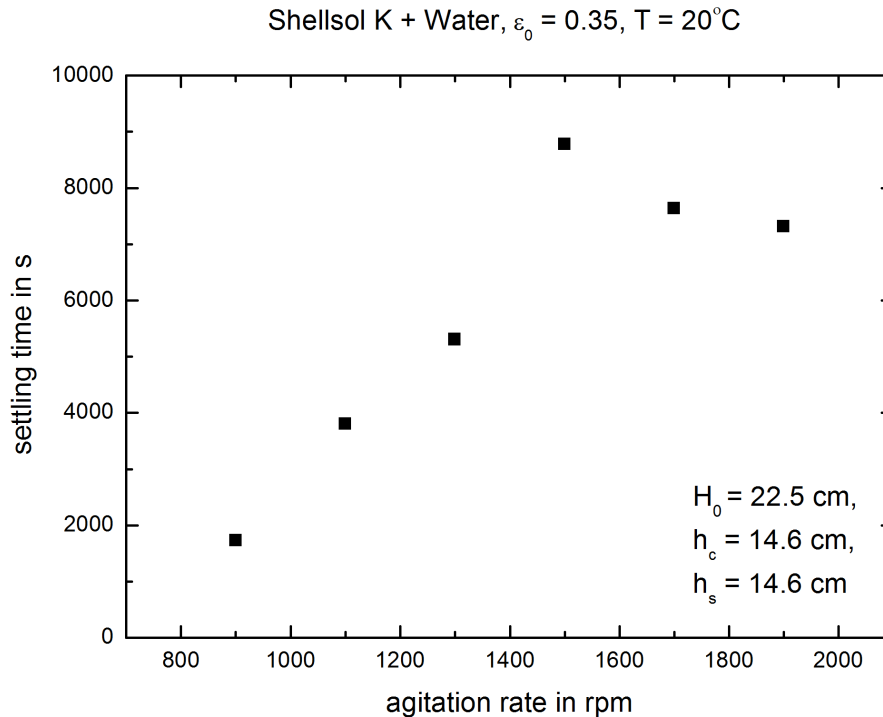


Figure 11.4.: Influence of the agitation rate on the separation time, ultrasonic evaluation

11.2. INFLUENCE OF THE HOLD-UP

The hold-up has been varied from 0.06 to 0.35 (0.05 to 0.3 wt.%) to quantify the differences in settling time. The agitation rate was kept constant at 1500 rpm. The result of this investigation can be seen in figure 11.5. It is obvious that the settling time increases linearly with increasing hold-up. The reason for this is that the number of droplets becomes larger. This leads to the formation of a thick dense packed zone, because coalescence is the time limiting step in this chemical system. Figure 11.6 shows that this zone is formed directly at the o/w interface with a high amount of solvent phase. Separation cannot be finished until this zone vanishes. The more droplets are inside the system the longer it takes to remove them by coalescence.

11. RESULTS - PREPARATION OF STABLE EMULSIONS

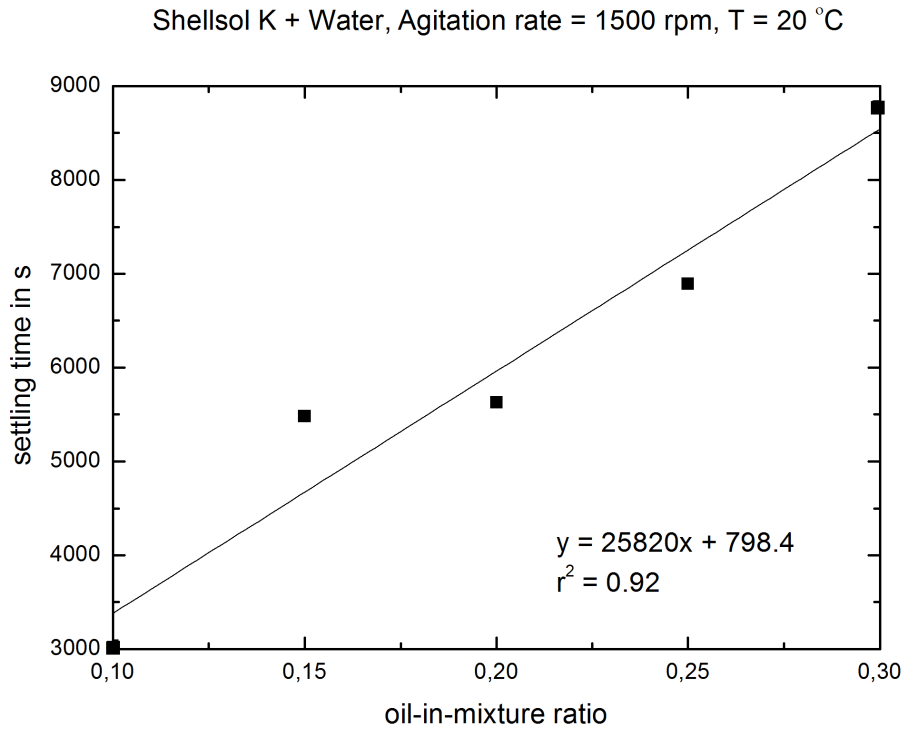


Figure 11.5.: Influence of the hold-up on the settling time

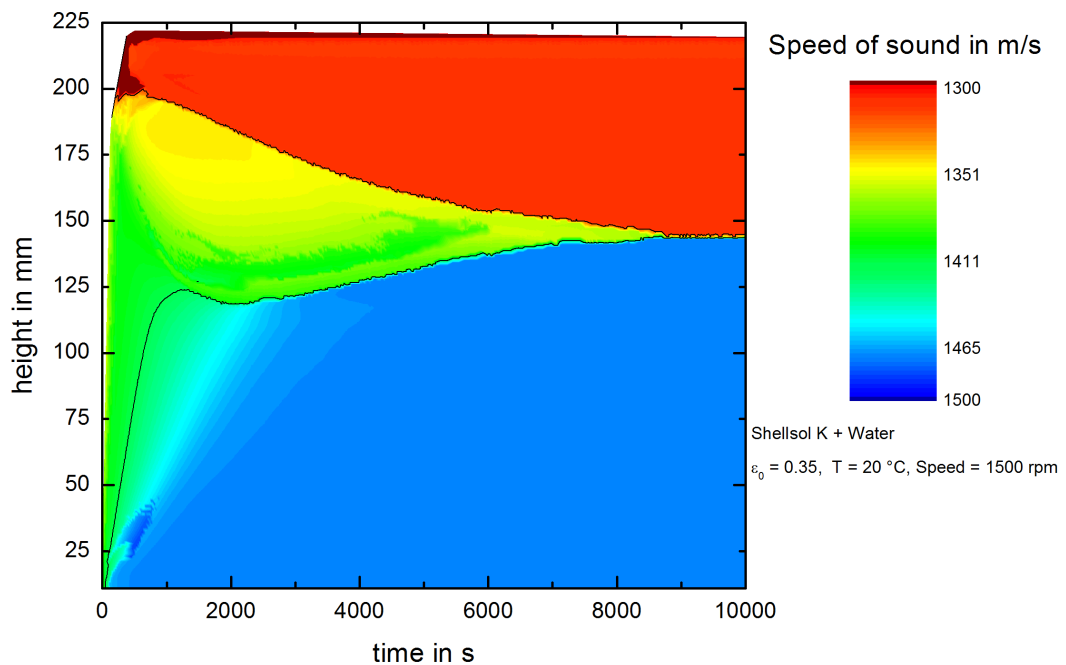


Figure 11.6.: Result of mechanically mixing an emulsion with an hold-up of 0.35 with a rotational speed of 1500 rpm

11.3. INFLUENCE OF THE SURFACTANT

It can be seen from the previous sections that the rotational speed of the agitator as well as the hold-up of the dispersed phase have an influence on emulsion stability. However, there is another effect to be considered. It is the type and the amount of surfactant. In this work only the anionic surfactant 4-DBSA is investigated. To determine the influence of 4-DBSA on emulsion stability 4 different proportions were added to the basic system SSK/water. One was chosen to be below the cmc of 4-DBSA ($2.45 \cdot 10^{-4}$ mol/l [102]) and three above it. The concentrations in the organic phase with the corresponding concentration in the aqueous phase (assuming that all 4-DBSA moves from the solvent to the aqueous phase) can be seen in table 11.1.

Figure 11.7 shows the emulsion stability with respect to the surfactant concentration. It can be seen that with a concentration lower than the cmc the emulsion is already quite stable. However, some splitting takes place, since clear solvent phase forms with time (red areas in the figure). Increasing the surfactant concentration above the cmc leads to a very stable emulsion. It is visible that the emulsion does not change any more within the investigated time span (100,000 seconds, which is approximately 28 hours).

Therefore, the concentration of 4-DBSA was chosen to be 0.1 wt.% with respect to the solvent phase to stabilise the emulsions produced.

Table 11.1.: 4-DBSA concentrations in the solvent and the aqueous phase at a hold-up of 0.35

<i>concentration in the solvent phase [wt.%]</i>	<i>concentration in the aqueous phase [mol/l]</i>
0.04	$1.34 \cdot 10^{-4}$
0.10	$3.49 \cdot 10^{-4}$
1.00	$3.38 \cdot 10^{-3}$
1.70	$5.88 \cdot 10^{-3}$

11. RESULTS - PREPARATION OF STABLE EMULSIONS

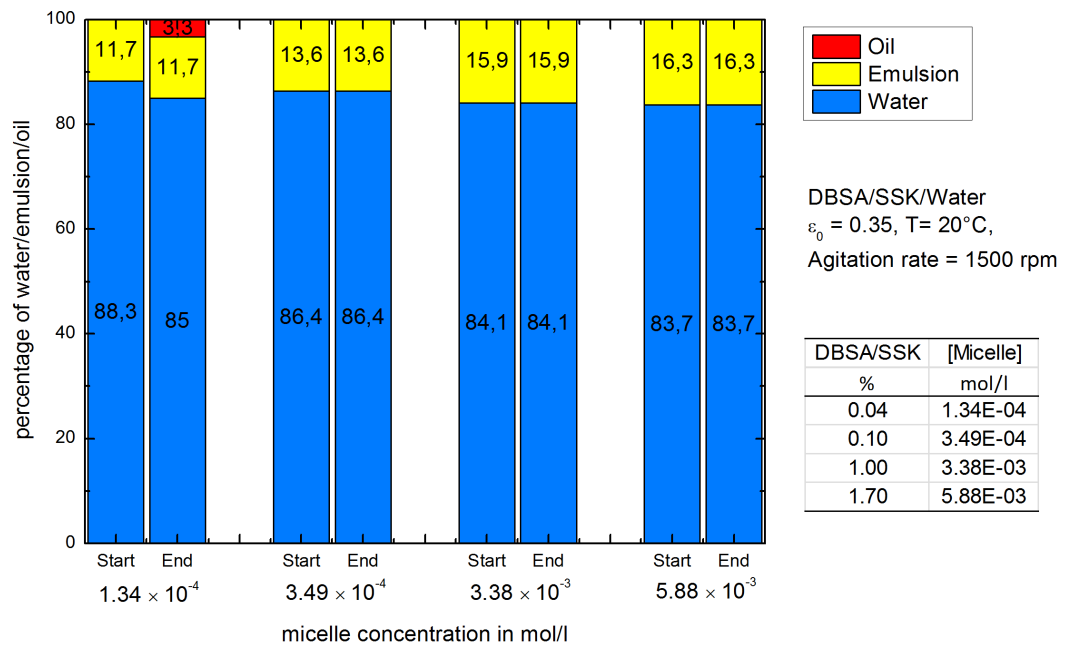


Figure 11.7.: Influence of the surfactant concentration on the emulsion stability

12. RESULTS - SPLITTING OF STABLE EMULSIONS

12.1. THERMAL SPLITTING

As described in the basic (see chapter 5.4) the splitting of emulsions can also be performed by providing thermal energy on the emulsion. This has been done for comparison reasons, whether conventional thermal splitting is an alternative splitting process or not.

In figure 12.1 the emulsion at the beginning of the thermal treatment is depicted. It is opaque and milky. Figure 12.2 shows the emulsion at the end of the splitting experiment (after 285 minutes). It can be seen that the emulsion became more translucent since the stir bar is visible at the bottom of the beaker. However, the separation has not been satisfactory. Additionally, the energy input is huge (46.5 kWh/m^3 emulsion) and a lot of emulsion is evaporated (approximately 17 % in 4.75 h). Due to this two problems thermal emulsion splitting cannot be regarded as an alternative to other splitting technologies and further investigation is not performed. The complete calculation as well as the temperature plotted over time are shown in appendix B.

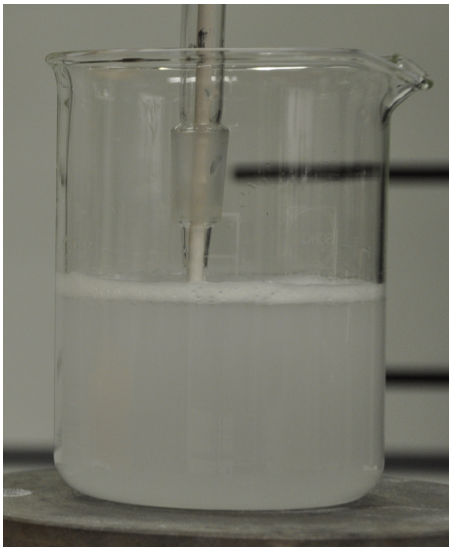


Figure 12.1.: Thermal splitting: Initial picture of the emulsion



Figure 12.2.: Thermal splitting: Picture of the final emulsion

12.2. CHEMICAL SPLITTING

An amount of 50 g isopropyl alcohol is put into a beaker. The emulsion consisting of 0.5 wt.% solvent phase in water is added dropwise. 0.1 wt.% of 4-DBSA are dissolved in the solvent phase.

Comparing the figures 12.3 and 12.4 it is visible that there is a change in cloudiness. While the mixture in figure 12.3 appears clear and transparent the two phase region is reached in figure 12.4 indicated by opaque stria at the bottom of the beaker after the addition of 76 ml of emulsion. This leads directly to the result that 660 l of isopropyl alcohol are necessary to "split" 1 m³ of emulsion. In fact, it is not a splitting procedure but a dissolution procedure. It increases the TOC-value in the system by a factor of approximately 100 (660 l compared to 0.5 wt.%), which makes it even more expensive to recover the water phase. Therefore, this kind of operation is not applicable in industrial emulsion splitting but is limited to analytical purposes to analyse the aqueous and the solvent phase in a homogeneous mixture.

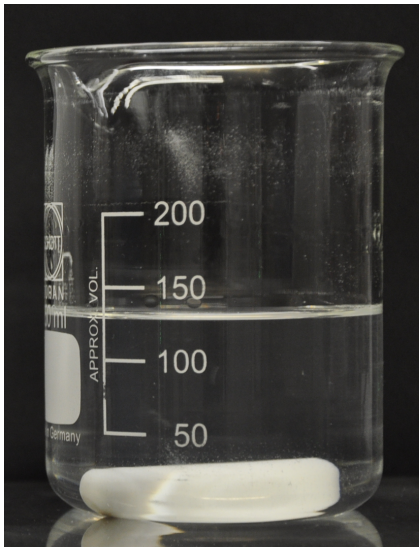


Figure 12.3.: Chemical splitting: Addition of 75 ml of emulsion to 50 ml of isopropyl alcohol

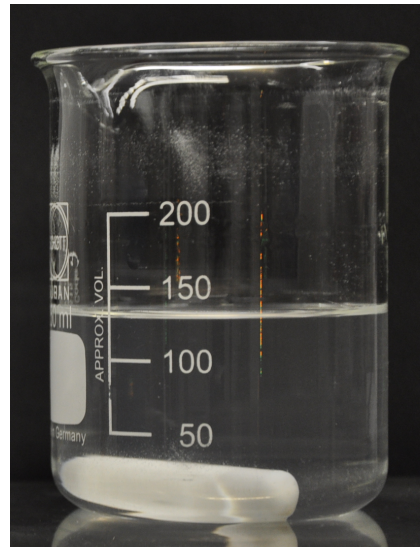


Figure 12.4.: Chemical splitting: Addition of 76 ml of emulsion to 50 ml of isopropyl alcohol

12.3. MECHANICAL SPLITTING

12.3.1. CENTRIFUGATION

As can be seen in figure 12.5 the application of centrifugal force leads to complete separation of the emulsion. Additionally, it is also obvious, that it takes only 30 minutes at a centrifugation number of 3000 until complete separation is realised. This is fast compared to other separation technologies like electrical splitting (see chapter 12.4). However, the high investment and operating costs (approximately 85,000 € and 2.75 kWh for a centrifuge with a maximum throughput of 80 l/min, respectively [103]) oppose the application of centrifugation.

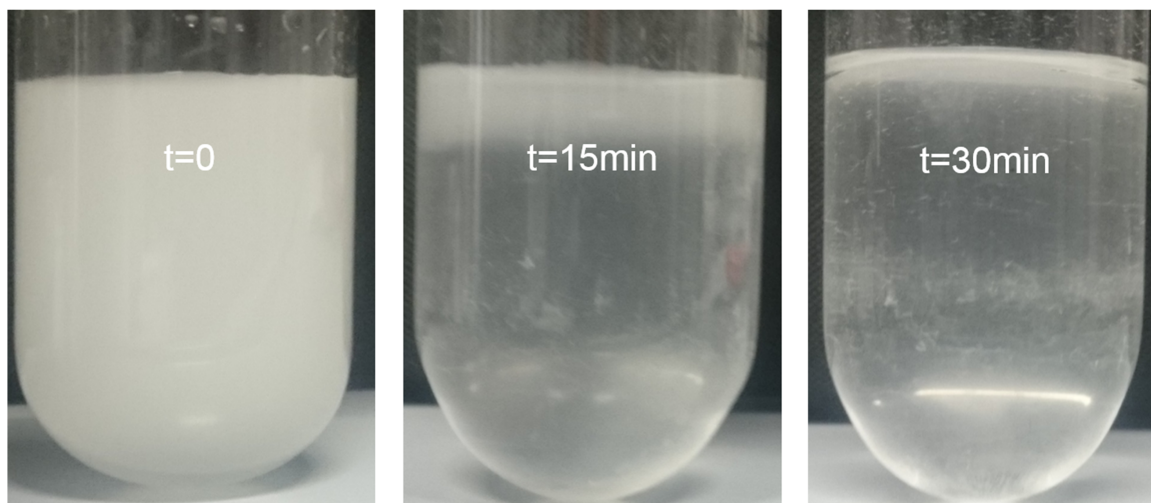


Figure 12.5.: Result of centrifugation at a centrifugation number of 3000 ($r=0.075\text{m}$ and 100 Hz)

12.3.2. FLOTATION

PRESSURIZED AIR FLOTATION

The pressurized air flotation has been performed with an emulsion consisting of 2 wt.% of solvent phase containing 0.1 wt.% 4-DBSA and SSK and deionized water as aqueous phase. In pictures 12.6 and 12.7 the beginning and the end after 35 minutes of flotation are depicted, respectively. Since there is hardly any difference in opacity, it is assumed that the bubble size produced by the frit is too large to split this emulsion. No further investigation of pressurized air flotation is performed.

ELECTROFLOTATION

The rod electrodes described in 8.4.2 serve as cathodes, while the expanded metal plate is used as anode. 5 different voltages, 3, 6, 9, 12 and 14.7 V have been applied to see the influence of the voltage on the separation efficiency. The result of all experiments is depicted in figure 12.8. It is obvious that the highest voltage leads to the highest separation rate. However, in the first 90 minutes the application of 12 or even 9 V lead to faster separation. The problem might be in this case that due to stochastic differences in bubble formation the emulsion brightness is increased faster at these lower voltages.

As can be seen in figure 12.9 the reproducibility is very good. This counteracts the theory of stochastic bubble formation. Another possible reason for the strange separation behaviour might be that there have been differences in electrode distance due to small differences in

12. RESULTS - SPLITTING OF STABLE EMULSIONS



Figure 12.6.: Pressurized air flotation at $t=0$



Figure 12.7.: Pressurized air flotation at $t=35$ min

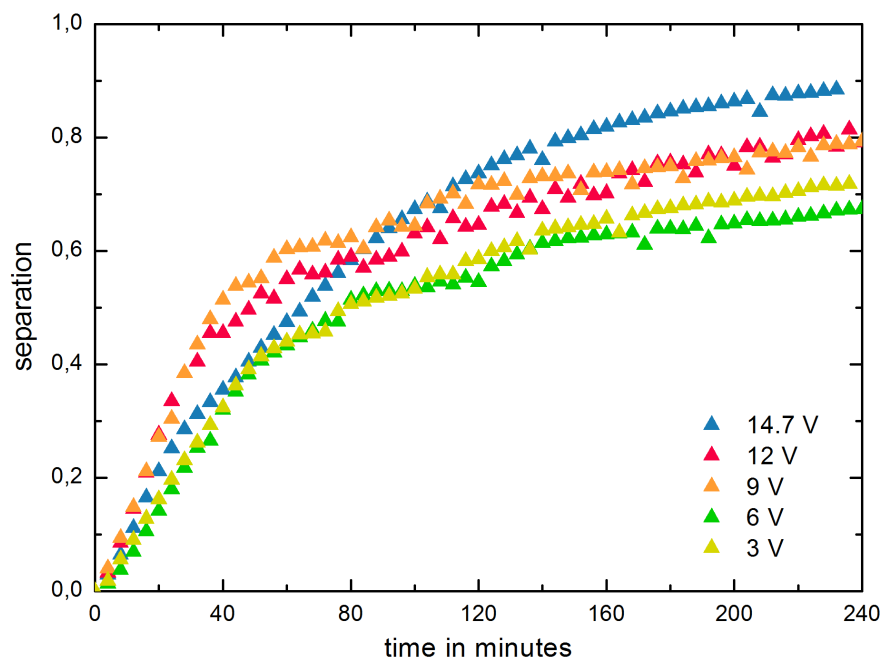


Figure 12.8.: Results of all electroflotation experiments

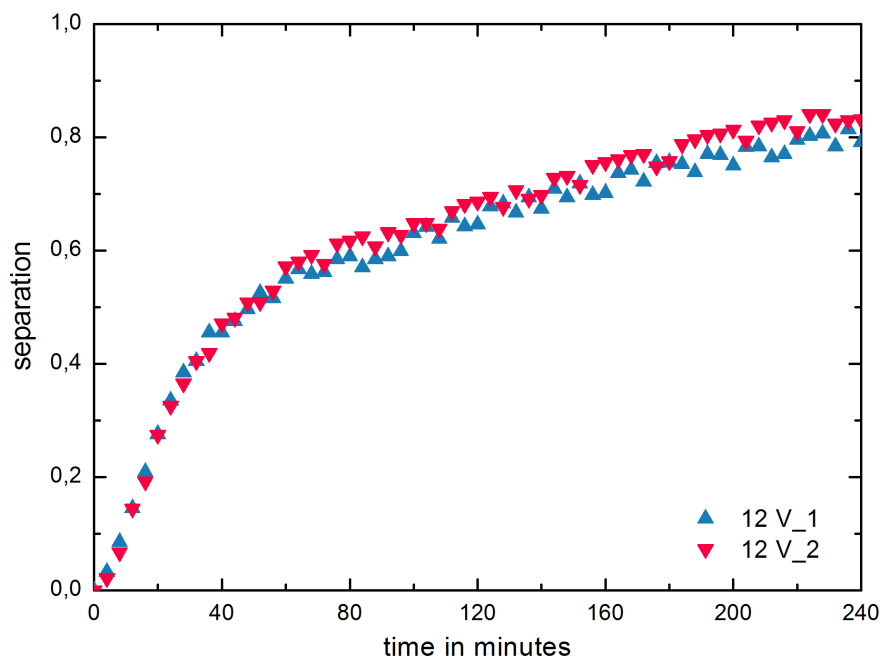


Figure 12.9.: Results of the electroflotation experiments at 12 V

setup. This would lead to higher electric field strengths at lower voltages and therefore to a higher bubble formation rate. A higher bubble formation rate would result in faster separation.

The experiments, which are not shown in this chapter, are depicted in appendix C.

12.4. ELECTRICAL SPLITTING - DIRECT CURRENT

Electrical splitting of o/w emulsions can only be performed in a DC field. The reason for this is that due to the higher electric conductivity of the aqueous phase compared to the solvent phase this would lead to electrolysis and therefore to another splitting principle (electro flotation, see chapter 12.3.2), which has not been the scope of this chapter. The diagrams depicted in the following chapters do not show all data points used in the modelling part in chapter 13. The reason for this is that the comparison of different experiments becomes difficult with increasing number of data points (compare figures 12.10 and 12.13, where the same experiments are depicted). Therefore, only every fourth data point is displayed in this section.

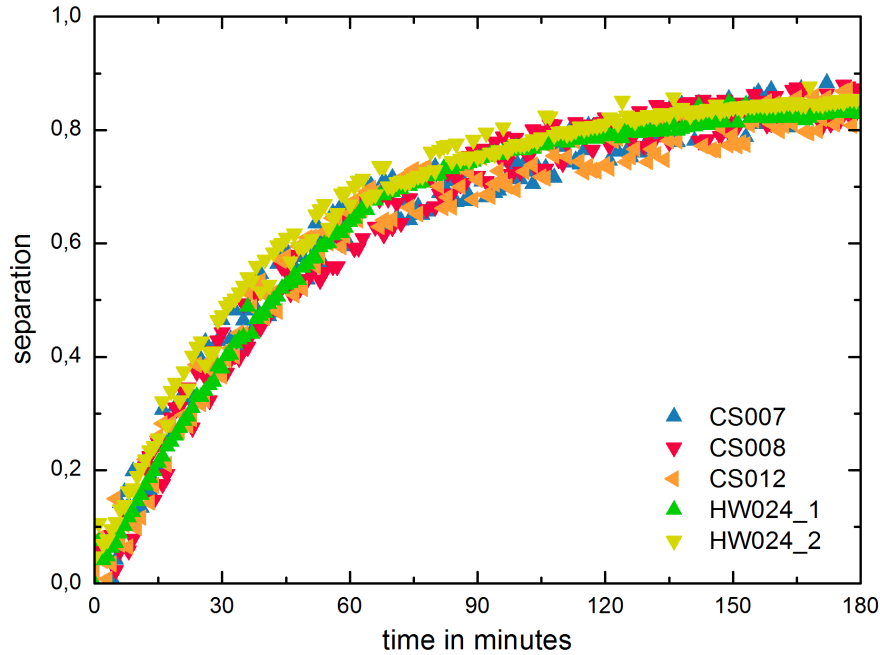


Figure 12.10.: Comparison of five experiments with two electrodes in a distance of 10 cm and an applied electric field strength of 100 V/m; all data points

12.4.1. REPRODUCIBILITY

The reproducibility of all setups is depicted in appendix E. In this chapter only two setups are discussed. The first setup is the preferably used, with the two electrodes arranged in a distance of 10 cm. In figure 12.11 three experiments with an applied electric field of 120 V/m are compared. It is obvious that the experimental data of these three experiments overlap very well. They show the same deviation around a mean value, the same slope and the same maximum separation after 3 hours.

The second setup is shown in figure 12.12. This example shows that reproducibility in this case is difficult to reach. Especially the experiment with the electrodes arranged in a distance of 10 cm and application of an electric field strength of 170 V/m and the experiment with the electrodes in a distance of 5 cm and an electric field strength of 339 V/m show deviations in the replicas. The reason for this is that the inclination was not adjustable to exactly 45 degrees but did deviate from the mean. This results in differences in electrode distance. These differences lead to differences in electric field, because the voltage is kept constant.

Since the general reproducibility is good, only one experiment per setting (number of electrodes, electrode angle, electrode distance and applied electric field strength) is used

12. RESULTS - SPLITTING OF STABLE EMULSIONS

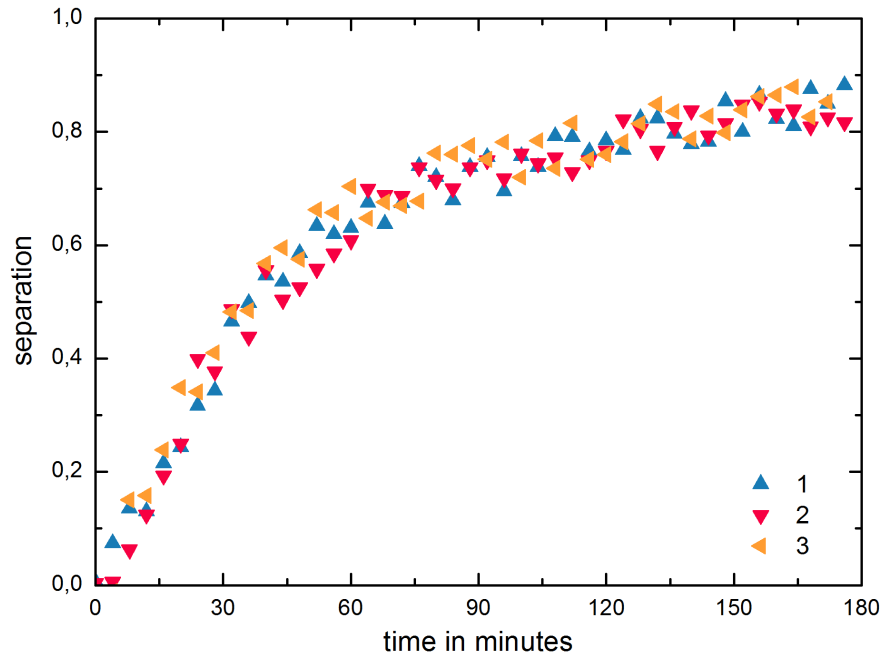


Figure 12.11.: Comparison of three experiments with two electrodes in a distance of 10 cm and an applied electric field strength of 120 V/m

for comparison. The comparison of all experiments of one setting is depicted in appendix E.

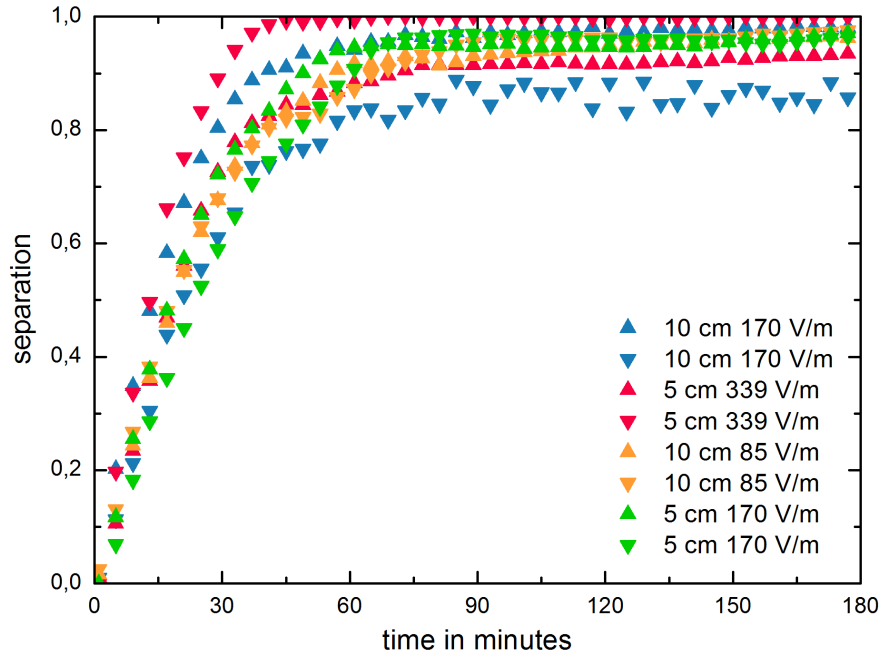


Figure 12.12.: Comparison of eight experiments with four different settings, where the two electrodes are inclined by 45 degrees with the anode on top of the cathode

12.4.2. COMPARISON OF DIFFERENT SETUPS

Figure 12.13 shows the comparison of three experiments in the standard cell and two experiments in the adopted cell, where inclined plates can be inserted. All experiments were performed with electrodes arranged in a distance of 10 cm and an electric field strength of 100 V/m. It can be seen that all experiments fit well together in slope at the beginning, the change in slope at 60 minutes and the final separation after 180 minutes. This confirms that the two setups are comparable despite the fact that the adopted cell contains approximately double the amount of emulsion.

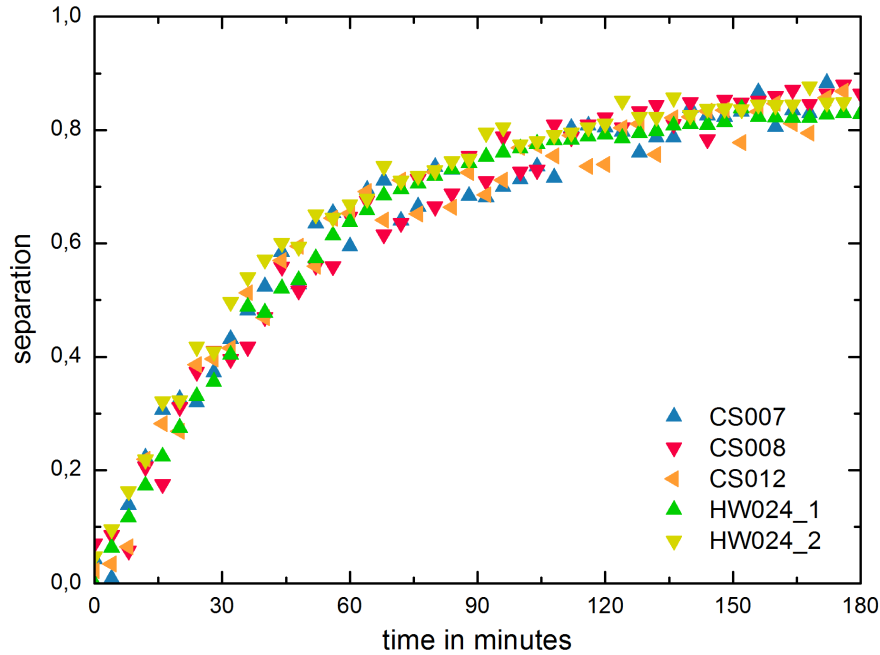


Figure 12.13.: Comparison of five experiments with two electrodes in a distance of 10 cm and an applied electric field strength of 100 V/m, where experiments 4 and 5 have been performed in a different vessel

12.4.3. RESULTS OF EXPERIMENTS WITH TWO PLATE ELECTRODES

In this chapter the results of the experiments carried out with two plate electrodes are discussed. The influence of the electrode distance at the same electric field strength is described. The same holds for the influence of the electric field strength at the same electrode distance. Additionally, the influence of the inclined plates is considered in these chapters. Furthermore, the arrangement of the inclined plates regarding whether the anode or the cathode is the upper electrode is investigated. Finally, the performance of the vertical arrangement of the plates is compared with the arrangement of the inclined plates.

INFLUENCE OF THE ELECTRODE DISTANCE AT A FIXED ELECTRIC FIELD STRENGTH

As can be seen in figure 12.14 there is hardly any difference identifiable in separation when comparing three experiments performed at an electric field strength of 100 V/m and electrode distances of 5, 10 and 15 cm. All experiments show the same slope, curvature and separation endpoint. This indicates that the electrode distance does not affect the separation rate and quality. The same holds for an electric field strength of 50 V/m and distances of 6, 12 and 24 cm (see figure 12.15). However, there is some different behaviour

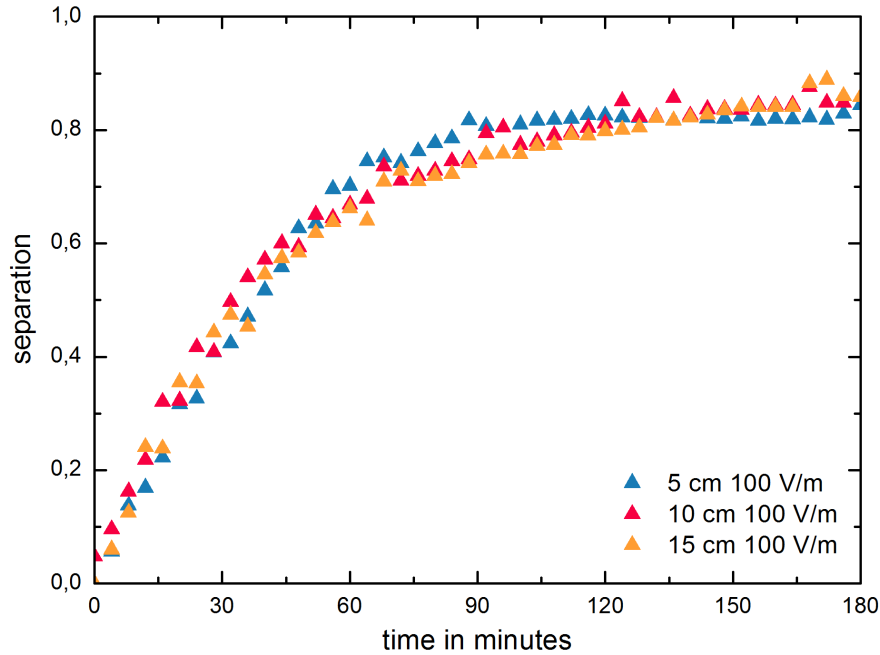


Figure 12.14.: Comparison of three experiments performed at 100 V/m and electrode distances of 5, 10 and 15 cm

observable at an electrode distance of 6 cm. In this experiment, the separation seems to be enhanced by the smaller distance. The slope is larger and the separation is finished much earlier than compared to an electrode distance of 12 and 24 cm.

INFLUENCE OF THE ELECTRIC FIELD STRENGTH AT A FIXED ELECTRODE DISTANCE

Figure 12.16 shows the influence of the electric field strength at a fixed electrode distance. It can be seen, that the separation increases with increasing electric field. Between 80 V/m and 100 V/m a step in splitting rate is visible. The differences in separation between 40 and 80 V/m and between 100 and 120 V/m is much smaller. The same holds for an electrode distance of 10 cm, where the same electric field strengths are compared (figure 12.17). The difference in separation between 80 V/m and 100 V/m compared to 40 and 80 V/m or 100 and 120 V/m is also much bigger in this case. However, the difference in separation between 40 and 80 V/m is bigger applying an electrode distance of 10 cm than compared to an electrode distance of 5 cm. This difference might result from experimental deviation.

12. RESULTS - SPLITTING OF STABLE EMULSIONS

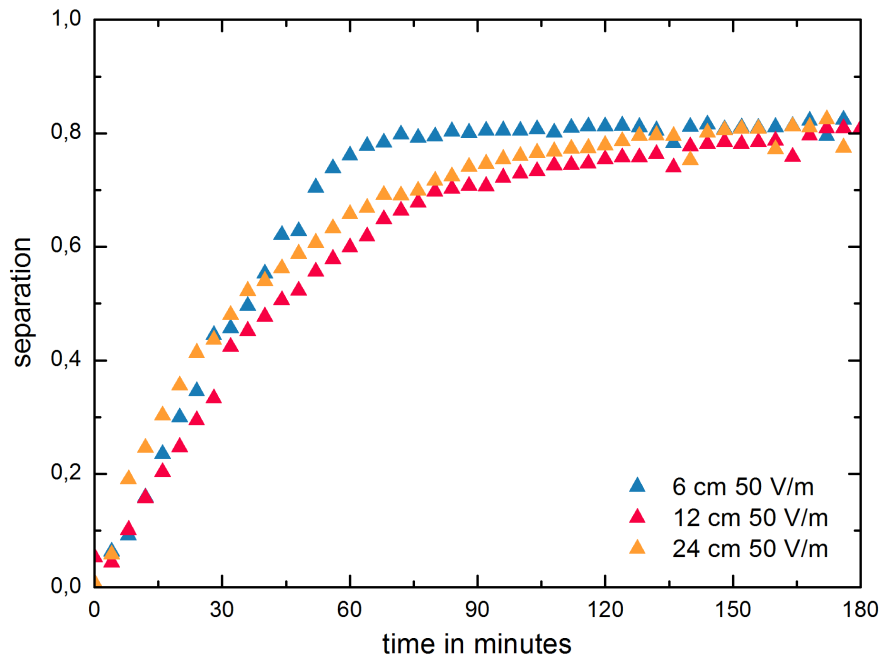


Figure 12.15.: Comparison of three experiments performed at 50 V/m and electrode distances of 6, 12 and 24 cm

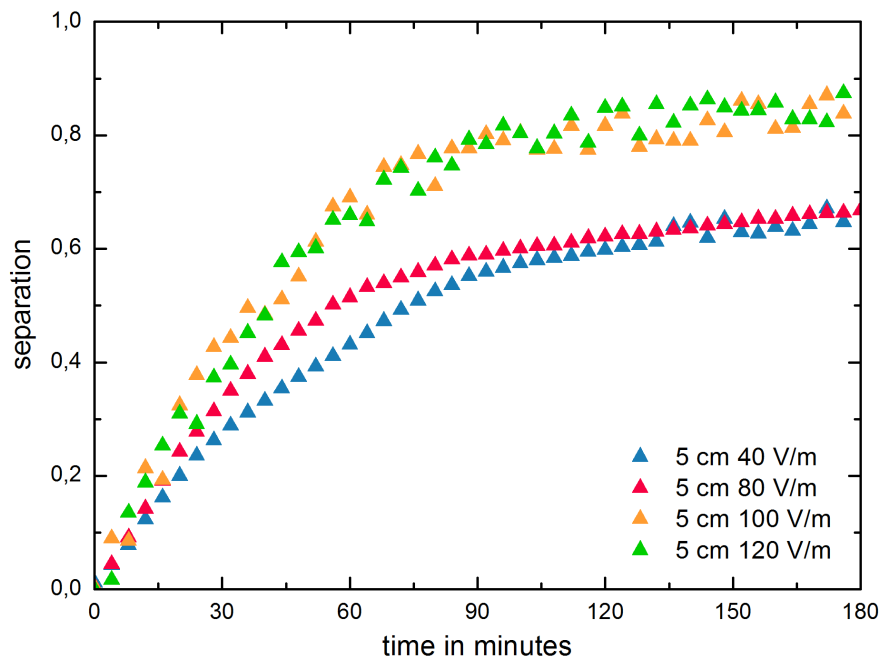


Figure 12.16.: Comparison of four experiments performed at 40, 80, 100 and 120 V/m and a fixed electrode distance of 5 cm

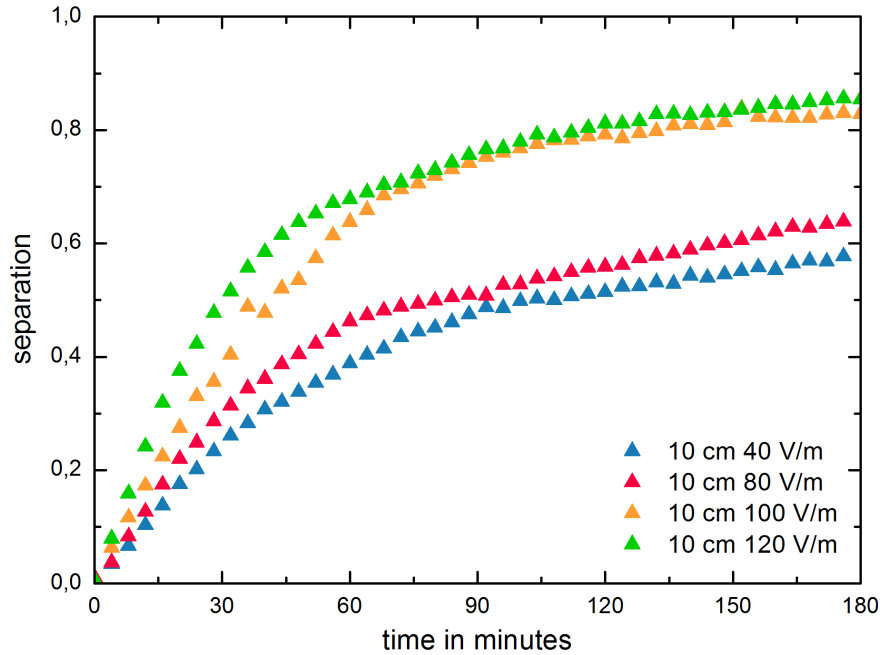


Figure 12.17.: Comparison of four experiments performed at 40, 80, 100 and 120 V/m and a fixed electrode distance of 10 cm

COMPARISON OF THE ARRANGEMENT OF INCLINED PLATE ELECTRODES

Since the reproducibility of experiments with inclined plates has not been very satisfactory, only qualitative findings are presented in this section. Using two inclined plates, it is advantageous to operate the upper electrode as the anode. In figure 12.18 all experiments with this electrode configuration perform better than the configuration placing the cathode above the anode. The abbreviation AnCa describes in a general way that the anode is the left electrode. Since the electrodes are inclined counter-clockwise, the anode becomes the lower electrode in this case. The inclination can be figured out best when comparing 12.19a and 12.19b.

COMPARISON OF THE SEPARATION USING VERTICAL PLATES AND INCLINED PLATE ELECTRODES

In figure 12.20 a comparison of two experiments with vertical and inclined plates is depicted. The other settings concerning electrode distance and electric field strength are nearly the same, which allows a comparison. As can be seen the inclined configuration with the anode as lower electrode performs better and additionally leads to a higher separation at the end of the experiment.

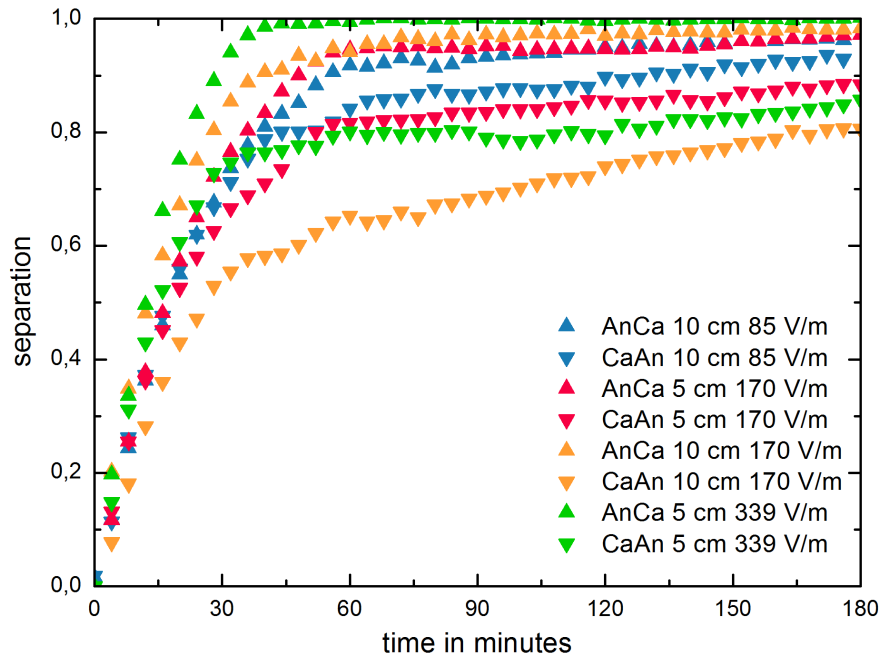


Figure 12.18.: Comparison of four experiments with an AnCa (cathode is the upper electrode) electrode configuration with four experiments at the same settings with an CaAn (anode is the upper electrode) electrode configuration



(a) Initial picture of an experiment using two vertical electrodes **(b)** Initial picture of an experiment using two inclined electrodes with CaAn configuration

Figure 12.19.: Electrode inclination

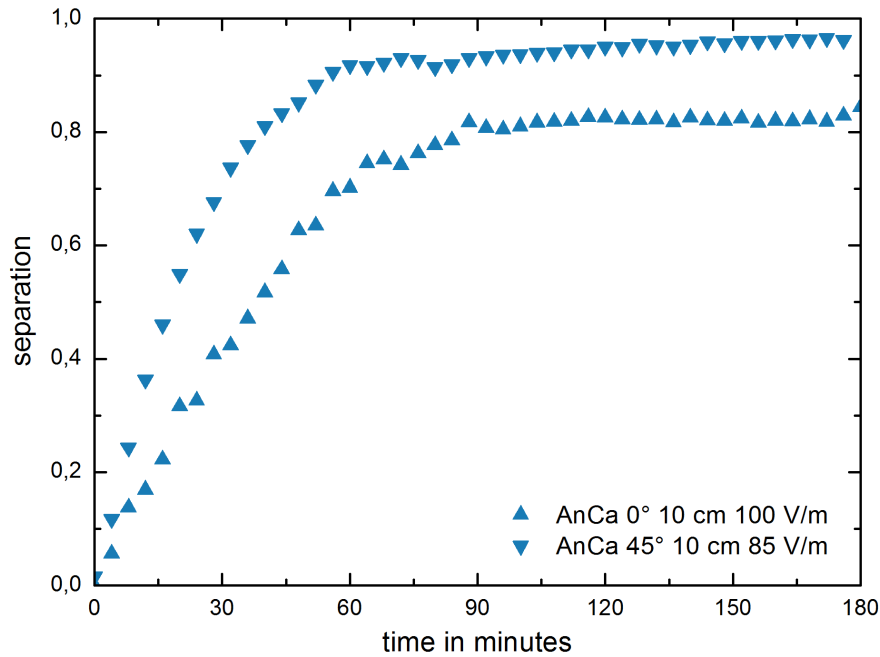


Figure 12.20.: Comparison of inclined (AnCa electrode configuration) with vertical plates at an electrode distance of 10 cm and at 85 and 100 V/m, respectively

12.4.4. RESULTS OF EXPERIMENTS WITH THREE PLATE ELECTRODES

In this chapter the results of the experiments carried out with three plate electrodes are discussed. Firstly, the influence of the electrode arrangement is investigated, since it is possible to use two anodes or two cathodes. Secondly, the results of experiments with different electrode distances at the same electric field strength are described. Thirdly, the influence of the electric field strength at the same electrode distance is discussed. Fourthly, the arrangement of the inclined plates regarding whether the anode or the cathode is the upper electrode is investigated and finally, the vertical arrangement of the plates is compared to the separation using inclined plates.

INFLUENCE OF THE ELECTRODE ARRANGEMENT

As can be seen in figure 12.21 the difference in performance regarding the separation is very small. However, the results indicate that the configuration CaAnCa performs better compared to the AnCaAn configuration. The reason for this could be the effect electrode edges have on field strength. If the anode is mounted between two cathodes, this effect might lead to better separation.

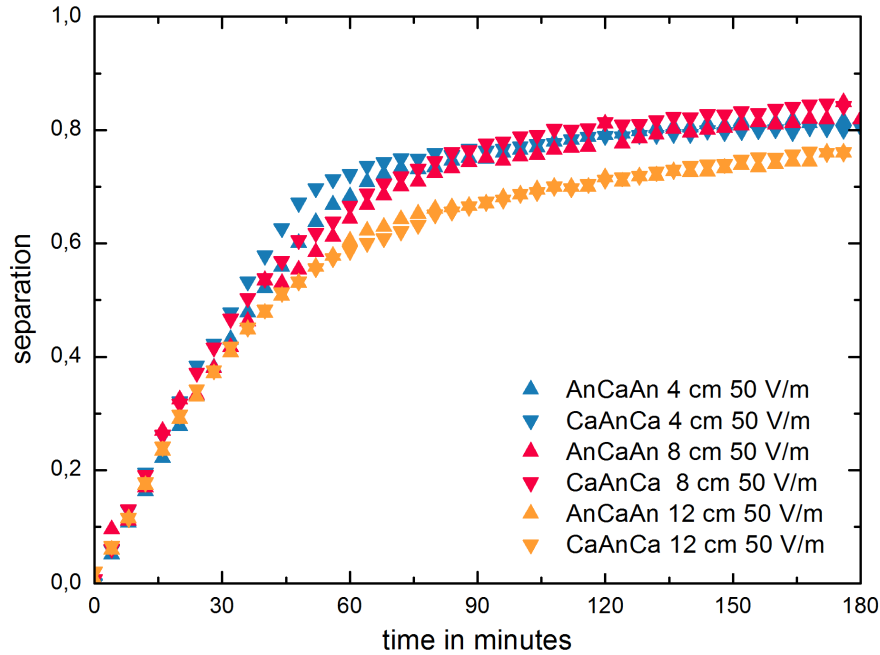


Figure 12.21.: Comparison of three experiments with an AnCaAn electrode configuration with three experiments at the same settings with a CaAnCa electrode configuration at a constant electric field strength of 50 V/m

The results at a constant electric field strength of 100 V/m, depicted in figure 12.22 show different behaviour. On the one hand, the configuration AnCaAn performs as good as the CaAnCa configuration and leads to the same separation after 180 minutes at 5 and 12 cm. On the other hand, applying an electrode distance of 4 or 8 cm, the CaAnCa configuration shows better separation after 180 minutes.

INFLUENCE OF THE ELECTRODE DISTANCE AT A FIXED ELECTRIC FIELD STRENGTH

As in chapter 12.4.3 the electrode distance with the same applied electric field strength affects neither the separation efficiency nor the separation speed. This can be seen in figure 12.21 and figure 12.22, where constant electric field strengths of 50 and 100 V/m are applied, respectively. In the latter case, a difference in separation can be seen. However, a tendency is not observable since the fastest separation is shown when applying an electrode distance of 8 cm. The second fastest separation can be observed mounting the electrodes in a distance of 4 cm, followed by 12 cm and finally 5 cm. It is assumed that this ranking is of coincidental nature, since the differences are not very large.

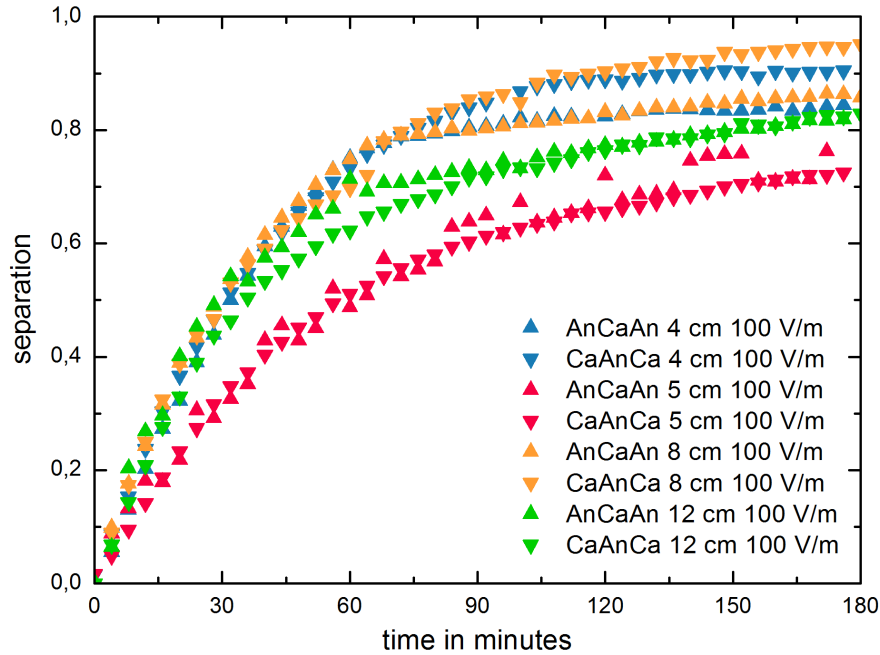


Figure 12.22.: Comparison of four experiments with an AnCaAn electrode configuration with four experiments at the same settings with an CaAnCa electrode configuration at a constant electric field strength of 100 V/m

INFLUENCE OF THE ELECTRIC FIELD STRENGTH AT A FIXED ELECTRODE DISTANCE

The influence of the electric field shows similar behaviour for two and three electrodes. As in chapter 12.4.3, the separation speed and separation maximum increase when applying an electric field strength of 50, 100, or 200 V/m on electrodes arranged in a distance of 4 cm (figure 12.23). In contrast to the installation of two electrodes, with a gap between 80 and 100 V/m, no gap is visible between 50 and 100 V/m installing three electrodes. The same observation can be made for the results of the experiments, where three electrodes are arranged in a distance of 8 cm (figure 12.24).

COMPARISON OF THE ARRANGEMENT OF INCLINED PLATE ELECTRODES

The behaviour observed in chapter 12.4.3, where two electrodes inclined by 45° are mounted, can not be seen in figure 12.25, where three electrodes are inclined. In this case, the CaAnCa configuration is faster compared to the AnCaAn configuration, no matter, which combination of electrode distance and electric field strength is applied. However, the difference is not as large as when arranging two inclined electrodes in the AnCa or CaAn configuration, but is comparable to the results of three vertical plates. In this case

12. RESULTS - SPLITTING OF STABLE EMULSIONS

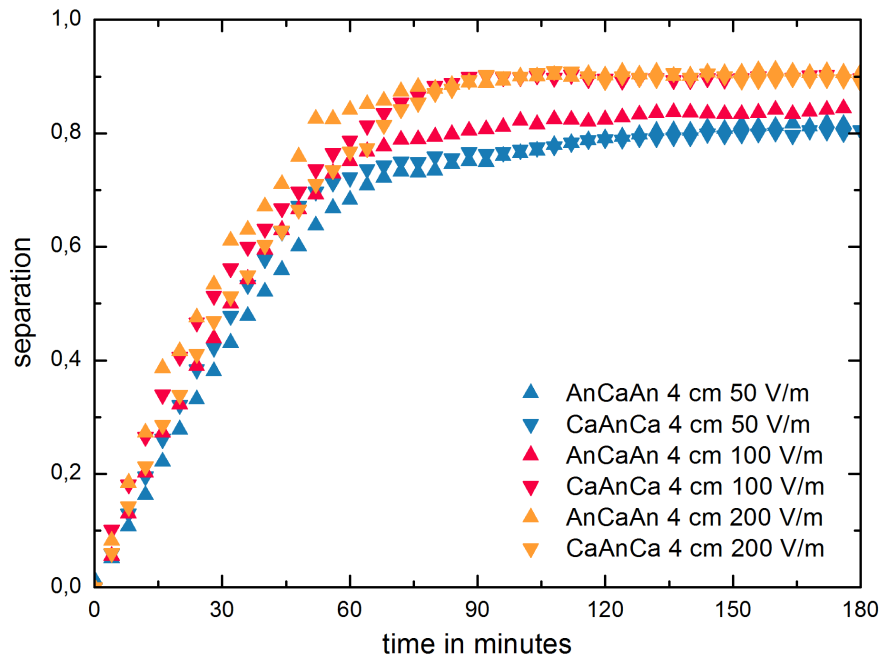


Figure 12.23.: Comparison of three experiments with an AnCaAn electrode configuration with three experiments at the same settings with a CaAnCa electrode configuration at a constant electrode distance of 4 cm

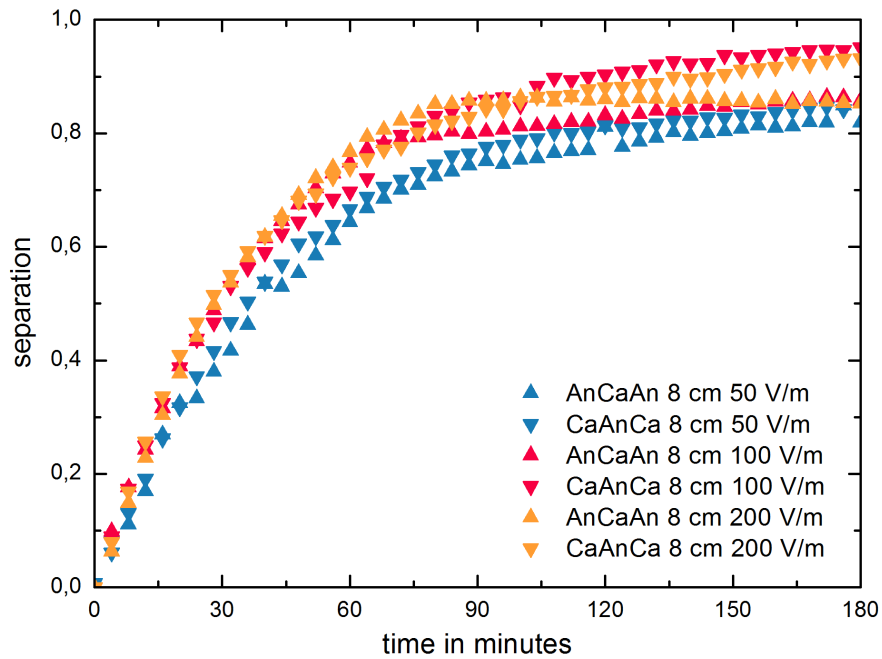


Figure 12.24.: Comparison of three experiments with an AnCaAn electrode configuration with three experiments at the same settings with a CaAnCa electrode configuration at a constant electrode distance of 8 cm

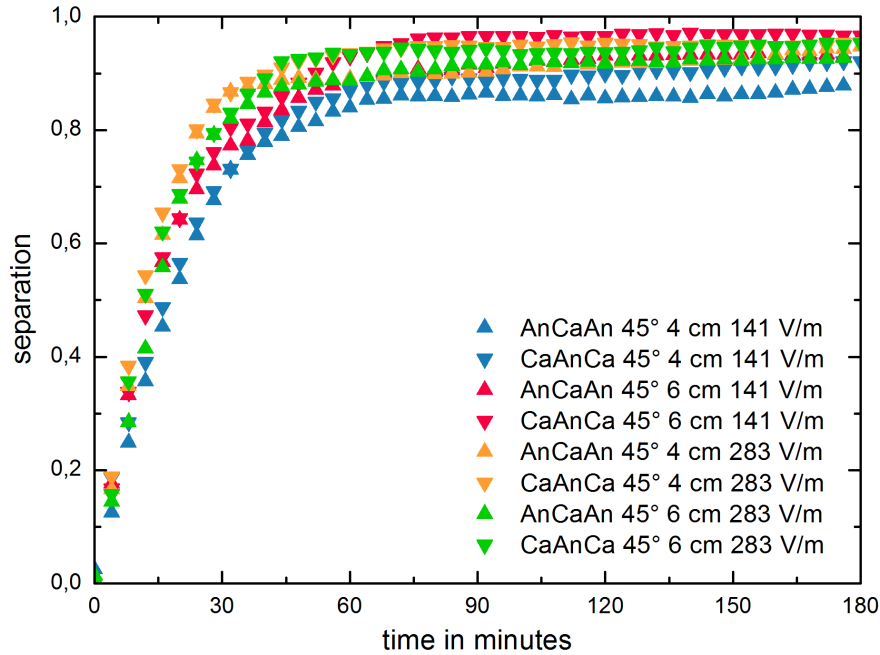


Figure 12.25.: Comparison of four experiments with an AnCaAn electrode configuration with four experiments at the same settings with a CaAnCa electrode configuration and an electrode inclination of 45°

also the CaAnCa configuration is the better one. The reason might be the same. The effects at the edges of the electrodes, especially of the anode, might lead to better separation.

COMPARISON OF THE SEPARATION USING VERTICAL PLATES AND INCLINED PLATE ELECTRODES

The comparison of the results using three inclined or three vertical plates shows that like in chapter 12.4.3 the inclination accelerates the separation. This can be seen in figure 12.26. The application of three inclined plates leads to much faster emulsion splitting, which is visible looking at the big slope of the separation curve. The splitting process is finished after 90 minutes. Additionally, the separation value reached at the end of the experiment is 0.2 higher compared to the result obtained using three vertical plates.

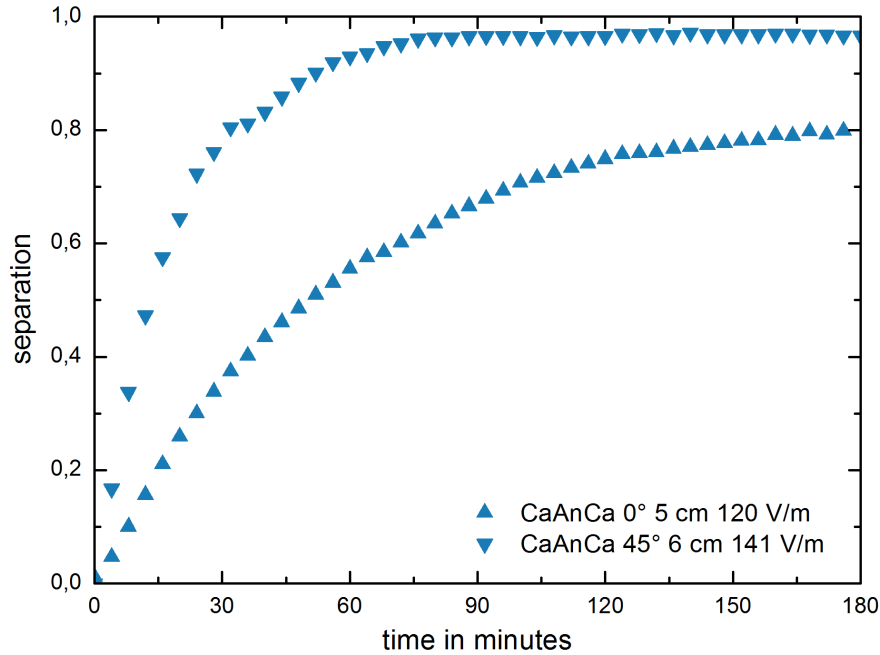


Figure 12.26.: Comparison of inclined with not inclined plates at an electrode distance of 10 cm and an electric field strength of 85 and 100 V/m, respectively; both CaAnCa electrode configuration

12.4.5. RESULTS OF EXPERIMENTS WITH FOUR PLATE ELECTRODES

As can be seen in figure 12.27 the splitting of the emulsion also works with four plate electrodes. However, there is an intersection between the results of an electric field strength of 300 V/m applied on electrodes in a distance of 1 cm and 100 V/m applied on electrodes in a distance of 3 cm. Possibly, there is an interaction of the droplets with the electrodes arranged in a distance of 1 cm to each other. Another option is that electrolysis occurs at this high operation voltage. Looking at figure 12.28, which shows the experiment at an electric field strength of 300 V/m at the end of the observation, obviously electrolysis occurred. The same holds for an electric field strength of 200 V/m. The end of this experiment is depicted in figure 12.29. However, the application of four plate electrodes works very well and shows a high splitting rate and a high separation at the end of the splitting process. When applying an electric field strength of 200 V/m the splitting process is finished after 90 minutes, while it takes 130 minutes when only 100 V/m are applied. The application of 300 V/m on electrodes mounted in a distance of 1 cm leads to an earlier end of separation. However, this end is at a lower level compared to the experiment with an applied electric field strength of 200 V/m. Additionally, the separation decreases again, which is also an indication for electrolysis, because raising bubbles could pull already separated droplets into the emulsion again.

12. RESULTS - SPLITTING OF STABLE EMULSIONS

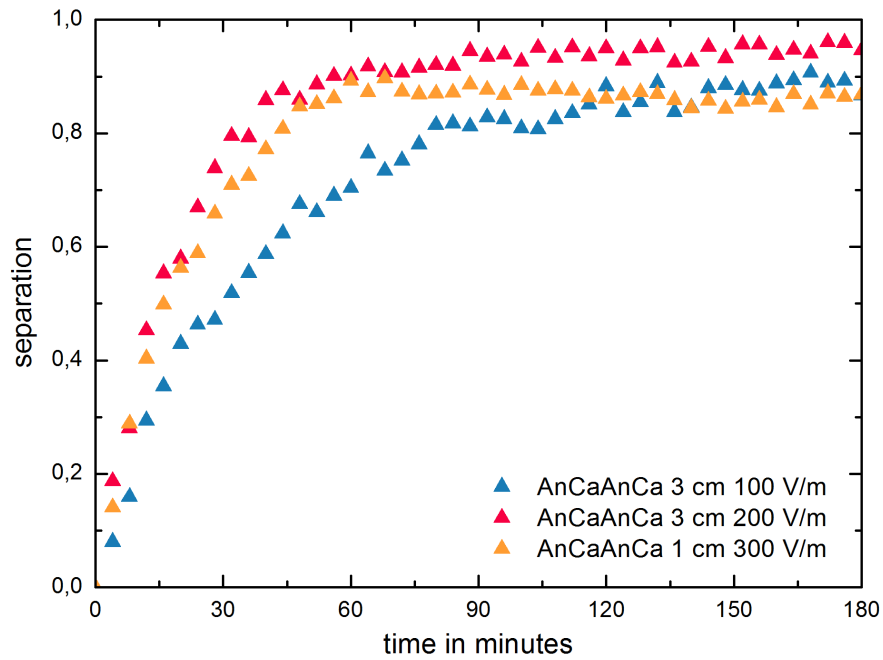


Figure 12.27.: Comparison of three experiments with four plate electrodes at an electric field strength of 100, 200 and 300 V/m



Figure 12.28.: Electric splitting experiment using four plate electrodes after 3 hours at an electric field strength of 300 V/m



Figure 12.29.: Electric splitting experiment using four plate electrodes after 3 hours at an electric field strength of 200 V/m

12.4.6. RESULTS OF EXPERIMENTS WITH FOUR PLATE ELECTRODES AND 3 TIMES 4 ROD ELECTRODES

In figure 12.30 three experiments, which have been performed using four plate electrodes and 3x4 rod electrodes, are depicted. The difference between them is the connection to the power supply and the applied voltage. It can be seen that the rod electrodes used as anodes deliver faster separation compared to the experiment, where the plate electrodes act as anodes. The reason for this behaviour might be the addition of electrophoresis of the anionic surfactant on the droplet surface and dielectrophoresis due to the inhomogeneous electric field, which is not the case, if the plate electrodes are used as anodes. Additionally, it is obvious that higher electric field strength leads to faster separation.

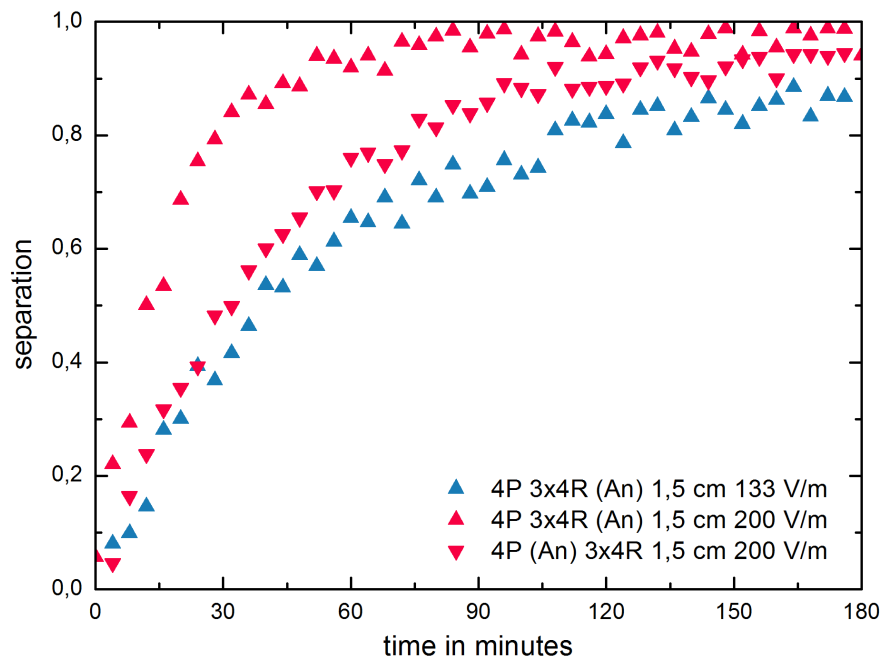


Figure 12.30.: Comparison of three experiments with four plate electrodes and three times four rod electrodes; two experiments, where the rods are connected as anode and one, where the plate electrodes are used as cathode

12.4.7. COMPARISON OF THE DIFFERENT ELECTRODE ARRANGEMENTS

Figure 12.31 shows the results of six different electrode setups at approximately the same electric field strength. It can be seen, that the setup with three electrodes in CaAnCa configuration inclined by 45° works best (141 V/m), followed by the setup with two inclined plates in AnCa configuration (85 V/m). These two show very similar separation speed and final separation. Both finish separation after 90 minutes at a separation of approximately 0.95. After 180 minutes, the setup containing three vertical electrodes in CaAnCa configuration also reaches this separation. However, the other setups, namely the application of two and four vertical plates and the application of four plate and 3x4 rod electrodes, which serve as the anode, with an electric field strength of 100, 100 and 133.3 V/m, respectively, do not reach this separation within the experimental time. These three experiments show similar speed and final separation.

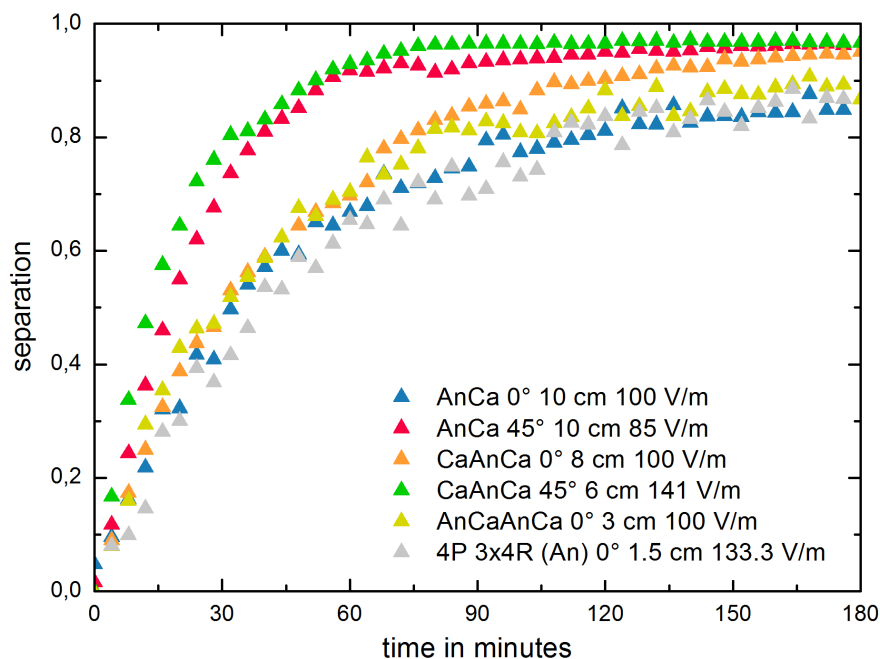


Figure 12.31.: Comparison of six different setups

12.4.8. ELECTRICAL SPLITTING OF A MULTI COMPONENT SYSTEM USING FOUR PLATE ELECTRODES

In this section the splitting experiments with the model effluent explained in 8.1 are discussed based on the optical comparison of the experiments. Four plate electrodes have been mounted and an electric field strength of 50 V/m was applied. Higher electric field strengths were not possible due to electrolysis. Due to the higher amount of surfactant electrolysis occurred at lower electric field strengths compared to the experiments explained before. The reason for this is the higher ion concentration in the emulsion, if more anionic surfactant is used. As can be seen in figure 12.32 the emulsion produced with methanol was very stable, even in the electric field. The height difference of the emulsion between the figures 12.32a and 12.32b results from air release, which has been inserted due to the intense mixing before the separation experiment. With increasing time a dense packed layer was formed, which was stable even after 21 hours (see figure 12.32h). Only a small layer of solvent phase formed after 9 hours (see figure 12.32d), which slightly increased. It is obvious that this emulsion cannot be split with the applied electric field.

A different result can be observed discussing the pictures in figure 12.33, where the emulsion splitting experiment with butanol used as alcohol for the esterification is shown. The splitting process is finished after 12 hours and clear aqueous and solvent phase can be formed.

When using octanol, which is virtually insoluble in water, for the reaction, a similar emulsion was formed as when using the completely soluble alcohol methanol. Again a dense packed zone was formed, as can be seen in figure 12.34. The progress in the experiment shows that some sedimentation occurred with increasing time. This sedimentation can be seen as the bottom of the vessel got more translucent. The bright zone increased with time. However, no separation occurred, since the emulsion remained cloudy even after 21 hours.

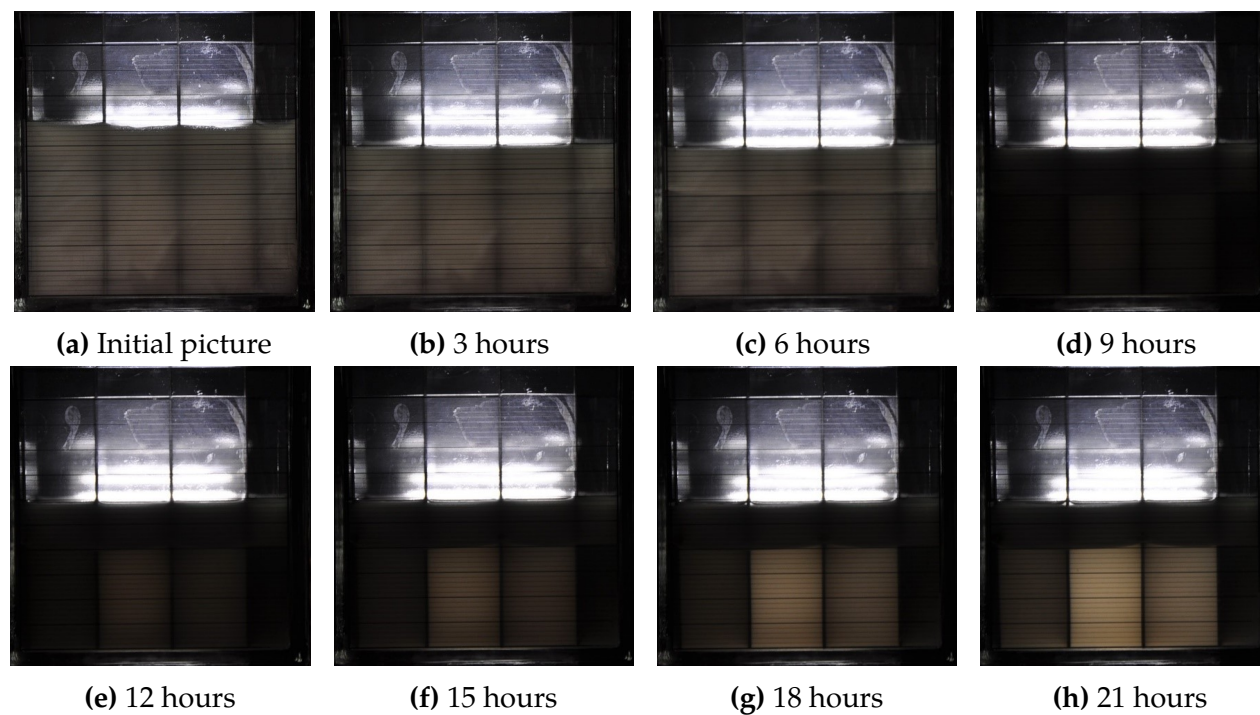


Figure 12.32.: Separation progress when applying an electric field strength of 50 V/m on an emulsion resulting from the esterification process of acetic acid with methanol

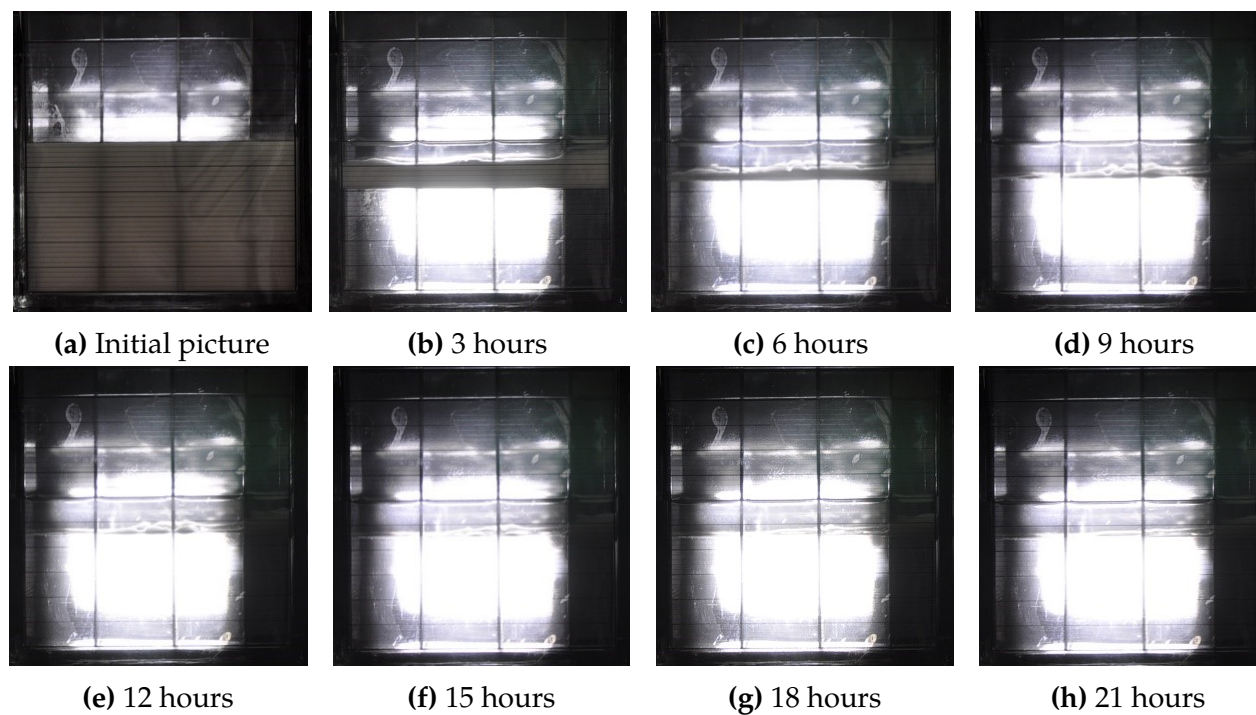


Figure 12.33.: Separation progress when applying an electric field strength of 50 V/m on an emulsion resulting from the esterification process of acetic acid with butanol

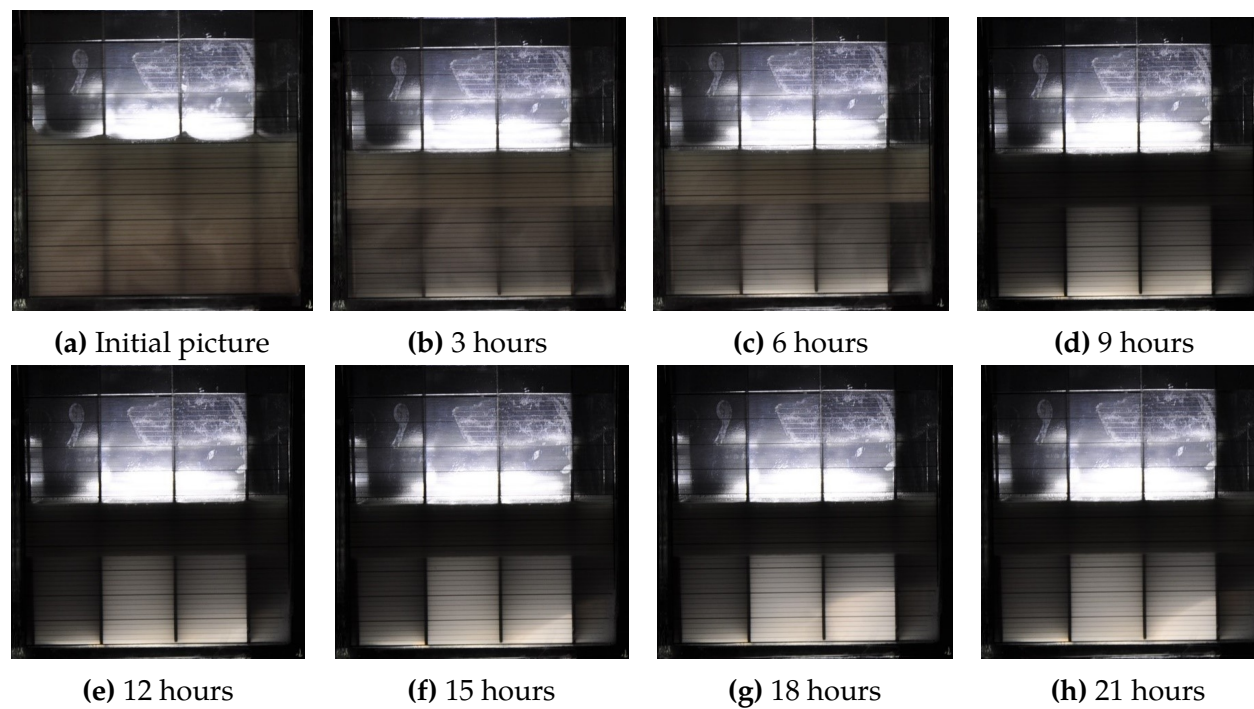


Figure 12.34.: Separation progress when applying an electric field strength of 50 V/m on an emulsion resulting from the esterification process of acetic acid with octanol

13. RESULTS - MODELLING OF THE ELECTRIC FIELD

SPLITTING PROGRESS

In this chapter the results of modelling are compared with the separation data of the corresponding experiments.

Figures 13.1 and 13.2 show the conformance between the model and the experimental data for different settings. One can conclude that the inaccuracy is very small. This goes along with the r^2 of the models, which is always greater than 0.96 (for more information, see chapter F in the appendix). In figure 13.3 5 experiments using two vertical plates arranged in a distance of 10 cm with an applied electric field strength of 100 V/m are compared. It is obvious that the model curves are all very similar and, considering their inaccuracies, the same separation degree is obtained after 180 minutes.

With the model described in chapter 10, the droplet diameter of the smallest droplet removable by a distinct setup can be calculated (equation 10.33). The connection between the electric field strength at a fixed electrode distance of 10 cm and the calculated droplet diameter is depicted in figures 13.4. In figure 13.5 the connection between the electrode distance at a fixed electric field strength of 100 V/m and the calculated droplet diameter is shown. Additionally, the values of the calculated droplet diameters and the corresponding electric field strengths or electrode distances are summarized in tables 13.1 and 13.2, respectively. The figures and the tables indicate that there is a systematic relation between these parameters. A low applied electric field strength does address large droplet diameters. The same holds for large electrode distances. The reason for this behaviour can be found in equation 10.28. For readability reasons this equation is reprinted in equation 13.1. It is obvious that for large values of the electric field strengths E_0 the rate of migration w becomes large, too. The larger w , the smaller the droplets, which can be removed within the same time span. With a small rate of migration, only larger droplets can be removed in a distinct time span, which leads to slow separation. This effect is depicted in 13.6. There, droplets of three dropsizes move in the electric field. Due to their different size, the rate of migration differs. It is obvious, that larger drops reach the electrodes faster than the smaller drops within the same time span at the same electric field strength. With increasing electric field strength, the rate of migration increases and does address smaller droplets to be removed within the same time span. This leads to a brighter picture and therefore to a higher separation value.

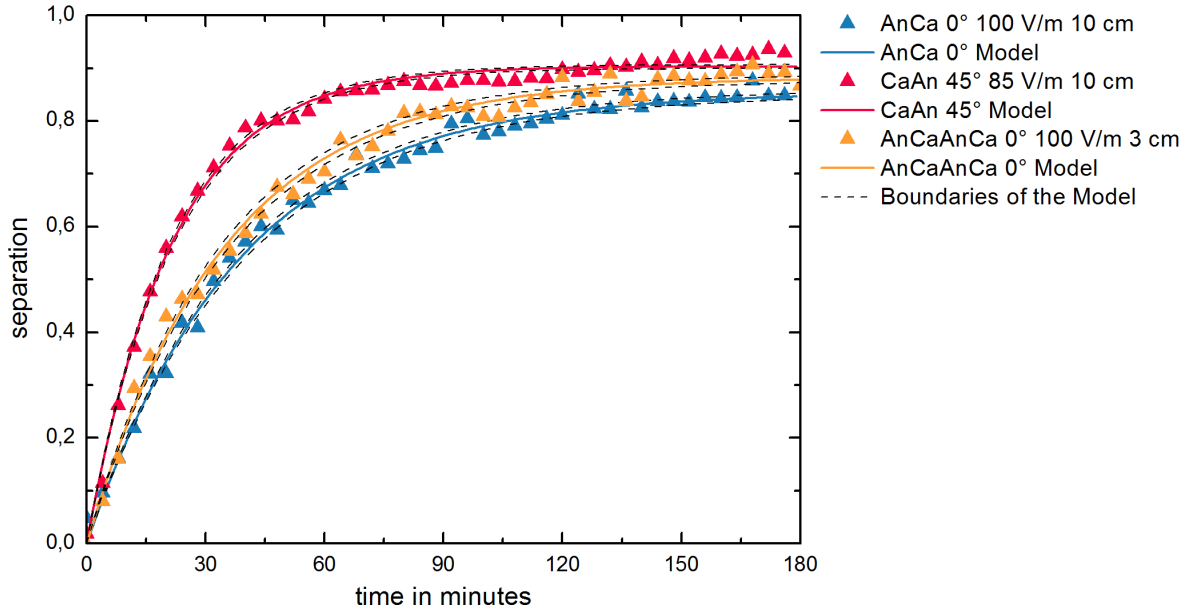


Figure 13.1.: Comparison of the model with experiments using two electrodes with an inclination of 0 and 45° as well as an experiment with four electrodes used

The correlation between the electrode distance and the observed droplet diameter, shown in figure 13.5, can be understood when discussing figure 13.7. There, uniform droplets move due to the applied electric field. Until they reach a surface (an electrode) the brightness and therefore the separation does not change. If, at a distinct time, a droplet reaches the electrode, the separation value increases (left marked droplet). The separation of droplets of the same diameter can be enhanced when reducing the electrode distance (right marked droplet).¹ Additionally, as described above, a larger droplet diameter leads to faster separation at a distinct electric field strength. Smaller droplets can be efficiently separated when using smaller electrode distances, which can be seen in figure 13.5.

$$w(x) = \frac{E_0^2 \cdot x}{4 \cdot \pi \cdot \eta_c} \quad (13.1)$$

¹The reduction in distance is visualised with a third electrode placed in the middle of the equipment. In fact, the direction of migration would change on one side of this third electrode due to the change in polarisation. For simplification reasons, this is not shown in the figure.

13. RESULTS - MODELLING OF THE ELECTRIC FIELD SPLITTING PROGRESS

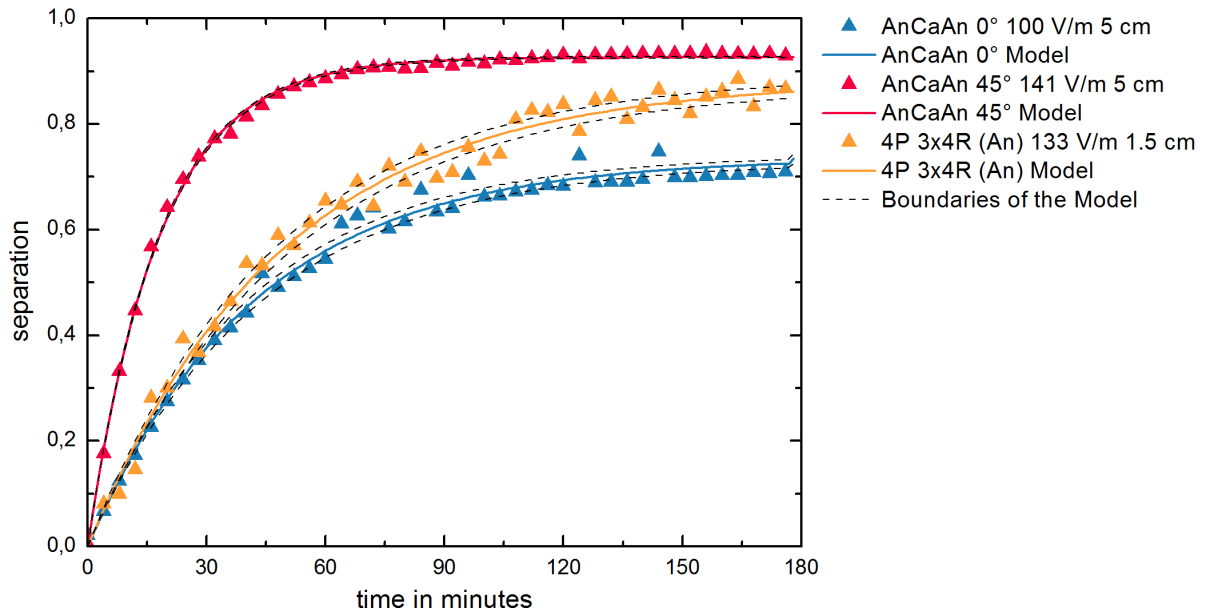


Figure 13.2.: Comparison of the model with experiments using three electrodes with an inclination of 0 and 45° as well as an experiment with four plate electrodes and 3x4 rod electrodes (An) used

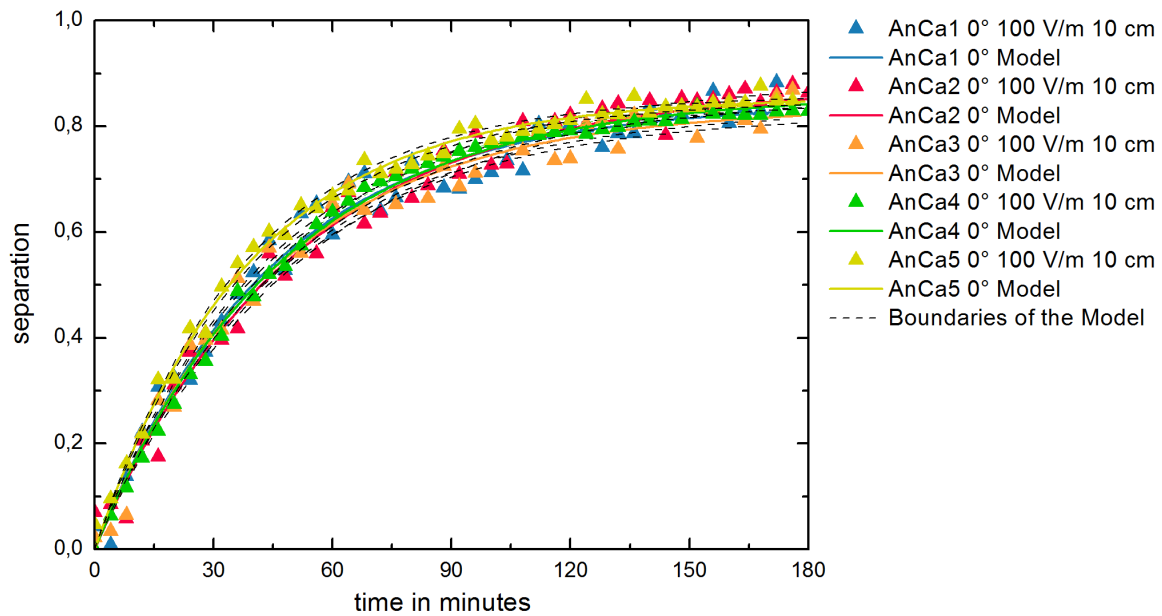


Figure 13.3.: Reproducibility of the model applied to five experiments with two plate electrodes in a distance of 10 cm and an electric field strength of 100 V/m

13. RESULTS - MODELLING OF THE ELECTRIC FIELD SPLITTING PROGRESS

Table 13.1.: Influence of the electric field strength on the droplet diameter at a constant electrode distance of 10 cm

<i>Electric field strength</i> V/m	<i>Droplet diameter</i> μm
40	2.1
60	1.3
80	0.6
100	0.5
120	0.4

Table 13.2.: Influence of the electrode distance on the droplet diameter at a constant electric field strength of 100 V/m

<i>Electrode distance</i> cm	<i>Droplet diameter</i> μm
5	0.2
10	0.5
15	0.6

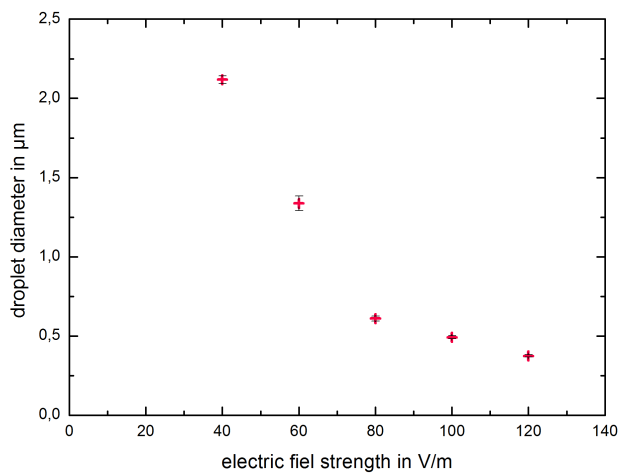


Figure 13.4.: Correlation between the droplet diameter and the electric field strength at a constant distance of 10 cm, error bars in black

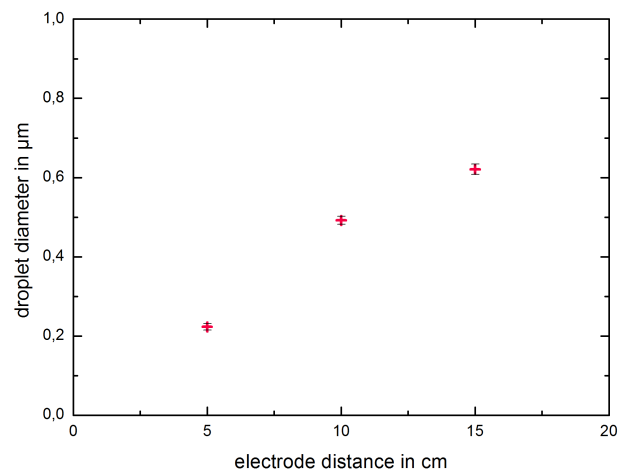


Figure 13.5.: Correlation between the droplet diameter and the electrode distance at a constant electric field strength of 100 V/m, error bars in black

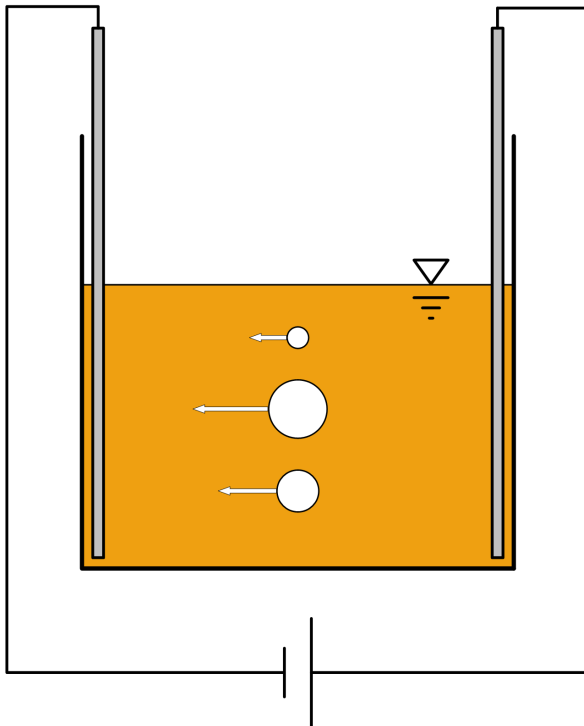


Figure 13.6.: Visualisation of the rate of migration for different drop diameters at the same electric field intensity

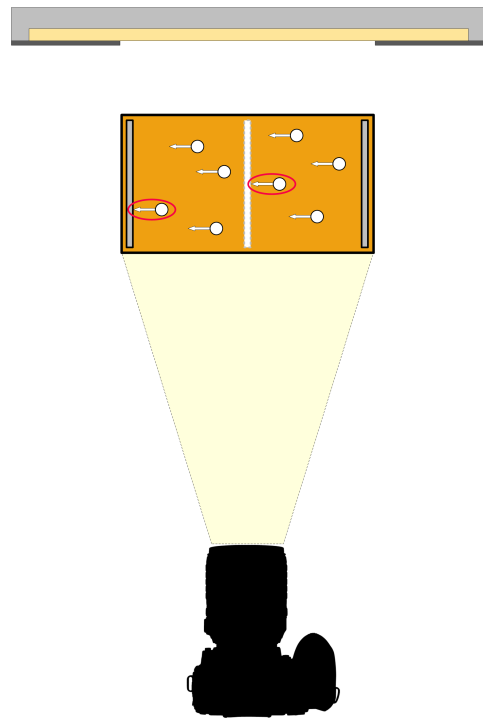


Figure 13.7.: Difference in separation for different electrode distance/number of electrodes; marked droplets separate

14. SUMMARY

The scope of this work was to investigate the separation behaviour of emulsions with a very low amount of solvent phase dispersed in the aqueous carrier phase in the electric field. The equipment was to be optimized regarding number, shape and inclination of the electrodes. For comparison other emulsion splitting techniques had to be investigated, too. A model based on physical data of the system was developed.

In a first step, the preparation of stable emulsions classified as turbidity was investigated. Agitation rate as well as hold-up were varied. The variation of the agitation rate showed a maximum separation time at approximately 1500 rpm, while the settling time increased with increasing hold-up of the solvent phase. The admixture of a surfactant stabilised the emulsion.

After preparing stable emulsions, the splitting process was investigated. The focus was laid on the splitting under electric field force. For comparison reasons also thermal, chemical and mechanical splitting were investigated.

Thermal splitting did not show good separation. The energy input was huge (46.5 kWh/m³ emulsion) and the emulsion did evaporate during the experiment (approximately 17 % in 4.75 h).

Chemical dissolution of the insoluble solvent phase using isopropyl alcohol did break turbidity. However, 660 l of isopropyl alcohol were necessary to dissolve the solvent phase per m³ of emulsion. The admixture of isopropyl alcohol increased the TOC-value by a factor of 100. Therefore, this kind of turbidity control is not applicable in industrial scale. It is limited to analytical applications to prepare emulsions for titration purposes.

Two techniques of the mechanical splitting have been investigated. On the one hand, centrifugation was tested. This technique showed fast separation (30 minutes at a centrifugation number of 3000). However, the high investment and operating cost oppose the application of centrifugation. On the other hand, two techniques of flotation were investigated. While pressurized air flotation could not be used to control turbidity, electroflotation showed fast separation.

Emulsion splitting under electric field force was investigated in deeper detail. Firstly, experiments with a two plate electrode setup were investigated for the effect of the electrode distance, the electric field strength and the inclination of the electrodes on turbidity control. The results show that there was hardly any difference in separation, when the electrode distance was varied at constant electric field strength. The higher the electric

14. SUMMARY

field strength at given electrode distance, the faster the progress of separation was. With two inclined plate electrodes, experiments did show that the upper electrode should be used as cathode, giving a clear indication for the particle surface charge. The comparison of the inclined with the vertical electrode arrangement showed that the inclined arrangement is favorable over the vertical arrangement of electrodes.

Experiments regarding the optimal arrangement of three plate electrodes were then performed. The results indicate that the configuration CaAnCa (cathode – anode – cathode) performed better compared to the AnCaAn (anode – cathode – cathode) configuration. Comparable to the experiments with two electrodes, the electrode distance did not have an influence on the separation. The influence of the electric field strength correlated with the separation in the same way for two and three electrode setups. The same held for the inclined arrangement. Again, the inclined setup led to faster separation compared to the vertical arrangement of the electrodes. The comparison of the inclined setups showed, that the CaAnCa configuration did control turbidity faster compared to the AnCaAn configuration. The combination of electrode distance and electric field strength did not have an influence on this finding.

Then, the performance of a four vertical plate electrode setup was investigated. In this setup high electric field strength was applied, which led to electrolysis above 200 V/m. However, the application of four plate electrodes worked very well and showed a high splitting rate and a high degree of phase separation at the end of the splitting process.

For comparison reasons the effect of inhomogeneous electric field with four plate electrodes and 3x4 rod electrodes was investigated. In this setup, faster separation was observed for rod electrodes as anodes. The increase of electric field strength led to an improvement of phase separation.

After the experiments have been performed, the different electrode arrangements were compared at approximately the same electric field strength. The setup with three electrodes arranged in CaAnCa configuration inclined by 45° showed the best performance of all setups. The application of two inclined plates in AnCa configuration showed comparable results.

The behaviour of the emulsions produced from treating a model effluent under the influence of the electric field was investigated. For that purpose acetic acid in the effluent was esterified with different alcohols. An electrode setup consisting of four vertically arranged plate electrodes was used for these experiments. When methanol was used as alcohol for the esterification process, the splitting was not possible while the usage of butanol led to complete separation after 12 hours. When using octanol, an emulsion similar to that when using the completely soluble alcohol methanol was formed.

14. SUMMARY

The model developed in this project was derived from a balance for the splitting equipment. It showed good accordance with the experimental data and allowed to determine the smallest droplet removable by a distinct setup and specified operation conditions. Low electric field strength led to removal of large droplets. The same was valid for large electrode distances. For high values of the electric field intensity E_0 the rate of migration w became large, too. Therefore, the diameter of the smallest removable diameter became smaller with increasing electric field strength. Large distance between electrodes does address migration of large droplets with a limited effect on turbidity control since turbidity correlates with the number of species.

The electric field direct current splitting of oil in water emulsions proved to be an effective splitting technology for very low solvent contamination of aqueous carriers. The simple setup (no turning equipment), risk (no formation of explosive gases) and the presumably low energy demand (only electric energy for rectifier) outweighed the disadvantage of the relatively long separation time. The model developed allows the prediction of either the electric field strength to be applied for droplets of given diameter to be removed, or it may recommend an electrode distance or forecast the time needed for separation.

ABBREVIATIONS

GENERAL ABBREVIATIONS

4-DBSA	<u>4</u> - <u>d</u> odecyl <u>b</u> enzenesulfonic <u>a</u> cid
AnCa	electrode configuration <u>a</u> node left, <u>c</u> athode right
AnCaAn	electrode configuration <u>a</u> node left, <u>c</u> athode middle, <u>a</u> node right
AnCaAnCa	electrode configuration <u>a</u> node first, <u>c</u> athode second, <u>a</u> node third, <u>c</u> athode last (from left to right)
CaAn	electrode configuration <u>c</u> athode left, <u>a</u> node right
CaAnCa	electrode configuration <u>c</u> athode left, <u>a</u> node middle, <u>c</u> athode right
cmc	<u>c</u> ritical <u>m</u> icelle <u>c</u> oncentration
DLVO-theory	theory named after the developers <u>D</u> erjaguin, <u>L</u> andau, <u>V</u> erwey and <u>O</u> verbeek
EIP	<u>E</u> mulsion <u>I</u> nversion <u>P</u> oint
HLB	<u>H</u> ydrophilic- <u>L</u> ipophilic <u>B</u> alance
IUPAC	<u>I</u> nternational <u>U</u> nion of <u>P</u> ure and <u>A</u> ppplied <u>C</u> hemistry
o/w	oil in water
PIT	<u>P</u> hase <u>I</u> nversion <u>T</u> emperature
SSK	<u>S</u> hell <u>S</u> ol- <u>K</u>
TOC	<u>T</u> otal <u>O</u> rganic <u>C</u> arbon
w/o	water in oil

GREEK SYMBOLS

α	angle of the electrodes
γ	interfacial tension
Δp_L	Laplace pressure
$\Delta\rho$	density difference of the continuous and the dispersed phase
ϵ	relative permittivity
η	shear viscosity
Θ	oil/water contact angle
$1/\kappa$	Debye length
ρ	density
σ	interfacial tension
ϕ_0	hold-up of dispersed phase at the top of the emulsion
$\phi(h)$	hold-up of dispersed phase at a distance h from the top of the emulsion
ω	circular velocity

SYMBOLS AND INDICES

0	initial state
1	continuous phase
2	dispersed phase
A	electrode area
A_H	Hamaker coefficient
A_s	parameter of the sigmoidal fit
A	amplitude
a	modelling parameter considering deviations
B_s	parameter of the sigmoidal fit
b	width of the electrodes, combination of constants in the modelling
C_s	parameter of the sigmoidal fit
c	concentration, critical value
D_m	average pore size of the membrane
D_p	particle size
D_s	parameter of the sigmoidal fit
d	horizontal distance between the electrodes
d^*	distance between the electrodes depending on the angle α
E_0	charging field strength
E_P	precipitating electric field
E	dispersed phase
F_b	bouyancy force
F_{El}	Coulomb-force
F_f	friction force
F_g	gravitational force
F_N	Newton force
F_{St}	Stokes resistance force
F_v	volume flow rate
g	gravitational constant
H	hydrophilic part
h	distance of flat infinite surfaces, distance from the top of the emulsion, height of the electrodes
I	current applied per meter of electrode
K	constant describing the mobility of ions
k	linear correlation coefficient
k_B	Boltzmann constant
L	lipophilic part

ABBREVIATIONS

M	molar mass
m	mass of the droplet
m	membrane
N_E	molar amount of the dispersed phase
n	number of lipophilic groups in the molecule, number of revolutions
ow	oil - water
P_c	critical pressure
q	charge of the droplet
R	receiver
R_1	principal radius 1 of curvature
R_2	principal radius 2 of curvature
r	radius of the dispersed droplet, radius of the centrifuge
r	area related rate of turbidity drop
S	solubility
Sr	separation rate
T	absolute temperature, transducer
t	experimental time
U	applied voltage
V	volume, van der Waals potential
v_{Stokes}	creaming or sedimentation velocity acc. to Stokes
w	particle migration rate induced by the electric field
x	droplet diameter
z	charge number, centrifugation number

BIBLIOGRAPHY

- [1] Hamley, I. W., *Introduction to Soft Matter*; John Wiley and Sons Ltd: Leeds, 2000.
- [2] Rosen, M. J.; Kunjappu, J. T., *Surfactants and Interfacial Phenomena: Fourth Edition*, 2012.
- [3] Hamley, I. W., *Introduction to Soft Matter – Revised Edition: Synthetic and Biological Self-Assembling Materials*, 2007.
- [4] Forgiarini, A.; Esquena, J.; González, C.; Solans, C. *Langmuir* **2001**, *17*, 2076–2083.
- [5] Tadros, T.; Izquierdo, P.; Esquena, J.; Solans, C. *Advances in Colloid and Interface Science* **2004**, *108-109*, 303–318.
- [6] Jafari, S. M.; Assadpoor, E.; He, Y.; Bhandari, B. *Food Hydrocolloids* **2008**, *22*, 1191–1202.
- [7] Lissant, K. J., *Demulsification*; Marcel Dekker Inc.: New York, 1983.
- [8] Treybal, R. E., *Liquid extraction*; McGraw-Hill Book Co. Inc.: New York, 1951.
- [9] Ichikawa, T.; Itoh, K.; Yamamoto, S.; Sumita, M. *Colloids and Surfaces A: Physicochemical and Engineering Aspects* **2004**, *242*, 21–26.
- [10] Toth, A. Intensivierung der Carbonsäureisolierung aus wässrigen Prozessströmen durch kombinierte Extraktion und Veresterung., Master Thesis, Graz University of Technology, 2015.
- [11] Godfrey, J. C.; Slater, M. J., *Liquid-Liquid Extraction Equipment*; John Wiley and Sons Ltd: Bradford, 1994.
- [12] Bataller, H.; Lamaallam, S.; Lachaise, J.; Graciaa, A.; Dicharry, C. *Journal of Materials Processing Technology* **2004**, *152*, 215–220.
- [13] Bensadok, K.; Benammar, S.; Lapicque, F.; Nezzal, G. *Journal of Hazardous Materials* **2008**, *152*, 423–430.
- [14] Derjaguin, B. V.; Landau, L. *Acta Physico-Chimica USSR* **1941**, *14*, 633–652.
- [15] Verwey, E. J. W.; Overbeek, J. T. G., *Theory of the Stability of Lyophobic Colloids: The Interaction of Sol Particles Having an Electric Double Layer*; Elsevier Publishing Company Inc.: Amsterdam, 1948.
- [16] Israelachvili, J. N. *Intermolecular and Surface Forces* **2011**, 133–149.
- [17] Marino, H. Phase Inversion Temperature Emulsification: From Batch to Continuous Process., Dissertation, Bath: University of Bath, 2010.

BIBLIOGRAPHY

- [18] Sjöblom, J., *Emulsions and Emulsion Stability*, Second; CRC Press: Bergen, 2006; Vol. 132.
- [19] Müller, P. *Pure and Applied Chemistry* **1994**, *66*, 1077–1184.
- [20] Pohling, R., *Chemische Reaktionen in der Wasseranalyse*; Springer Berlin Heidelberg: Berlin, Heidelberg, 2015.
- [21] Griffin, W. C. *Journal of Cosmetic Science* **1954**, *5*, 249–256.
- [22] Davies, J. *Gas/Liquid and Liquid/Liquid Interfaces* **1957**, 426–438.
- [23] Griffin, W. C. *Journal of Cosmetic Science* **1949**, *1*, 311–326.
- [24] Poonyaratanasrikhajon, A. O/W-Emulsions, Production and Stability., Master Thesis, Graz University of Technology, 2016.
- [25] Walstra, P. *Chemical Engineering Science* **1993**, *48*, 333–349.
- [26] McClements, D. J., *Food Emulsions: Principles Practices, and Techniques*, Second; CRC Press: 2005.
- [27] Einstein, A. *Annalen der Physik* **1906**, *324*, 371–381.
- [28] Tadros, T. F., *Emulsion Formation and Stability*; Tadros, T. F., Ed.; Wiley-VCH Verlag GmbH & Co. KGaA: Weinheim, Germany, 2013.
- [29] Vitale, S. A.; Katz, J. L. *Langmuir* **2003**, *19*, 4105–4110.
- [30] Fernandez, P.; André, V.; Rieger, J.; Kühnle, A. *Colloids and Surfaces A: Physicochemical and Engineering Aspects* **2004**, *251*, 53–58.
- [31] Shinoda, K.; Saito, H. *Journal of Colloid and Interface Science* **1969**, *30*, 258–263.
- [32] Förster, T.; Von Rybinski, W.; Wadle, A. *Advances in Colloid and Interface Science* **1995**, *58*, 119–149.
- [33] Dunstan, T. S.; Fletcher, P. D. I.; Mashinchi, S. *Langmuir* **2012**, *28*, 339–349.
- [34] Nakashima, T.; Shimizu, M.; Kukizaki, M. *Key Engineering Materials* **1992**, *61-62*, 513–516.
- [35] Katoh, R.; Asano, Y.; Furuya, A.; Sotoyama, K.; Tomita, M. *Journal of Membrane Science* **1996**, *113*, 131–135.
- [36] Stang, M.; Schuchmann, H.; Schubert, H. *Engineering in Life Sciences* **2001**, *1*, 151–157.
- [37] Schultz, S.; Wagner, G.; Urban, K.; Ulrich, J. *Chemical Engineering and Technology* **2004**, *27*, 361–368.
- [38] Crum, L. A.; Mason, T. J.; Reisse, J. L.; Suslick, K. S., *Sonochemistry and Sonoluminescence*; Crum, L. A., Mason, T. J., Reisse, J. L., Suslick, K. S., Eds.; Springer Netherlands: Dordrecht, 1999.

BIBLIOGRAPHY

- [39] Urban, K.; Wagner, G.; Schaffner, D.; Röglin, D.; Ulrich, J. *Chemical Engineering and Technology* **2006**, *29*, 24–31.
- [40] Henschke, M. Dimensionierung liegender Flüssig-flüssig-Abscheider anhand diskontinuierlicher Absetzversuche., Dissertation, RWTH Aachen, 1995.
- [41] Demetriades, K.; Coupland, J. N.; McClements, D. J. *Journal of Food Science* **1997**, *62*, 462–467.
- [42] Demetriades, K.; Coupland, J. N.; McClements, D. J. *Journal of Food Science* **1997**, *62*, 342–347.
- [43] Binks, B. P., *Modern Aspects of Emulsion Science*; Binks, B. P., Ed.; Royal Society of Chemistry: Cambridge, 1998.
- [44] Taylor, P. *Colloids and Surfaces A: Physicochemical and Engineering Aspects* **1995**, *99*, 175–185.
- [45] Taylor, P. *Advances in Colloid and Interface Science* **1998**, *75*, 107–163.
- [46] Porras, M.; Solans, C.; González, C.; Gutiérrez, J. M. *Colloids and Surfaces A: Physicochemical and Engineering Aspects* **2008**, *324*, 181–188.
- [47] Hiemenz, P. C., *Surface Tension and Contact Angle: Application to Pure Substances*, 1997, pp 248–286.
- [48] Larson, K.; Raghuraman, B.; Wiencek, J. *Journal of Membrane Science* **1994**, *91*, 231–248.
- [49] Nour, A. H.; Abu Hassan, M. A.; Yunus, R. M. Characterization and demulsification of water-in-crude oil emulsions., 2007.
- [50] Sutherland, K., *Filters and Filtration Handbook*, 2008.
- [51] Zhang, Z.; Xu, G. Y.; Wang, F.; Dong, S. L.; Li, Y. M. *Journal of Colloid and Interface Science* **2004**, *277*, 464–470.
- [52] Cottrell, F. G. Process for Separating and Collecting Particles of one Liquid Suspended in another Liquid., 1911.
- [53] Draxler, J.; Furst, W.; Marr, R. *Journal of Membrane Science* **1988**, *38*, 281–293.
- [54] Lee, C.; Sams, G.; Wagner, J. *Journal of Electrostatics* **2001**, *53*, 1–24.
- [55] Perles, C. E.; Volpe, P. L. O.; Bombard, A. J. *Energy and Fuels* **2012**, *26*, 6914–6924.
- [56] Eow, J. S.; Ghadiri, M.; Sharif, A. *Journal of Electrostatics* **2001**, *51-52*, 463–469.
- [57] Draxler, J. Flüssige Membranen für die Abwasserreinigung., Habilitation, Graz University of Technology, 1992.

BIBLIOGRAPHY

- [58] Cottrell, F. G.; Speed, J. B. Separating and Collecting Particles of one Liquid Suspended in another Liquid., 1911.
- [59] Pearce, C. a. R. *British Journal of Applied Physics* **1954**, 5, 136–143.
- [60] Hosseini, M.; Shahavi, M. H. *Chinese Journal of Chemical Engineering* **2012**, 20, 654–658.
- [61] Hirato, T.; Koyama, K.; Tanaka, T.; Awakura, Y.; Majima, H. Demulsification of Water-In-Oil Emulsion by an Electrostatic Coalescence Method., 1991.
- [62] Wallau, W.; Patel, R.; Mujtaba, I.; Arellano-Garcia, H. In *Proceedings of the 24th European Symposium on Computer Aided Process Engineering*2, Elsevier: 2014; Vol. 24.
- [63] Wallau, W.; Schlawitschek, C.; Arellano-Garcia, H. *Industrial and Engineering Chemistry Research* **2016**, 55, 4585–4598.
- [64] Mhatre, S.; Vivacqua, V.; Ghadiri, M.; Abdullah, A. M.; Al-Marri, M. J.; Hassanpour, A.; Hewakandamby, B.; Azzopardi, B.; Kermani, B. *Chemical Engineering Research and Design* **2015**, 96, 177–195.
- [65] Chen, T. Y.; Mohammed, R. A.; Bailey, A. I.; Luckham, P. F.; Taylor, S. E. *Colloids and Surfaces A: Physicochemical and Engineering Aspects* **1994**, 83, 273–284.
- [66] Williams, T. J.; Bailey, A. G. *IEEE Transactions on Industry Applications* **1986**, IA-22, 536–541.
- [67] Cañizares, P.; Martínez, F.; Lobato, J.; Rodrigo, M. A. *Journal of Hazardous Materials* **2007**, 145, 233–240.
- [68] Evans, R.; Napper, D. H. *Journal of Colloid And Interface Science* **1975**, 52, 260–264.
- [69] Clayfield, E.; Lumb, E. *Journal of Colloid and Interface Science* **1966**, 22, 269–284.
- [70] Derjaguin, B. V.; Churaev, N. V.; Muller, V. M., *Surface Forces*; Springer US: Boston, MA, 1987.
- [71] Manciu, M.; Ruckenstein, E. *Langmuir* **2001**, 17, 2455–2463.
- [72] Ichikawa, T. *Colloids and Surfaces A: Physicochemical and Engineering Aspects* **2007**, 302, 581–586.
- [73] Alinezhad, K.; Hosseini, M.; Movagarnejad, K.; Salehi, M. *Korean Journal of Chemical Engineering* **2010**, 27, 198–205.
- [74] Fernández-Morales, F. H.; Duarte, J. E.; Samitier-Martí, J. *Anais da Academia Brasileira de Ciencias* **2008**, 80, 627–638.
- [75] Ichikawa, T.; Nakajima, Y. *Colloids and Surfaces A: Physicochemical and Engineering Aspects*, 242, 27–37.

BIBLIOGRAPHY

- [76] Melin, T.; Rautenbach, R., *Membranverfahren*; VDI-Buch; Springer Berlin Heidelberg: Berlin, Heidelberg, 2007.
- [77] Stewart, M.; Arnold, K., *Emulsions and Oil Treating Equipment*, First; Gulf Professional Publishing: 2008.
- [78] Behr, A.; Agar, D. W.; Jörissen, J., *Einführung in die Technische Chemie*; Springer Berlin Heidelberg: Dortmund, 2010.
- [79] Förtsch, G.; Meinholz, H., *Handbuch Betrieblicher Gewässerschutz*; Springer Fachmedien Wiesbaden: Wiesbaden, 2014.
- [80] Hahn, H. H., *Wassertechnologie*; Springer Berlin Heidelberg: Berlin, Heidelberg, 1987.
- [81] Rubio, J.; Souza, M.; Smith, R. *Minerals Engineering* **2002**, *15*, 139–155.
- [82] Evdokimov, I. N.; Losev, A. P. *Journal of Petroleum Science and Engineering* **2014**, *115*, 24–30.
- [83] Xia, L.; Lu, S.; Cao, G. *Journal of Colloid and Interface Science* **2004**, *271*, 504–506.
- [84] Martínez-Palou, R.; Cerón-Camacho, R.; Chávez, B.; Vallejo, A. A.; Villanueva-Negrete, D.; Castellanos, J.; Karamath, J.; Reyes, J.; Aburto, J. *Fuel* **2013**, *113*, 407–414.
- [85] Guzmán-Lucero, D.; Flores, P.; Rojo, T.; Martínez-Palou, R. *Energy and Fuels* **2010**, *24*, 3610–3615.
- [86] Wang, S.; Yang, J.; Xu, X. *Fuel* **2011**, *90*, 987–991.
- [87] Da Silva, E. B.; Santos, D.; De Brito, M. P.; Guimarães, R. C. L.; Ferreira, B. M. S.; Freitas, L. S.; De Campos, M. C. V.; Franceschi, E.; Dariva, C.; Santos, A. F.; Fortuny, M. *Fuel* **2014**, *128*, 141–147.
- [88] Binner, E. R.; Robinson, J. P.; Kingman, S. W.; Lester, E. H.; Azzopardi, B. J.; Dimitrakis, G.; Briggs, J. *Energy & Fuels* **2013**, *27*, 3173–3178.
- [89] Kim, S. H.; Lee, S. Y.; Yi, G.-R.; Pine, D. J.; Yang, S.-M. *Journal of the American Chemical Society* **2006**, *128*, 10897–10904.
- [90] SDS Search and Product Safety Center, Sigma Aldrich Co. LCC., <http://www.sigmaaldrich.com/safety-center.html>, 30.08.2017.
- [91] Chemical Book - Chemical Search Engine., http://www.chemicalbook.com/ChemicalProductProperty_EN_CB6310466.htm, 27.10.2017.
- [92] GESTIS-Stoffdatenbank, Institut für Arbeitsschutz der Deutschen Gesetzlichen Unfallversicherung., <http://gestis.itrust.de>, 30.08.2017.
- [93] ChemSpider Search and share chemistry., <http://www.chemspider.com/>, 27.10.2017.

BIBLIOGRAPHY

- [94] Chemicals Safety Data Sheets, Shell Chemicals Ltd., <http://www.shell.com/business-customers/chemicals/safe-product-handling-and-transportation/chemicals-safety-data-sheets.html>, 30.08.2017.
- [95] Bol, P. Investigation of drop dispersions in batch settling processes., Dissertation, Graz University of Technology, 2015.
- [96] Separating a Mixture of Oil and Water Using a Separating Funnel., <http://highschoolchemistryguide.com/separating-a-mixture-of-oil-and-water/1>, 29.01.2016.
- [97] Tantichumnan, C. Influence of Viscosity on Sedimentation and Coalescence Behavior., Master Thesis, Graz University of Technology, 2014.
- [98] Rajcharak, B. Modeling of drop sedimentation in liquid-liquid phase separation., Master Thesis, Graz University of Technology, 2015.
- [99] Deutsch, W. *Annalen der Physik* **1922**, 373, 335–344.
- [100] White, H. J. *Industrial & Engineering Chemistry* **1955**, 47, 932–939.
- [101] White, H. J., *Entstaubung industrieller Gase mit Elektrofiltern*; VEB Deutscher Verlag für Grundstoffindustrie: Leipzig, 1969.
- [102] Balbay, S.; Acikgoz, C.; Akin, D. *Proceeding of the 14th International Conference on Environmental Science and Technology Rhodes, Greece* **2015**, 3–5.
- [103] Vornefeld, M. Personal Communciation., 2014.
- [104] Matlab online documentation of the least-squares (model fitting) algorithms., <https://de.mathworks.com/help/optim/ug/least-squares-model-fitting-algorithms.html>, 24.10.2017.
- [105] Matlab online documentation of the command "fitoptions"., <https://de.mathworks.com/help/curvefit/fitoptions.html>, 23.10.2017.

LIST OF FIGURES

2.1.	Schematic energy versus distance profiles of the DLVO interaction [16] . . .	7
2.2.	Scheme of electrical stabilisation layers, adopted from [17]	8
2.3.	Scheme of steric stabilisation of emulsions	12
2.4.	Scheme of the Gibbs-Marangoni effect [26]	13
3.1.	Influence of surfactant concentration on emulsion stability, droplet size and interfacial tension [28]	15
3.2.	Schematic illustration of transitional and catastrophic phase inversion [30]	16
3.3.	Scheme of curvature change inside an emulsion due to transitional or catastrophic phase inversion (adopted from [30])	18
4.1.	Scheme of various breakdown processes in emulsions (adopted from [28])	24
4.2.	Main coalescence steps (adopted from [40])	24
4.3.	Force balance of an ascending droplet	25
4.4.	different potential energy curves versus distance of droplets with charged surface [3]	26
4.5.	Ostwald ripening (adopted from [26])	28
5.1.	Schematic of the dipole-dipole interaction [57]	30
5.2.	Schematic of the electrophoresis [57]	31
5.3.	Schematic of the dielectrophoresis [57]	31
5.4.	Mechanism of electrical demulsification acc. to [72]	33
5.5.	Operation principle of a hydrocyclone [77]	36
5.6.	Flotation principle, adopted from [79]	37
7.1.	Principle of the ultrasonic scanner [95]	43
7.2.	Mixing unit with scheme	43
7.3.	Separation funnel [96]	43
7.4.	Scheme of the optical cell equipment	44
7.5.	Ultrasonic Scanner [97]	45
8.1.	Laboratory equipment pressurized air flotation	49
8.2.	Laboratory equipment electroflotation	49
8.3.	Scheme of the electrode setup	50
8.4.	Picture of the three plate arrangement; distance between electrodes: 1 cm	51

LIST OF FIGURES

8.5.	Plate rod configuration with four plates and 3x4 rods; distance between electrodes: 1 cm	51
8.6.	Scheme of the apparatus for investigating the electric field with inclined plates	51
8.7.	Scheme of inclined plates and the electric field force applied between them	52
8.8.	Scheme of the monitoring setup	53
8.9.	Whole separation area with additional equipment devices	53
8.10.	Microsoft Excel® spreadsheet of the input	54
8.11.	Image containing the original reference, start and last picture of the experiment as well as the cut pictures	55
8.12.	Sigmoidal Fit and experimental data	56
8.13.	Microsoft Excel® spreadsheet of the results of the modelling; the result file of the fit has a similar structure	57
9.1.	delay of separation (red line); experiment performed with 2 electrodes with a distance of 10 cm and an applied voltage of 10 V (CS007)	60
9.2.	No delay; experiment performed with two electrodes with a distance of 10 cm and an applied voltage of 10 V (CS012)	60
9.3.	Delay is not taken into account; experiment performed with two electrodes with a distance of 10 cm and an applied voltage of 10 V (CS007 without delay time of 7 min)	61
10.1.	Balance for the splitting equipment	63
10.2.	Force balance for a droplet in the electric field	64
11.1.	Influence of the agitation rate on the coalescence curve	70
11.2.	Influence of the agitation rate on the coalescence time, optical evaluation .	70
11.3.	Linear decrease of the coalescence time for agitation rate between 1500 and 1900 rpm, optical evaluation	71
11.4.	Influence of the agitation rate on the separation time, ultrasonic evaluation	72
11.5.	Influence of the hold-up on the settling time	73
11.6.	Result of mechanically mixing an emulsion with an hold-up of 0.35 with a rotational speed of 1500 rpm	73
11.7.	Influence of the surfactant concentration on the emulsion stability	75
12.1.	Thermal splitting: Initial picture of the emulsion	77
12.2.	Thermal splitting: Picture of the final emulsion	77
12.3.	Chemical splitting: Addition of 75 ml of emulsion to 50 ml of isopropyl alcohol	78

LIST OF FIGURES

12.4.	Chemical splitting: Addition of 76 ml of emulsion to 50 ml of isopropyl alcohol	78
12.5.	Result of centrifugation at a centrifugation number of 3000 ($r=0.075m$ and 100 Hz)	79
12.6.	Pressurized air flotation at $t=0$	80
12.7.	Pressurized air flotation at $t=35$ min	80
12.8.	Results of all electroflotation experiments	80
12.9.	Results of the electroflotation experiments at 12 V	81
12.10.	Comparison of five experiments with two electrodes in a distance of 10 cm and an applied electric field strength of 100 V/m; all data points	82
12.11.	Comparison of three experiments with two electrodes in a distance of 10 cm and an applied electric field strength of 120 V/m	83
12.12.	Comparison of eight experiments with four different settings, where the two electrodes are inclined by 45 degrees with the anode on top of the cathode	84
12.13.	Comparison of five experiments with two electrodes in a distance of 10 cm and an applied electric field strength of 100 V/m, where experiments 4 and 5 have been performed in a different vessel	85
12.14.	Comparison of three experiments performed at 100 V/m and electrode distances of 5, 10 and 15 cm	86
12.15.	Comparison of three experiments performed at 50 V/m and electrode distances of 6, 12 and 24 cm	87
12.16.	Comparison of four experiments performed at 40, 80, 100 and 120 V/m and a fixed electrode distance of 5 cm	87
12.17.	Comparison of four experiments performed at 40, 80, 100 and 120 V/m and a fixed electrode distance of 10 cm	88
12.18.	Comparison of four experiments with an AnCa (cathode is the upper electrode) electrode configuration with four experiments at the same settings with an CaAn (anode is the upper electrode) electrode configuration	89
12.19.	Electrode inclination	89
12.20.	Comparison of inclined (AnCa electrode configuration) with vertical plates at an electrode distance of 10 cm and at 85 and 100 V/m, respectively	90
12.21.	Comparison of three experiments with an AnCaAn electrode configuration with three experiments at the same settings with a CaAnCa electrode configuration at a constant electric field strength of 50 V/m	91

LIST OF FIGURES

12.22.	Comparison of four experiments with an AnCaAn electrode configuration with four experiments at the same settings with an CaAnCa electrode configuration at a constant electric field strength of 100 V/m	92
12.23.	Comparison of three experiments with an AnCaAn electrode configuration with three experiments at the same settings with a CaAnCa electrode configuration at a constant electrode distance of 4 cm	93
12.24.	Comparison of three experiments with an AnCaAn electrode configuration with three experiments at the same settings with a CaAnCa electrode configuration at a constant electrode distance of 8 cm	93
12.25.	Comparison of four experiments with an AnCaAn electrode configuration with four experiments at the same settings with a CaAnCa electrode configuration and an electrode inclination of 45°	94
12.26.	Comparison of inclined with not inclined plates at an electrode distance of 10 cm and an electric field strength of 85 and 100 V/m, respectively; both CaAnCa electrode configuration	95
12.27.	Comparison of three experiments with four plate electrodes at an electric field strength of 100, 200 and 300 V/m	96
12.28.	Electric splitting experiment using four plate electrodes after 3 hours at an electric field strength of 300 V/m	96
12.29.	Electric splitting experiment using four plate electrodes after 3 hours at an electric field strength of 200 V/m	96
12.30.	Comparison of three experiments with four plate electrodes and three times four rod electrodes; two experiments, where the rods are connected as anode and one, where the plate electrodes are used as cathode	97
12.31.	Comparison of six different setups	98
12.32.	Separation progress when applying an electric field strength of 50 V/m on an emulsion resulting from the esterification process of acetic acid with methanol	100
12.33.	Separation progress when applying an electric field strength of 50 V/m on an emulsion resulting from the esterification process of acetic acid with butanol	101
12.34.	Separation progress when applying an electric field strength of 50 V/m on an emulsion resulting from the esterification process of acetic acid with octanol	102
13.1.	Comparison of the model with experiments using two electrodes with an inclination of 0 and 45° as well as an experiment with four electrodes used	104

LIST OF FIGURES

13.2.	Comparison of the model with experiments using three electrodes with an inclination of 0 and 45° as well as an experiment with four plate electrodes and 3x4 rod electrodes (An) used	105
13.3.	Reproducibility of the model applied to five experiments with two plate electrodes in a distance of 10 cm and an electric field strength of 100 V/m	105
13.4.	Correlation between the droplet diameter and the electric field strength at a constant distance of 10 cm, error bars in black	106
13.5.	Correlation between the droplet diameter and the electrode distance at a constant electric field strength of 100 V/m, error bars in black	106
13.6.	Visualisation of the rate of migration for different drop diameters at the same electric field intensity	107
13.7.	Difference in separation for different electrode distance/number of electrodes; marked droplets separate	107
A.1.	Microsoft Excel® spreadsheet of the input	132
B.1.	Temperature over time of the thermal splitting experiment (RMA006) . . .	157
C.1.	Reproducibility of the electro flotation experiment performed at 3 V	160
C.2.	Reproducibility of the electro flotation experiment performed at 6 V	160
C.3.	Reproducibility of the electro flotation experiment performed at 9 V	161
C.4.	Reproducibility of the electro flotation experiment performed at 14.7 V . .	161
D.1.	Calibration of the ultrasonic scanner	163
E.1.	Reproducibility of the electric splitting experiment with two plate electrodes and an applied electric field of 40 V/m	177
E.2.	Reproducibility of the electric splitting experiment with two plate electrodes and an applied electric field of 50 V/m	177
E.3.	Reproducibility of the electric splitting experiment with two plate electrodes and an applied electric field of 60 V/m	178
E.4.	Reproducibility of the electric splitting experiment with two plate electrodes and an applied electric field of 80 V/m	178
E.5.	Reproducibility of the electric splitting experiment with two plate electrodes and an applied electric field of 100 V/m	179
E.6.	Reproducibility of the electric splitting experiment with two plate electrodes and an applied electric field of 120 V/m	179
E.7.	Reproducibility of the electric splitting experiment with two inclined plate electrodes with an AnCa configuration	180

LIST OF FIGURES

E.8. Reproducibility of the electric splitting experiment with two inclined plate electrodes with an CaAn configuration 180

E.9. Reproducibility of the electric splitting experiment with three plate electrodes with an AnCaAn configuration and an applied electric field of 40 V/m 181

E.10. Reproducibility of the electric splitting experiment with three plate electrodes with an AnCaAn configuration and an applied electric field of 50 V/m 181

E.11. Reproducibility of the electric splitting experiment with three plate electrodes with an AnCaAn configuration and an applied electric field of 60 V/m 182

E.12. Reproducibility of the electric splitting experiment with three plate electrodes with an AnCaAn configuration and an applied electric field of 80 V/m 182

E.13. Reproducibility of the electric splitting experiment with three plate electrodes with an AnCaAn configuration and an applied electric field of 100 V/m 183

E.14. Reproducibility of the electric splitting experiment with three plate electrodes with an AnCaAn configuration and an applied electric field of 120 V/m 183

E.15. Reproducibility of the electric splitting experiment with three plate electrodes with an AnCaAn configuration and an applied electric field of 200 V/m 184

E.16. Reproducibility of the electric splitting experiment with three plate electrodes with an CaAnCa configuration and an applied electric field of 40 V/m 184

E.17. Reproducibility of the electric splitting experiment with three plate electrodes with an CaAnCa configuration and an applied electric field of 50 V/m 185

E.18. Reproducibility of the electric splitting experiment with three plate electrodes with an CaAnCa configuration and an applied electric field of 80 V/m 185

E.19. Reproducibility of the electric splitting experiment with three plate electrodes with an CaAnCa configuration and an applied electric field of 100 V/m 186

LIST OF FIGURES

E.20. Reproducibility of the electric splitting experiment with three plate electrodes with an CaAnCa configuration and an applied electric field of 120 V/m 186

E.21. Reproducibility of the electric splitting experiment with three plate electrodes with an CaAnCa configuration and an applied electric field of 200 V/m 187

E.22. Reproducibility of the electric splitting experiment with three inclined plate electrodes with an AnCaAn configuration and an applied electric field of 141 V/m 187

E.23. Reproducibility of the electric splitting experiment with three inclined plate electrodes with an AnCaAn configuration and an applied electric field of 283 V/m 188

E.24. Reproducibility of the electric splitting experiment with three inclined plate electrodes with an CaAnCa configuration and an applied electric field of 141 V/m 188

E.25. Reproducibility of the electric splitting experiment with three inclined plate electrodes with an CaAnCa configuration and an applied electric field of 283 V/m 189

E.26. Reproducibility of the electric splitting experiment with four plate electrodes with an AnCaAnCa configuration 189

E.27. Reproducibility of the electric splitting experiment with four inclined plate electrodes and 3x4 rod electrodes with the rods acting as anodes 190

E.28. Reproducibility of the electric splitting experiment with four inclined plate electrodes and 3x4 rod electrodes with the plates acting as anodes 190

LIST OF TABLES

1.1.	Properties of different emulsion types [1, 3, 6]	2
2.1.	Fields of application of surfactants with distinct HLB [23]	10
2.2.	HLB group numbers [22]	11
3.1.	Comparison of different types of emulsification systems [6]	22
6.1.	Chemicals used	41
11.1.	4-DBSA concentrations in the solvent and the aqueous phase at a hold-up of 0.35	74
13.1.	Influence of the electric field strength on the droplet diameter at a constant electrode distance of 10 cm	106
13.2.	Influence of the electrode distance on the droplet diameter at a constant electric field strength of 100 V/m	106
A.1.	Fit options in MATLAB®[105]	148
A.2.	Options of the model parameter finding procedure different from the fitting options [105]	148
B.1.	Assumptions made for thermal splitting power calculation	157
D.1.	Data of the ultrasonic scanner calibration	163
E.1.	Experimental settings of the experiments using 2 plate electrodes	165
E.2.	Experimental settings of the experiments using 2 inclined plate electrodes	167
E.3.	Experimental settings of the experiments using 3 plate electrodes in AnCaAn configuration	168
E.4.	Experimental settings of the experiments using 3 plate electrodes in CaAnCa configuration	170
E.5.	Experimental settings of the experiments using 3 inclined plate electrodes in AnCaAn and CaAnCa configuration	172
E.6.	Experimental settings of the experiments using 4 plate electrodes in AnCaAnCa configuration	173
E.7.	Experimental settings of the experiments using 4 plate electrodes and 3x4 rod electrodes (anodes)	174

LIST OF TABLES

E.8. Experimental settings of the experiments using 4 plate electrodes (anodes) and 3x4 rod electrodes 175

E.9. Experimental settings of the experiments using 4 plate electrodes in An-CaAnCa configuration investigating the industrial effluents 176

F.1. Model parameters of all electric field experiments 192

F.2. Fit parameters of all electric field experiments 201

Appendix

APPENDIX A. MATLAB CODE

The MATLAB® code itself consists of four parts. These are explained shortly in the following chapters and in deeper detail in the code itself.

Additionally, a Microsoft Excel file has been set up containing all the data of the experiment. After evaluation of the program code all important data are stored in separated spreadsheets. The input sheet is shown in figure A.1. The program `PictureAnalysisAndFit` reads the necessary information from this spreadsheet and processes the evaluation of the brightness as well as the fitting and modelling. How to determine each parameter can be read in the documentation of the program in chapter A.

APPENDIX A. MATLAB CODE

Date	30.11.2016
Electrode configuration	2 plates
Anode	left
electrode distance	10 cm
aqueous phase	water
solvent phase	SSK 0.1 gew% SSK
phase ratio	0,005
voltage	10 V
experiment duration (approx.)	180 min
amount aq. phase	497,5
amount sol. phase	2,5
Notes	
photos to be deleted before exp. data (incl. reference)	1
photos to be deleted after exp. data (incl. reference)	0
interval between photos	1 min
time of first photograph	0
Information concerning the <u>reference</u> picture	
Number of reference picture	1
Cutting information	
Top left	
x-coordinate	1085
y-coordinate	1025
Bottom right	
x-coordinate	1980
y-coordinate	1650
Information concerning the <u>other</u> pictures in the experiment	
Cutting information	
Top left	
x-coordinate	1105
y-coordinate	965
Bottom right	
x-coordinate	2000
y-coordinate	1590

Figure A.1.: Microsoft Excel[®] spreadsheet of the input

FPA

```

1 % Main File for analysing picture sequences in multiple folders.
2 % To analyse the pictures an Excel file with input information is
3 % needed. The required information can be seen in the
4 % documentation of the program PictureAnalysisAndFit, which is
5 % necessary for the complete analysis. The programs FA and
6 % FolderAnalysis are needed for easier analysis of the data
7 % generated.
8
9 function FPA % FolderPictureAnalysis
10 close all; clc;
11 tic; % Starts the stopwatch
12
13 %% Input
14 % Determining the interval between the pictures to be analysed.
15 % 1 = every picture is analysed
16 % 2 = every second picture is analysed
17
18 AnalysisInterval = 1; % [1, 2, 5, 10];
19
20 angle = 0; % rotates the image; negative values for clockwise
21
22 % Defining the weight factor for the first point.
23 % (zero separation)
24
25 weightZero = 1; % 1 means same weight as the other points
26
27 % Option: Display all .png files related to the current analysis
28 % show = 0 --> Figures are not displayed
29 % show = 1 --> Figures are displayed
30
31 show = 1;
32
33 % Defining the extension of the excel sheet and the figures to
34 % distinguish between different settings:
35

```

```

36 for AIvar = 1:length(AnalysisInterval) % control variable, if
37     % more than one analysis interval is defined.
38     for w0var = 1:length(weightZero) % control variable, if more
39         % than one weight factor for the startpoint is defined.
40
41     % Define a part of the name of the Excel-Spreadsheet:
42
43     extension = strcat('AI_', num2str(AnalysisInterval(AIvar)), '_w0_',
44         num2str(weightZero(w0var)));
45
46     %% Reading of the folders to be analysed
47     % Finds the number of folders inside the current folder
48     % Get a list of all subfolders in the current directory
49     allSubFolders = genpath(cd);
50
51     % Parse into a cell array.
52
53     remain = allSubFolders;
54     listOfFolderNames = {};
55     while true
56         [singleSubFolder, remain] = strtok(remain, ';');
57         if isempty(singleSubFolder)
58             break;
59         end
60         listOfFolderNames = [listOfFolderNames singleSubFolder];
61     end
62
63     numberOfFolders = length(listOfFolderNames);
64
65     startFolder = 2; % starts at number 2 because 1 is the current
66     % directory
67     endFolder = numberOfFolders; % Defines the last folder to be
68     % analysed. "numberOfFolders" is the number of the last folder
69     % in the directory. Other numbers smaller than this one are
70     % possible too.
71

```



```

72 %% Analysis of all folders in the current directory using the
73 % program "PictureAnalysisAndFit"
74
75 for i=startFolder:endFolder
76     actualFolder = listOfFolderNames{i};
77     pathParts = strsplit(actualFolder, '\');
78     fprintf('\n\nAnalysis of experiment %s\n', pathParts{end})
79     resultsPAAF = PictureAnalysisAndFit(actualFolder,
        AnalysisInterval(AIvar), weightZero(w0var), extension,
        angle);
80     cd(listOfFolderNames{1});
81 end
82
83 disp('----- FPA FINISH -----')
84
85 %% Summarizing all data with FA
86
87 FA(AnalysisInterval(AIvar), extension, startFolder, endFolder, show)
88     end
89 end
90
91 endtimesek = toc
92 endtimemin = endtimesek/60
93 endtimeh = endtimesek/3600
94 clear all

```

PICTUREANALYSISANDFIT

In table A.1 all data of the fitting algorithm are listed. Additionally, a short explanation is given. Table A.2 shows the parameters of the model application different from the fitting parameters.

It can be seen that the method "non linear least squares" is applied using the trust-region algorithm. In general, least squares is the problem of finding a local minimizer to a function. This function is a sum of squares. [104]

Using the trust-region algorithm the fit is tested whether it is possible to improve it or not. This is done by approximating the non linear least squares function in the neighbourhood of

the current solution. This neighbourhood is the trust region. Then, a trial step is computed. The current solution point is updated by addition of the trial step if the trial step leads to an improved solution. If this is not the case the trust region is shrunk and the trial step is repeated. [104]

```

1 % This program analyses the pictures in the Folder "actualFolder"
2 % and determines the brightness of each of them. For this reason,
3 % all pictures are cropped to the area of interest, which is
4 % defined beforehand. The corners of this area are written to
5 % the input excel file.
6 % To find out the corners, any picture has to be read (not the
7 % initial one, because camera or emulsion position might
8 % have changed) with
9 %
10 % -----
11 % | pic2 = imread('NAME_OF_THE_PICTURE.jpg') |
12 % | imshow(pic2) % opens the picture      |
13 % -----
14 %
15 % Using the data cursor in the figure the top left and the
16 % bottom right point of the area of interest can be defined. The
17 % same procedure has to be performed to find the corners of the
18 % reference picture.
19 %
20 % Excluding pictures from the separation calculation might be
21 % necessary due to the following reasons:
22 %     The reference picture
23 %     Pictures of surrounding equipment
24 %     Close ups of the clear emulsion
25 %
26 % CAVE: The reference picture is not part of the separation
27 % progress itself. However, it is necessary for the calculation
28 % of the separation, since it defines the endpoint of complete
29 % separation (clear liquid). Therefore it is mandatory to take
30 % one and to define its number in the set of pictures.
31 %
32 % It is possible to set a time interval between the
33 % pictures, if for example a longer experiment is performed and

```

APPENDIX A. MATLAB CODE

```

34 % pictures are taken every fifth minute.
35 % The starttime for the first picture is also set in case of
36 % starting the experiment and forgetting to start the camera.
37 % Then, the separation is calculated with respect to the first
38 % picture (separation = 0) and a reference picture complete
39 % separation (separation = 1).
40 % Afterwards, the separation is fitted using a sigmoidal fitting
41 % approach to determine the initial dead time. For the following
42 % modelling step the dead time is subtracted from the separation
43 % data, i.e. the data are shifted to the left. This is only done
44 % for dead times greater than 1. If the dead time is equal to or
45 % lower than 0, subtraction is not performed. The applied model
46 % results form a force balance around the droplets and is
47 % reduced to an exponential model with two parameters.
48 % The data of the sigmoidal fit as well as of the modelling are
49 % saved to the excel sheet with the input information.
50
51 function [result_sig] = PictureAnalysisAndFit(actualFolder,
        AnalysisInterval, weightZero, extension, angle)
52
53 %% Reading the folder analysed and all .jpg files in this folder
54 cd(actualFolder)
55 CurrentDirectory = actualFolder;
56 [up, folder, ~] = fileparts(CurrentDirectory);
57 Expname = folder; % Name of the analysed experiment/folder
58
59 % Check whether the Excel file exists
60
61 filecheck = exist(strcat(Expname, '.xlsx'), 'file');
62 if filecheck~=2
63     fprintf('Warning: File does not exist: %s \n\nContinuing with
        next experiment. \n', strcat(Expname, '.xlsx'));
64     result_sig = [];
65     return
66 end
67
68 %% Necessary input, which is read from the input excel sheet.

```

```

69
70 etac = 1; % mPas
71 input = xlsread(Expname, 'Tabelle1', 'b14:b39');
72 ElDist = xlsread(Expname, 'Tabelle1', 'b4'); % [cm]
73 Voltage = xlsread(Expname, 'Tabelle1', 'b8'); % [V]
74 E0 = Voltage*100/(ElDist*cos(angle*pi/180)); % [V/m]
75
76 c1 = input(1);
77 c2 = input(2);
78 interval = input(3); % [min]
79 starttime = input(4); % [min]
80
81 % Check if the input is valid, i.e. if the cutting information is
82 % correct.
83
84 InputWarning = 0;
85 if c1<0 || c2<0 || interval<=0
86     fprintf(2, '      One input parameter is smaller than 0! Check
      the excel sheet of %s \n      Going to the next experiment
      \n', folder);
87     InputWarning = 1;
88     result_sig = [];
89     return
90 elseif isnan(c1)==1 || isnan(c2)==1 || isnan(interval)==1 ||
      isnan(starttime)==1
91     fprintf(2, '      One input parameter is not a number! Check
      the excel sheet of %s \n      Going to the next experiment
      \n', folder);
92     InputWarning = 1;
93     result_sig = [];
94     return
95 end
96
97 %% Input for average brightness calculation of all pictures
98
99 % Top left
100 x1 = input(21); y1 = input(22);

```

```

101
102 % Bottom right
103 x2 = input(25); y2 = input(26);
104
105 % Input for average brightness calculation of reference picture
106
107 ref = input(7); % defines the position of the reference picture
108             % in "allpics"
109
110 % Top left
111 xref1 = input(11); yref1 = input(12);
112
113 % Bottom right
114 xref2 = input(15); yref2 = input(16);
115
116 % Check if the input for cutting the images is valid
117
118 CropWarning = 0;
119 if ref<=0 || x1<0 || y1<0 || x2<0 || y2<0 || xref1<0 || yref1<0
    || xref2<0 || yref2<0
120     fprintf(2,'      One input parameter for cutting the picture
    is smaller than 0! Check the excel sheet of %s \n
    Going to the next experiment \n',folder);
121     CropWarning = 1;
122     result_sig = [];
123     return
124 elseif isnan(ref)==1 || isnan(x1)==1 || isnan(y1)==1 || isnan(x2)
    ==1 || isnan(y2)==1 || isnan(xref1)==1 || isnan(yref1)==1 ||
    isnan(xref2)==1 || isnan(yref2)==1
125     fprintf(2,'      One input parameter for cutting the picture
    is not a number! Check the excel sheet of %s \n      Going
    to the next experiment \n',folder);
126     CropWarning = 1;
127     result_sig = [];
128     return
129 end
130

```

```

131 fprintf('End of input \n\n')
132
133 % ----- %
134 % ----- %
135 % ----- END OF INPUT ----- %
136 % ----- %
137 % ----- %
138
139 %% Reading the pictures
140
141 jpegFiles = dir('*.jpg');
142 numfiles = length(jpegFiles);
143 allpics = cell(1, numfiles);
144
145 % All pictures are stored to allpics
146 for k = 1:numfiles
147     allpics{k} = imread(jpegFiles(k).name,angle);
148 end
149 fprintf('Reading of all foto data finished \n\n')
150
151 %% Start of calculation
152 %% Calculation of the average brightness for all pictures
153 % All pictures are cropped to the area defined above
154
155 crpics = {1,length(numfiles-c2)};
156 cravg = length(numfiles-c2);
157
158 % Cut pictures to the emulsion range and calculate the average
159 % brightness of all pictures of the experiment.
160
161 for i=1:(numfiles-c1-c2)/AnalysisInterval
162     crpics{1,i}=imcrop(allpics{1,i+(i-1)*(AnalysisInterval-1)+c1
163         }, [x1 y1 x2-x1 y2-y1]);
164     cravg(i)= mean(reshape(crpics{1,i}, [], 1))/255;
165 end
166 %% Calculation of average brightness of reference picture

```

```

167
168 crref=imcrop(allpics{1,ref}, [xref1 yref1 xref2-xref1 yref2-yref1
    ]);
169
170 % Calculate the average brightness of the initial picture
171
172 avgref= mean(reshape(crref,[],1))/255;
173
174 % Calculate the relative brightness (i.e. separation progress)
175
176 div=(cavg-cavg(1))./(avgref-cavg(1));
177
178 % x-axis for the plot
179
180 time = (linspace (starttime,length(div)+starttime-1,
    length(div)).').*interval*AnalysisInterval;
181
182 % Transposes div to make it usable as y-axis
183
184 separation = div.';
185
186 fprintf('End of analyis\n\n')
187
188 %% Plot all important pictures
189
190 figure
191 subplot(2,3,1),imshow(allpics{1,1});
192     subplot(2,3,2),imshow(allpics{1,c1+1});title(Expname);
193     subplot(2,3,3),imshow(allpics{1,numfiles-c2- (AnalysisInterval
    -1)});
194     subplot(2,3,4),imshow(crref);
195     subplot(2,3,5),imshow(crpics{1,c1+1});
196     subplot(2,3,6),imshow(crpics{1,length(cavg)});
197 print(strcat('cutfigure',extension,Expname),'-dpng')
198
199 clear allpics % releases the RAM again
200

```

```

201 %% Fitting the result
202
203 fprintf('Fitting the sigmoidal fit for determination of dead time
        \n\n')
204 weightFactors_Sig = ones(length(separation),1);
205 weightFactors_Sig(1) = weightZero;
206 boundariesLow_Sig = [-inf,-inf,-inf,-inf];
207 boundariesHigh_Sig = [inf,inf,inf,inf];
208
209 close all
210
211 % Sigmoidal fit incl. random start parameter (as)
212
213 SigFitName = 'Sig_SP_';
214 [f1, gof1, output1] = fit(time, separation, 'as+(bs-as)/(1+exp(-(
        x-cs)/ds))', 'StartPoint', [-5, 1, -20, 15], 'MaxIter',
        1000000, 'MaxFunEvals', 1000000, 'Weight', weightFactors_Sig, '
        Lower', boundariesLow_Sig, 'Upper', boundariesHigh_Sig);
215
216 as = [f1.as];
217 bs = [f1.bs];
218 cs = [f1.cs];
219 ds = [f1.ds];
220 fprintf('End of fitting the sigmoidal fit for determination of
        dead time \n\n')
221
222 %% Plot the fit
223
224 plot(time, separation, '+', 'LineWidth',1.5); hold on
225 plot(f1, 'k')
226 legend(Expname, 'fit', 'location', 'SouthEast');
227 hold off
228 xlabel('time in min');
229 ylabel('separation')
230 axis([0,inf,0,1]);
231
232 % Save the figure of the fit

```



```

233
234 print(strcat('figure_',SigFitName,extension,Expname),'-dpng')
235
236 %% Prepare the fit data for saving
237
238 abcd_sig = (coeffnames(f1));
239 coeff1 = [as; bs; cs; ds];
240
241 result_fit_sig = [coeff1, confint(f1).'];
242 result_gof_sig = [gof1.sse; gof1.rsquare; gof1.dfe; gof1.
    adjrsquare; gof1.rmse];
243 description_gof_sig = fields(gof1);
244 outputm_sig = {output1.message};
245 fitdata_sig = result_fit_sig(1,:)+(result_fit_sig(2,:)-
    result_fit_sig(1,:))./(1+exp(-(time-result_fit_sig(3,:))./
    result_fit_sig(4,:)));
246
247 %% Applying the model
248
249 fprintf('Applying the model\n\n')
250
251 % Determining the time where the sigmoidal fit intersects with
252 % the x-axis (dead time)
253
254 syms tfit
255 tdead = double(round(solve(as+(bs-as)/(1+exp(-(tfit-cs)/ds))==0,
    tfit)));
256 if tdead<0
257     tdead=0;
258 end
259
260 % Excluding the delay in separation start
261
262 time_red = time - tdead;
263
264 modvar = 0;
265 for tvar=1:length(time)

```

```

266     if tvar<=length(time) && time_red(tvar)>=0
267         modvar=modvar+1;
268         time_mod(modvar) = time_red(tvar);
269         separation_mod(modvar) = separation(tvar);
270         cravg_mod(modvar) = cravg(tvar);
271         tvar=tvar+1;
272     else
273         tvar=tvar+1;
274     end
275 end
276
277 time_mod=time_mod';
278 separation_mod = separation_mod';
279
280 close all
281
282 % Modelling acc. to Chemical Reaction Engineering incl. random
283 % startparameter
284
285 ModelName = 'CRE_SP_';
286
287 weightFactors_Mod = ones(length(separation_mod),1);
288 weightFactors_Mod(1) = weightZero;
289 boundariesLow_Mod = [-inf,-inf];
290 boundariesHigh_Mod = [inf,inf];
291
292 [f2, gof2, output2] = fit(time_mod, separation_mod, 'am*(1-exp(-
    bm*x))', 'StartPoint', [1, 0], 'MaxIter', 1000000, 'MaxFunEvals
    ', 1000000, 'Weight', weightFactors_Mod, 'Lower',
    boundariesLow_Mod, 'Upper', boundariesHigh_Mod);
293
294 am = [f2.am];
295 bm = [f2.bm];
296
297 fprintf('End of fitting the model to the adopted experimental
    data \n\n')
298

```

```

299 %% Plot the model
300
301 plot(time_mod, separation_mod, '+', 'LineWidth',1.5); hold on
302 plot(f2, 'r')
303 legend(Expname, 'Model', 'location', 'SouthEast');
304 hold off
305 xlabel('time in min');
306 ylabel('separation')
307 axis([0,inf,0,1]);
308 print(strcat('figure_',ModelName,extension,Expname),'-dpng')
309
310 %% Prepare the modelling data for saving
311
312 abcd_mod = (coeffnames(f2));
313 coeff2 = [am; bm];
314 result_fit_mod = [coeff2, confint(f2).'];
315 result_gof_mod = [gof2.sse; gof2.rsquare; gof2.dfe; gof2.
    adjrsquare; gof2.rmse];
316 description_gof_mod = fields(gof2);
317 outputm_mod = {output2.message};
318 fitdata_mod = result_fit_mod(1,:).*(1-exp(-result_fit_mod(2,:).*
    time_mod));
319
320 %% Calculate the droplet diameter
321
322 DropDiameter = ((10^4)/(6*1.05^2))*result_fit_mod(2,:)*4*pi*etac*
    Eldist/E0^2; % [micro meter]
323
324 %% Saving the important results to a .mat file and an Excel sheet
325
326 fprintf('Begin of saving \n\n')
327
328 result_sig = [time, separation, fitdata_sig, cravg.'];
329 save(strcat('results_',SigFitName,Expname,extension),'result_sig'
    );
330
331 result_mod = [time_mod, separation_mod, fitdata_mod, cravg_mod

```

```

    .'];
332 save(strcat('results_',ModelName,Expname,extension),'result_mod')
    ;
333
334 ending = '.xlsx';
335 tabledesc_fit = {'time [min]', 'separation [-]', 'fit data [-]',
    'fit data lower boundary[-]', 'fit data higher boundary[-]', '
    avg.brightness [-]', 'brighthness ref. [-]', ' ', ' ', 'values
    parameter', 'confidence intervall lower boundary', 'confidence
    intervall upper boundary', ' ', ' ', 'goodness of fit', '
    message'};
336 warning off MATLAB:xlswrite:AddSheet;
337
338 % Data of sigmoidal fit is saved
339
340 xlswrite(strcat(Expname,ending),tabledesc_fit,strcat(SigFitName,
    Expname,extension));
341 xlswrite(strcat(Expname,ending),result_sig,strcat(SigFitName,
    Expname,extension), 'A2');
342 xlswrite(strcat(Expname,ending),avgref,strcat(SigFitName,Expname,
    extension), 'G2');
343 xlswrite(strcat(Expname,ending),abcd_sig,strcat(SigFitName,
    Expname,extension), 'I2');
344 xlswrite(strcat(Expname,ending),result_fit_sig,strcat(SigFitName,
    Expname,extension), 'J2');
345 xlswrite(strcat(Expname,ending),description_gof_sig,strcat(
    SigFitName,Expname,extension), 'N2');
346 xlswrite(strcat(Expname,ending),result_gof_sig,strcat(SigFitName,
    Expname,extension), 'O2');
347 xlswrite(strcat(Expname,ending),outputm_sig,strcat(SigFitName,
    Expname,extension), 'P2');
348
349 tabledesc_cre = {'time [min]', 'separation [-]', 'model data [-]'
    , 'model data lower boundary [-]', 'model data upper boundary
    [-]', 'avg.brightness [-]', 'brighthness ref. [-]', 'deadtime [
    min]', ' ', 'values parameter ', 'confidence intervall lower
    boundary', 'confidence intervall upper boundary', ' ', ' ', '

```

```
    goodness of fit', 'message'});
350
351 % Data of modelling is saved
352
353 xlswrite(strcat(Expname, ending), tabledesc_cre, strcat(ModelName,
    Expname, extension));
354 xlswrite(strcat(Expname, ending), result_mod, strcat(ModelName,
    Expname, extension), 'A2');
355 xlswrite(strcat(Expname, ending), avgref, strcat(ModelName, Expname,
    extension), 'G2');
356 xlswrite(strcat(Expname, ending), tdead, strcat(ModelName, Expname,
    extension), 'H2');
357 xlswrite(strcat(Expname, ending), abcd_mod, strcat(ModelName, Expname
    , extension), 'I2');
358 xlswrite(strcat(Expname, ending), {'drop diameter'}, strcat(
    ModelName, Expname, extension), 'I5');
359 xlswrite(strcat(Expname, ending), DropDiameter, strcat(ModelName,
    Expname, extension), 'J5');
360 xlswrite(strcat(Expname, ending), {'micrometer'}, strcat(ModelName,
    Expname, extension), 'M5');
361 xlswrite(strcat(Expname, ending), result_fit_mod, strcat(ModelName,
    Expname, extension), 'J2');
362 xlswrite(strcat(Expname, ending), description_gof_mod, strcat(
    ModelName, Expname, extension), 'N2');
363 xlswrite(strcat(Expname, ending), result_gof_mod, strcat(ModelName,
    Expname, extension), 'O2');
364 xlswrite(strcat(Expname, ending), outputm_mod, strcat(ModelName,
    Expname, extension), 'P2');
```

Table A.1.: Fit options in MATLAB[®] [105]

<i>Option</i>	<i>Value</i>	<i>Explanation</i>
Normalize	'Off'	Option to center and scale the data
Exclude	[]	Points to exclude from fit
Weights	[1xlength(separation) double]=ones	Weight factors for the fit
Method	Non Linear Least Squares	see text
Robust	'Off'	Robust linear least-squares fitting method
Start Point	[-5 1 -20 15]	Initial values for coefficients
Lower	[-Inf -Inf -Inf -Inf]	Lower boundaries for the coefficients to be fitted
Upper	[Inf Inf Inf Inf]	Upper boundaries for the coefficients to be fitted
Algorithm	'Trust-Region'	Algorithm to use for the fitting procedure
DiffMinChange	1e-08	Minimum change in coefficients for finite difference gradients
DiffMaxChange	0.1	Maximum change in coefficients for finite difference gradients
Display	'Notify'	displays output only if the fit does not converge
MaxFunEvals	1000000	Maximum number of evaluations of model allowed
MaxIter	1000000	Maximum number of iterations allowed for fit
TolFun	1.0000e-06	Termination tolerance on model value
TolX	1.0000e-06	Termination tolerance on coefficient values

Table A.2.: Options of the model parameter finding procedure different from the fitting options [105]

<i>Option</i>	<i>Value</i>	<i>Explanation</i>
Start Point	[1 0]	Initial values for coefficients
Lower	[-Inf -Inf]	Lower boundaries for the coefficients to be fitted
Upper	[Inf Inf]	Upper boundaries for the coefficients to be fitted

FA

```

1 % Main file for folder analysis (FA) and summarizing the data
2 % generated from picture analysis. An excel sheet with 4
3 % spreadsheet filled with data is produced. The first one
4 % contains the separation data of all experiments. Into the
5 % second spreadsheet the modelling data including the lower and
6 % the upper boundary of the model is stored. The third one
7 % provides the model parameters, the respective confidence
8 % intervals including the relative deviation from the parameter
9 % and the rsquare as a measure of model quality. Additionally
10 % all messages of the fit are stored in this spreadsheet. The
11 % last spreadsheet contains information about the input data of
12 % all experiments written to the input spreadsheet.
13
14 function [StorePng]=FA(AnalysisInterval,extension,startFolder,
    endFolder,show)
15 close all;
16
17 % Defining the name of the output Excel-Sheet
18
19 ExcelName =strcat('CRE_ExperimentalData_comb',extension, '.xlsx');
20
21 %% Folder analysis
22 % Finds the number of folders inside the current folder
23 % Get a list of all subfolders in the current directory
24
25 allSubFolders = genpath(cd);
26
27 % Parse into a cell array.
28
29 remain = allSubFolders;
30 listOfFolderNames = {};
31 while true
32     [singleSubFolder, remain] = strtok(remain, ';');
33     if isempty(singleSubFolder)
34         break;

```

```

35         end
36         listOfFolderNames = [listOfFolderNames singleSubFolder];
37     end
38
39     % Define the time vector and give starting values for parameters.
40
41     time = (linspace(0,2000,2000/1+1).').*AnalysisInterval;
42     k=1;
43     allSeparationData = zeros(450/AnalysisInterval,200);
44
45     % Start the actual analysis.
46
47     for i=startFolder:endFolder
48         actualFolder = listOfFolderNames{i};
49         pathParts = strsplit(actualFolder,'\');
50         fprintf('\n\nAnalysis of folder %s\n', pathParts{end})
51         [StorePng, inputData, separationData, fitData, fitDataLB,
52          fitDataHB, fitParameters, rsquare, message, boundaries] =
53          Folderanalysis(actualFolder,AnalysisInterval,extension);
54
55     % Check, whether there is anything to store. If this is not the
56     % case, nothing is done and the next folder is analysed.
57
58         if size(StorePng)==0
59             else
60
61             %% Show all stored result pictures of the folder analysed
62             % before. This is done for every folder.
63
64                 if show==1
65                     figure;
66                     imshow(StorePng{1});
67                     figure;
68                     imshow(StorePng{2});
69                 else
70                     end

```



```

70 %% Store the fit data as well as the lower boundary and the
71 % higher boundary data.
72
73     for j=1:length(separationData)
74         allSeparationData(j,k) = separationData(j);
75         allFitData(j,k) = fitData(j);
76         allFitDataLB(j,k)= fitDataLB(j);
77         allFitDataHB(j,k)= fitDataHB(j);
78     end
79
80 %% Store the fit parameters as well as some additional
81 % information.
82
83     for j=1:length(fitParameters)
84         allFitParameters(k,j) = fitParameters(j);
85     end
86
87     allFitParameters(k,3) = rsquare;
88     allMessages{k,:} = message;
89     ExpName{1,k} = pathParts{end};
90     allBoundaries(k,:) = boundaries;
91     allInputData(:,k) = inputData;
92
93     if k>1
94         ExpNameModel{1,k+2*k-2} = pathParts{end};
95     else
96     end
97     k=k+1;
98 end
99
100 % Set the current directory back to the one where the programs
101 % are to go to save all data into the same file and proceed to
102 % the next experiment.
103
104     cd(listOfFolderNames{1});
105 end
106

```

```

107 % Prepare data for saving to excel.
108
109 ExpNameModel{1,1} = ExpName{1};
110 colvar=1;
111 for expvar = 1:length(allFitParameters)
112     for rowvar = 1: length(allFitData)
113         ModelData(rowvar,colvar) = allFitData(rowvar,expvar);
114         ModelData(rowvar,colvar+1) = allFitDataLB(rowvar,expvar);
115         ModelData(rowvar,colvar+2) = allFitDataHB(rowvar,expvar);
116     end
117     colvar= colvar + 3;
118 end
119
120 for i=1:length(allFitParameters)
121     relDeva(i) = sqrt(((allFitParameters(i,1)-allBoundaries(i,1))
122         ./allFitParameters(i,1)).^2).*100;
123     relDevb(i) = sqrt(((allFitParameters(i,2)-allBoundaries(i,2))
124         ./allFitParameters(i,2)).^2).*100;
125 end
126
127 % Define the headings of the spreadsheets
128
129
130 timename = {'time in min'};
131 HeadingFitPar = {'Name of the experiment', 'a', 'b', 'rsquare', '
132     confidence a lower', 'confidence b lower', 'confidence a
133     higher', 'confidence b higher', 'relative deviation of
134     confidence intervall of parameter a in %', 'relative deviation
135     of confidence intervall of parameter b in %', ' ', ' ', '
136     Message'};
137
138 HeadingInputData = {'Name of the experiment', 'Date', 'Electrode
139     configuration', 'Anode', 'Electrode distance', 'Aqueous phase'
140     , 'Solvent phase', 'Phase ratio', 'Voltage', 'Experiment
141     duration (approx.)', 'Amount aq. phase', 'Amount sol. phase',
142     'Notes'};
143
144 SubheadingModel = {'Separation Data Model', 'LowerBoundary', '

```

```

    HigherBoundary'}';
133
134 % Spread the Subheading of the model is repeated for all models.
135
136 colvar=1;
137 while colvar<length(allFitParameters)*3
138     SubHeadingAllModels(colvar)=SubheadingModel(1);
139     colvar=colvar+1;
140     SubHeadingAllModels(colvar)=SubheadingModel(2);
141     colvar=colvar+1;
142     SubHeadingAllModels(colvar)=SubheadingModel(3);
143     colvar=colvar+1;
144 end
145
146 %% Writing the results into the excel sheet named before
147 % (Excelname).
148
149 % Separation data
150
151 warning off MATLAB:xlswrite:AddSheet;
152 xlswrite(ExcelName, ExpName, 'Separation Data', 'B1');
153 xlswrite(ExcelName, allSeparationData, 'Separation Data', 'B4');
154 xlswrite(ExcelName, time, 'Separation Data', 'A4');
155 xlswrite(ExcelName, timename, 'Separation Data', 'A1');
156
157 % Modelling data
158
159 xlswrite(ExcelName, ExpNameModel, 'Modelling Data', 'B1');
160 xlswrite(ExcelName, SubHeadingAllModels, 'Modelling Data', 'B3');
161 xlswrite(ExcelName, ModelData, 'Modelling Data', 'B4');
162 xlswrite(ExcelName, time, 'Modelling Data', 'A4');
163 xlswrite(ExcelName, timename, 'Modelling Data', 'A1');
164
165 % Model parameters
166
167 xlswrite(ExcelName, ExpName, 'Model Parameters', 'A2');
168 xlswrite(ExcelName, HeadingFitPar, 'Model Parameters', 'A1');

```

```

169 xlswrite(ExcelName, allFitParameters, 'Model Parameters', 'B2');
170 xlswrite(ExcelName, allBoundaries, 'Model Parameters', 'E2');
171 xlswrite(ExcelName, relDeva.', 'Model Parameters', 'I2');
172 xlswrite(ExcelName, relDevb.', 'Model Parameters', 'J2');
173 xlswrite(ExcelName, allMessages, 'Model Parameters', 'M2');
174
175 % Overview about the input data
176
177 xlswrite(ExcelName, HeadingInputData, 'Overview Input Data', 'A1');
178 xlswrite(ExcelName, ExpName.', 'Overview Input Data', 'A2');
179 xlswrite(ExcelName, allInputData.', 'Overview Input Data', 'B2');
180
181 disp('----- FA FINISH -----')

```

FOLDERANALYSIS

```

1 % This function reads the .png files in the actual Folder
2 % (actualFolder) and stores it to a specified folder
3 % (storeFolder). Additionally all input and result data including
4 % the model parameters are read from the excel file.
5
6 function [allpng, inputData, separationData, fitData, fitDataLB,
7         fitDataHB, fitParameters, rsquare, message, boundaries] =
8         Folderanalysis(actualFolder, AnalysisInterval, extension)
9
10 cd(actualFolder)
11 CurrentDirectory = actualFolder;
12 [up, folder, ~] = fileparts(CurrentDirectory);
13 Expname = folder; % Name of the analysed experiment/folder
14
15 % The first part is a check, whether the result .png file exists.
16 % This is done to avoid error messages due to empty result
17 % matrices. filecheck~=2 means, that it is not true that there is
18 % a .png file with the name searched for. If so, the result
19 % matrices are built as empty vectors and a warning is displayed.
20
21 filecheck = exist(strcat('figure_CRE_SP_', extension, Expname,

```

```

    .png'), 'file');
20 if filecheck~=2
21     fprintf('Warning: File does not exist: %s \n\nContinuing with
        next experiment. \n', strcat('figure_CRE_SP_',extension,
            Expname, '.png'));
22     allpng = [];
23     inputData =[];
24     separationData =[];
25     fitData =[];
26     fitDataLB =[];
27     fitDataHB =[];
28     fitParameters = [];
29     rsquare = [];
30     message = [];
31     boundaries = [];
32     return
33 end
34
35 % Reading the .png files of interest, i.e. those with a
36 % specified name
37
38 pngFitFiles = dir(strcat('figure_CRE_SP_',extension,Expname,
        '*.png'));
39 pngCutFiles = dir(strcat('cutfigure',extension,Expname, '*.png'));
40 numfiles = length(pngFitFiles);
41 allpng = cell(2, numfiles);
42
43 % All .png files of interest are stored into allpng
44
45 for k = 1:numfiles
46     allpng{1,k} = imread(pngCutFiles(k).name);
47     allpng{2,k} = imread(pngFitFiles(k).name);
48 end
49
50 % Reading the result excel file and saving the data to
51 % several variables for further processing.
52

```

```

53 [~,~,allthingsexp] = xlsread(strcat(Expname, '.xlsx'),
    strcat('CRE_SP_',Expname,extension));
54 ExcelComplete = xlsread(strcat(Expname, '.xlsx'),
    strcat('CRE_SP_',Expname,extension));
55 fitParameters = xlsread(strcat(Expname, '.xlsx'),
    strcat('CRE_SP_',Expname,extension), 'J2:J3');
56 rsquare = xlsread(strcat(Expname, '.xlsx'), strcat('CRE_SP_',
    Expname,extension), '03');
57 lowerBoundaries = xlsread(strcat(Expname, '.xlsx'),
    strcat('CRE_SP_',Expname,extension), 'K2:K3');
58 upperBoundaries = xlsread(strcat(Expname, '.xlsx'),
    strcat('CRE_SP_',Expname,extension), 'L2:L3');
59
60 separationData = ExcelComplete(:,2);
61 fitData = ExcelComplete(:,3);
62 fitDataLB = ExcelComplete(:,4);
63 fitDataHB = ExcelComplete(:,5);
64 message = allthingsexp{2,16};
65 boundaries = [lowerBoundaries',upperBoundaries'];
66
67 % Reading the input spreadsheet and saving the data to
68 % inputData for further processing.
69 [~,~,allInput] = xlsread(strcat(Expname, '.xlsx'), 'Tabelle1');
70
71 for i= 1:12
72     inputData{i,1} = allInput{i,2};
73 end
74
75 fprintf('Reading and saving of all .png files finished \n\n')

```

© 2017 The MathWorks, Inc. MATLAB and Simulink are registered trademarks of The MathWorks, Inc. See mathworks.com/trademarks for a list of additional trademarks. Other product or brand names may be trademarks or registered trademarks of their respective holders.

APPENDIX B. THERMAL SPLITTING

In this chapter the temperature over time of the thermal splitting experiment (figure B.1 as well as the calculation for the power demand are shown.

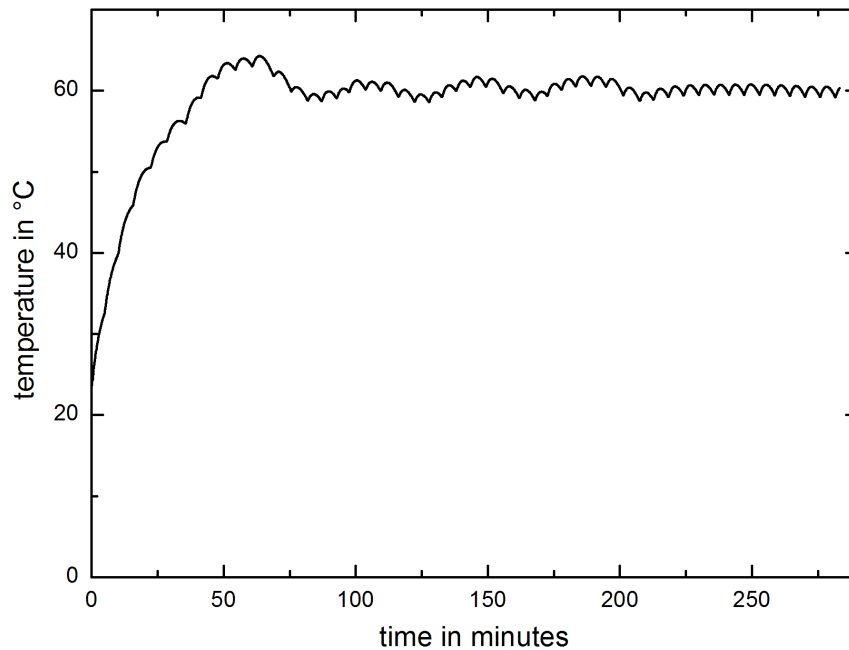


Figure B.1.: Temperature over time of the thermal splitting experiment (RMA006)

The assumptions to calculate the power demand are summarized in table B.1. Equation B.1 is used to perform this calculation. The numbers are put inside in equation B.2. 46.52 kWh are necessary to heat 1 m³ of emulsion from 20 to 60 °C. Heat losses or cooling power necessary to avoid evaporation are not included.

Table B.1.: Assumptions made for thermal splitting power calculation

<i>Assumption</i>	<i>Unit</i>	<i>Value [93]</i>	<i>Notes</i>
Volume	m ³	1	pure water
c_p	kJ/kg K	4.187	pure water
ΔT	K	40	from 20 to 60 °C
Density ρ	kg/m ³	1000	pure water

APPENDIX B. THERMAL SPLITTING

$$Q = m \cdot c_p \cdot \Delta T = V \cdot \rho \cdot c_p \cdot \Delta T \quad (\text{B.1})$$

$$Q = 1 \cdot 1000 \cdot 4.187 \cdot 40 = 167480 \text{kJ} = 46.52 \text{kWh} \quad (\text{B.2})$$

APPENDIX C. FLOTATION

In this chapter the reproducibility of the electro flotation experiments is shown.

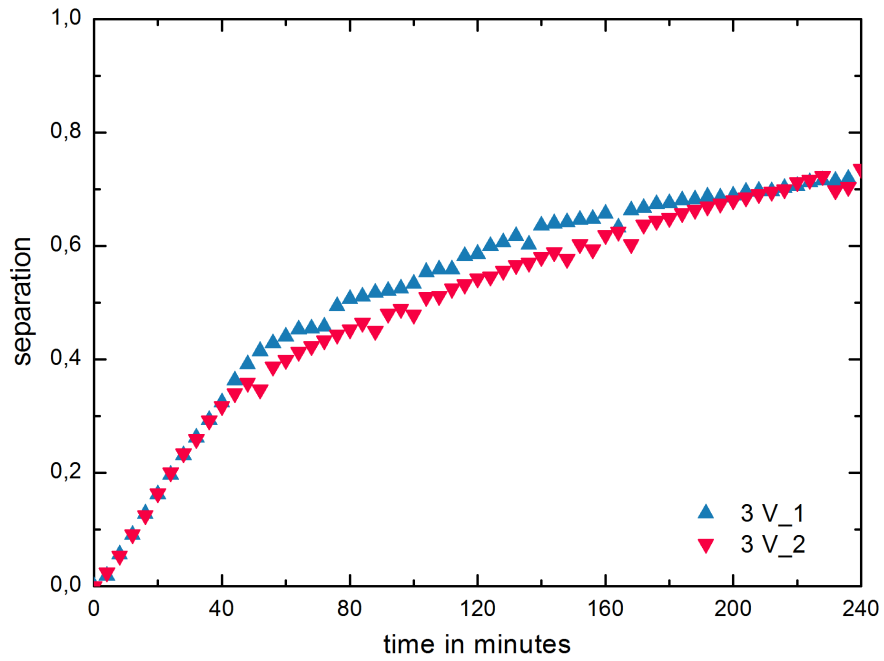


Figure C.1.: Reproducibility of the electro flotation experiment performed at 3 V

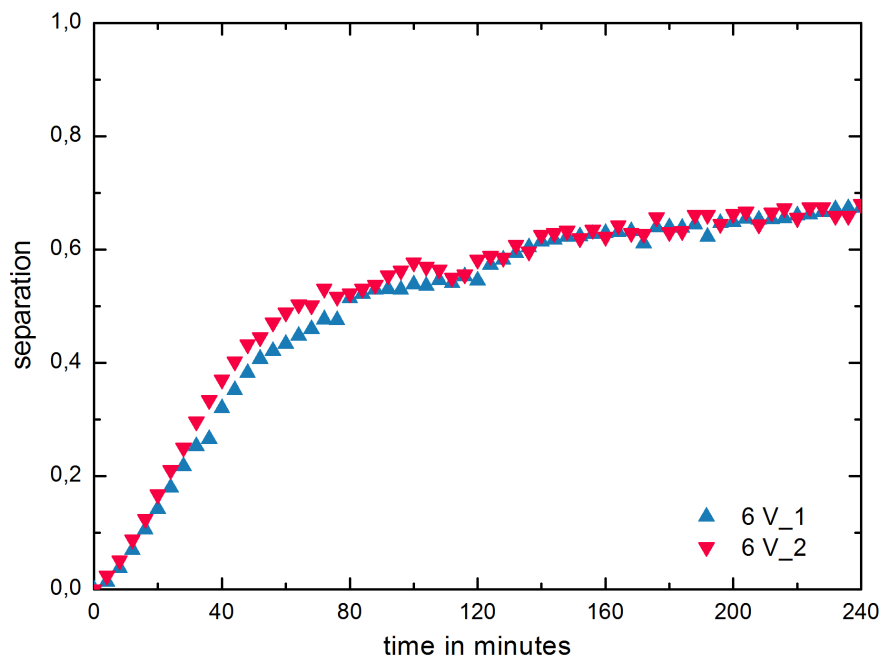


Figure C.2.: Reproducibility of the electro flotation experiment performed at 6 V

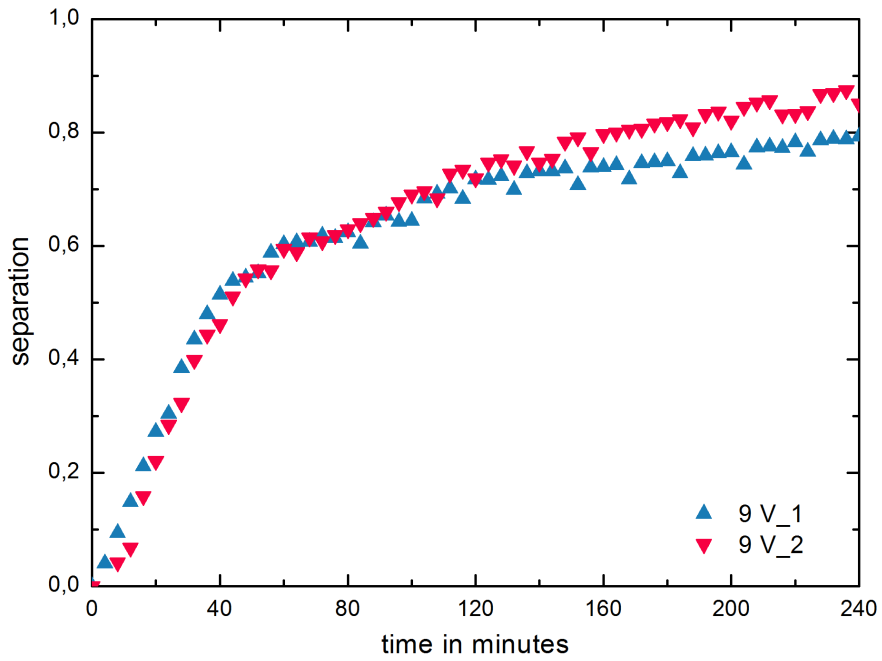


Figure C.3.: Reproducibility of the electro flotation experiment performed at 9 V

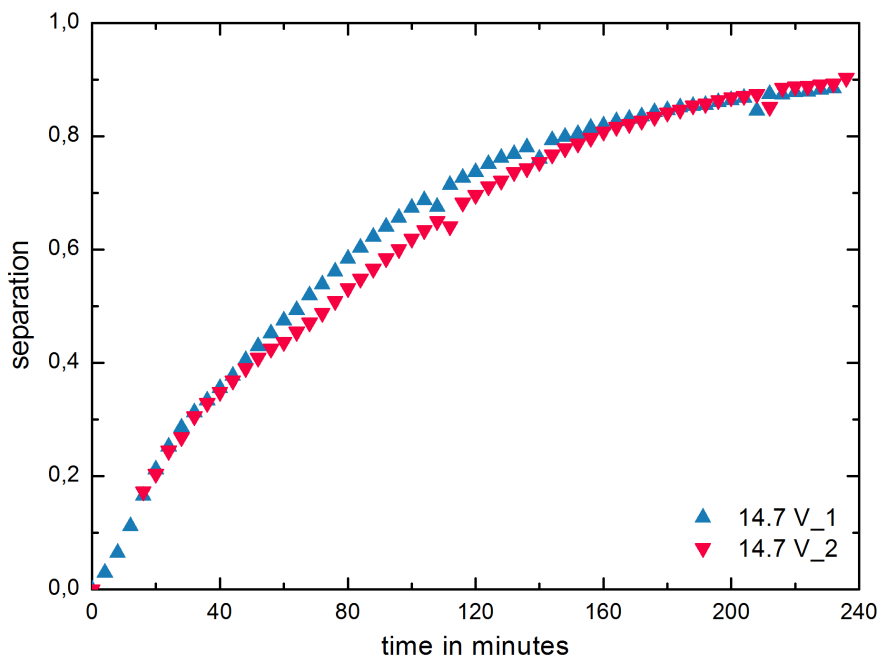


Figure C.4.: Reproducibility of the electro flotation experiment performed at 14.7 V

APPENDIX D. CALIBRATION OF THE ULTRASONIC SCANNER

For calibrating the ultrasonic scanner different mixtures of SSK and water have been produced and analysed in the equipment. Additionally, pure water is analysed in the ultrasonic scanner to get the end point of the calibration. The result is depicted in figure D.1.

In table D.1 the values of the calibration are compiled.

Shellsol K + Water, SSK = 30%wt, $\varepsilon_0 = 0.35$, $T = 20^\circ\text{C}$, Mixing time = 60 s

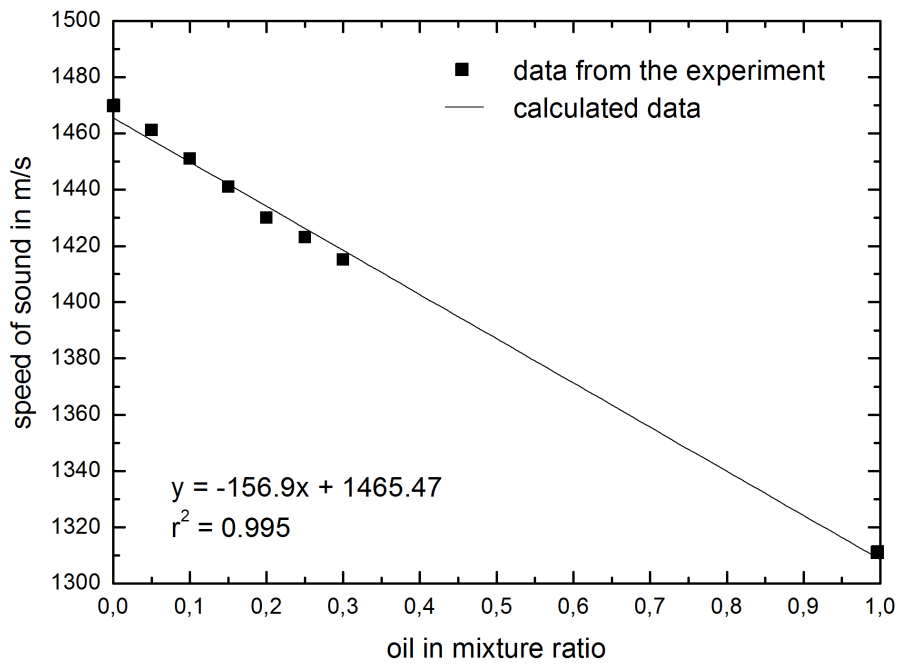


Figure D.1.: Calibration of the ultrasonic scanner

Table D.1.: Data of the ultrasonic scanner calibration

<i>Oil-in-mixture</i> <i>wt. %</i>	<i>Speed of sound</i> <i>m/s</i>
0	1472
0.05	1461
0.1	1451
0.15	1441
0.2	1430
0.25	1423
0.3	1415
1.0	1311

APPENDIX E. REPRODUCIBILITY OF THE ELECTRIC FIELD EXPERIMENTS

In this chapter the reproducibility of the electric field splitting experiments is shown for each setting. The names of the experiments and the respective settings including electrode distance, voltage, electric field strength, angle, electrode arrangement and mass weighed in are shown in tables E.1 to E.9.

Table E.1.: Experimental settings of the experiments using 2 plate electrodes

<i>Name</i>	<i>Electrode distance</i> <i>in cm</i>	<i>Voltage</i> <i>in V</i>	<i>Electric field strength</i> <i>in V/m</i>	<i>Angle</i>	<i>Electrode arrangement</i>	<i>Weight H₂O</i> <i>in g</i>	<i>Weight solvent</i> <i>in g</i>
CS020	5	2	40	0	A K	497.50	2.50
CS021	5	2	40	0	A K	497.48	2.48
CS024	5	2	40	0	A K	497.50	2.52
CS015	10	4	40	0	A K	497.50	2.50
CS017	10	4	40	0	A K	497.52	2.52
CS018	10	4	40	0	A K	497.50	2.50
HW020_1	6	3	50	0	A K	1243.77	6.28
HW020_2	6	3	50	0	A K	1243.81	6.26
HW021_1	12	6	50	0	A K	1243.69	6.29
HW021_2	12	6	50	0	A K	1243.72	6.21
HW022_1	24	12	50	0	A K	1243.76	6.24
HW022_2	24	12	50	0	A K	1243.78	6.29
RMA030	10	6	60	0	A K	497.76	2.50
RMA031	10	6	60	0	A K	497.72	2.50
CS019	5	4	80	0	A K	497.50	2.50
CS022	5	4	80	0	A K	497.52	2.50
CS023	5	4	80	0	A K	497.49	2.50
CS013	10	8	80	0	A K	497.50	2.50
CS014	10	8	80	0	A K	497.50	2.50
CS016	10	8	80	0	A K	497.50	2.50

Table E.1.: Experimental settings of the experiments using 2 plate electrodes (continued)

<i>Name</i>	<i>Electrode distance</i> <i>in cm</i>	<i>Voltage</i> <i>in V</i>	<i>Electric field strength</i> <i>in V/m</i>	<i>Angle</i>	<i>Electrode arrangement</i>	<i>Weight H₂O</i> <i>in g</i>	<i>Weight solvent</i> <i>in g</i>
CS009	5	5	100	0	A K	497.50	2.50
CS010	5	5	100	0	A K	497.50	2.50
CS011	5	5	100	0	A K	497.50	2.50
HW023_1	5	5	100	0	A K	1243.80	6.27
HW023_2	5	5	100	0	A K	1243.81	6.22
CS007	10	10	100	0	A K	497.50	2.50
CS008	10	10	100	0	A K	497.50	2.50
CS012	10	10	100	0	A K	497.50	2.50
HW024_1	10	10	100	0	A K	1243.79	6.27
HW024_2	10	10	100	0	A K	1243.71	6.26
HW025_1	15	15	100	0	A K	1243.74	6.29
HW025_2	15	15	100	0	A K	1243.71	6.28
CS002	5	6	120	0	A K	497.50	2.50
CS005	5	6	120	0	A K	497.50	2.50
CS006	5	6	120	0	A K	497.50	2.50
CS001	10	12	120	0	A K	497.50	2.50
CS003	10	12	120	0	A K	497.50	2.50
CS004	10	12	120	0	A K	497.50	2.50
HW001_1	10	12	120	0	A K	1243.71	6.26
HW001_2	10	12	120	0	A K	1243.79	6.26
RMA029	10	12	120	0	A K	497.59	2.48
RMA032	10	12	120	0	A K	497.75	2.50

Table E.2.: Experimental settings of the experiments using 2 inclined plate electrodes

<i>Name</i>	<i>Electrode distance</i> <i>in cm</i>	<i>Voltage</i> <i>in V</i>	<i>Electric field strength</i> <i>in V/m</i>	<i>Angle</i>	<i>Electrode arrangement</i>	<i>Weight H₂O</i> <i>in g</i>	<i>Weight solvent</i> <i>in g</i>
HW008_1	10	6	85	45	A K	1243.73	6.25
HW008_2	10	6	85	45	A K	1243.76	6.3
HW010_1	5	6	170	45	A K	1243.79	6.3
HW010_2	5	6	170	45	A K	1243.74	6.29
HW004_1	10	12	170	45	A K	1243.72	6.25
HW004_2	10	12	170	45	A K	1243.81	6.25
HW006_1	5	12	339	45	A K	1243.78	6.25
HW006_2	5	12	339	45	A K	1243.79	6.29
HW009_1	10	6	85	45	K A	1243.78	6.29
HW009_2	10	6	85	45	K A	1243.81	6.28
HW011_1	5	6	170	45	K A	1243.77	6.26
HW011_1	5	6	170	45	K A	1243.69	6.29
HW005_1	10	12	170	45	K A	1243.62	6.29
HW005_2	10	12	170	45	K A	1243.74	6.27
HW007_1	5	12	339	45	K A	1243.71	6.26
HW007_2	5	12	339	45	K A	1243.74	6.24

Table E.3.: Experimental settings of the experiments using 3 plate electrodes in AnCaAn configuration

<i>Name</i>	<i>Electrode distance</i> <i>in cm</i>	<i>Voltage</i> <i>in V</i>	<i>Electric field strength</i> <i>in V/m</i>	<i>Angle</i>	<i>Electrode arrangement</i>	<i>Weight H₂O</i> <i>in g</i>	<i>Weight solvent</i> <i>in g</i>
CS044	5	2	40	0	A K A	497.52	2.52
CS047	5	2	40	0	A K A	497.52	2.49
CS048	5	2	40	0	A K A	497.50	2.50
HW026_1	4	2	50	0	A K A	1243.76	6.26
HW026_2	4	2	50	0	A K A	1243.81	6.27
HW028_1	8	4	50	0	A K A	1243.76	6.27
HW028_2	8	4	50	0	A K A	1243.78	6.29
HW030_1	12	6	50	0	A K A	1243.76	6.27
HW030_2	12	6	50	0	A K A	1243.77	6.24
TM035	5	3	60	0	A K A	497.50	2.51
TM039	5	3	60	0	A K A	497.50	2.61
TM054	5	3	60	0	A K A	497.57	2.51
CS043	5	4	80	0	A K A	497.48	2.52
CS045	5	4	80	0	A K A	497.49	2.49
CS046	5	4	80	0	A K A	497.50	2.52
TM041	3	3	100	0	A K A	497.53	2.52
TM042	3	3	100	0	A K A	497.49	2.50
HW032_1	4	4	100	0	A K A	1243.73	6.22
HW032_2	4	4	100	0	A K A	1243.81	6.26
CS038	5	5	100	0	A K A	497.50	2.50
CS040	5	5	100	0	A K A	497.50	2.56
CS042	5	5	100	0	A K A	497.50	2.50

Table E.3.: Experimental settings of the experiments using 3 plate electrodes in AnCaAn configuration (continued)

<i>Name</i>	<i>Electrode distance</i> <i>in cm</i>	<i>Voltage</i> <i>in V</i>	<i>Electric field strength</i> <i>in V/m</i>	<i>Angle</i>	<i>Electrode arrangement</i>	<i>Weight H₂O</i> <i>in g</i>	<i>Weight solvent</i> <i>in g</i>
HW034_1	8	8	100	0	A K A	1243.75	6.24
HW034_2	8	8	100	0	A K A	1243.76	6.28
HW036_1	12	12	100	0	A K A	1243.76	6.28
HW036_2	12	12	100	0	A K A	1243.73	6.24
CS037	5	6	120	0	A K A	497.49	2.49
CS039	5	6	120	0	A K A	497.50	2.51
CS041	5	6	120	0	A K A	497.52	2.50
TM036	5	6	120	0	A K A	497.50	2.51
TM038	5	6	120	0	A K A	497.50	2.61
HW002_1	10	12	120	0	A K A	1243.68	6.25
HW002_2	10	12	120	0	A K A	1243.61	6.29
TM045	3	6	200	0	A K A	497.59	2.50
TM046	3	6	200	0	A K A	497.54	2.50
TM058	3	6	200	0	A K A	497.50	2.51
HW038_1	4	8	200	0	A K A	1243.78	6.27
HW038_2	4	8	200	0	A K A	1243.71	6.25
HW040_1	8	16	200	0	A K A	1243.70	6.28
HW040_2	8	16	200	0	A K A	1243.74	6.23
TM040	5	12	240	0	A K A	497.53	2.52
TM043	5	12	240	0	A K A	497.49	2.50
TM044	3	9	300	0	A K A	497.59	2.50
TM059	3	9	300	0	A K A	497.61	2.52

Table E.4.: Experimental settings of the experiments using 3 plate electrodes in CaAnCa configuration

<i>Name</i>	<i>Electrode distance</i> <i>in cm</i>	<i>Voltage</i> <i>in V</i>	<i>Electric field strength</i> <i>in V/m</i>	<i>Angle</i>	<i>Electrode arrangement</i>	<i>Weight H₂O</i> <i>in g</i>	<i>Weight solvent</i> <i>in g</i>
CS034	5	2	40	0	K A K	497.50	2.50
CS035	5	2	40	0	K A K	497.51	2.51
CS036	5	2	40	0	K A K	497.52	2.49
HW027_1	4	2	50	0	K A K	1243.73	6.23
HW027_2	4	2	50	0	K A K	1243.75	6.28
HW029_1	8	4	50	0	K A K	1243.80	6.24
HW029_2	8	4	50	0	K A K	1243.78	6.21
HW031_1	12	6	50	0	K A K	1243.76	6.27
HW031_2	12	6	50	0	K A K	1243.73	6.23
CS030	5	4	80	0	K A K	497.50	2.50
CS031	5	4	80	0	K A K	497.49	2.52
CS033	5	4	80	0	K A K	497.51	2.50
HW033_1	4	4	100	0	K A K	1243.79	6.24
HW033_2	4	4	100	0	K A K	1243.72	6.27
CS028	5	5	100	0	K A K	497.52	2.54
CS029	5	5	100	0	K A K	497.53	2.50
CS032	5	5	100	0	K A K	497.51	2.52
HW035_1	8	8	100	0	K A K	1243.72	6.25
HW035_2	8	8	100	0	K A K	1243.81	6.26
HW037_1	12	12	100	0	K A K	1243.72	6.22
HW037_2	12	12	100	0	K A K	1243.75	6.28

Table E.4.: Experimental settings of the experiments using 3 plate electrodes in CaAnCa configuration (continued)

<i>Name</i>	<i>Electrode distance</i> <i>in cm</i>	<i>Voltage</i> <i>in V</i>	<i>Electric field strength</i> <i>in V/m</i>	<i>Angle</i>	<i>Electrode arrangement</i>	<i>Weight H₂O</i> <i>in g</i>	<i>Weight solvent</i> <i>in g</i>
CS025	5	6	120	0	K A K	497.52	2.50
CS026	5	6	120	0	K A K	497.50	2.49
CS027	5	6	120	0	K A K	497.51	2.51
HW003_1	10	12	120	0	K A K	1243.72	6.27
HW003_2	10	12	120	0	K A K	1243.77	6.26
HW039_1	4	8	200	0	K A K	1243.76	6.26
HW039_2	4	8	200	0	K A K	1243.78	6.24
HW041_1	8	16	200	0	K A K	1243.76	6.25
HW041_2	8	16	200	0	K A K	1243.75	6.28

Table E.5.: Experimental settings of the experiments using 3 inclined plate electrodes in AnCaAn and CaAnCa configuration

<i>Name</i>	<i>Electrode distance</i> <i>in cm</i>	<i>Voltage</i> <i>in V</i>	<i>Electric field strength</i> <i>in V/m</i>	<i>Angle</i>	<i>Electrode arrangement</i>	<i>Weight H₂O</i> <i>in g</i>	<i>Weight solvent</i> <i>in g</i>
HW018_1	4	4	141	45	A K A	1243.71	6.28
HW018_2	4	4	141	45	A K A	1243.76	6.21
HW014_1	6	6	141	45	A K A	1243.74	6.24
HW014_2	6	6	141	45	A K A	1243.76	6.23
HW016_1	4	8	283	45	A K A	1243.74	6.25
HW016_2	4	8	283	45	A K A	1243.79	6.27
HW012_1	6	12	283	45	A K A	1243.78	6.29
HW012_2	6	12	283	45	A K A	1243.76	6.22
HW019_1	4	4	141	45	K A K	1243.79	6.22
HW019_2	4	4	141	45	K A K	1243.80	6.27
HW015_1	6	6	141	45	K A K	1243.80	6.23
HW015_2	6	6	141	45	K A K	1243.77	6.21
HW017_1	4	8	283	45	K A K	1243.72	6.24
HW017_2	4	8	283	45	K A K	1243.78	6.26
HW013_1	6	12	283	45	K A K	1243.76	6.21
HW013_2	6	12	283	45	K A K	1243.78	6.26

Table E.6.: Experimental settings of the experiments using 4 plate electrodes in AnCaAnCa configuration

<i>Name</i>	<i>Electrode distance</i> <i>in cm</i>	<i>Voltage</i> <i>in V</i>	<i>Electric field strength</i> <i>in V/m</i>	<i>Angle</i>	<i>Electrode arrangement</i>	<i>Weight H₂O</i> <i>in g</i>	<i>Weight solvent</i> <i>in g</i>
TM048	3	3	100	0	A K A K	497.53	2.56
TM051	3	3	100	0	A K A K	497.60	2.51
TM049	3	6	200	0	A K A K	497.53	2.56
TM050	3	6	200	0	A K A K	497.60	2.51
TM052	1	3	300	0	A K A K	497.59	2.50
TM053	1	3	300	0	A K A K	497.53	2.51

Table E.7.: Experimental settings of the experiments using 4 plate electrodes and 3x4 rod electrodes (anodes)

<i>Name</i>	<i>Electrode distance</i> <i>in cm</i>	<i>Voltage</i> <i>in V</i>	<i>Electric field strength</i> <i>in V/m</i>	<i>Angle</i>	<i>Electrode arrangement</i>	<i>Weight H₂O</i> <i>in g</i>	<i>Weight solvent</i> <i>in g</i>
TM055	1.5	1	66.67	0	4P 3x4R(A)	497.52	2.52
TM033	1.5	2	133.33	0	4P 3x4R(A)	497.53	2.51
TM061	1.5	2	133.33	0	4P 3x4R(A)	497.52	2.51
RMA033	1.5	3	200	0	4P 3x4R(A)	497.50	2.48
TM032	1.5	3	200	0	4P 3x4R(A)	497.51	2.50
TM056	1.5	3	200	0	4P 3x4R(A)	497.49	2.50

Table E.8.: Experimental settings of the experiments using 4 plate electrodes (anodes) and 3x4 rod electrodes

<i>Name</i>	<i>Electrode distance</i> <i>in cm</i>	<i>Voltage</i> <i>in V</i>	<i>Electric field strength</i> <i>in V/m</i>	<i>Angle</i>	<i>Electrode arrangement</i>	<i>Weight H₂O</i> <i>in g</i>	<i>Weight solvent</i> <i>in g</i>
TM060	1.5	0.5	33.33	0	4P(A) 3x4R	497.51	2.50
TM057	1.5	3	200	0	4P(A) 3x4R	497.59	2.51
TM034	1.5	3	200	0	4P(A) 3x4R	497.53	2.51

Table E.9.: Experimental settings of the experiments using 4 plate electrodes in AnCaAnCa configuration investigating the industrial effluents

<i>Name</i>	<i>Electrode distance</i> <i>in cm</i>	<i>Voltage</i> <i>in V</i>	<i>Electric field strength</i> <i>in V/m</i>	<i>Angle</i>	<i>Electrode arrangement</i>	<i>Duration</i> <i>in h</i>
TM011	3	1.5	50	0	A K A K	6.5
TM012	3	1.5	50	0	A K A K	5.5
TM013	3	1.5	50	0	A K A K	6
TM014	3	1.5	50	0	A K A K	5

Table E.9.: Experimental settings of the experiments using 4 plate electrodes in AnCaAnCa configuration investigating the industrial effluents (continued)

<i>Name</i>	<i>Weight acetic acid</i> <i>in g</i>	<i>Weight alcohol</i> <i>in g</i>	<i>Weight n-undecane</i> <i>in g</i>	<i>Weight 4-DBSA</i> <i>in g</i>	<i>Weight aqueous phase</i> <i>in g</i>	<i>Weight solvent phase</i> <i>in g</i>	<i>Notes</i>
TM011	30.07	37.21	73.97	7.42	270.99	67.18	BuOH + HAc in water (overall volume 500 ml)
TM012	30.06	16.02	74.01	7.42	271.25	67.26	MeOH + HAc in water (overall volume 500 ml)
TM013	30.00	74.03	0	7.49	271.00	67.28	HAc in water (overall volume 500 ml), solvent OcOH
TM014	30.01	16.04	74.12	7.45	274.39	67.31	MeOH + HAc in water (overall volume 500 ml)

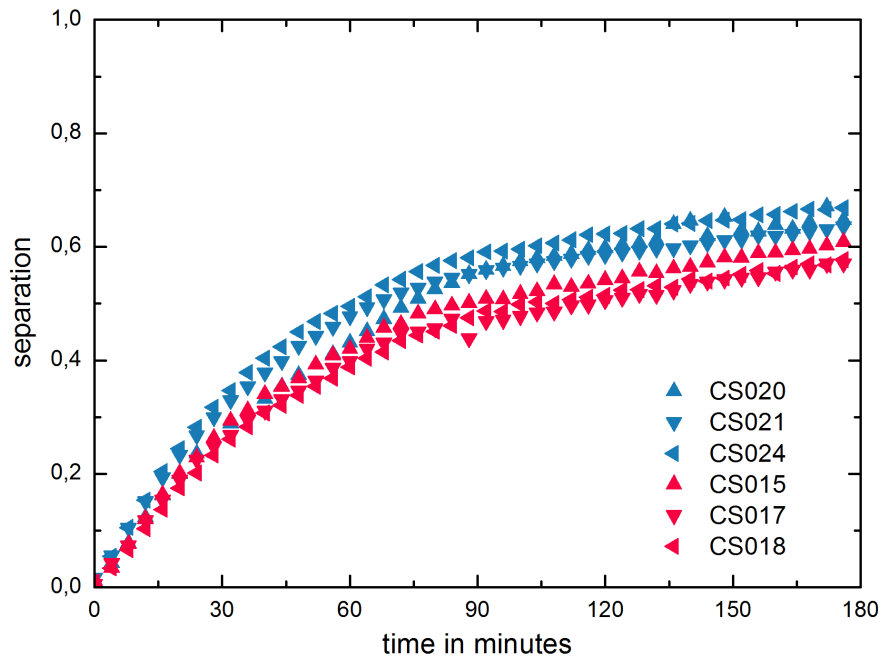


Figure E.1.: Reproducibility of the electric splitting experiment with two plate electrodes and an applied electric field of 40 V/m

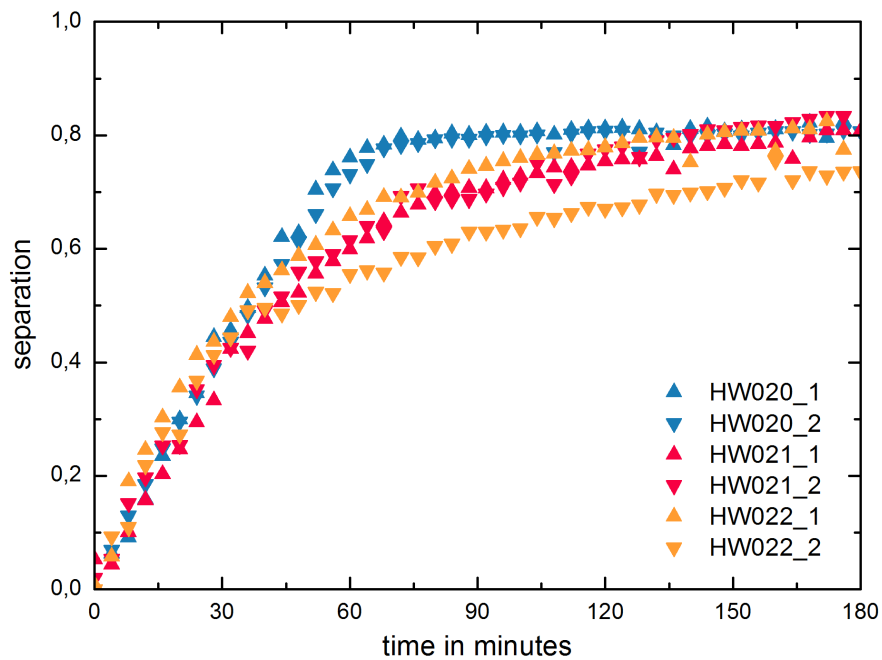


Figure E.2.: Reproducibility of the electric splitting experiment with two plate electrodes and an applied electric field of 50 V/m

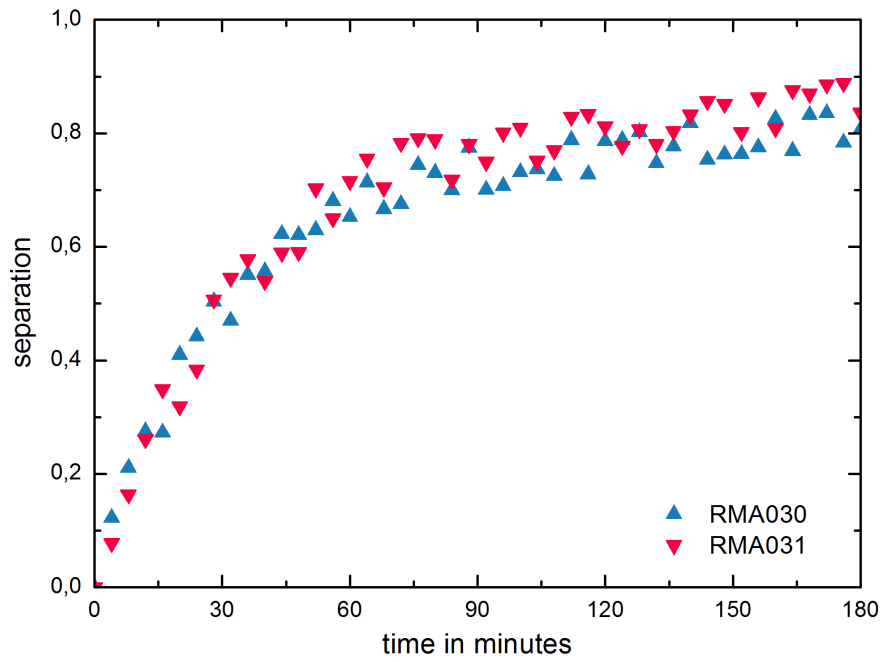


Figure E.3.: Reproducibility of the electric splitting experiment with two plate electrodes and an applied electric field of 60 V/m

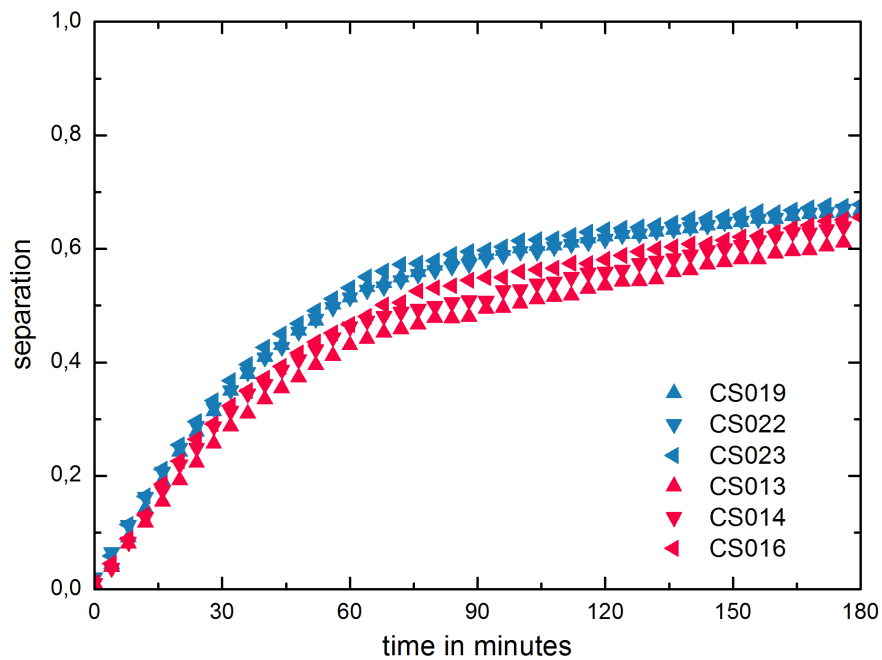


Figure E.4.: Reproducibility of the electric splitting experiment with two plate electrodes and an applied electric field of 80 V/m

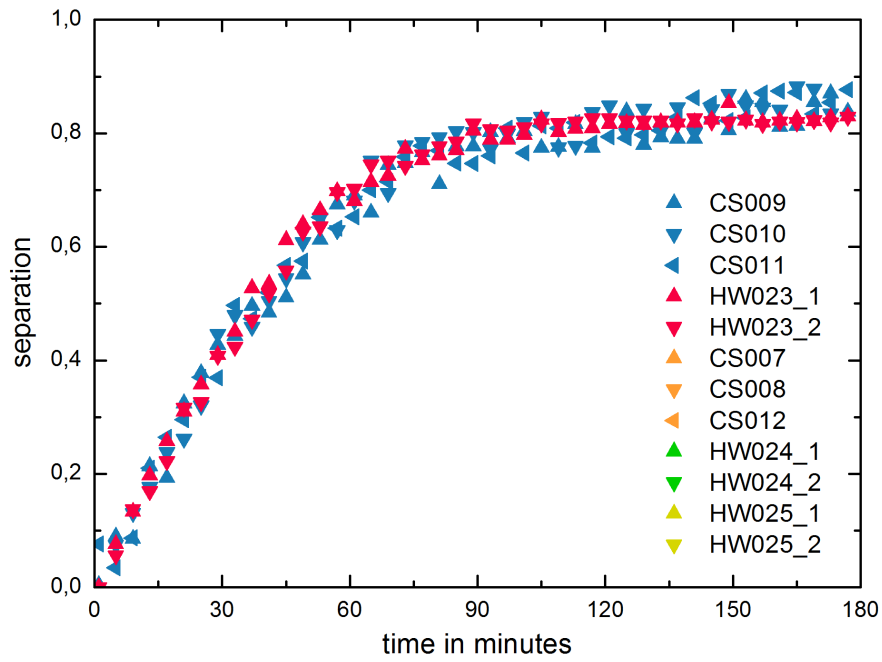


Figure E.5.: Reproducibility of the electric splitting experiment with two plate electrodes and an applied electric field of 100 V/m

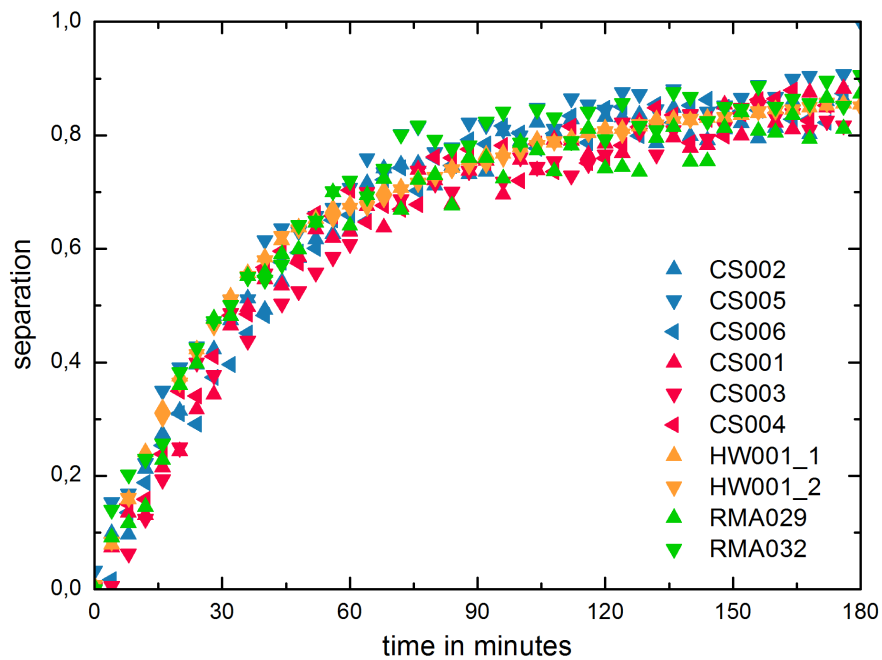


Figure E.6.: Reproducibility of the electric splitting experiment with two plate electrodes and an applied electric field of 120 V/m

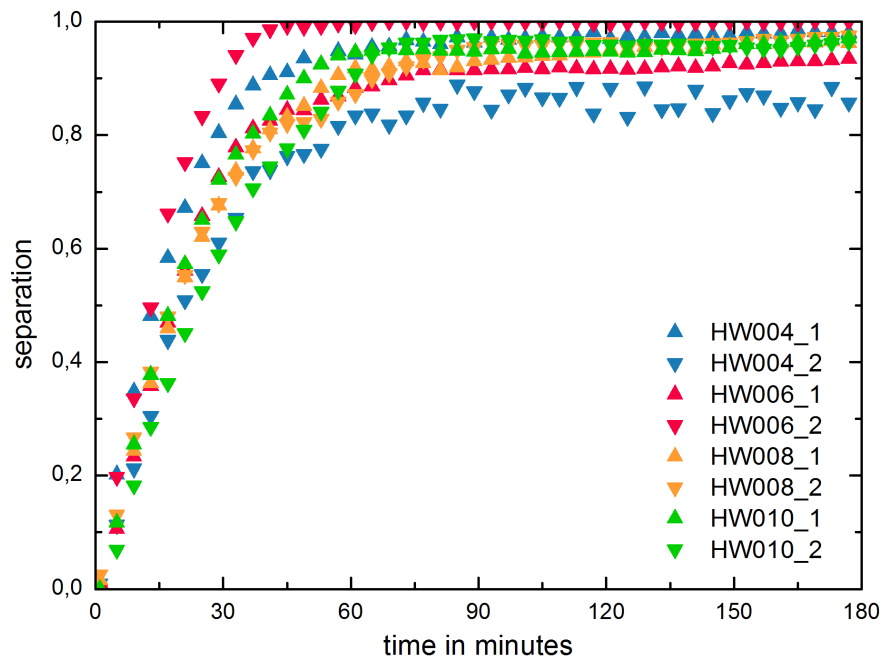


Figure E.7.: Reproducibility of the electric splitting experiment with two inclined plate electrodes with an AnCa configuration

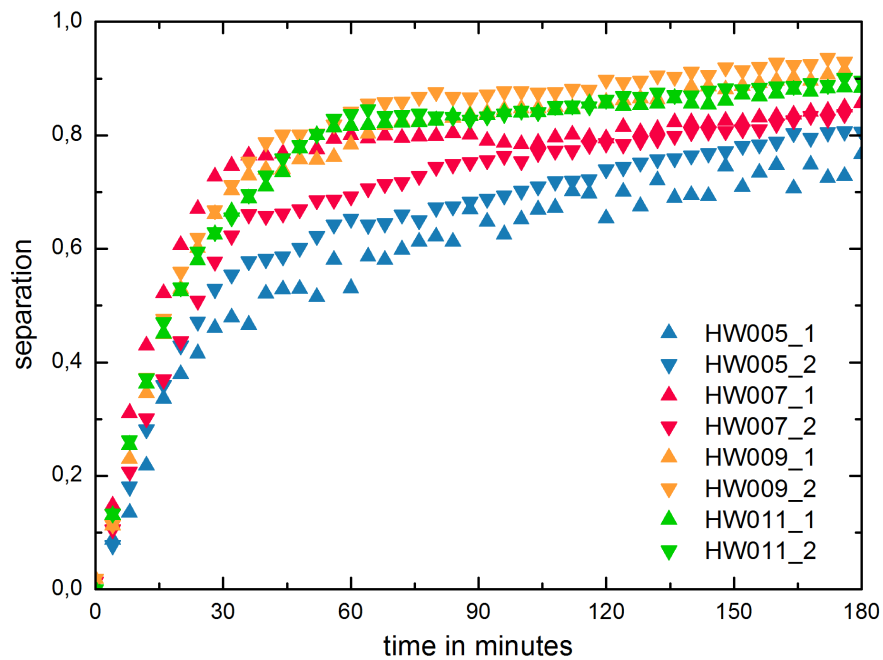


Figure E.8.: Reproducibility of the electric splitting experiment with two inclined plate electrodes with an CaAn configuration

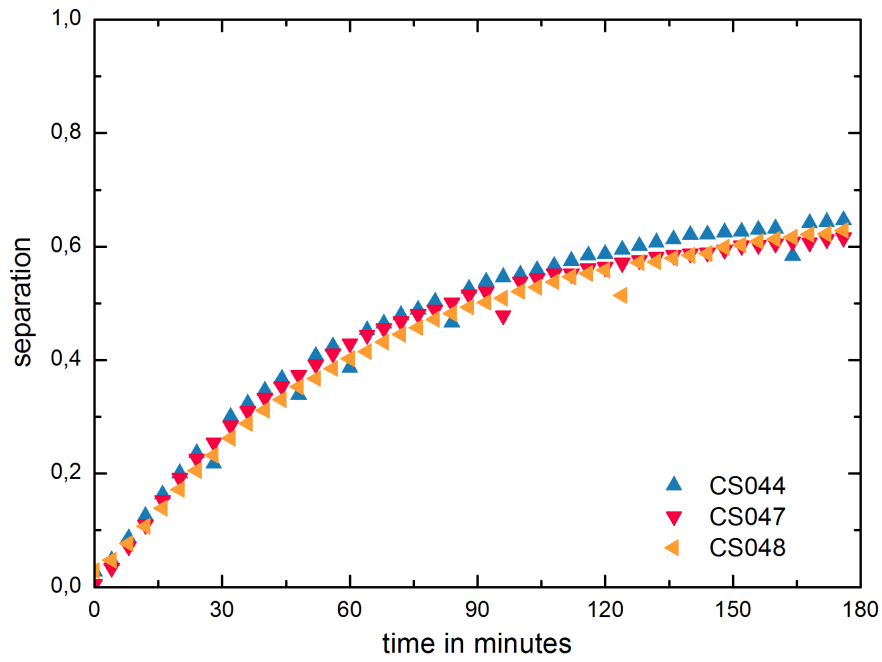


Figure E.9.: Reproducibility of the electric splitting experiment with three plate electrodes with an AnCaAn configuration and an applied electric field of 40 V/m

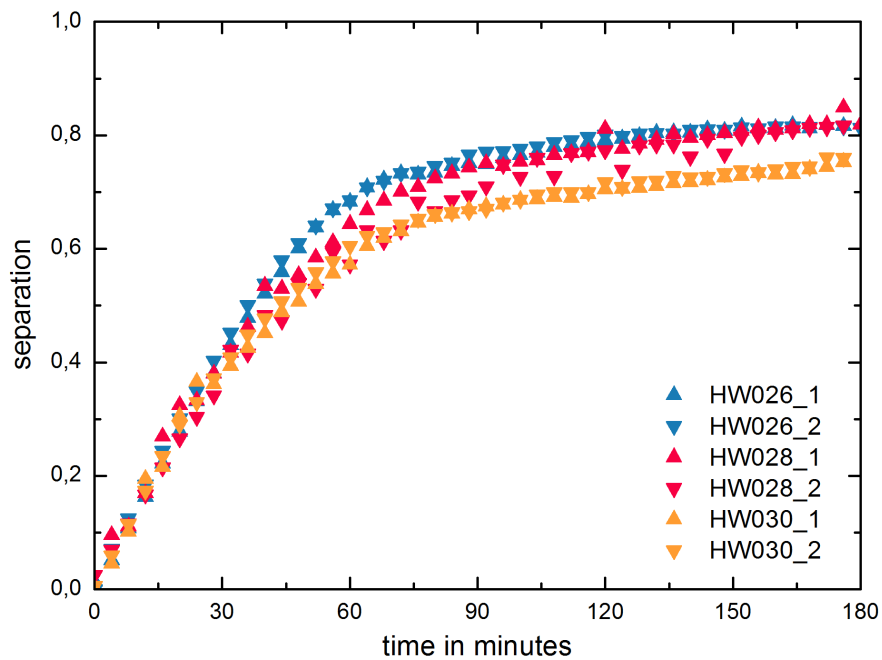


Figure E.10.: Reproducibility of the electric splitting experiment with three plate electrodes with an AnCaAn configuration and an applied electric field of 50 V/m

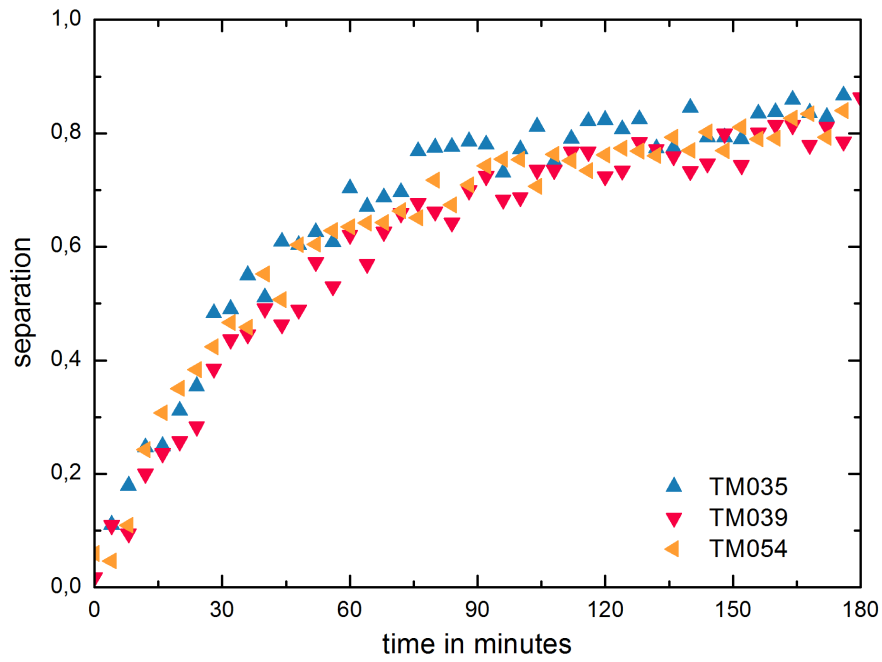


Figure E.11.: Reproducibility of the electric splitting experiment with three plate electrodes with an AnCaAn configuration and an applied electric field of 60 V/m

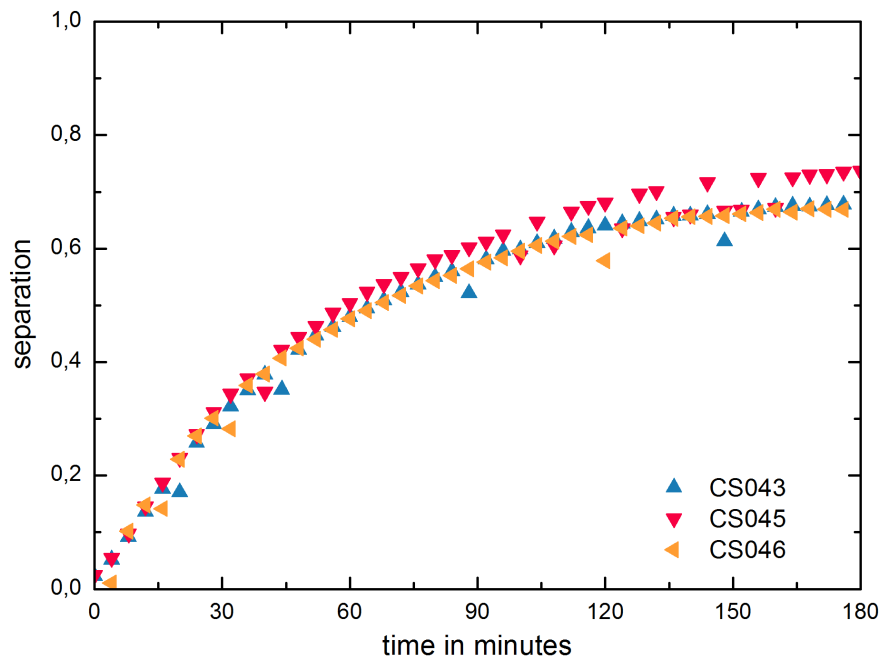


Figure E.12.: Reproducibility of the electric splitting experiment with three plate electrodes with an AnCaAn configuration and an applied electric field of 80 V/m

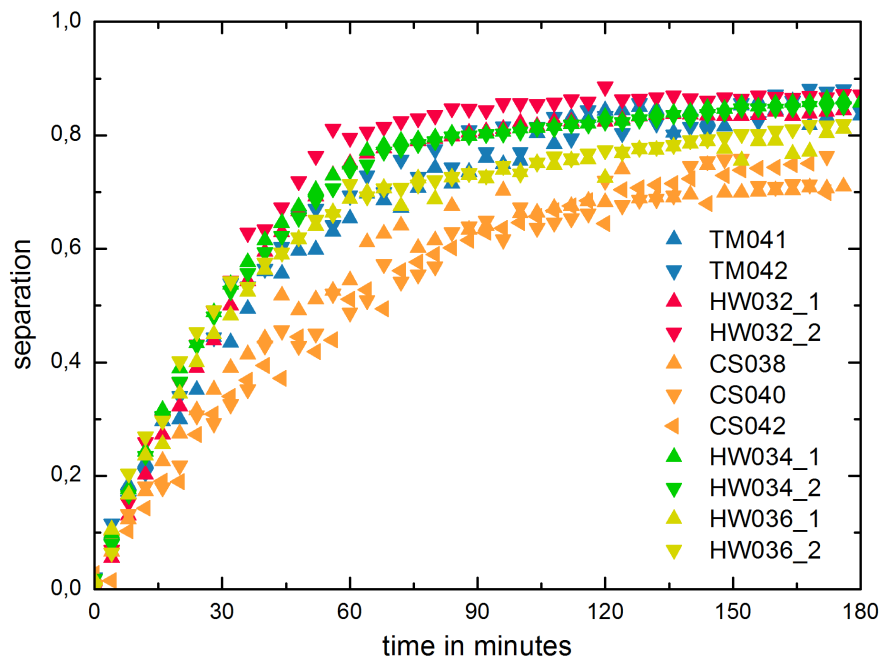


Figure E.13.: Reproducibility of the electric splitting experiment with three plate electrodes with an AnCaAn configuration and an applied electric field of 100 V/m

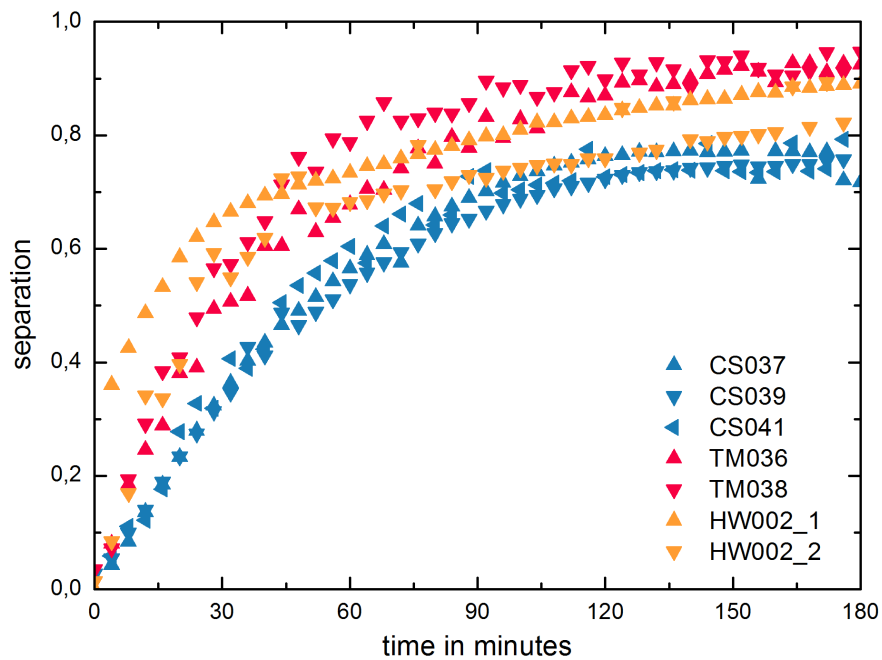


Figure E.14.: Reproducibility of the electric splitting experiment with three plate electrodes with an AnCaAn configuration and an applied electric field of 120 V/m

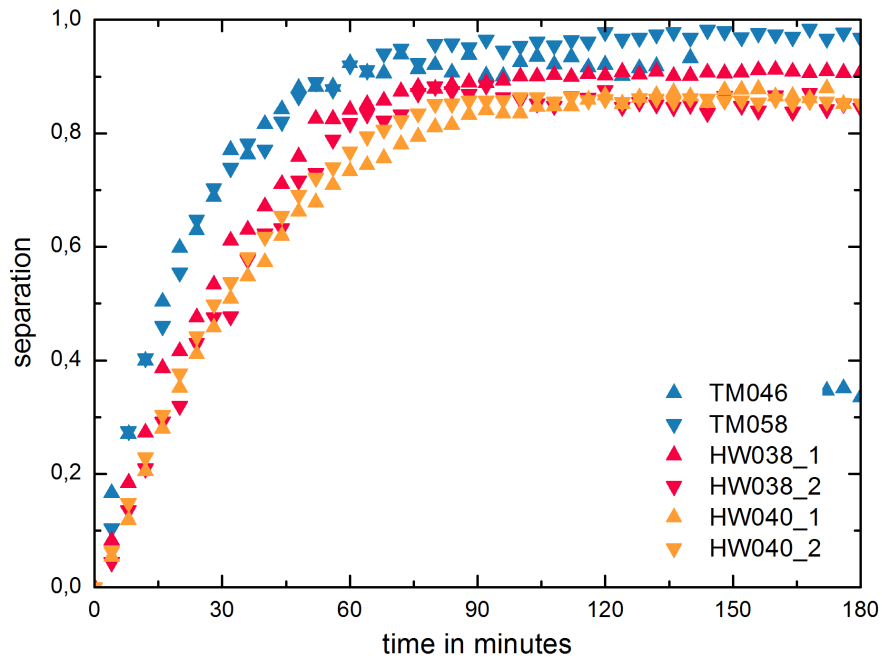


Figure E.15.: Reproducibility of the electric splitting experiment with three plate electrodes with an AnCaAn configuration and an applied electric field of 200 V/m

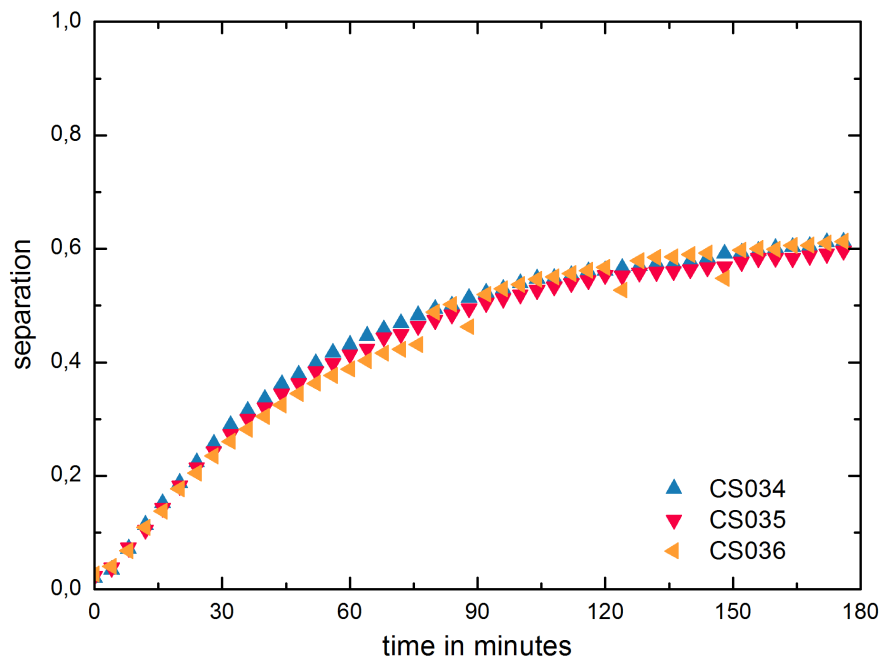


Figure E.16.: Reproducibility of the electric splitting experiment with three plate electrodes with an CaAnCa configuration and an applied electric field of 40 V/m

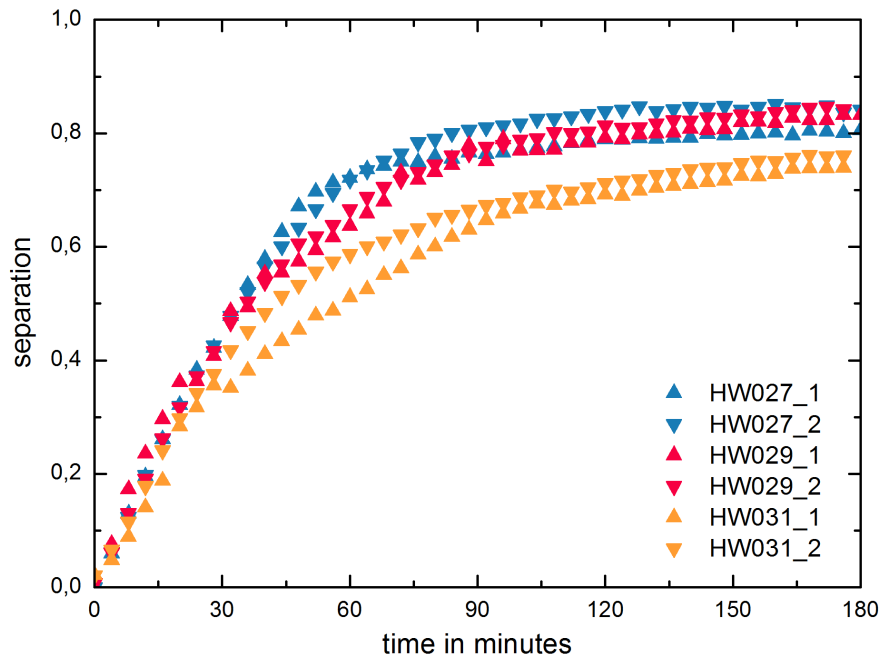


Figure E.17.: Reproducibility of the electric splitting experiment with three plate electrodes with an CaAnCa configuration and an applied electric field of 50 V/m

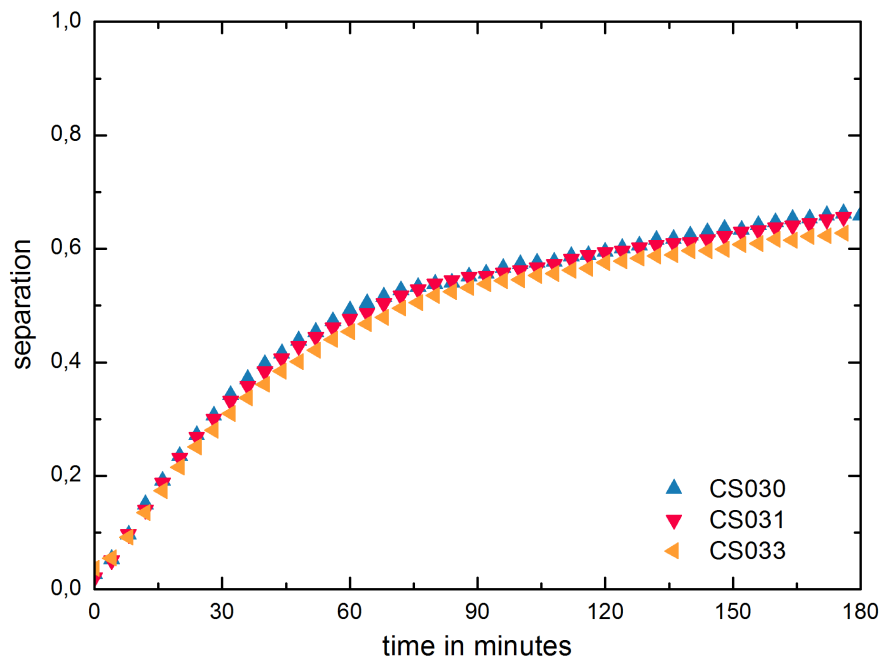


Figure E.18.: Reproducibility of the electric splitting experiment with three plate electrodes with an CaAnCa configuration and an applied electric field of 80 V/m

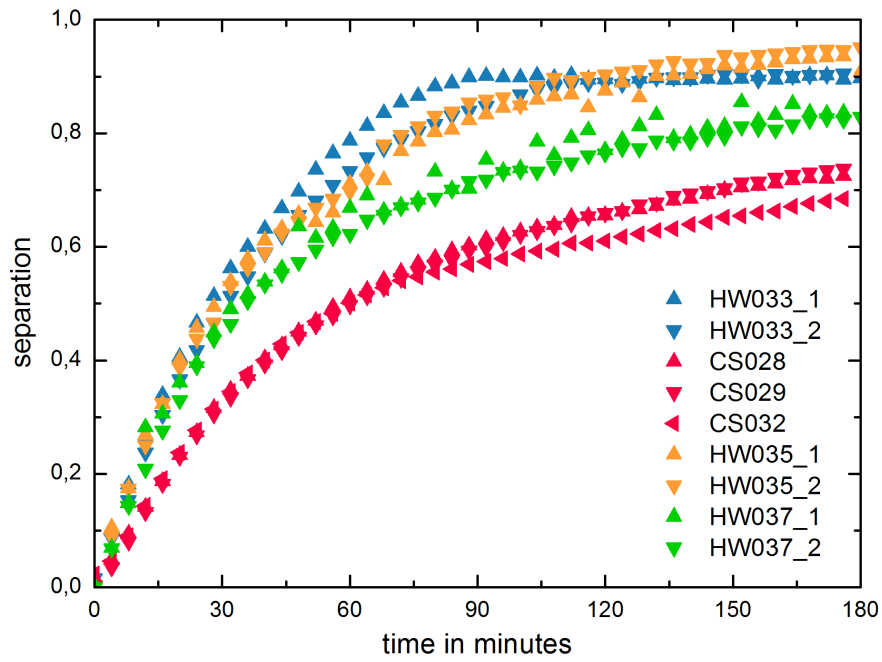


Figure E.19.: Reproducibility of the electric splitting experiment with three plate electrodes with an CaAnCa configuration and an applied electric field of 100 V/m

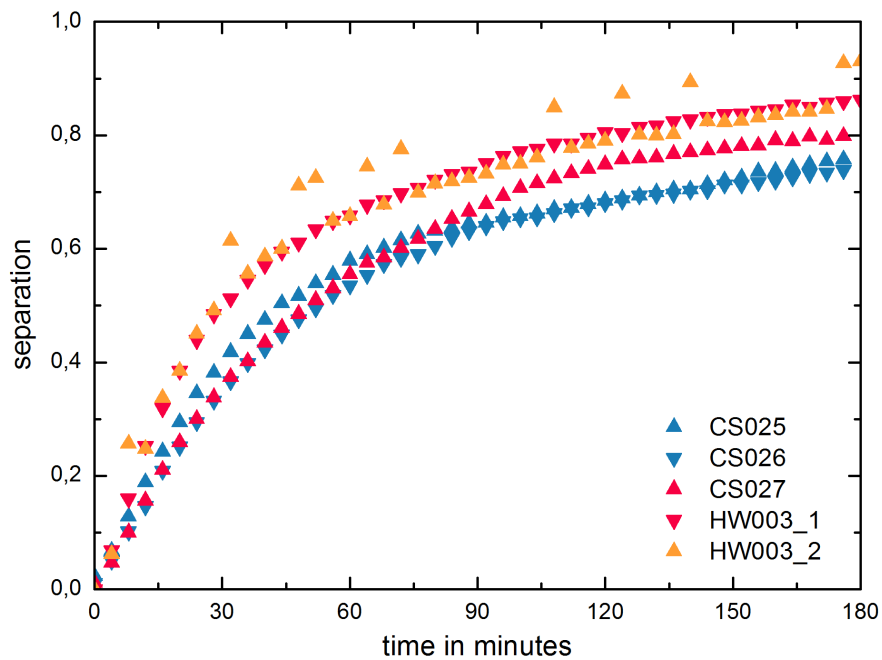


Figure E.20.: Reproducibility of the electric splitting experiment with three plate electrodes with an CaAnCa configuration and an applied electric field of 120 V/m

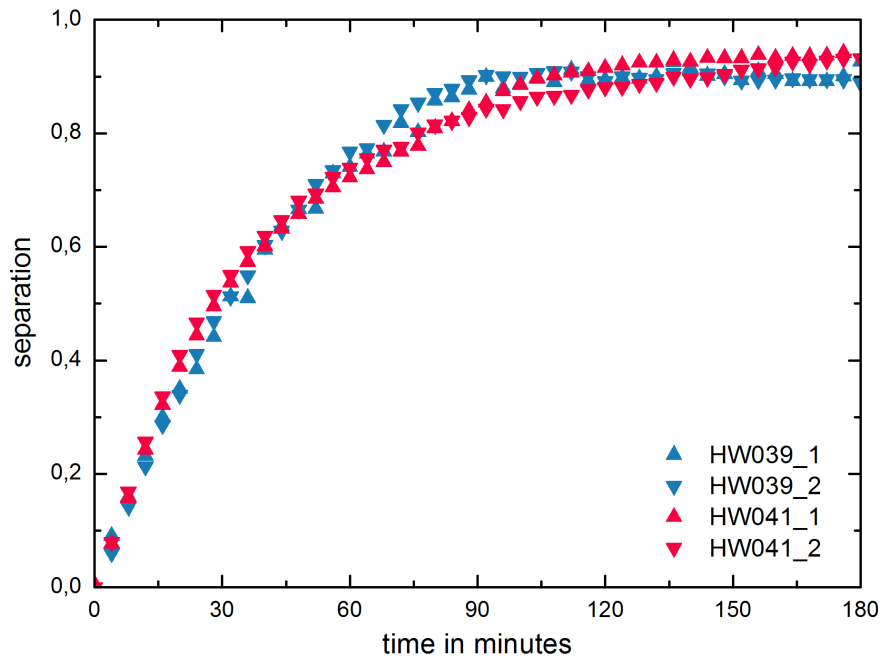


Figure E.21.: Reproducibility of the electric splitting experiment with three plate electrodes with an CaAnCa configuration and an applied electric field of 200 V/m

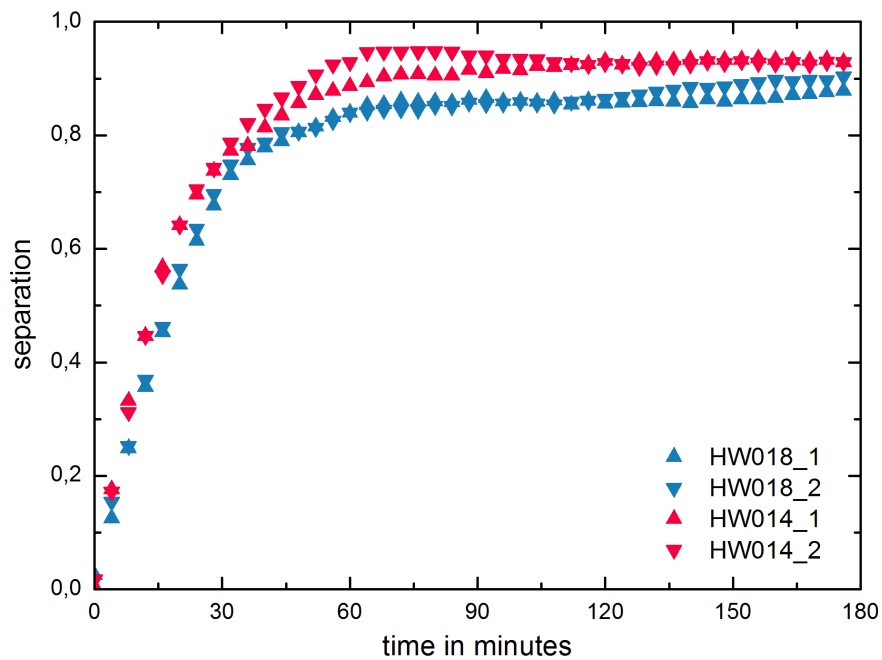


Figure E.22.: Reproducibility of the electric splitting experiment with three inclined plate electrodes with an AnCaAn configuration and an applied electric field of 141 V/m

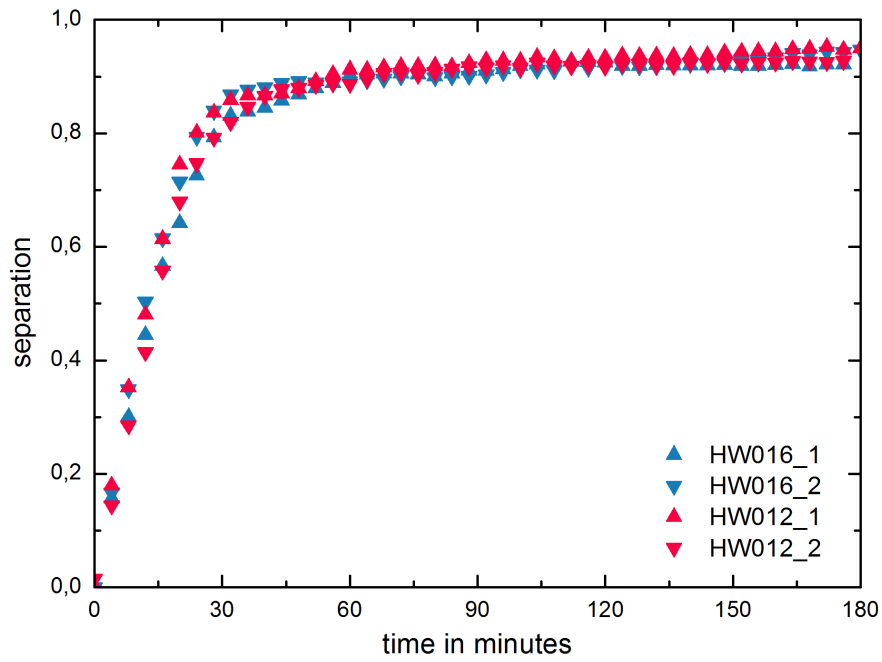


Figure E.23.: Reproducibility of the electric splitting experiment with three inclined plate electrodes with an AnCaAn configuration and an applied electric field of 283 V/m

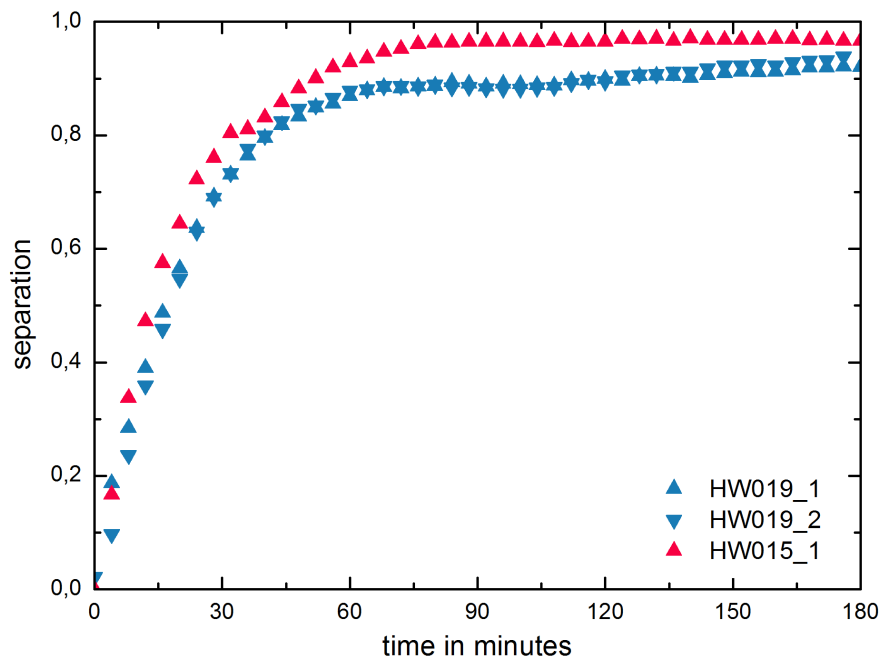


Figure E.24.: Reproducibility of the electric splitting experiment with three inclined plate electrodes with an CaAnCa configuration and an applied electric field of 141 V/m

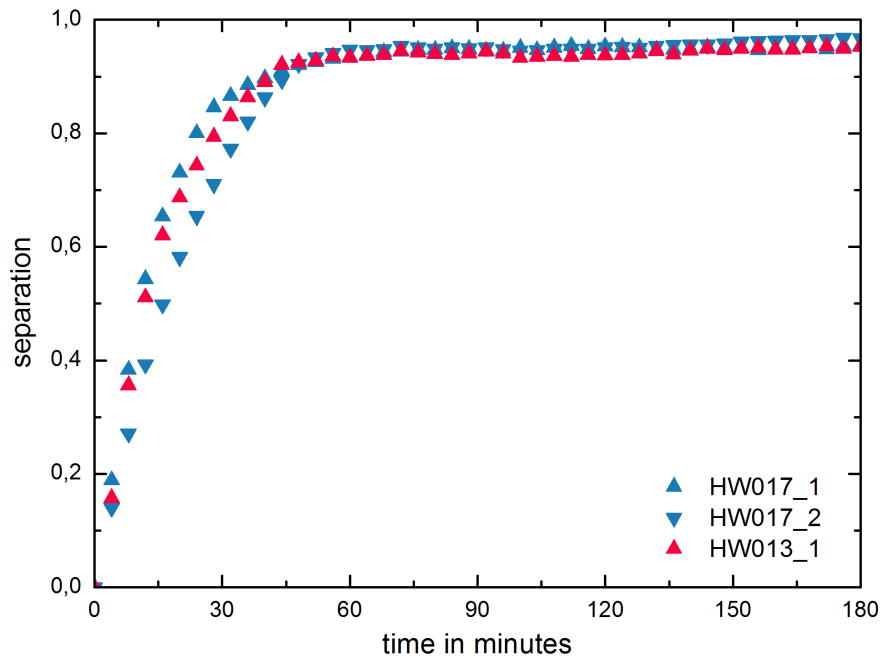


Figure E.25.: Reproducibility of the electric splitting experiment with three inclined plate electrodes with an CaAnCa configuration and an applied electric field of 283 V/m

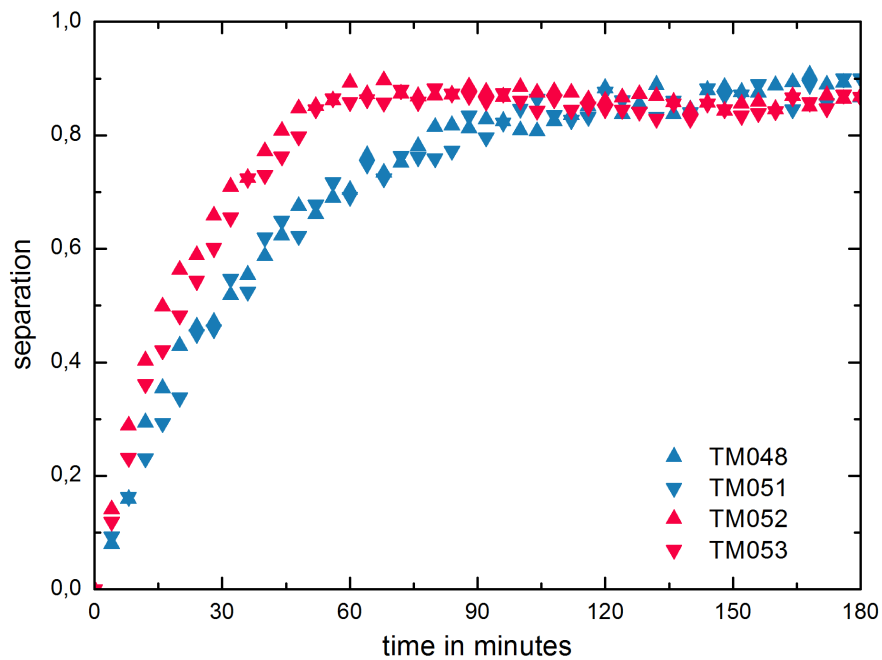


Figure E.26.: Reproducibility of the electric splitting experiment with four plate electrodes with an AnCaAnCa configuration

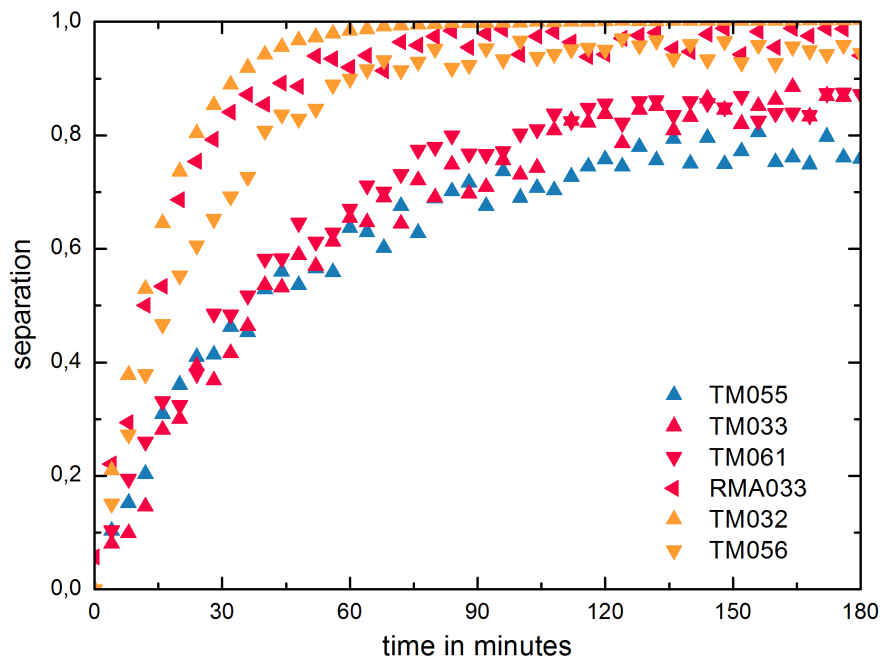


Figure E.27.: Reproducibility of the electric splitting experiment with four inclined plate electrodes and 3x4 rod electrodes with the rods acting as anodes

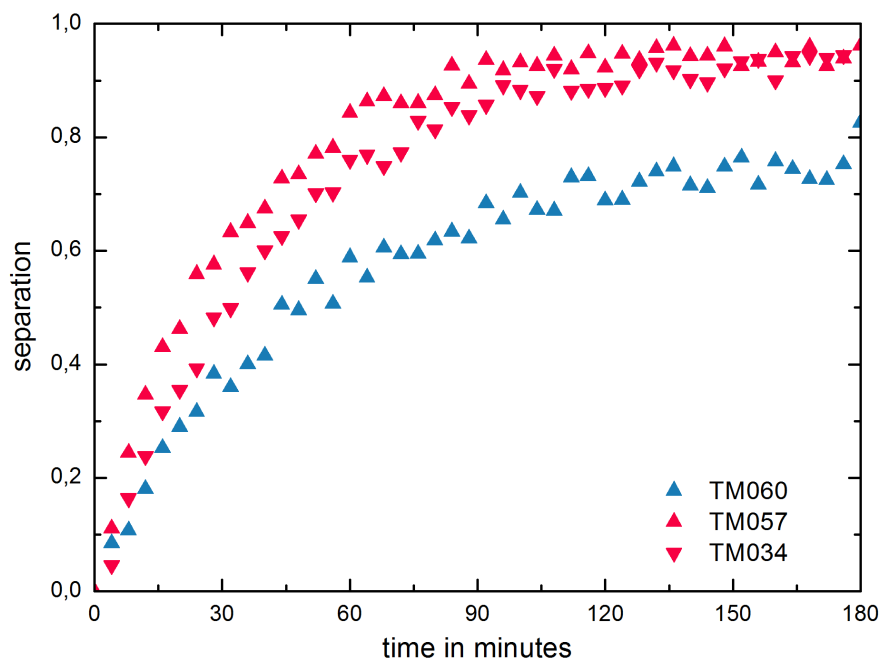


Figure E.28.: Reproducibility of the electric splitting experiment with four inclined plate electrodes and 3x4 rod electrodes with the plates acting as anodes

APPENDIX F. MODELLING RESULTS FOR THE ELECTRICAL FIELD SPLITTING

In this chapter the modelling results as well as the data from the sigmoidal fit of all electrical field splitting experiments are listed. The parameters of the model and the fit are shown in the tables F.1 and F.2, respectively.

The model was not able to analyse TM044 properly. The reason was a program error. DCamCapture stopped working and led to incomplete documentation of the experiment. In the experiment TM046 the camera has been moved. For this reasons the r^2 of these experiments are low.

Table F.1.: Model parameters of all electric field experiments

<i>Name of the experiment</i>	<i>a</i>	<i>b</i>	<i>r</i> ²	<i>confidence interval a lower</i>	<i>confidence interval b lower</i>	<i>confidence interval a higher</i>	<i>confidence interval b higher</i>	<i>relative deviation of confidence interval of parameter a in %</i>	<i>relative deviation of confidence interval of parameter b in %</i>
CS001	0.864	2.099E-2	0.979	0.852	2.010E-2	0.876	2.189E-2	1.39	4.27
CS002	0.850	2.474E-2	0.984	0.841	2.389E-2	0.858	2.560E-2	1.00	3.46
CS003	0.847	2.237E-2	0.980	0.836	2.144E-2	0.858	2.330E-2	1.31	4.16
CS004	0.855	2.376E-2	0.977	0.844	2.271E-2	0.867	2.481E-2	1.34	4.42
CS005	0.986	2.137E-2	0.990	0.977	2.073E-2	0.995	2.200E-2	0.95	2.96
CS006	0.886	2.149E-2	0.985	0.876	2.071E-2	0.896	2.228E-2	1.16	3.63
CS007	0.844	2.257E-2	0.978	0.832	2.161E-2	0.855	2.354E-2	1.35	4.28
CS008	0.874	2.012E-2	0.983	0.863	1.934E-2	0.886	2.089E-2	1.29	3.86
CS009	0.857	2.353E-2	0.984	0.848	2.269E-2	0.867	2.438E-2	1.08	3.59
CS010	0.876	2.318E-2	0.983	0.865	2.229E-2	0.886	2.408E-2	1.19	3.86
CS011	0.874	2.396E-2	0.984	0.865	2.312E-2	0.883	2.480E-2	1.04	3.51
CS012	0.835	2.235E-2	0.978	0.824	2.139E-2	0.847	2.331E-2	1.34	4.29
CS013	0.605	1.947E-2	0.995	0.600	1.906E-2	0.609	1.989E-2	0.74	2.14
CS014	0.628	2.056E-2	0.993	0.623	2.006E-2	0.633	2.107E-2	0.82	2.47
CS015	0.610	1.966E-2	0.998	0.607	1.937E-2	0.613	1.995E-2	0.51	1.48
CS016	0.647	2.105E-2	0.996	0.643	2.068E-2	0.650	2.142E-2	0.57	1.77
CS017	0.571	1.962E-2	0.996	0.568	1.924E-2	0.575	1.999E-2	0.66	1.92
CS018	0.591	1.784E-2	0.999	0.588	1.762E-2	0.594	1.805E-2	0.44	1.18
CS019	0.673	2.291E-2	0.997	0.671	2.260E-2	0.676	2.321E-2	0.38	1.32
CS020	0.688	1.704E-2	0.997	0.684	1.675E-2	0.693	1.733E-2	0.64	1.70

Table F.1.: Model parameters of all electric field experiments (continued)

<i>Name of the experiment</i>	<i>a</i>	<i>b</i>	<i>r</i> ²	<i>confidence interval a lower</i>	<i>confidence interval b lower</i>	<i>confidence interval a higher</i>	<i>confidence interval b higher</i>	<i>relative deviation of confidence interval of parameter a in %</i>	<i>relative deviation of confidence interval of parameter b in %</i>
CS021	0.633	2.300E-2	0.999	0.631	2.278E-2	0.635	2.322E-2	0.29	0.95
CS022	0.665	2.359E-2	0.998	0.663	2.333E-2	0.667	2.385E-2	0.33	1.11
CS023	0.645	2.325E-2	0.998	0.643	2.300E-2	0.647	2.349E-2	0.31	1.06
CS024	0.673	2.262E-2	0.999	0.671	2.243E-2	0.674	2.281E-2	0.26	0.83
CS025	0.719	2.391E-2	0.995	0.715	2.344E-2	0.723	2.439E-2	0.59	1.98
CS026	0.725	2.335E-2	0.999	0.723	2.317E-2	0.726	2.353E-2	0.23	0.77
CS027	0.813	1.837E-2	0.999	0.810	1.820E-2	0.816	1.854E-2	0.33	0.93
CS028	0.706	2.162E-2	0.998	0.703	2.132E-2	0.709	2.192E-2	0.44	1.40
CS029	0.738	1.812E-2	0.999	0.735	1.790E-2	0.742	1.834E-2	0.44	1.22
CS030	0.654	2.158E-2	0.997	0.651	2.125E-2	0.657	2.191E-2	0.48	1.51
CS031	0.636	2.144E-2	0.998	0.633	2.114E-2	0.638	2.173E-2	0.44	1.37
CS032	0.671	2.149E-2	0.997	0.668	2.113E-2	0.675	2.185E-2	0.54	1.68
CS033	0.660	1.965E-2	0.998	0.657	1.942E-2	0.663	1.988E-2	0.40	1.17
CS034	0.644	1.799E-2	0.999	0.643	1.782E-2	0.647	1.816E-2	0.34	0.94
CS035	0.620	1.933E-2	0.999	0.619	1.919E-2	0.622	1.948E-2	0.26	0.75
CS036	0.726	1.260E-2	0.992	0.714	1.214E-2	0.738	1.305E-2	1.67	3.58
CS037	0.820	1.837E-2	0.989	0.810	1.775E-2	0.830	1.898E-2	1.20	3.35
CS038	0.750	2.219E-2	0.988	0.742	2.149E-2	0.757	2.289E-2	0.99	3.15
CS039	0.800	1.763E-2	0.997	0.795	1.732E-2	0.805	1.795E-2	0.67	1.79
CS040	0.789	1.687E-2	0.988	0.777	1.624E-2	0.800	1.750E-2	1.46	3.74

Table F.1.: Model parameters of all electric field experiments (continued)

<i>Name of the experiment</i>	<i>a</i>	<i>b</i>	<i>r</i> ²	<i>confidence interval a lower</i>	<i>confidence interval b lower</i>	<i>confidence interval a higher</i>	<i>confidence interval b higher</i>	<i>relative deviation of confidence interval of parameter a in %</i>	<i>relative deviation of confidence interval of parameter b in %</i>
CS041	0.830	1.873E-2	0.986	0.819	1.799E-2	0.842	1.947E-2	1.40	3.94
CS042	0.799	1.543E-2	0.990	0.787	1.486E-2	0.811	1.599E-2	1.52	3.67
CS043	0.674	1.822E-2	0.990	0.667	1.765E-2	0.682	1.879E-2	1.15	3.15
CS044	0.668	1.638E-2	0.992	0.660	1.587E-2	0.676	1.688E-2	1.22	3.11
CS045	0.773	1.622E-2	0.993	0.768	1.585E-2	0.780	1.659E-2	0.77	2.29
CS046	0.707	1.789E-2	0.992	0.700	1.738E-2	0.715	1.840E-2	1.05	2.84
CS047	0.636	1.764E-2	0.997	0.631	1.732E-2	0.640	1.797E-2	0.66	1.77
CS048	0.655	1.531E-2	0.997	0.650	1.500E-2	0.661	1.563E-2	0.84	2.05
HW001_1	0.841	2.840E-2	0.996	0.837	2.793E-2	0.844	2.886E-2	0.43	1.64
HW001_2	0.842	2.739E-2	0.995	0.838	2.689E-2	0.846	2.788E-2	0.49	1.82
HW002_1	0.825	5.922E-2	0.828	0.814	5.448E-2	0.835	6.396E-2	1.32	8.00
HW002_2	0.804	3.539E-2	0.960	0.795	3.367E-2	0.813	3.710E-2	1.10	4.84
HW003_1	0.839	2.747E-2	0.992	0.834	2.686E-2	0.844	2.809E-2	0.60	2.23
HW003_2	0.828	3.133E-2	0.961	0.819	2.982E-2	0.838	3.284E-2	1.18	4.82
HW004_1	0.978	5.893E-2	0.997	0.976	5.824E-2	0.980	5.961E-2	0.19	1.16
HW004_2	0.870	4.474E-2	0.987	0.866	4.354E-2	0.875	4.594E-2	0.52	2.68
HW005_1	0.711	3.028E-2	0.965	0.703	2.892E-2	0.719	3.164E-2	1.12	4.48
HW005_2	0.754	3.606E-2	0.967	0.747	3.453E-2	0.761	3.759E-2	0.95	4.25
HW006_1	0.929	4.863E-2	0.989	0.925	4.743E-2	0.933	4.983E-2	0.46	2.47
HW006_2	1.007	6.766E-2	0.987	1.003	6.588E-2	1.011	6.943E-2	0.40	2.62

Table F.1.: Model parameters of all electric field experiments (continued)

<i>Name of the experiment</i>	<i>a</i>	<i>b</i>	<i>r</i> ²	<i>confidence interval a lower</i>	<i>confidence interval b lower</i>	<i>confidence interval a higher</i>	<i>confidence interval b higher</i>	<i>relative deviation of confidence interval of parameter a in %</i>	<i>relative deviation of confidence interval of parameter b in %</i>
HW007_1	0.816	6.600E-2	0.987	0.812	6.424E-2	0.819	6.776E-2	0.41	2.66
HW007_2	0.797	3.995E-2	0.984	0.792	3.876E-2	0.802	4.113E-2	0.62	2.97
HW008_1	0.960	4.397E-2	0.995	0.957	4.327E-2	0.963	4.467E-2	0.31	1.58
HW008_2	0.968	4.213E-2	0.998	0.966	4.167E-2	0.970	4.260E-2	0.22	1.11
HW009_1	0.872	4.465E-2	0.987	0.867	4.348E-2	0.876	4.581E-2	0.51	2.60
HW009_2	0.904	4.639E-2	0.993	0.900	4.549E-2	0.907	4.730E-2	0.37	1.95
HW010_1	0.966	4.745E-2	0.991	0.962	4.637E-2	0.970	4.852E-2	0.43	2.27
HW010_2	0.985	3.484E-2	0.984	0.978	3.372E-2	0.993	3.597E-2	0.74	3.23
HW011_1	0.863	4.559E-2	0.996	0.861	4.495E-2	0.865	4.622E-2	0.27	1.39
HW011_2	0.871	4.637E-2	0.994	0.868	4.556E-2	0.874	4.719E-2	0.34	1.76
HW012_1	0.935	6.830E-2	0.989	0.932	6.665E-2	0.939	6.996E-2	0.37	2.42
HW012_2	0.925	6.012E-2	0.988	0.921	5.855E-2	0.929	6.168E-2	0.43	2.60
HW013_1	0.948	6.435E-2	0.995	0.946	6.334E-2	0.950	6.536E-2	0.25	1.57
HW014_1	0.927	5.572E-2	0.998	0.925	5.518E-2	0.928	5.626E-2	0.17	0.96
HW014_2	0.938	5.679E-2	0.994	0.935	5.581E-2	0.941	5.777E-2	0.29	1.73
HW015_1	0.969	5.389E-2	0.999	0.967	5.344E-2	0.970	5.435E-2	0.15	0.84
HW016_1	0.921	6.018E-2	0.993	0.918	5.900E-2	0.924	6.137E-2	0.32	1.97
HW016_2	0.922	7.049E-2	0.987	0.918	6.860E-2	0.925	7.239E-2	0.40	2.69
HW017_1	0.951	7.134E-2	0.996	0.949	7.032E-2	0.953	7.235E-2	0.21	1.43
HW017_2	0.966	4.924E-2	0.991	0.962	4.816E-2	0.970	5.032E-2	0.40	2.19

Table F.1.: Model parameters of all electric field experiments (continued)

<i>Name of the experiment</i>	<i>a</i>	<i>b</i>	<i>r</i> ²	<i>confidence interval a lower</i>	<i>confidence interval b lower</i>	<i>confidence interval a higher</i>	<i>confidence interval b higher</i>	<i>relative deviation of confidence interval of parameter a in %</i>	<i>relative deviation of confidence interval of parameter b in %</i>
HW018_1	0.871	5.070E-2	0.993	0.868	4.974E-2	0.874	5.165E-2	0.34	1.89
HW018_2	0.879	5.116E-2	0.991	0.875	5.000E-2	0.882	5.232E-2	0.41	2.26
HW019_1	0.908	5.003E-2	0.998	0.906	4.947E-2	0.910	5.060E-2	0.21	1.13
HW019_2	0.916	4.682E-2	0.991	0.912	4.574E-2	0.920	4.789E-2	0.44	2.30
HW020_1	0.844	2.837E-2	0.968	0.833	2.698E-2	0.855	2.976E-2	1.29	4.91
HW020_2	0.836	2.733E-2	0.974	0.826	2.612E-2	0.846	2.853E-2	1.19	4.42
HW021_1	0.815	2.118E-2	0.991	0.807	2.058E-2	0.822	2.178E-2	0.91	2.84
HW021_2	0.841	2.164E-2	0.993	0.835	2.114E-2	0.847	2.213E-2	0.72	2.27
HW022_1	0.812	2.731E-2	0.995	0.808	2.680E-2	0.816	2.782E-2	0.51	1.88
HW022_2	0.709	2.712E-2	0.982	0.703	2.622E-2	0.716	2.802E-2	0.90	3.33
HW023_1	0.850	2.673E-2	0.991	0.844	2.606E-2	0.856	2.739E-2	0.68	2.48
HW023_2	0.863	2.466E-2	0.981	0.854	2.371E-2	0.873	2.560E-2	1.11	3.83
HW024_1	0.860	2.138E-2	0.995	0.854	2.096E-2	0.865	2.180E-2	0.63	1.98
HW024_2	0.855	2.590E-2	0.994	0.850	2.536E-2	0.860	2.643E-2	0.58	2.06
HW025_1	0.807	2.179E-2	0.994	0.802	2.134E-2	0.813	2.226E-2	0.69	2.17
HW025_2	0.861	2.314E-2	0.993	0.855	2.263E-2	0.867	2.366E-2	0.67	2.22
HW026_1	0.840	2.448E-2	0.989	0.833	2.376E-2	0.848	2.520E-2	0.86	2.94
HW026_2	0.836	2.589E-2	0.993	0.831	2.531E-2	0.842	2.648E-2	0.63	2.26
HW027_1	0.814	3.022E-2	0.986	0.808	2.928E-2	0.821	3.116E-2	0.78	3.12
HW027_2	0.872	2.625E-2	0.993	0.867	2.564E-2	0.878	2.685E-2	0.64	2.31

Table F.1.: Model parameters of all electric field experiments (continued)

<i>Name of the experiment</i>	<i>a</i>	<i>b</i>	<i>r</i> ²	<i>confidence interval a lower</i>	<i>confidence interval b lower</i>	<i>confidence interval a higher</i>	<i>confidence interval b higher</i>	<i>relative deviation of confidence interval of parameter a in %</i>	<i>relative deviation of confidence interval of parameter b in %</i>
HW028_1	0.838	2.335E-2	0.995	0.833	2.290E-2	0.843	2.381E-2	0.58	1.95
HW028_2	0.829	2.069E-2	0.993	0.822	2.019E-2	0.835	2.119E-2	0.80	2.41
HW029_1	0.830	2.663E-2	0.995	0.826	2.615E-2	0.834	2.710E-2	0.49	1.79
HW029_2	0.857	2.456E-2	0.998	0.854	2.428E-2	0.859	2.485E-2	0.34	1.17
HW030_1	0.748	2.442E-2	0.996	0.744	2.400E-2	0.752	2.484E-2	0.50	1.71
HW030_2	0.753	2.501E-2	0.997	0.750	2.466E-2	0.756	2.536E-2	0.40	1.39
HW031_1	0.769	1.923E-2	0.995	0.763	1.883E-2	0.774	1.963E-2	0.72	2.08
HW031_2	0.760	2.439E-2	0.998	0.758	2.411E-2	0.763	2.466E-2	0.33	1.14
HW032_1	0.860	2.871E-2	0.989	0.854	2.791E-2	0.867	2.952E-2	0.73	2.81
HW032_2	0.889	3.177E-2	0.986	0.882	3.079E-2	0.895	3.275E-2	0.75	3.08
HW033_1	0.921	3.082E-2	0.993	0.916	3.017E-2	0.926	3.148E-2	0.52	2.12
HW033_2	0.925	2.591E-2	0.998	0.922	2.562E-2	0.928	2.620E-2	0.31	1.11
HW034_1	0.859	3.140E-2	0.997	0.856	3.097E-2	0.861	3.183E-2	0.34	1.38
HW034_2	0.853	3.037E-2	0.997	0.850	2.994E-2	0.856	3.080E-2	0.36	1.41
HW035_1	0.923	2.583E-2	0.994	0.918	2.530E-2	0.929	2.637E-2	0.58	2.07
HW035_2	0.956	2.411E-2	0.997	0.952	2.376E-2	0.960	2.446E-2	0.43	1.46
HW036_1	0.789	2.967E-2	0.990	0.784	2.891E-2	0.794	3.042E-2	0.65	2.53
HW036_2	0.796	3.250E-2	0.989	0.791	3.168E-2	0.801	3.332E-2	0.61	2.52
HW037_1	0.825	2.694E-2	0.989	0.819	2.621E-2	0.832	2.767E-2	0.74	2.70
HW037_2	0.813	2.515E-2	0.996	0.809	2.471E-2	0.817	2.558E-2	0.49	1.73

Table F.1.: Model parameters of all electric field experiments (continued)

<i>Name of the experiment</i>	<i>a</i>	<i>b</i>	<i>r</i> ²	<i>confidence interval a lower</i>	<i>confidence interval b lower</i>	<i>confidence interval a higher</i>	<i>confidence interval b higher</i>	<i>relative deviation of confidence interval of parameter a in %</i>	<i>relative deviation of confidence interval of parameter b in %</i>
HW038_1	0.925	3.389E-2	0.989	0.920	3.303E-2	0.931	3.476E-2	0.59	2.56
HW038_2	0.893	3.058E-2	0.967	0.882	2.909E-2	0.904	3.207E-2	1.21	4.87
HW039_1	0.941	2.527E-2	0.990	0.933	2.459E-2	0.948	2.595E-2	0.76	2.69
HW039_2	0.934	2.673E-2	0.986	0.926	2.590E-2	0.942	2.756E-2	0.84	3.11
HW040_1	0.894	2.660E-2	0.993	0.888	2.599E-2	0.900	2.721E-2	0.63	2.28
HW040_2	0.883	3.100E-2	0.989	0.877	3.018E-2	0.888	3.183E-2	0.65	2.65
HW041_1	0.957	2.448E-2	0.998	0.953	2.416E-2	0.960	2.480E-2	0.38	1.29
HW041_2	0.919	2.774E-2	0.998	0.916	2.743E-2	0.922	2.806E-2	0.30	1.13
RMA029	0.845	2.500E-2	0.966	0.837	2.397E-2	0.854	2.603E-2	1.02	4.13
RMA030	0.835	2.671E-2	0.957	0.829	2.575E-2	0.841	2.767E-2	0.72	3.60
RMA031	0.879	2.534E-2	0.968	0.873	2.447E-2	0.886	2.621E-2	0.74	3.43
RMA032	0.883	2.663E-2	0.983	0.877	2.586E-2	0.890	2.741E-2	0.72	2.92
RMA033	0.969	5.551E-2	0.981	0.967	5.443E-2	0.971	5.660E-2	0.21	1.95
TM032	1.003	6.521E-2	0.998	1.002	6.461E-2	1.005	6.581E-2	0.14	0.92
TM033	0.884	2.062E-2	0.988	0.874	1.995E-2	0.893	2.129E-2	1.07	3.24
TM034	0.955	2.409E-2	0.991	0.947	2.346E-2	0.962	2.472E-2	0.78	2.61
TM035	0.840	2.589E-2	0.990	0.832	2.501E-2	0.848	2.677E-2	0.95	3.39
TM036	0.926	2.334E-2	0.991	0.919	2.277E-2	0.933	2.392E-2	0.73	2.48
TM037	0.925	1.524E-2	0.960	0.913	1.379E-2	0.937	1.669E-2	1.28	9.51
TM038	0.923	3.317E-2	0.991	0.918	3.243E-2	0.927	3.391E-2	0.52	2.23

Table F.1.: Model parameters of all electric field experiments (continued)

<i>Name of the experiment</i>	<i>a</i>	<i>b</i>	<i>r</i> ²	<i>confidence interval a lower</i>	<i>confidence interval b lower</i>	<i>confidence interval a higher</i>	<i>confidence interval b higher</i>	<i>relative deviation of confidence interval of parameter a in %</i>	<i>relative deviation of confidence interval of parameter b in %</i>
TM039	0.814	2.095E-2	0.985	0.805	2.020E-2	0.824	2.169E-2	1.17	3.57
TM040	0.916	4.397E-2	0.987	0.911	4.278E-2	0.921	4.517E-2	0.54	2.72
TM041	0.861	2.374E-2	0.990	0.855	2.315E-2	0.867	2.433E-2	0.72	2.49
TM042	0.858	2.743E-2	0.988	0.852	2.668E-2	0.865	2.818E-2	0.74	2.74
TM043	0.923	3.552E-2	0.989	0.918	3.460E-2	0.929	3.644E-2	0.58	2.59
TM044	0.952	0.115	0.932	0.944	0.108	0.960	0.123	0.80	6.46
TM045	0.900	4.441E-2	0.990	0.896	4.342E-2	0.904	4.541E-2	0.43	2.24
TM046	0.745	8.296E-2	0.279	0.706	5.087E-2	0.783	0.115	5.22	38.68
TM048	0.883	2.920E-2	0.990	0.877	2.849E-2	0.888	2.991E-2	0.62	2.44
TM049	0.939	4.482E-2	0.986	0.934	4.359E-2	0.944	4.605E-2	0.54	2.75
TM050	0.946	5.222E-2	0.994	0.943	5.139E-2	0.948	5.305E-2	0.27	1.60
TM051	0.883	2.746E-2	0.990	0.877	2.678E-2	0.889	2.814E-2	0.66	2.48
TM052	0.873	5.329E-2	0.985	0.869	5.182E-2	0.877	5.477E-2	0.48	2.77
TM053	0.867	4.657E-2	0.982	0.862	4.509E-2	0.872	4.804E-2	0.60	3.16
TM054	0.793	2.626E-2	0.982	0.785	2.534E-2	0.801	2.719E-2	0.97	3.51
TM055	0.790	2.543E-2	0.980	0.782	2.455E-2	0.798	2.631E-2	0.95	3.45
TM056	0.957	4.215E-2	0.992	0.953	4.129E-2	0.961	4.301E-2	0.41	2.05
TM057	0.952	3.385E-2	0.994	0.948	3.322E-2	0.956	3.447E-2	0.43	1.85
TM058	0.977	4.225E-2	0.996	0.974	4.165E-2	0.980	4.286E-2	0.29	1.43
TM059	0.989	4.969E-2	0.996	0.987	4.900E-2	0.992	5.039E-2	0.26	1.41

Table F.1.: Model parameters of all electric field experiments (continued)

<i>Name of the experiment</i>	<i>a</i>	<i>b</i>	<i>r</i> ²	<i>confidence interval a lower</i>	<i>confidence interval b lower</i>	<i>confidence interval a higher</i>	<i>confidence interval b higher</i>	<i>relative deviation of confidence interval of parameter a in %</i>	<i>relative deviation of confidence interval of parameter b in %</i>
TM060	0.770	2.181E-2	0.988	0.763	2.115E-2	0.778	2.248E-2	0.97	3.06
TM061	0.881	2.466E-2	0.988	0.876	2.413E-2	0.885	2.519E-2	0.50	2.15
TM062	0.706	1.665E-2	0.984	0.695	1.597E-2	0.717	1.733E-2	1.56	4.08
TM063	0.692	1.633E-2	0.985	0.681	1.568E-2	0.703	1.698E-2	1.55	3.99

Table F.2.: Fit parameters of all electric field experiments

<i>Name of the experiment</i>	A_s	B_s	C_s	D_s	r^2	<i>deadtime in minutes</i>
CS001	-5.090	0.853	-71.965	42.078	0.981	3
CS002	-1.369	0.831	-14.009	29.761	0.986	1
CS003	-4.272	0.837	-59.815	39.175	0.982	4
CS004	-2.825	0.842	-36.081	34.898	0.980	6
CS005	-10484.205	0.878	-336.632	35.923	0.987	1
CS006	-0.686	0.848	5.792	27.706	0.991	0
CS007	-44715.612	0.844	-480.979	44.823	0.982	7
CS008	-5.668	0.865	-82.304	44.793	0.984	2
CS009	-0.843	0.829	2.374	27.448	0.989	3
CS010	-0.806	0.843	7.234	27.122	0.988	6
CS011	-0.793	0.846	2.280	26.603	0.989	1
CS012	-1.648	0.816	-22.498	34.217	0.979	2
CS013	-8571.565	0.599	-474.929	50.031	0.995	4
CS014	-9632.565	0.622	-451.424	47.099	0.993	3
CS015	-11018.887	0.607	-486.465	49.739	0.998	1
CS016	-22042.252	0.645	-490.425	47.265	0.996	3
CS017	-16977.016	0.569	-521.398	50.672	0.996	1
CS018	-2968.435	0.580	-444.173	52.524	0.997	4
CS019	-1821.304	0.670	-331.683	42.377	0.997	3
CS020	-4709.885	0.686	-509.563	57.928	0.997	2
CS021	-4995.978	0.628	-379.310	42.443	0.998	2
CS022	-8149.424	0.663	-396.648	42.290	0.998	2
CS023	-7564.776	0.673	-372.093	40.021	0.998	1
CS024	-9591.753	0.672	-418.321	43.847	0.999	1
CS025	-16135.571	0.733	-392.229	39.294	0.995	1
CS026	-19565.623	0.743	-478.212	47.275	0.999	3
CS027	-8807.012	0.831	-496.530	53.820	0.999	2
CS028	-7353.463	0.731	-454.832	49.615	0.998	2
CS029	-21607.328	0.755	-570.171	55.787	0.998	2
CS030	-7099.867	0.651	-413.288	44.618	0.996	2
CS031	-6741.677	0.643	-412.587	44.851	0.997	3
CS032	-10861.384	0.671	-429.573	44.461	0.996	1
CS033	-6327.462	0.626	-430.865	46.904	0.998	2
CS034	-4.300	0.623	-89.817	47.237	0.999	1

Table F.2.: Fit parameters of all electric field experiments (continued)

<i>Name of the experiment</i>	A_s	B_s	C_s	D_s	r^2	<i>deadtime in minutes</i>
CS035	-1.814	0.603	-47.640	44.628	0.999	2
CS036	-4253.361	0.648	-530.401	60.623	0.993	2
CS037	-0.573	0.776	9.193	29.342	0.994	0
CS038	-21115.888	0.736	-431.196	42.254	0.988	3
CS039	-16310.643	0.797	-524.339	53.217	0.996	4
CS040	-3037.283	0.755	-420.407	51.379	0.986	6
CS041	-0.52	0.759	11.954	27.391	0.989	2
CS042	-12154.628	0.788	-570.265	59.720	0.991	6
CS043	-17710.318	0.703	-548.511	54.383	0.991	3
CS044	-28469.951	0.667	-601.833	56.767	0.992	3
CS045	-7976.773	0.750	-493.665	53.575	0.992	3
CS046	-19300.209	0.695	-533.085	52.406	0.992	3
CS047	-7392.655	0.636	-504.468	54.260	0.997	3
CS048	-20094.617	0.663	-665.016	64.739	0.997	3
HW001_1	-15643.439	0.840	-345.405	35.207	0.996	1
HW001_2	-29337.084	0.841	-381.051	36.494	0.995	1
HW002_1	-16897.671	0.860	-352.666	34.215	0.951	0
HW002_2	-10430.917	0.801	-262.510	27.897	0.964	2
HW003_1	-15281.596	0.839	-362.108	36.849	0.992	0
HW003_2	-17653.880	0.828	-324.889	32.507	0.962	0
HW004_1	-1.811	0.975	-9.059	13.772	0.998	0
HW004_2	-1.199	0.863	-4.396	16.441	0.991	1
HW005_1	-13598.637	0.714	-347.157	35.032	0.968	0
HW005_2	-20143.107	0.754	-289.447	28.316	0.968	0
HW006_1	-0.540	0.918	8.234	12.193	0.997	2
HW006_2	-0.470	1.000	6.059	8.605	0.999	0
HW007_1	-1.661	0.812	-8.008	11.736	0.989	0
HW007_2	-7637.276	0.795	-225.134	24.655	0.985	1
HW008_1	-1.232	0.951	-3.497	16.581	0.998	1
HW008_2	-415.226	0.967	-140.548	23.364	0.998	1
HW009_1	-228.565	0.870	-120.938	22.048	0.988	2
HW009_2	-41.657	0.902	-79.577	21.055	0.993	1
HW010_1	-0.746	0.957	3.281	13.609	0.998	0
HW010_2	-0.527	0.967	10.920	16.492	0.997	1

Table F.2.: Fit parameters of all electric field experiments (continued)

<i>Name of the experiment</i>	A_s	B_s	C_s	D_s	r^2	<i>deadtime in minutes</i>
HW011_1	-297.999	0.860	-122.436	21.001	0.996	0
HW011_2	-840.777	0.868	-141.712	20.668	0.994	0
HW012_1	-1.331	0.930	-3.368	10.517	0.993	0
HW012_2	-0.487	0.916	6.927	9.608	0.997	1
HW013_1	-2.389	0.944	-11.209	12.524	0.998	0
HW014_1	-14.964	0.927	-48.070	17.842	0.997	2
HW014_2	-1.332	0.934	-4.284	13.567	0.997	1
HW015_1	-2571.308	0.969	-146.646	18.607	0.999	0
HW016_1	-0.907	0.915	1.115	11.317	0.997	1
HW016_2	-0.744	0.916	2.150	9.024	0.994	0
HW017_1	-2.320	0.948	-9.571	11.171	0.999	0
HW017_2	-0.647	0.958	4.426	13.040	0.998	0
HW018_1	-0.698	0.863	3.280	13.111	0.999	1
HW018_2	-1.069	0.872	-1.952	13.986	0.994	1
HW019_1	-3.001	0.904	-20.811	17.252	0.998	0
HW019_2	-1.045	0.907	-0.751	14.712	0.996	1
HW020_1	-0.191	0.813	21.666	15.111	0.996	0
HW020_2	-0.145	0.806	23.636	16.207	0.996	0
HW021_1	-0.825	0.783	-0.575	30.223	0.994	1
HW021_2	-9277.606	0.841	-431.640	46.446	0.994	1
HW022_1	-11418.390	0.809	-342.333	35.931	0.995	1
HW022_2	-23779.315	0.714	-412.110	39.385	0.985	0
HW023_1	-0.599	0.826	6.658	22.832	0.997	0
HW023_2	-0.216	0.827	22.334	19.201	0.997	0
HW024_1	-0.811	0.828	-0.306	30.244	0.998	0
HW024_2	-1419.051	0.847	-275.206	37.189	0.993	1
HW025_1	-27558.559	0.804	-470.687	45.181	0.994	1
HW025_2	-22705.384	0.856	-424.687	41.741	0.993	0
HW026_1	-0.474	0.807	12.973	22.311	0.998	1
HW026_2	-0.567	0.810	7.619	23.132	0.999	0
HW027_1	-0.375	0.791	13.063	17.640	0.998	0
HW027_2	-0.652	0.847	6.010	23.167	1.000	0
HW028_1	-1.479	0.822	-20.663	33.093	0.996	0
HW028_2	-8457.005	0.824	-434.837	47.395	0.993	3

Table F.2.: Fit parameters of all electric field experiments (continued)

<i>Name of the experiment</i>	A_s	B_s	C_s	D_s	r^2	<i>deadtime in minutes</i>
HW029_1	-5271.764	0.824	-316.908	36.192	0.995	0
HW029_2	-2.526	0.842	-34.717	32.921	0.999	1
HW030_1	-4.006	0.742	-60.412	36.811	0.996	2
HW030_2	-2.231	0.741	-33.719	32.608	0.998	2
HW031_1	-15514.893	0.760	-492.456	49.768	0.995	1
HW031_2	-8727.256	0.758	-377.122	40.442	0.998	1
HW032_1	-0.498	0.835	11.333	19.650	0.999	1
HW032_2	-0.447	0.867	11.457	17.481	0.998	0
HW033_1	-0.795	0.906	1.417	22.114	0.997	0
HW033_2	-661.132	0.925	-252.491	38.571	0.998	1
HW034_1	-1.425	0.848	-13.461	24.569	0.998	0
HW034_2	-1.357	0.840	-11.303	24.839	0.999	1
HW035_1	-34518.142	0.927	-422.923	40.094	0.994	0
HW035_2	-12792.635	0.956	-399.775	41.999	0.997	0
HW036_1	-2.966	0.782	-37.836	29.045	0.991	1
HW036_2	-4260.872	0.796	-262.224	30.767	0.990	2
HW037_1	-55472.096	0.825	-414.925	37.381	0.990	1
HW037_2	-9731.997	0.811	-373.735	39.750	0.996	0
HW038_1	-0.607	0.909	6.834	18.084	0.998	0
HW038_2	-0.193	0.868	20.519	15.084	0.990	0
HW039_1	-0.567	0.913	9.343	24.094	0.996	0
HW039_2	-0.495	0.907	12.109	21.340	0.997	0
HW040_1	-0.909	0.870	1.375	24.455	0.998	2
HW040_2	-0.655	0.864	5.636	19.937	0.998	0
HW041_1	-32088.364	0.955	-424.022	40.762	0.998	1
HW041_2	-11189.303	0.917	-334.962	35.614	0.998	0
RMA029	-23450.987	0.843	-399.610	39.188	0.968	1
RMA030	-15660.048	0.837	-395.533	39.929	0.961	0
RMA031	-13402.124	0.877	-370.966	38.519	0.967	0
RMA032	-12637.832	0.882	-363.415	37.888	0.983	0
RMA033	-5.276	0.969	-27.687	16.717	0.983	1
TM032	-1.994	1.000	-8.863	12.452	1.000	0
TM033	-12403.115	0.876	-445.020	46.899	0.988	3
TM034	-1.511	0.933	-11.849	30.403	0.993	3

Table F.2.: Fit parameters of all electric field experiments (continued)

<i>Name of the experiment</i>	A_s	B_s	C_s	D_s	r^2	<i>deadtime in minutes</i>
TM035	-3.834	0.832	-48.447	33.717	0.986	3
TM036	-12311.360	0.925	-409.027	43.022	0.991	0
TM037	-26093.638	0.921	-630.802	61.460	0.959	0
TM038	-6.283	0.919	-52.949	27.935	0.992	1
TM039	-4906.853	0.805	-396.941	45.783	0.984	2
TM040	-4.536	0.913	-31.357	20.636	0.988	2
TM041	-15658.548	0.860	-414.731	42.219	0.991	0
TM042	-10050.278	0.854	-331.353	35.478	0.989	1
TM043	-0.930	0.911	0.140	19.407	0.993	1
TM044	6.400E-2	0.944	9.816	3.029	0.965	2
TM045	-1.570	0.896	-11.930	18.644	0.991	0
TM046	-6.800E-2	0.744	10.595	5.959	0.293	0
TM048	-21071.850	0.881	-342.745	34.071	0.991	1
TM049	-0.523	0.928	6.753	13.733	0.994	0
TM050	-3.359	0.944	-22.804	17.344	0.995	0
TM051	-2.386	0.877	-33.019	31.427	0.991	0
TM052	-0.698	0.868	1.634	13.213	0.990	0
TM053	-0.505	0.859	5.952	13.809	0.990	0
TM054	-6556.320	0.783	-321.944	35.779	0.981	1
TM055	-37359.862	0.800	-478.016	44.140	0.985	0
TM056	-1.210	0.950	-5.145	17.790	0.995	0
TM057	-3073.972	0.951	-239.554	29.598	0.994	0
TM058	-23.392	0.975	-71.057	22.514	0.997	0
TM059	-39.125	0.990	-74.304	20.354	0.996	1
TM060	-11887.127	0.766	-429.764	44.664	0.989	1
TM061	-15668.271	0.882	-409.994	41.788	0.989	0
TM062	-37841.412	0.702	-645.574	59.237	0.984	0
TM063	-9701.892	0.685	-579.321	60.505	0.985	0

APPENDIX G. PUBLICATIONS

ORAL PRESENTATIONS

2017

Macher-Ambrosch, R.; Siebenhofer, M.:

Turbidity Control

in: 13th Minisymposium Chemical and Process Engineering and 4th Austrian Particle Forum,
Innsbruck, Austria, 29/03/17 - 30/03/17

Macher-Ambrosch, R.; Siebenhofer, M.:

Turbidity Control

in: AIChE Annual Meeting 2017,
Minneapolis, USA, 29/10/17 - 03/11/17

Macher-Ambrosch, R.; Siebenhofer, M.:

Turbidity Control

in: 21st International Solvent Extraction Conference,
Miyazaki, Japan, 05/11/17 - 09/11/17

2016

Macher-Ambrosch, R.; Siebenhofer, M.:

Turbidity control

in: 42. Tief-Temperatur-Thermodynamik-Kolloquium TTTK 2016,
Canazei, Italy, 21/02/16 - 27/02/16

Macher-Ambrosch, R.; Siebenhofer, M.:

Turbidity Control - Cleavage of Stable Emulsions

in: AIChE Annual Meeting 2016,
San Francisco, USA, 14/11/16 - 19/11/16

Toth, A.; Macher-Ambrosch, R.; Painer, D.; Lux, S.; Siebenhofer, M.:

Intensified Liquid-Liquid Extraction with Chemical Reaction By Emulsification

in: AIChE Annual Meeting 2016,

San Francisco, USA, 14/11/16 - 19/11/16

Toth, A.; Macher-Ambrosch, R.; Painer, D.; Lux, S.; Siebenhofer, M.:

Isolation of Carboxylic Acids from Dilute Aqueous Solutions - Intensifying Approach By Conversion in Emulsified Reactive Solvents

in: AIChE Annual Meeting 2016,

San Francisco, USA, 14/11/16 - 19/11/16

2015

Macher-Ambrosch, R.; Siebenhofer, M.:

Turbidity control in liquid-liquid extraction

in: AIChE Annual Meeting 2015,

Salt Lake City, USA, 08/11/15 - 13/11/15

2014

Macher, R.; Pfennig, A.:

Numerische Modellierung von Zentrifugalabscheidern basierend auf experimentellen Daten

in: Jahrestreffen der Fachgruppen Extraktion und Fluidverfahrenstechnik,

Fulda, Germany, 27/03/14 - 28/03/14

POSTER

2016

Macher-Ambrosch, R.; Siebenhofer, M.:

Turbidity control

in: 12th Minisymposium Verfahrenstechnik 2016,
Graz, Austria, 30/03/2016 - 31/03/2016

Poonyaratanasrihajan, A.; Macher-Ambrosch, R.; Kangsadan, T.; Siebenhofer, M.:

O/W-Emulsions, Production and Stability

in: 12th Minisymposium Verfahrenstechnik 2016,
Graz, Austria, 30/03/2016 - 31/03/2016

Macher-Ambrosch, R.; Siebenhofer, M.:

Turbidity Control - Spaltung von stabilen Öl/Wasser Emulsionen

in: ProcessNet-Jahrestagung und 32. DECHEMA-Jahrestagung der Biotechnologie 2016,
Aachen, Germany, 12/09/16 - 15/09/16

Macher-Ambrosch, R.; Toth, A.; Siebenhofer, M.:

Phase Separation of Emulsification Reaction Broths

in: 19th Symposium on Separation Science and Technology for Energy Applications,
Gatlinburg, USA, 10/10/16 - 12/10/16

Toth, A.; Macher-Ambrosch, R.; Lux, S.; Siebenhofer, M.:

Intensification of Liquid-Liquid Extraction with Chemical Reaction through Emulsification

in: 19th Symposium on Separations Science and Technology for Energy Applications,
Gatlinburg, USA, 10/10/16 - 12/10/16

2014

Macher, R.; Bol, P.; Pfennig, A.:

Charakterisierung und Abtrennung von Feinsttrübungen mithilfe von Zentrifugalabscheidern

in: ProcessNet-Jahrestagung und 31. Jahrestagung der Biotechnologen 2014,
Aachen, Germany, 29/09/14 - 02/10/14

Macher, R.; Pfennig, A.:

Numerical Modelling of Centrifugal Settlers Based on Experimental Data

in: ISEC 20th International Solvent Extraction Conference,

Frankfurt, Germany, 7/09/14 - 11/09/14

CONTRIBUTIONS IN CONFERENCE PROCEEDINGS

2017

Macher-Ambrosch, R.; Siebenhofer, M.:

Turbidity control

in: Conference Proceedings of the 13th Minisymposium Verfahrenstechnik. (2017)

2016

Macher-Ambrosch, R.; Siebenhofer, M.:

Turbidity control

in: Conference Proceedings of the 12th Minisymposium Verfahrenstechnik. (2016)

Poonyaratanasrihajan, A.; Macher-Ambrosch, R.; Kangsadan, T.; Siebenhofer, M.:

O/W-Emulsions, Production and Stability

in: Conference Proceedings of the 12th Minisymposium Verfahrenstechnik. (2016)

2014

Macher, R.; Pfennig, A.:

Numerical Modelling of Centrifugal Settlers Based on Experimental Data.

in: ISEC 19th International Solvent Extraction Conference. (2014)

CONTRIBUTIONS IN JOURNALS

2017

Leis, D.; Lauß, B.; Macher-Ambrosch, R.; Pfennig, A.; Nidetzky, B.; Kratzer, R.:
Integration of whole-cell reaction and product isolation: Highly hydrophobic solvents promote *in situ* substrate supply and simplify extractive product isolation
in: Journal of Biotechnology. 257, p. 110-117

2016

Macher-Ambrosch, R.; Siebenhofer, M.:
Turbidity control
in: CEET konkret 2016, p. 18-19

2015

Macher-Ambrosch, R.; Siebenhofer, M.:
Turbidity control
in: CEET konkret 2015, p. 14-15

2014

Macher, R.; Bol, P.; Pfennig, A.:
Charakterisierung und Abtrennung von Feinsttrübungen mithilfe von Zentrifugalabscheidern
in: Chemie-Ingenieur Technik. 86, 9 p. 1465 (2014)

Macher, R.:
Phasentrennung in Gravitations- und Zentrifugalabscheidern
in: CEET konkret 2014, p. 24-25

2013

Macher, R.:
Phasentrennung in Zentrifugalextraktoren
in: CEET konkret 2013, p. 24-25